Synthesis, Characterizations and Applications of Mesoporous Carbon Composites

by

Mingzhi Dai

A Dissertation Presented in Partial Fulfillment
of the Requirements for the Degree
Doctor of Philosophy

Approved November 2012 by the
Graduate Supervisory Committee:

Bryan Vogt, Chair
Jeffrey LaBelle
Lenore Dai
David Nielsen
Cesar Torres

ARIZONA STATE UNIVERSITY

December 2012

ABSTRACT

This dissertation provides a fundamental understanding of the properties of mesoporous carbon based materials and the utilization of those properties into different applications such as electrodes materials for super capacitors, adsorbents for water treatments and biosensors. The thickness of mesoporous carbon films on Si substrates are measured by Ellipsometry method and pore size distribution has been calculated by Kelvin equation based on toluene adsorption and desorption isotherms monitored by Ellipsometer.

The addition of organometallics cobalt and vanalyl acetylacetonate in the synthesis precursor leads to the metal oxides in the carbon framework, which largely decreased the shrink of the framework during carbonization, resulting in an increase in the average pore size. In addition to the structural changes, the introduction of metal oxides into mesoporous carbon framework greatly enhances the electrochemical performance as a result of their pseudocapacitance. Also, after the addition of Co into the framework, the contraction of mesoporous powders decreased significantly and the capacitance increased prominently because of the solidification function of CoO nanoparticles. When carbon-cobalt composites are used as adsorbent, the adsorption capacity of dye pollutant in water is remarkably higher (90 mg/g) after adding Co than the mesoporous carbon powder (2 mg/g). Furthermore, the surface area and pore size of mesoporous composites can be greatly increased by addition of tetraethyl orthosilicate into the precursor with

subsequent etching, which leads to a dramatic increase in the adsorption capacity from 90 mg/g up to 1151 mg/g.

When used as electrode materials for amperometric biosensors, mesoporous carbons showed good sensitivity, selectivity and stability. And fluorine-free and low-cost poly (methacrylate)s have been developed as binders for screen printed biosensors. With using only 5wt% of poly (hydroxybutyl methacrylate), the glucose sensor maintained mechanical integrity and exhibited excellent sensitivity on detecting glucose level in whole rabbit blood. Furthermore, extremely high surface area mesoporous carbons have been synthesized by introducing inorganic Si precursor during self-assembly, which effectively determined norepinephrine at very low concentrations.

ACKNOWLEDGEMENTS

I would like to thank everyone who helped and encouraged me during my doctoral study. My deep gratitude goes first to my advisor, Professor Bryan D. Vogt, who expertly guided me through my 3.5 years of research life. His unwavering passion and sharp insight for research kept inspiring me constantly engaged my research. Without his guidance and persistent help, this dissertation would not have been possible. My sincere appreciation goes to my co-advisor Professor Jeffrey T. La Belle, who generously accepted me in his group and provided me everything I need for my continuous research in the last year. I would not be able to finish my dissertation by now without his support and guidance. I would also like to thank the rest of my dissertation committees: Prof. Lenore Dai, Prof. David R. Nielsen and Prof. César I. Torres for their insightful questions and advices during my comprehensive exam and dissertation.

Thank my fellow labmate Todd Prichard for his help and support. Thank Dr. Lingyan Song, Dr. Xinxin Li, Vicki Chavez for their training on the equipments and suggestions on the experiments during my first year of PhD study. Thank Dr. Jessica M Torres and Alpha Labiano for their friendship and support. Thank Brittney Haselwood and Stephanie Maxwell in Dr. La Belle's group for assisting me through the last two biosensor projects.

Lastly, I would like to thank my parents for their tremendous love and support on the way of chasing my dreams. Thank my lovely sisters and brother in law for their encouragement and love. Their faith in me is the power source

for me to achieve my goals. Thank my parents in law for their love and support. Thank my husband Huxiao who accompanied me through these years, shared my frustration, excitement, as well as happiness and offered me the greatest support and love along this journey.

TABLE OF CONTENTS

Page

CHAPTER Page

CHAPTER Page

CHAPTER Page

LIST OF FIGURES

Figure Page

Figure Page

Figure Page

Figure Page

Figure Page

LIST OF TABLES

Table Page

CHAPTER 1

INTRODUCTION

1.1 Overview

Mesoporous carbons with high surface area, tunable pore size, narrow pore size distribution and biocompatibility have developed tremendously during last two decades. Particularly, ordered mesoporous carbons have received much attention because of their wide applications such as high surface area adsorbents,[1-5] solid supports for sensors,[6-9] electrodes for batteries[10-14] and catalyst support for fuel cells.[15-18] In recent years, extensive efforts have focused on their synthesis and performances in order to obtain well-defined nanostructured materials with controlled modification of the framework for specific applications.[19-21]

Mesoporous carbon based materials, with both high surface area and good electrolyte accessibility, provide the optimum amount of charge to be stored and delivered. Combined with pseudo-capacitive materials (for example, metal oxides), the supercapacitors are able to store energy using both adsorption (from porous carbon) and fast surface redox reactions (metal oxides), providing very high capacitance. As a sustainable and renewable resource, these supercapacitors provide a promising way to solve the climate change and decreasing availability of fossil fuels problems.

When make the mesoporous carbon magnetic, with the huge interface and large pore space, they can effectively remove unfavorable heavy metal anions or organic pollutants as separable adsorbents for water pollution control.

Through adjusting of the pore size and surface area, adsorbents can be designed to target specific type and amount of certain pollutant. Magnetic separable carbon based adsorbents offer an efficient alternative approach to change the aggravating environment pollution situation with low cost.

With increasing demands in the development of inexpensive, reliable and simple devices for rapid and accurate tests in diagnostics of disease, disposable screen printed electrodes can serve as biosensors to meet requirements. By selecting suitable components of electrode materials, the low sensitive screen printed electrodes can be modified to provide high signal and accuracy. With unique electronic, chemical, biocompatible properties, as well as tunable pore size, high surface area carbon materials provide high sensitivity, reproducibility and selectivity to the biosensors. Combining with environmental friendly polymer binders, sensors with optimum sensitivity and integrity can be achieved.

The goal of this research is to exploit the advantageous properties of ordered mesoporous carbon-based materials and adjust those properties according to the requirements for different applications such as electrodes for energy storage, magnetically separable adsorbents for water treatments and electrode materials for disposable biosensors. To ensure a good control of the pore frameworks, it is important to understand their properties such as pore size, pore shape, pore volume, porosity, wall thickness, and stability during treatments. Introducing metal oxides into the mesoporous carbon framework leads to mesoporous carbon composite electrodes with high capacitance;

adding Si inorganic template and organometallic into the precursor result in mesoporous carbon with large adsorption capacity; using poly methacrylate binder and mesoporous carbons as electrode materials produces glucose and norepinephrine sensors with great sensitivity.

In this introduction, a brief summary of each chapter is provided, along with in depth discussion on the development of the synthesis methods for mesoporous materials, characterizations of mesoporous thins films and powders on pore size calculation, pore framework structure investigation, as well as the applications with using the mesoporous materials.

In Chapter 2, ordered mesoporous composites thin films with incorporation of cobalt and vanadium oxides via the triconstituent synthesis method by using $Co(acac)_3$ and $VO(acac)_2$ as precursors have been synthesized. Evaporation induced self-assembly (EISA) of low-molecular weight phenolic resin (resols),[22] commercially available triblock copolymers (Pluronic F127) and metal (acac) is utilized to form highly ordered mesoporous carbon composite thin films after pyrolysis at 800 ℃. The porous morphology of the films is investigated by X-ray diffraction, transmission electron microscopy (TEM), and ellipsometric porosimetry. Additionally, the electrical and electrochemical properties of these films are examined as a function of composite film composition. These results illustrate the versatility of the triconstituent assembly approach for fabrication of ordered mesoporous carbon composites with potential applications in catalysis, energy storage, and sensing.

In Chapter 3, Mesoporous carbons containing cobalt nanoparticles are synthesized by tri-or quad-constituent self assembly of Pluronic F127, phenol-formaldehyde oligomer (resol), cobalt acetylacetonate (acac), and optionally tetraethyl orthosilicate (TEOS, optional). Upon pyrolysis in N_2 atmosphere, the resol provides sufficient carbon yield to maintain the ordered structure, while decomposition of the Co(acac) yields cobalt nanoparticles. To provide increased surface area, the dispersed silicate from condensation of TEOS can be etched after carbonization to yield micropores, Without silica templated micropores, the surface area decreases as the cobalt content increases, but there is a concurrent increase in the volume-average pore diameter (BHJ) and a dramatic increase in the adsorption capacity of methylene green with the equilibrium adsorption capacity from 2 to 90 mg/g with increasing Co content. Moreover, the surface area and pore size of mesoporous composites can be dramatically increased by addition of TEOS and subsequent etching. These composites exhibit extremely high adsorption capacity up to 1151 mg g^{-1}, which also increases with increases in the Co content. Additionally, the inclusion of cobalt nanoparticles provides magnetic separation from aqueous suspension. The in situ synthesis of the Co nanoparticles yields to a carbon shell that can partially protect the Co from leaching in acidic media; after 96 h in 2 M HCl, the powders remain magnetic.

In Chapter 4, two ordered, soft-templated mesoporous carbon powders with cubic and hexagonal framework structure and four different commercial, low cost methacrylate-based polymer binders with widely varying physical

properties are investigated as screen printed electrodes for glucose sensors using glucose oxidase and ferricyanide as the mediator. Both the chemistry and concentration of the binder in the electrode formulation can significantly impact the performance. Poly(hydroxybutyl methacrylate) as the binder provides hydrophilicity to enable transport of species in the aqueous phase to the carbon surface, but yet is sufficiently hydrophobic to provide mechanical robustness to the sensor. The current from the mesoporous carbon electrodes can be more than an order of magnitude greater than for a commercial printed carbon electrode (Zensor) with improved sensitivity for model glucose solutions. Even when applying these sensors to rabbit whole blood, the performance of these glucose sensors compares favorably to a standard commercial glucose meter with the lower detection limit of the mesoporous electrode being approximately 20 mg dL^{-1} despite the lack of a separation membrane to prevent non-specific events; these results suggest that the small pore sizes and high surface areas associated with ordered mesoporous carbons may effectively decrease some non-specific inferences for electrochemical sensing.

In Chapter 5, norepinephrine (NE) is detected amperometrically using enzyme Phenylethanolamine N-methyl transferase and cofactor S-(5′-Adenosyl)-L-methionine chloride dihydrochloride on screen printed mesoporous carbon electrodes. The role of internal surface area and pore size of the mesoporous carbon is systematically examined by using soft templated mesoporous silica-carbon powder with highly microporous walls obtained

from etching of the silica to produce powders with surface areas ranging from 671-2339 m^2/g. As the surface area increases, the sensitivity of the biosensor at very low NE concentrations (0-500 pg mL^{-1}) in PBS increases with an increase in the slope of the current from 6 to $117\frac{\mu A}{ng/ml}$. The best performing electrode provides similar sensitivity in whole rabbit blood despite no added membrane layer to filter the non-desired reactants; the small (<5 nm) pore size and large internal surface area acts to minimize non-specific events that decrease sensitivity.

In Chapter 6, a brief description of future work is given, including work aimed at further control of porous materials at macro-scale, as well as their applications in biosensors. The steps of synthesizing three macroporous carbon materials with uniform pore size around 50, 100 and 200 nm for each, without using template surfactant are proposed. The next step after successfully synthesize macroporous carbons is to apply them on the application of antibody biosensors. Different as the fabrication of previous biosensors, this time the antibody will be immobilized into the pores first, and then it will be used to detect the target under electrochemical measurements. The impact of the pore size of the carbon, applied potential, pH value and temperature on the performance of the biosensors will be studied.

1.2 Synthesis methods of mesoporous materials

According to the International Union of Pure and Applied Chemistry (IUPAC), the definition of pore size is that micropores are smaller than 2nm in

diameter, mesopores are 2 to 50nm and macropores are larger than 50nm.[23] Numerous methods have been proposed to synthesize mesoporous materials in the past two plus decades. The development of the synthesis methods will be discussed as below according to the breakthrough of mesoporous products in history.

1.2.1 Templated mesoporous aluminosilicates using ionic surfactants

The report by Mobil researchers in 1992 of the synthesis of a family ordered mesoporous molecular aluminosilicates sieves (denoted as MCM-41) has sparked tremendous interest in the field of mesoporous materials.[24,25] This initial breakthrough extended ordered porous materials from microporous to mesoporous with relatively large, uniform and easily adjustable pore sizes. Long-chain ionic quaternary ammonium surfactant hexadecyltrimethylammonium ($C_{16}H_{33}(CH_3)_3N^+OH/Cl$) was used as structure directing agents under basic conditions, and the electrostatic interactions between cationic surfactant (S^+) and anionic inorganic precursors (I^-) triggered the self-assembly of the mesoporous structure during hydrothermal synthesis.[24] In this self-assembly process, the pore size of the mesoporous structured MCM-41 family can be controlled (from 15 Å to 100 Å) by the choice of surfactant, auxiliary chemicals and reaction conditions.[24] For example, the pore size can be reduced by decreasing the alkyl chain length, n, from 16 to 8 in the ammonium surfactant ($C_nH_{2n+1}(CH_3)_3N^+$), while increasing the pore size increased by adding the organic solvent mesitylene.[24] As shown in the Figure 1, decreasing n leads to the shorter chain lengths inside the

micelles, which results in smaller radius of the micelles and thus smaller pore size after removal of the surfactant. As a contrast, addition of organic auxiliary chemicals such as mesitylene would swell the hydrophobic cores of the micelles, leading to larger pore size. However, the cooperative organization mechanism via electrostatic interactions is not limited to ion-pairs between the cationic surfactants (S^+) and anionic inorganic species (I^-).[26] Besides the mechanism mentioned above, the electrostatic templating concept has been extended to charge reversed S^-I^+ (anionic surfactants such as sulfonates and cationic inorganic precursors), counter ion-mediated $S^+X^-I^+$ ($X^- = Cl^-$ or Br^-), and $S^-M^+I^-$ ($M^+ = Na^+$ or K^+) pathways.[27-29]

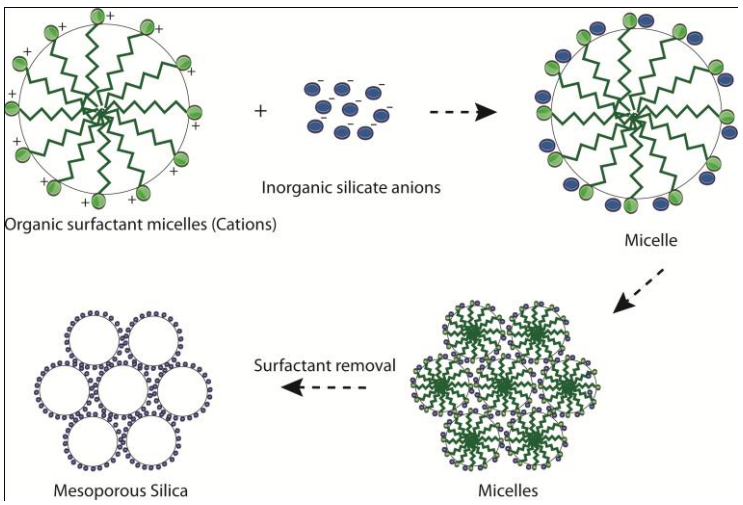

Figure 1 Ionic surfactant templating mechanism.[26]

1.2.2 Neutral and non-ionic templating mesoporous silica molecular sieves

In 1994, neutral (N^0I^0)[30] and a non-ionic (S^0I^0)[31] templating techniques by using alkylamines and polyethylene oxide-based surfactants were reported and the products are denoted HMS and MSU-X, respectively. The neutral

templating route is based on hydrogen bonding and self - organization between neutral primary amine micelles or non-ionic surfactant micelles (S^0) and neutral inorganic precursors (I^0). As shown in Figure 2, for the HMS synthesis, tetraethyl orthosilicate is first partially hydrolyzed to a neutral species and then through hydrogen bonding interact with the head group of amine surfactant. Also, the product MSU-X templated by non-ionic polyethylene oxide (PEO) surfactants has drawn much attention at that time because PEO is low cost and environmentally compatible. Actually the templating procedure is quite simply by the hydrolysis of TEOS in the presence of PEO surfactants, and the pore size can be adjusted by changing the number of hydrophobic carbon units or hydrophilic EO units and the ratio of TEOS and PEO,

$$Si(OEt)_4 + H_2O \rightleftharpoons Si(OEt)_{4-x}(OH)_x$$

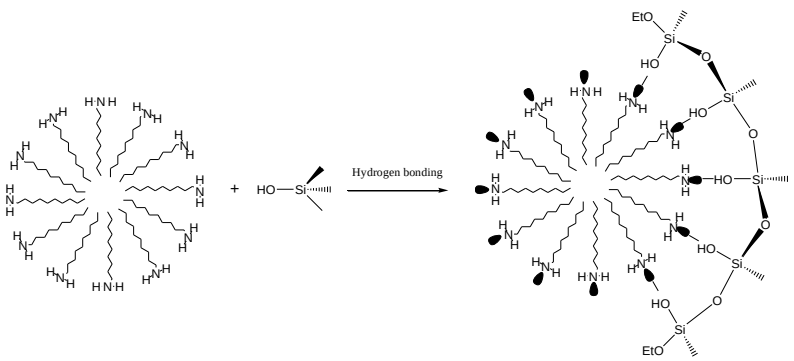

Figure 2 Neutral templating mechanism.[26,32]

Nonionic amphiphilic PEO surfactants are commercially available, relatively low cost, nontoxic and biodegradable,[33] and also have excellent properties such as association properties,[34] self-aggregation[35] and phase

behaviors.[36] Thus much attention has been paid to PEO amphiphilic block copolymers as the templates. But it was hard to obtain mesoporous materials with ordered structure by the neutral templating method (HMS and MSU-X are both disordered). However, in 1998, Stucky and co-workers[37,38] made a major contribution by synthesis of a family of ordered siliceous mesoporous materials (SBA-X) with using various PEO block copolymers in acidic aqueous solutions. Since then, remarkable progress has been made on the synthesis of new silica mesophases. In Stucky's work, highly ordered large pore (up to 300nm) mesoporous silica materials 2D hexagonal (*p6mm*) SBA-15[37] and cubic (*Im3m*) SBA-16[38] were synthesized under acidic conditions with the presence of triblock polymers such as $EO_{20}PO_{70}EO_{20}$ (P123), $EO_{106}PO_{70}EO_{106}$ (F127), $EO_{132}PO_{50}EO_{132}$(F108) and $EO_{39}BO_{47}EO_{39}$(B50-6600) as structure-directing agents. In particular SBA-15 has attracted considerable interest due to its high quality structure regularity, thick inorganic walls, excellent stability, and also the synthesis is simple and reproducible synthesis.[37,39]

Because various structures and properties can be obtained by the block architecture and controllable repeating number of hydrophobic and hydrophilic blocks, nonionic block copolymers have become a popular choice as template for mesoporous materials.[23] For preparing mesoporous materials from block copolymers, two key requirements have to be satisfied: first, the etchable materials (surfactant) need to be able to physically access to the solvent and reagent; second, the matrix material should be able to support the

resultant mesoporous structure after template removal, otherwise the mesoporous structure will be collapsed.[21]

1.3 Synthesis of mesoporous carbons

The inorganic-organic self-assembly method has been widely used to synthesize ordered mesoporous metal oxides,[40,41] metal sulfides[42] and silica sieves[32]. A frequently used approach of fabricating mesoporous materials involved using hard silica template as precursor and matrix materials for the resulting porous framework. For example, in order to prepare mesoporous carbon replicas, first is to fill the carbon sources into silica channels, following by carbonizing the material, and then etch the hard silicate template by HF or NaOH solution. However, because of the high formation energy of C-C bonds, the preparation of ordered mesoporous carbon materials is difficult.[22] Due to the extensive potential high-tech applications such as energy storage,[43,44] adsorption,[45,46] catalysis,[47] separation,[48,49] supercapacitors,[13,50] significant research has been carried out to develop mesoporous carbons. Dai's group firstly tried using the self-assembly of block copolymers to synthesize large-scale, highly ordered nanoporous carbon films in 2004.[51] And In 2006, Meng and coworkers[22] at Fudan University successfully synthesized a family of highly ordered mesoporous carbon frameworks through organic assembly of triblock copolymers by an evaporation induced self-assembly strategy (EISA).

First, a hydrophilic resin (denoted resol) with small molecular weight was synthesized (Figure 3). As shown in Figure 2, high curvature can be obtained by increasing phenol/surfactant template ratio or the PEO/PPO ratio

in the block copolymers, and the pore structure can shift from lamellar to cylinder and to spheres. As a result, different structure ordered mesoporous carbons FDU-15(hexagonal) and FDU-16 (cubic) were obtained by controlling the ratio of organic triblock copolymer/phenol and the type of triblock copolymers.[22] Particularly FDU-16-800 has drawn much attention because of its high surface area (820 cm^2 g^{-1}), nicely ordered cubic structure, high stability (over 1400 ℃) and easily reproducibility. The synthesis approach involves four major steps: resol precursor preparation (matrix), mix resol and triblock copolymers in organic solvent, evaporate the solvent, thermopolymerization under ~100 ℃ to solidify the framework by crosslinking and carbonization to remove the surfactant template.

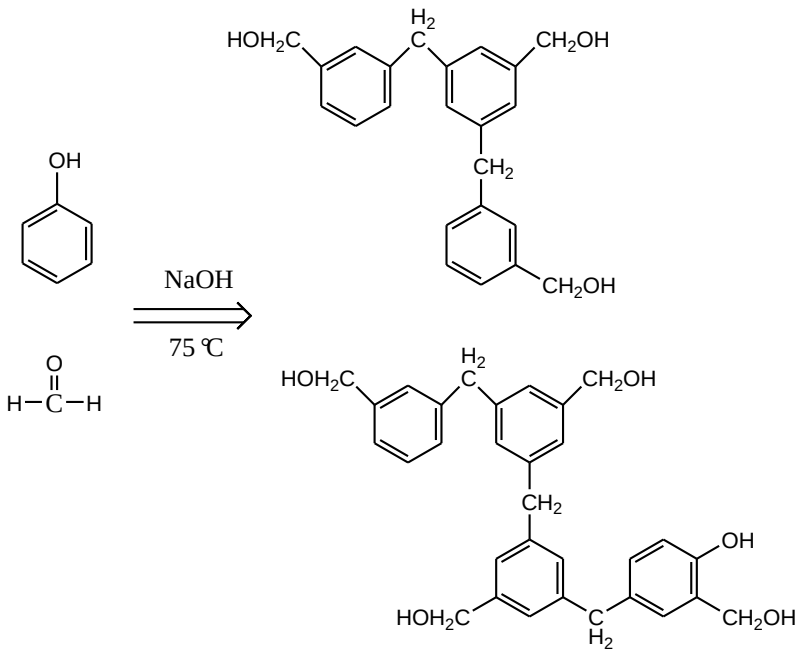

Figure 3 Synthesize resol by phenol and formaldehyde.[22]

1. 4 Surface area and porosity properties of mesoporous powders

An important tool to understand the surface area and porosity in unknown samples is controlled gas adsorption.[52] The adsorption isotherm, provides the relationship between the amount of adsorbed adsorbate (normally nitrogen is used) and the equilibrium pressure or relative pressure at a known temperature, typically 77K for nitrogen.[53] Van der Waals adsorption isotherms of gases can be divided into five types following the seminal work of Brunauer, Deming, Deming and Teller in 1940.[54] Each of the five isotherms shapes is depicted in Figure 4 and reflects certain unique properties of the material of interest. Type I is the well-known Langmuir adsorption isotherm and it occurs when adsorption is limited to only a few molecular layers. In the case of physical adsorption, the condition for type I isotherms to occur is that microporous powders have pore size not larger than a few adsorbate molecular diameters, indicating no additional adsorption after the micropores have been filled.[53,55] When adsorption on nonporous powders or powders with pore diameters larger than micropores, Types II isotherms usually are encountered.[54,55] With increasing the relative pressure after the first adsorbed monolayer completed, second and higher layers occur and the number of adsorbed layers increases until at saturation. In type III adsorption isotherms, the adsorbate interaction with an adsorbed layer is greater than with the adsorbent surface, leading to additional adsorption on the adsorbed layer. Type IV isotherms are encountered on porous adsorbents with pore size in the range of 15 -1000 Angstroms.[55] Comparing to type II isotherms, the slope increases

in type IV adsorption curve at high relative pressures means an increasing uptake of adsorbate as the pores are being filled. In this case, capillary condensation occurs after the initial monolayer–multilayer adsorption on the mesoporous walls.[53] Basically, the situation for type V isotherms to occur is between type III and type IV. It involves small adsorbate-adsorbent interaction potentials which are similar to the type III isotherms, and type V isotherms are also associated with pore size in the same range as in type IV isotherms. The adsorption phenomenon for mesoporous powder materials normally falls in type IV isotherms, which is the area of interest for this work.

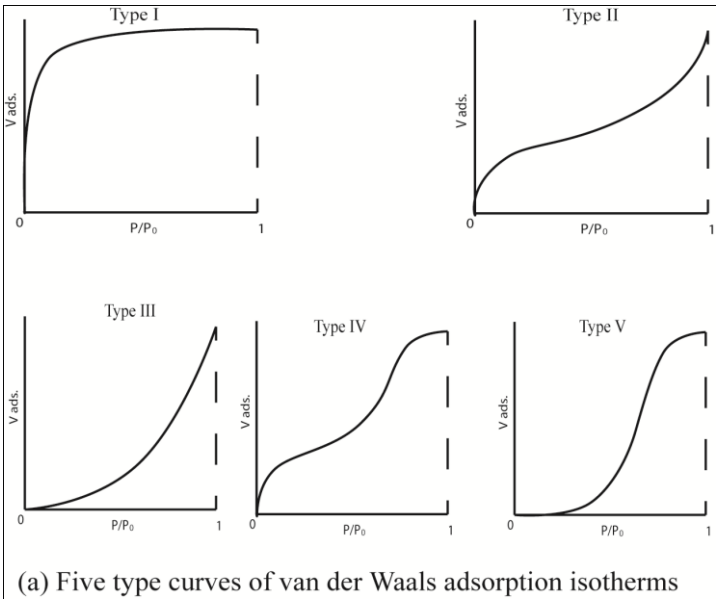

(a) Five type curves of van der Waals adsorption isotherms

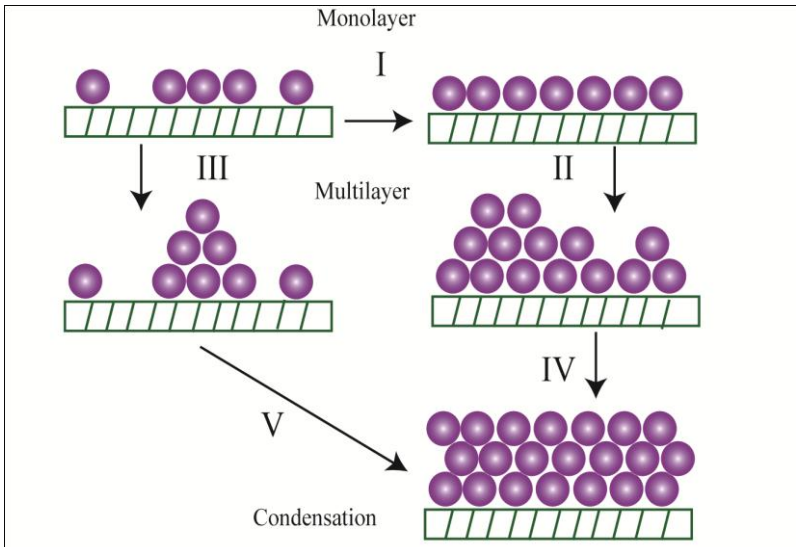

(b) Illustrations of five types of van der Waals adsorption isotherms

Figure 4 Five types of van der Waals adsorption isotherms.

In 1938, Brunauer, Emmett and Teller[56] (BET) proposed the theory of multilayer adsorption, and then the number of molecules of vapor needed to complete a monolayer on the solid surface can be calculated from an adsorption isotherm.[57] Since then, the BET has been extensively applied to

physical adsorption isotherms since it makes an good method of calculating surface area.[58] In the BET theory, the adsorbed molecules in the first adsorbed layer are assumed to act as sites for the second-layer adsorbates, which are subsequently considered to be the sites for the higher layer adsorbates. At a given temperature, when the rate of condensation (adsorption) is equal to the rate of evaporation (desorption), equilibrium is obtained. The equation[53] for adsorption in each layer at equilibrium is:

$$a_i p\theta_{i-1} = b_i\theta_i \exp(\frac{-E_i}{RT}) \quad (1)$$

where θ_{i-1} and θ_i represent the fractions of surface covered by the *i*–1th and *i*th layers, respectively, a_i and b_i are adsorption and desorption constants, and E_i is the heat of adsorption for the *i*th layer.[56] In order to simplify the summation of the amounts adsorbed, assume for all layers after the first, these parameters remain constant

$$E_2 = E_3 = \cdots = E_i = E_L \quad (2)$$

where $E_L$the heat of liquefaction of the gas, and

$$\frac{b_2}{a_2} = \frac{b_3}{a_3} = \cdots \frac{b_i}{a_i} = q \quad (3)$$

By assuming heat of adsorption E_i is independent of the number of adsorbed molecules already present in the first layer and q is a constant that the evaporation-condensation properties of the molecules in the second and higher adsorbed layers are the same as those of the liquid state, the well-known BET equation is thus formed[56]

$$\frac{\frac{p}{p^0}}{[n\left(\frac{1-p}{p^0}\right)]} = \left(\frac{1}{n_m C}\right) + \left[\frac{(C-1)}{n v_m C}\right]\left(\frac{p}{p^0}\right) \quad (4)$$

where n is the adsorbed gas quantity, n_m is the monolayer adsorbed quantity and C is a measure of the adsorbent-adsorbate interaction energy.[59] The parameter C is defined by the equation

$$C = \exp[\frac{(E_1 - E_L)}{RT}] \quad (5)$$

In equation (4), if plot $p/n(p^0-p)$ versus p/p^0, n_m and C can be easily calculated from the slope and intercept of the linear plot. But the linearity is found to be limited in the p/p^0 range 0.05-0.3 for various gases such as CO_2, Argon, Nitrogen and Oxygen, and the plot of experimental data would deviate more and more strongly from the straight line as relative pressure exceeds 0.35.[53,55,56] The specific surface area can be obtained from n_m by the equation

$$\alpha_{BET} = n_m L \sigma \quad (6)$$

where L is the Avogadro's constant, and σ is the area occupied by each adsorbate molecule in the completed monolayer. The adsorbent gas molecules should not possess permanent dipole moments as to be physically adsorbed on the adsorbate. Given the cost and error value caused by E_1-E_L from the assumption in equation (2), Nitrogen (77K) is normally considered as the most suitable adsorptive for the determination of surface area of all kinds of solids, and the adsorbate nitrogen molecule is found to be 0.162 m^2. Thus, it is possible to evaluate BET-nitrogen area from n_m by equation (6).

1.5 Properties and characterizations of ordered mesoporous carbon thin films

Porous thin films (typically thinner than 2 microns) are more and more important in modern materials field because of their numerous potential applications in energy storage devices, sensors, separations and microelectronics.[60,61] Ordered mesoporous carbon thin films can be prepared by spin coating the resol and amphiphilic triblock copolymer solution (same ratio as powder product FDU-16/FDU-15) onto a clean silicon wafer, and then followed by solvent evaporation, thermopolymerization and carbonization processes, just the same steps as powder FDU-16 product. To make sure good adhesion between the carbon film and silicon wafer, it's important to treat the wafer surface by Piranha acid or UV light in order to obtain a clean surface and enrich the –OH groups. Mesoporous carbon powder product is prepared by pouring the solution into petri dish instead of spin coating on silicon wafer. However, even if for the same solution, same solvent evaporation time and same time and temperature for thermopolymerization and carbonization, the morphology properties such as pore size, porosity, contraction degree, and of course the final structure framework, are much different between films and powders.

1.5.1 Pore size distribution (PSD) of thin films

Pore size is the one of the most important properties for porous materials, because it defines the dielectric, mechanical, thermal and chemical properties of the material.[61] Ellipsometric Porosimetry (EP) is a very informative, powerful and non-destructive technique to measure the pore size

distribution of thin films, first reported by Baklanov and co-workers in 2000.[61,62] By detecting the change of the optical characteristics of the porous film during vapor adsorption and desorption, it determines the mass of an adsorptive condensed/adsorbed in pores instead of direct weighing.[61] Actually, ellipsometry measures a change in polarization when light reflects or transmits from a material structure, which depends on optical properties and thickness of the films (Figure 5). At very first, ellipsometry was used to determine the thickness and optical constant of the films (refractive index). In EP approach, the principle has been extended to use the change of the refractive index (n) and the film thickness (d) to estimate the amount of adsorbate adsorbed/condensed in the film, allowing us to directly measure the pore size distribution of a thin porous film in a simple way. [60,63]

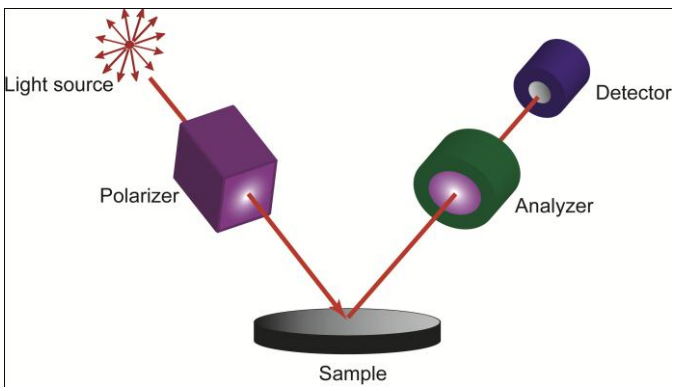

Figure 5 Schematic of ellipsometry.

In EP approach to measure pore size in the film, a non-polar organic solvent (such as toluene, heptanes and tetrachloride) is used to fill and empty the pores by changing the vapor pressure in room temperature, which is called adsorption and desorption isotherms.[61] The amount of adsorptive inside of the

pores can be calculated from the change of optical constant in the materials during vapor adsorption/desorption. The refractive index of the film will be measured and recorded by the computer when relative pressure of the solvent vapor changes from 0 to 1 in adsorption and from 1 to 0 in desorption (Figure 6).

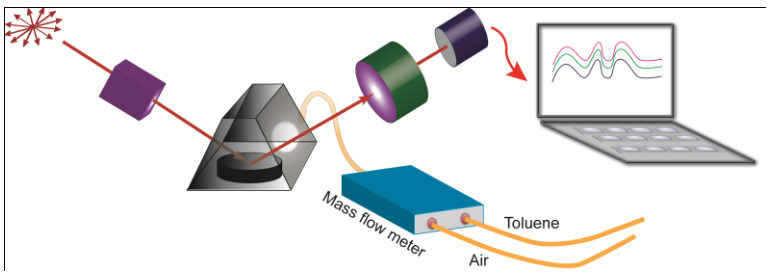

Figure 6 Set up for measuring adsorption/desorption isotherms.

The typical adsorption/desorption isotherm curves for mesoporous films are shown in Figure 7. The curve BCD shows the path along adsorption isotherms as the relative pressure is increased, and curve DFB displays the path along desorption isotherms as the relative pressure is reduced. Capillary condensation of toluene occurred in the pores as vapor pressure increased, resulted in the increase in the average refractive index of the film. Initially, the refractive index increased slowly.[64] When the vapor pressure reached a critical value, the refractive index increased dramatically due to a large amount filling of pores of certain size. And accordingly, refractive index reduced distinctly because of the pore emptying in desorption process when the vapor pressure dropped. The hysteresis loop in desorption/adsorption isotherms in the Figure

7 is from the mesoporous polymer film, which falls into type V isotherms.[20,65-70]

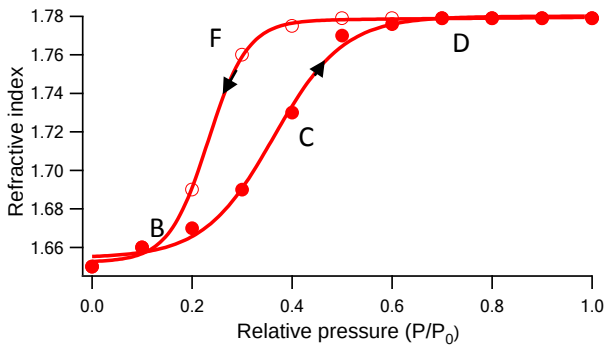

Figure 7 Adsorption and desorption isotherms for toluene in mesoporous polymer film FDU-16 as determined by the changes in the refractive index (λ = 632 nm) as a function of the adsorbate (toluene) relative pressure.

Figure 8 schematically shows the desorption/adsorption isotherms process in a vertical single cylindrical mesopore.[23] First, monolayer adsorption of the vapor happens on the pore wall (Figure 8A). After the completion of the monolayer formation, multilayer adsorption occurs automatically (Figure 8B). When the thickness of the adsorption layer on the pore wall reaches a critical value t at relative pressure ~0.2 point in Figure 7, capillary condensation happens in the core of the pore (from Figure 8C to 8D) in the range of relative pressure from 0.2 to 0.6 in Figure 7. The narrower the pore size distribution in the materials, the sharper pore condensation transition from Figure 8C to 8 D will be observed. During the pressure changes from 0.6 to 1, full adsorption of the solvent vapor in the pore has reached. When the partial pressure decreases from 1 to 0, however, desorption curve does not exactly follow the adsorption.

As can be seen from the isotherms in Figure 7, a hysteresis loop between adsorption and desorption is observed. Lower pressure is needed (~0.4) for pore evaporation to occur than full capillary condensation point in adsorption (~0.6), which is because the pore emptying happens from the center of the pore leading to smaller meniscus in desorption than condensation in adsorption as showed in Figure 6E. What is more, in the ink-bottle type of pores,[71] there is a "bottle-neck" effect during the desorption process.[61,72] When a pore is connecting with a smaller pore (or neck), the solvent will fill the big pore first and then the small pore. So the pressure needed for capillary condensation is based on the size of the big pore (higher pressure than smaller pore). However, during desorption process, pore evaporation first happens on the small pore as shown in Figure 9B. After the completion of emptying the small pore, the big pore starts to evaporate. So the pressure needed for pore evaporation is according to the size of the small pore, which means lower pressure is required. As a result of "bottle-neck" effect, pore evaporation is controlled by the connecting small pore, the "window size" of desorption. [67,73,74]

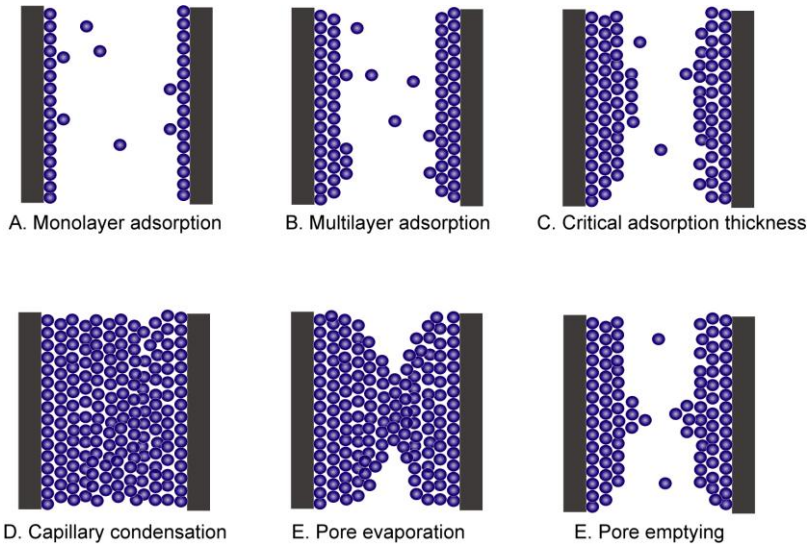

Figure 8 Adsorption/desorption process in a single cylindrical pore.[23]

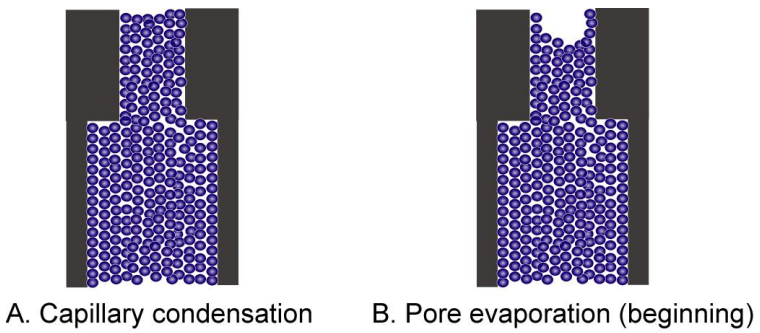

Figure 9 (A) Capillary condensation in ink-bottle pore; (B) the "bottle – neck" of desorption in ink-bottle pore.

In the calculation of pore size in the mesoporous think films, Kelvin equation is of great importance because it builds up the relationship between the size of a filled pore to the partial pressure and physical properties of an adsorbing gas.

$$ln\frac{P}{P_0} = -\frac{2\gamma V_m}{r_k RT} \quad (5)$$

Where P is the vapor pressure and P_0 is the saturated vapor pressure; r is the surface tension of the adsorbing species; γ is the surface tension of the adsorbing species; V_m is the adsorbate molar volume in the condensed state; r_k is the Kelvin radius; R is the gas constant, and T is temperature. Mesoporous radius is calculated as $r_p = r_k + t$, where r_k is the Kelvin radius and t is the thickness of the adsorbed layer of vapor in the pore before capillary condensation occurs[61], as shown in Figure 8C. The adsorbed layer thickness t is defined by the BET equation (equation 2) and obtained from the adsorption of nonporous sample with similar surface.[61,64] The pore size distribution can be calculated by Kelvin equation and BET equation, which is as shown in Figure 8. The peak position of the distribution curve stands for the most popular size of the pores. The narrower the pore size distribution, means the more uniform the size of the pores in the materials, the sharper the peak will be observed Figure 8.[62]

$$t = \frac{d_0 CK \cdot (P/P_0)}{\left[1 - K\left(\frac{P}{P_0}\right)\right] \cdot [1 + K(C-1)(P/P_0)]} \quad (6)$$

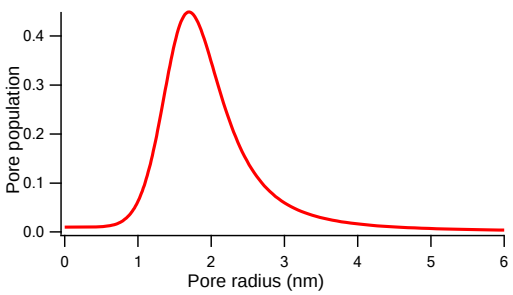

Figure 10 Calculated pore size distribution of FDU16-350 film based upon the desorption branch of the isotherms.

1.6 Morphology characteristics of mesoporous materials

1.6.1 TEM characterization

Because of limited image resolution in light microscopes as imposed by the wavelength of visible light, TEMs were developed. Transmission electron microscopy provides a way to look at the microstructures of solid at atomic level, generating signals telling us about the sample chemistry and crystallography.[75]

The major limitation of TEM is the requirements for the preparation of specimens to be imaged. In order to get good signal from TEM, the specimens have to be very thin, which means electron transparent. It must be thin enough to transmit sufficient electrons so that enough intensity falls on the screen to obtain an interpretable image. For 100-KeV electrons, normally the thickness of the specimen should be below 100 nm for TEM and below 50nm for high-resolution TEM.[75] There are many ways to prepare specimens for TEM. Which method to choose is depending on the type of the material and the information one needs to obtain. But no matter which way one may choose to produce TEM sample, the preparation process should not alter the interested properties of the material. The ultimate objective of sample preparation is to obtain an electron transparent thin specimen which is also representative of the bulk materials one wants to study. For mesoporous thin films coated on Si substrate, cross-section specimens preparation method was usually used as schemed in Figure 11.

Figure 11-1 is a thin mesoporous carbon layer on Si substrate (yellow side is the film and dark side is Si wafer). In Figure 1.11-2, the Si substrate is cut into 4 stripes (~3mm width). In Figure 1.11-3, select two best film and glue them together face to face. Also glue other two stripes outside as support. In Figure 11-4, squeeze the glued pieces and bake them in oven at 90 ℃ for 30 min. In Figure 11-5, cut the glued film into small pieces with ~3mm width. Then polish both sides of the small piece of film to about 100μm in thickness (one side needs to be polished with fine sand paper to get mirror like surface) as shown in Figure 11-7. In Figure 11-8, use cloth wheel and then copper wheel to grind a very think spot in the center until yellow light can be seen from the light on the bottom (color would change from red to orange to yellow as the thickness decreasing in the center). In Figure 11-9, after glue the sample on a copper grid, use ion beam to hit the center thin area until a hole shows up. Under TEM, the edge of the hole along the glue line is the interested area (Figure 11-10).

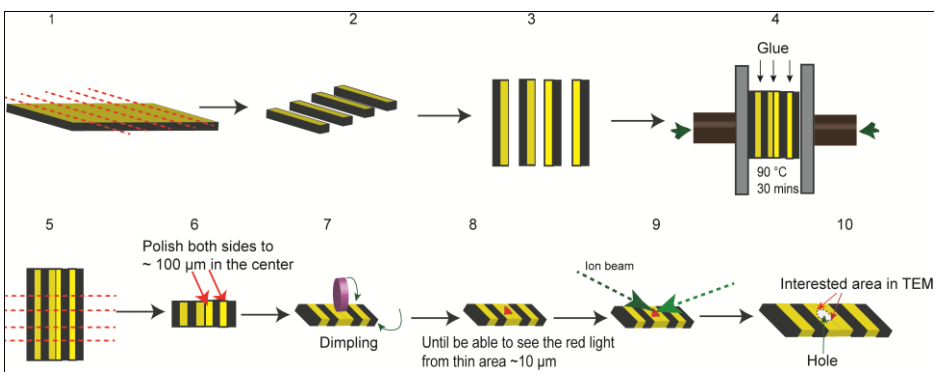

Figure 11 Cross section TEM sample preparation procedures.

TEM is the most direct and informative approach to directly show the morphology of mesoporous materials. However, one limitation is that only a very small area is observed under TEM and artifacts may appear in some circumstances, sometimes other techniques such as X-ray diffraction (XRD) are need in order to confirm the structure of the whole film.

1.6.2 X-ray diffraction determination of the ordered structure of polymer/carbon thin films

In 1912, the phenomenon of XRD by crystals was discovered and the confirmed wave nature of x-rays provided a new method for investigating the fine structure of matter.[76] Diffraction is due to existence of certain phase relations between two or more waves, can indirectly reveal details of internal structure. Actually, diffraction is a scattering phenomenon involving with a large number of atoms. For crystals, the atoms are arranged periodically on a lattice, the scattered rays by them have definite phase relations between them. As a result, destructive interference occurs in most directions of scattering, but in a few directions constructive interference takes place and diffraction beams are formed.[76] The essential condition that must be met for diffraction to occur can be described in Bragg's law.

$$n\lambda = 2d\ sin\theta \quad (7)$$

In the equation, n is called the order of diffraction; λ is the wavelength of incident x-rays; d is spacing distance; θ is Bragg angle measured between the incident beam and the considered particular crystal planes.

Experimentally, by using Bragg's law, the spacing d of different planes can be determined by applying a known wavelength and measuring θ in the meantime. The important features are shown in Figure 12. The incident x-ray can be set to any desired angle to sample by rotating the sample. Normally, the x-ray tube is fixed, and the detector rotates 2 θ if the sample rotate θ angle in order to measure the intensity of the diffracted x-rays.

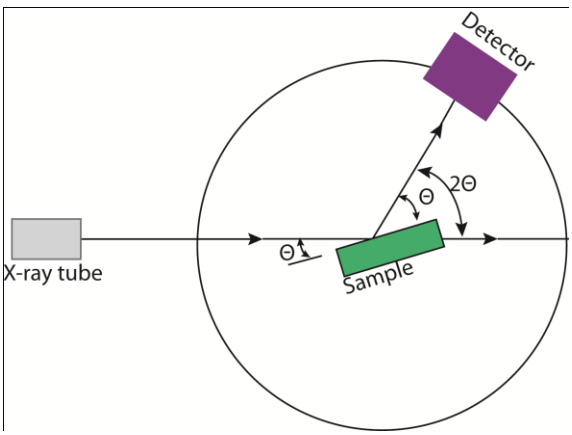

Figure 12 Schematic of x-ray spectrometer.

Although ordered mesoporous materials are not crystalline, they still diffract because of periodic voids in the amorphous framework or periodic contrasts in the electron density corresponding to surfactant regions. Therefore, x-ray diffraction also can be used to determine the mesophase structure such as the ordering of the pores and pore to pore distance.[77,78] Actually, x-ray diffraction is one of the first techniques used to characterize these micelles – templated structures. If the pores are uniformed distributed through the film, a sharp resolved diffraction peak can be observed as in Figure 13a. The position of the peak depends on the d-spacing of the pore planes, and larger d-spacing

leads to smaller diffraction angle (Figure 13b). In the case of the pore arrangement is not so well ordered, the diffraction peak would become broad with low intensity (Figure 13c). No diffraction peak will be observed if the pores are completely disordered.

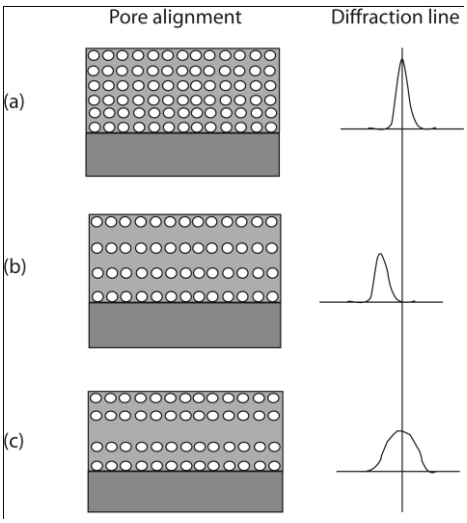

Figure 13 Effect of uniform and non-uniform distributed pores on diffraction peak position and width. (a) Highly ordered mesopores with uniform d-spacing, (b) Ordered mesoporous with uniform large d-spacing, (c) Not so well ordered mesostructure with non-uniform d-spacing.[76]

However, mesoporous films that are oriented perpendicular to the substrate (co-exist) do not contribute to the observed diffraction because the diffraction from other channel orientations is not collected by the detector.[78] Also, certain peaks will be absent if the film has some domains where the channels are parallel to the substrate surface.[78] Alternatively, other diffraction techniques may be used to determine the channel orientation such as

orientation imaging microscopy.[79] small-angle X-ray scattering,[80] 2D X-ray scattering,[77] grazing angle of incidence small-angle X-ray scattering.[19,81-83]

1.7 Electrochemical properties

Electrochemistry is a branch of chemistry focusing on the interrelation of electrical and chemical effects, in which most of the field deals with the study of chemical changes caused by the passage of an electric current and electrical energy produced by chemical reactions.[84] From electrochemical measurements, people may want to obtain thermodynamic data about a reaction, or they are interested in generating an unstable intermediate and study its rate of decay, or they are seeking to analyze a solution for trace amounts of metal ions or other pieces. Electrochemical properties of the systems are of primary interest if they want to design a new electrode for battery, a glucose sensor or a new power source.

Batteries, fuel cells and electrochemical capacitors are popular electrochemical energy storage and conversion systems. Despite of their different energy storage differences, they all have "electrochemical similarities" as the systems are composed of two electrodes in contact with an electrolyte solution.[85] However, batteries are normally closed systems with electrical energy generated by conversion of chemical energy through redox reactions at the anode and cathode, while fuel cells are open systems with continuous supply of fuel gas. In electrochemical capacitors, energy is delivered though the formation and release of the electrical double layers, which is caused by the movement of electrons when alter the orientation of electrolyte ions at the

electrolyte/electrolyte interface.[85] Electrochemical capacitors are also known as supercapacitors or ultracapacitors because of their ability to store and deliver energy at high rates.[86] Based on the electrode materials used and the charge storage mechanisms, electrochemical supercapacitors are generally classified into two types: (a) electrochemical double layer capacitors (EDLCs) composed of solid electrolytes and carbon,[50] and (b) redox supercapacitors with insertion of transition metal oxides such as RuO_2, MnO_2, V_2O_5, NiO and CoO.[10,87-91]

EDLCs store energy by means of charge separation, which is about the same way as traditional capacitor. However, compared to traditional capacitors of most of batteries, EDLCs store substantially more energy because of the small distance in the electrical double layer where the charge separation takes place and a large amount of ions can be stored in high surface area.[92] The adsorption process of ions from electrolyte onto the surface of materials is reversible and electrochemically stable, and the double layer capacitance C is described by Helmholtz in the formula:[93]

$$C = \frac{\varepsilon_r \varepsilon_0 A}{d} \quad (8)$$

where ε_r is the electrolyte dielectric constant, ε_0 is the dielectric constant of the vacuum, d is the effective thickness of the double layer and A is the electrode surface area. Since there is no faradic (redox) reaction at EDLC electrodes as a result of the electrostatic charge storage, swelling in the active material can be avoid so that the electrodes can survive millions of

cycles.[93] Only the surface accessible to electrolyte ions contributes to charge storage, which allows very fast energy uptake and delivery due to the surface storage mechanism.[93,94]

In contrast, for pseudo-capacitors, most of the charge is transferred at the surface of the solid electrode and Faradaic reactions are involved in the interaction between solid material and the electrolyte.[94,95] In this case, charges accumulated in the capacitor are voltage-dependent and accordingly the pseudo-capacitance is strongly related to voltage:

$$C = \frac{dQ}{dV} \tag{9}$$

where C is the capacitance of the pseudo-capacitor, Q is the quantity of charge and V is the potential. The specific capacitance of pseudo-capacitors is typically much higher than that of EDLCs, but pseudo-capacitors often suffer from low power density and lack of stability during cycling because redox reactions are used.

Hybrid capacitors are referred to ultracapacitors that are fabricated with one double layer material electrode (power source) and one pseudo-capacitor materials (energy source) electrode.[93,95] Hybrid capacitors offer an alternative to pseudo-capacitors or EDLCs by combining them together to improve the properties in both energy and powder densities. Currently, people have developed two types of hybrid systems: pseudo-capacitive metal oxides with capacitive carbon electrode and lithium-insertion electrodes with capacitive electrode.[93] Recently, mesoporous materials have drawn much

attention in the development of electrochemical supercapacitors for high power applications. For high surface area mesoporous carbon materials, the double layer formation at the electrode-electrolyte interface provides high capacitance.[90,96,97] The combination of mesoporous carbon and transition metal has become more and more popular, and high capacitance with high stability has been achieved through this type of hybrid capacitors.[10,87,98-101] Mesoporous electrode material not only increase the amount of electrolyte adsorbed into the electrode, but also blocks undesired heavy anions enter into the electrode obstructing the actual charge exchange process.[90]

1.8 Applications

Mesoporous materials have extensive applications because they possess a unique set of properties that the bulk correspondent materials do not have such as high specific area, fluid permeability and molecular sieving and shape-selective effects. For example, properties like high adsorption capacity, high selectivity, favorable adsorption kinetics, excellent mechanical properties, good stability and durability are determining mesoporous materials have excellent performance as good adsorbent.

1.8.1 Mesoporous carbon-based electrode materials for supercapacitors

Although lithium ion batteries are attractive as the most promising candidates with high energy density, the power density is generally low because of their poor electronic conductivity and low diffusion rate.[102-104] In order to achieve a high rate capability of lithium batteries, it is necessary to improve ionic and electronic diffusion.[103] In this circumstance, mesoporous

materials are quite useful as hosts for Li intercalation because their high surface area can provide large space to accommodate ions, thin walls can shorten the Li diffusion distance in the solid phase and pores can facilitate the penetration of liquid electrolyte ions into the electrode material, which make major contribution to the low conductivity and diffusion rate issues.[102] As electrode materials, carbon materials have already attracted numerous interests for the applications of electrochemical capacitors due to their electrical conductivity, chemical stability and low cost.[94] Mesoporous carbon materials possessing unique electrical properties and well controlled pore sizes and structures would facilitate fast ion and electron transportation, which would further improve the conductivity and diffusion problems.

Extensive previous work has proven that mesoporous carbon materials have great potential as electrode candidate for supercapacitors.[105-111] For example, an ordered mesoporous carbon with large pore size of 6.7 nm prepared by organic-inorganic-surfactant tri-constituent co-assembly route exhibited 112 F g^{-1} specific capacitance and good cycling ability over 50 cycles.[99] Mesoporous carbon microspheres prepared by hydrothermal emulsion-activated approach with diameters 0.5-2.0 μm and pore size of 2.6 - 4.0 nm showed 157 F g^{-1} specific capacitance and current density 10Ag^{-1} in 6M KOH solution.[112] Also, a highly ordered three-dimensional cubic mesoporous carbon CMK-8 synthesized by nanocasting method displayed 246 F g^{-1} specific capacitance.[113]

Further enhancement in capacitance of mesoporous carbon as electrode can be obtained through introducing of metal oxide to the mesoporous channels based on pseudocapacitance for charge-store.[114] Transition oxides such as nickel oxides,[115] cobalt oxides,[116] vanadium oxides,[10] $RuO_{2,}$[111] $SnO_{2,}$[117] iron oxides,[118] copper oxides,[119] Zirconium dioxide,[120] manganese oxides[121-124] have been extensively investigated as electrode materials for supercapacitors. A Mn_3O_4 worm-like mesoporous carbon[121] prepared through microwave method showed enhanced specific capacitance of 266 F/g. The specific capacitance of the same worm-like structure mesoporous carbon@Bi(2)O(3) by the same synthesis method reached up to 386 F/g, which is three times higher than pure worm-like mesoporous carbon.[122] Thus, the combination of transition metal oxides and mesoporous carbon has great potential as supercapacitors.

1.8.2 Mesoporous carbon-based environmental separation adsorbents

Water pollution has been always the leading issue of environment pollution. Numerous treatment methods have been investigated in order to remove the contaminants and recycle water. Among all the approaches, adsorption-based process is one of the most efficient routes to control the pollution problem. With high surface area, regular and tunable pore sizes and large pore volumes, mesoporous materials are highly efficient adsorbents.[125] Recently, various functional mesoporous adsorbents have been reported to efficiently adsorb all kinds of pollutants from water.[126-137] For adsorbing metal ions from water, a SBA-15 molecular sieve was synthesized via hydrothermal

method adsorbed 98.49% Pb(2+) from water.[127] Significantly, based on mesoporous crystalline materials-41, silica sorbents were functionalized to selectively extract mercury (II) ions from water contaminated with a wide range of heavy metal ions.[129] Also, mesoporous materials are widely investigated as adsorbents to remove organic pollutant from water. For example, Hu and coworkers[132] studied the adsorption kinetics and equilibrium of three commercial anionic dyes (orange II, reactive red and acid black 1) by ordered mesoporous carbon CMK-3. Comparing with commercial activated carbon, CMK-3 showed much higher uptake rate and adsorption capacity of these three dyes. As reported by Bui.,[128] after organically functionalized mesoporous SBA is capable of selectively removing pharmaceuticals from water.

Recently, increasing attention is in magnetically separable adsorbents by incorporating magnetic metals into mesoporous carbon materials. In this case, the most popular metal is Fe due to strong magnetization property and low cost.[138-140] Other transitional magnetic metals are also extensively studied, such as Ni,[1] Ag[141] and Co.[142] Through proper fabrication, mesoporous materials can serve as excellent adsorbents to as an efficient way to control the contamination of water.

1.8.3 Mesoporous carbon-based electrode materials for biosensors

The first report of electrochemical biosensing is in 1962 by Clark and Lyons[143], who designed the first glucose enzyme electrode using enzyme glucose oxidase to detect glucose in blood plasma. Since then, the research on

enzyme based glucose sensors has been widely conducted. Electrochemical measurements are based on the monitoring of oxygen consumed on cathode

$$glucose + O_2 \xrightarrow{glucose\ oxidase} gluconic\ acid + H_2O_2 \quad (10)$$

$$O_2 + 4H^+ + 4e^- \rightarrow 2\,H_2O_2 \quad (11)$$

or amperometric (anodic) monitoring of the hydrogen peroxide [144]

$$H_2O_2 \rightarrow O_2 + 2H^+ + 2e^- \quad (12)$$

In 1973, Guilbault and Lubrano firstly reported the direct amperometric measurement of hydrogen peroxide produced to determine glucose with using an enzyme electrode.[145] After that, amperometric enzyme electrodes have been extensively studied with different electrodes materials or immobilization approach, because it provides rapid, reliable, simple and economical approach to determine glucose in biological fluids.

Ordered mesoporous carbon possesses uniform pore structure, high specific surface area, chemical inertness and biocompatibility, which make it a good candidate for electrode materials in electrochemical sensors.[8,146,147] As a matter of fact, ordered mesoporous carbon has already been extensively utilized in the electrode materials for glucose sensors.[147-150] With high current signal resulted from high surface area and adjustable pore size, mesoporous carbons allow the simple disposable screen printed electrodes exhibit both high sensitivity and selectivity even without using membrane.[148] In order to detect very low concentration neurotransmitters (such as norepinephrine) in blood plasma, the surface area of mesoporous carbons can be further increased

by adding inorganic Si compound in to the synthesis precursor and remove it afterwards, resulting in increased current signal.

As modern electroanalytical chemistry is more and more relied on electrode material, with possessing so many admirable properties such as high surface area, well defined pore size, mechanical and thermal stability, electrical conductivity, as well as adjustable framework, ordered mesoporous carbons might be the future electrode material for biosensors.

1.9 References

1. Huang, C.-h.; Doong, R.-a.; Gu, D.; Zhao, D., Dual-template synthesis of magnetically-separable hierarchically-ordered porous carbons by catalytic graphitization. *Carbon* **2011**, *49*, 3055-3064.

2. Park, I.-S.; Choi, M.; Kim, T.-W.; Ryoo, R., Synthesis of magnetically separable ordered mesoporous carbons using furfuryl alcohol and cobalt nitrate in a silica template. *Journal of Materials Chemistry* **2006**, *16*, 3409-3416.

3. Vinu, A.; Streb, C.; Murugesan, V.; Hartmann, M., Adsorption of cytochrome c on new mesoporous carbon molecular sieves. *The Journal of Physical Chemistry B* **2003**, *107*, 8297-8299.

4. Gierszal, K. P.; Kim, T.-W.; Ryoo, R.; Jaroniec, M., Adsorption and structural properties of ordered mesoporous carbons synthesized by using various carbon precursors and ordered siliceous p6mm and ia3̄d mesostructures as templates. *The Journal of Physical Chemistry B* **2005**, *109*, 23263-23268.

5. Darmstadt, H.; Roy, C.; Kaliaguine, S.; Kim, T.-W.; Ryoo, R., Surface and pore structures of cmk-5 ordered mesoporous carbons by adsorption and surface spectroscopy. *Chemistry of Materials* **2003**, *15*, 3300-3307.

6. Zheng, D.; Ye, J.; Zhou, L.; Zhang, Y.; Yu, C., Simultaneous determination of dopamine, ascorbic acid and uric acid on ordered mesoporous carbon/nafion composite film. *Journal of Electroanalytical Chemistry* **2009**, *625*, 82-87.

7. Zhou, M.; Shang, L.; Li, B.; Huang, L.; Dong, S., Highly ordered mesoporous carbons as electrode material for the construction of electrochemical dehydrogenase- and oxidase-based biosensors. *Biosensors and Bioelectronics* **2008**, *24*, 442-447.

8. Zhou, M.; Shang, L.; Li, B.; Huang, L.; Dong, S., The characteristics of highly ordered mesoporous carbons as electrode material for electrochemical sensing as compared with carbon nanotubes. *Electrochemistry Communications* **2008**, *10*, 859-863.

9. Bo, X.; Bai, J.; Wang, L.; Guo, L., In situ growth of copper sulfide nanoparticles on ordered mesoporous carbon and their application as nonenzymatic amperometric sensor of hydrogen peroxide. *Talanta* **2010**, *81*, 339-345.

10. Dai, M.; Song, L.; LaBelle, J. T.; Vogt, B. D., Ordered mesoporous carbon composite films containing cobalt oxide and vanadia for electrochemical applications. *Chemistry of Materials* **2011**, *23*, 2869-2878.

11. Jia, N.; Wang, Z.; Yang, G.; Shen, H.; Zhu, L., Electrochemical properties of ordered mesoporous carbon and its electroanalytical application for selective determination of dopamine. *Electrochemistry Communications* **2007**, *9*, 233-238.

12. Ryoo, R.; Joo, S. H.; Kruk, M.; Jaroniec, M., Ordered mesoporous carbons. *Advanced Materials* **2001**, *13*, 677-681.

13. Zhou, M.; Guo, L.-p.; Lin, F.-y.; Liu, H.-x., Electrochemistry and electrocatalysis of polyoxometalate-ordered mesoporous carbon modified electrode. *Analytica Chimica Acta* **2007**, *587*, 124-131.

14. Zhou, M.; Ding, J.; Guo, L.-p.; Shang, Q.-k., Electrochemical behavior of l-cysteine and its detection at ordered mesoporous carbon-modified glassy carbon electrode. *Analytical Chemistry* **2007**, *79*, 5328-5335.

15. Levario, T. J.; Dai, M.; Yuan, W.; Vogt, B. D.; Nielsen, D. R., Rapid adsorption of alcohol biofuels by high surface area mesoporous carbons. *Microporous and Mesoporous Materials* **2012**, *148*, 107-114.

16. Ding, J.; Chan, K.-Y.; Ren, J.; Xiao, F.-s., Platinum and platinum–ruthenium nanoparticles supported on ordered mesoporous carbon and their electrocatalytic performance for fuel cell reactions. *Electrochimica Acta* **2005**, *50*, 3131-3141.

17. Joo, S. H.; Pak, C.; You, D. J.; Lee, S.-A.; Lee, H. I.; Kim, J. M.; Chang, H.; Seung, D., Ordered mesoporous carbons (omc) as supports of electrocatalysts for direct methanol fuel cells (dmfc): Effect of carbon precursors of omc on dmfc performances. *Electrochimica Acta* **2006**, *52*, 1618-1626.

18. Calvillo, L.; Lázaro, M. J.; García-Bordejé, E.; Moliner, R.; Cabot, P. L.; Esparbé, I.; Pastor, E.; Quintana, J. J., Platinum supported on functionalized ordered mesoporous carbon as electrocatalyst for direct methanol fuel cells. *Journal of Power Sources* **2007**, *169*, 59-64.

19. Tate, M. P.; Urade, V. N.; Kowalski, J. D.; Wei, T.-c.; Hamilton, B. D.; Eggiman, B. W.; Hillhouse, H. W., Simulation and interpretation of 2d diffraction patterns from self-assembled nanostructured films at arbitrary angles of incidence: From grazing incidence (above the critical angle) to transmission perpendicular to the substrate. *The Journal of Physical Chemistry B* **2006**, *110*, 9882-9892.

20. Meng, Y.; Gu, D.; Zhang, F.; Shi, Y.; Yang, H.; Li, Z.; Yu, C.; Tu, B.; Zhao, D., Ordered mesoporous polymers and homologous carbon frameworks: Amphiphilic surfactant templating and direct transformation. *Angewandte Chemie* **2005**, *117*, 7215-7221.

21. Hillmyer, M.; Abetz, V., Ed.; Springer Berlin / Heidelberg: 2005; Vol. 190, p 137-181.

22. Meng, Y.; Gu, D.; Zhang, F.; Shi, Y.; Cheng, L.; Feng, D.; Wu, Z.; Chen, Z.; Wan, Y.; Stein, A.; Zhao, D., A family of highly ordered mesoporous polymer resin and carbon structures from organic−organic self-assembly. *Chemistry of Materials* **2006**, *18*, 4447-4464.

23. Lu, G. Q.; Zhao, X. S. *Nanoporous materials science and engineering*; Imperial College Press, 2004; Vol. 4.

24. Beck, J. S.; Vartuli, J. C.; Roth, W. J.; Leonowicz, M. E.; Kresge, C. T.; Schmitt, K. D.; Chu, C. T. W.; Olson, D. H.; Sheppard, E. W., A new family of mesoporous molecular sieves prepared with liquid crystal templates. *Journal of the American Chemical Society* **1992**, *114*, 10834-10843.

25. Kresge, C. T.; Leonowicz, M. E.; Roth, W. J.; Vartuli, J. C.; Beck, J. S., Ordered mesoporous molecular sieves synthesized by a liquid-crystal template mechanism. *Nature* **1992**, *359*, 710-712.

26. *The chemistry of nanostructured materials*; Yang, P., Ed.; World Scientific Publishing Co. Pte. Ltd, 2003.

27. Firouzi, A.; Kumar, D.; Bull, L.; Besier, T.; Sieger, P.; Huo, Q.; Walker, S.; Zasadzinski, J.; Glinka, C.; Nicol, J.; et, a., Cooperative organization of inorganic-surfactant and biomimetic assemblies. *Science* **1995**, *267*, 1138-1143.

28. Huo, Q.; Margolese, D. I.; Ciesla, U.; Feng, P.; Gier, T. E.; Sieger, P.; Leon, R.; Petroff, P. M.; Schuth, F.; Stucky, G. D., Generalized synthesis of periodic surfactant/inorganic composite materials. *Nature* **1994**, *368*, 317-321.

29. Firouzi, A.; Atef, F.; Oertli, A. G.; Stucky, G. D.; Chmelka, B. F., Alkaline lyotropic silicate−surfactant liquid crystals. *Journal of the American Chemical Society* **1997**, *119*, 3596-3610.

30. Tanev, P. T.; Pinnavaia, T. J., A neutral templating route to mesoporous molecular-sieves. *Science* **1995**, *267*, 865-867.

31. Bagshaw, S. A.; Prouzet, E.; Pinnavaia, T. J., Templating of mesoporous molecular-sieves by nonionic polyethylene oxide surfactants. *Science* **1995**, *269*, 1242-1244.

32. Tanev, P. T.; Pinnavaia, T. J., Mesoporous silica molecular sieves prepared by ionic and neutral surfactant templating: A comparison of physical properties. *Chemistry of Materials* **1996**, *8*, 2068-2079.

33. Zentner, G. M.; Rathi, R.; Shih, C.; McRea, J. C.; Seo, M.-H.; Oh, H.; Rhee, B. G.; Mestecky, J.; Moldoveanu, Z.; Morgan, M.; Weitman, S., Biodegradable block copolymers for delivery of proteins and water-insoluble drugs. *Journal of Controlled Release* **2001**, *72*, 203-215.

34. Booth, C.; Attwood, D., Effects of block architecture and composition on the association properties of poly(oxyalkylene) copolymers in aqueous solution. *Macromolecular Rapid Communications* **2000**, *21*, 501-527.

35. Leibler, L., Theory of microphase separation in block copolymers. *Macromolecules* **1980**, *13*, 1602-1617.

36. Lodge, T. P.; Pudil, B.; Hanley, K. J., The full phase behavior for block copolymers in solvents of varying selectivity. *Macromolecules* **2002**, *35*, 4707-4717.

37. Zhao, D. Y.; Feng, J. L.; Huo, Q. S.; Melosh, N.; Fredrickson, G. H.; Chmelka, B. F.; Stucky, G. D., Triblock copolymer syntheses of mesoporous silica with periodic 50 to 300 angstrom pores. *Science* **1998**, *279*, 548-552.

38. Zhao, D.; Huo, Q.; Feng, J.; Chmelka, B. F.; Stucky, G. D., Nonionic triblock and star diblock copolymer and oligomeric surfactant syntheses of highly ordered, hydrothermally stable, mesoporous silica structures. *Journal of the American Chemical Society* **1998**, *120*, 6024-6036.

39. Komarneni, S.; Smith, D. M.; Beck, J. S. *Advances in porous materials*; Materials Research Society, 1994; Vol. 371.

40. Yang, P.; Zhao, D.; Margolese, D. I.; Chmelka, B. F.; Stucky, G. D., Generalized syntheses of large-pore mesoporous metal oxides with semicrystalline frameworks. *Nature* **1998**, *396*, 152-155.

41. Tian, B.; Liu, X.; Tu, B.; Yu, C.; Fan, J.; Wang, L.; Xie, S.; Stucky, G. D.; Zhao, D., Self-adjusted synthesis of ordered stable mesoporous minerals by acid-base pairs. *Nat Mater* **2003**, *2*, 159-163.

42. Braun, P. V.; Osenar, P.; Tohver, V.; Kennedy, S. B.; Stupp, S. I., Nanostructure templating in inorganic solids with organic lyotropic liquid crystals. *Journal of the American Chemical Society* **1999**, *121*, 7302-7309.

43. Frackowiak, E.; Béguin, F., Carbon materials for the electrochemical storage of energy in capacitors. *Carbon* **2001**, *39*, 937-950.

44. Planeix, J. M.; Coustel, N.; Coq, B.; Brotons, V.; Kumbhar, P. S.; Dutartre, R.; Geneste, P.; Bernier, P.; Ajayan, P. M., Application of carbon nanotubes as supports in heterogeneous catalysis. *Journal of the American Chemical Society* **1994**, *116*, 7935-7936.

45. Netzer, A.; Hughes, D. E., Adsorption of copper, lead and cobalt by activated carbon. *Water Research* **1984**, *18*, 927-933.

46. M, K., Removal of cr(vi) from aqueous solutions by adsorption onto hazelnut shell activated carbon: Kinetic and equilibrium studies. *Bioresource Technology* **2004**, *91*, 317-321.

47. Deck, C. P.; Vecchio, K., Prediction of carbon nanotube growth success by the analysis of carbon–catalyst binary phase diagrams. *Carbon* **2006**, *44*, 267-275.

48. Zouboulis, A. I.; Lazaridis, N. K.; Zamboulis, D., Powdered activated carbon separation from water by foam flotation. *Separation Science and Technology* **1994**, *29*, 385-400.

49. Zheng, M.; Jagota, A.; Semke, E. D.; Diner, B. A.; McLean, R. S.; Lustig, S. R.; Richardson, R. E.; Tassi, N. G., DNA-assisted dispersion and separation of carbon nanotubes. *Nat Mater* **2003**, *2*, 338-342.

50. Ishikawa, M.; Morita, M.; Ihara, M.; Matsuda, Y., Electric double-layer capacitor composed of activated carbon fiber cloth electrodes and solid polymer electrolytes containing alkylammonium salts. *Journal of The Electrochemical Society* **1994**, *141*, 1730-1734.

51. Liang, C.; Hong, K.; Guiochon, G. A.; Mays, J. W.; Dai, S., Synthesis of a large-scale highly ordered porous carbon film by self-assembly of block copolymers. *Angewandte Chemie International Edition* **2004**, *43*, 5785-5789.

52. Storck, S.; Bretinger, H.; Maier, W. F., Characterization of micro- and mesoporous solids by physisorption methods and pore-size analysis. *Applied Catalysis A: General* **1998**, *174*, 137-146.

53. Neimark, A. V.; Sing, K. S. W.; Thommes, M. In *Handbook of heterogeneous catalysis*; Wiley-VCH Verlag GmbH & Co. KGaA: 2008.

54. Brunauer, S.; Deming, L. S.; Deming, W. E.; Teller, E., On a theory of the van der waals adsorption of gases. *Journal of the American Chemical Society* **1940**, *62*, 1723-1732.

55. Lowel, S.; Shields, J. E. *Powder surface area and porosity*; Second ed.; Chapman and Hall, 1984.

56. Brunauer, S.; Emmett, P. H.; Teller, E., Adsorption of gases in multimolecular layers. *Journal of the American Chemical Society* **1938**, *60*, 309-319.

57. Harkins, W. D.; Jura, G., Surfaces of solids. Xiii. A vapor adsorption method for the determination of the area of a solid without the assumption of a molecular area, and the areas occupied by nitrogen and other molecules on the surface of a solid. *Journal of the American Chemical Society* **1944**, *66*, 1366-1373.

58. Anderson, R. B., Modifications of the brunauer, emmett and teller equation1. *Journal of the American Chemical Society* **1946**, *68*, 686-691.

59. Jerzy, H., Chapter 3.1 surface area and porosity. *Catalysis Today* **1994**, *20*, 11-16.

60. Boissiere, C.; Grosso, D.; Lepoutre, S.; Nicole, L.; Bruneau, A. B.; Sanchez, C., Porosity and mechanical properties of mesoporous thin films

assessed by environmental ellipsometric porosimetry. *Langmuir* **2005**, *21*, 12362-12371.

61. Baklanov, M. R.; Mogilnikov, K. P.; Polovinkin, V. G.; Dultsev, F. N., Determination of pore size distribution in thin films by ellipsometric porosimetry. *Journal of Vacuum Science & Technology B: Microelectronics and Nanometer Structures* **2000**, *18*, 1385-1391.

62. Baklanov, M. R.; Mogilnikov, K. P., Non-destructive characterisation of porous low-k dielectric films. *Microelectronic Engineering* **2002**, *64*, 335-349.

63. Dultsev, F. N.; Baklanov, M. R., Nondestructive determination of pore size distribution in thin films deposited on solid substrates. *Electrochemical and Solid-State Letters* **1999**, *2*, 192-194.

64. Li, X.; Vogt, B. D., Carbon dioxide mediated synthesis of mesoporous silica films: Tuning properties using pressure. *Chemistry of Materials* **2008**, *20*, 3229-3238.

65. Morishige, K.; Tateishi, N., Adsorption hysteresis in ink-bottle pore. *The Journal of Chemical Physics* **2003**, *119*, 2301-2306.

66. Branton, P. J.; Hall, P. G.; Sing, K. S. W.; Reichert, H.; Schuth, F.; Unger, K. K., Physisorption of argon, nitrogen and oxygen by mcm-41, a model mesoporous adsorbent. *Journal of the Chemical Society, Faraday Transactions* **1994**, *90*, 2965-2967.

67. Thommes, M.; Smarsly, B.; Groenewolt, M.; Ravikovitch, P. I.; Neimark, A. V., Adsorption hysteresis of nitrogen and argon in pore networks and characterization of novel micro- and mesoporous silicas. *Langmuir* **2005**, *22*, 756-764.

68. Dongyuan, Z.; Peidong, Y.; Nick, M.; Jianglin, F.; Bradley, F. C.; Galen, D. S., Continuous mesoporous silica films with highly ordered large pore structures. *Advanced Materials* **1998**, *10*, 1380-1385.

69. Yang, Z. X.; Xia, Y. D.; Mokaya, R., Zeolite zsm-5 with unique supermicropores synthesized using mesoporous carbon as a template. *Advanced Materials* **2004**, *16*, 727-732.

70. Machin, W. D., Temperature dependence of hysteresis and the pore size distributions of two mesoporous adsorbents. *Langmuir* **1994**, *10*, 1235-1240.

71. Moro, F.; Böhni, H., Ink-bottle effect in mercury intrusion porosimetry of cement-based materials. *Journal of Colloid and Interface Science* **2002**, *246*, 135-149.

72. Štěpánek, F.; Šoóš, M.; Rajniak, P., Characterisation of porous media by the virtual capillary condensation method. *Colloids and Surfaces A: Physicochemical and Engineering Aspects* **2007**, *300*, 11-20.

73. Han, Y.-J.; Watson, J. T.; Stucky, G. D.; Butler, A., Catalytic activity of mesoporous silicate-immobilized chloroperoxidase. *Journal of Molecular Catalysis B: Enzymatic* **2002**, *17*, 1-8.

74. Ravikovitch, P. I.; Neimark, A. V., Experimental confirmation of different mechanisms of evaporation from ink-bottle type pores: Equilibrium, pore blocking, and cavitation. *Langmuir* **2002**, *18*, 9830-9837.

75. *Transmission electron microscopy: A textbook for material science*; Williams, B. D.; Carter, B. C., Eds., 2008.

76. Cullity, B. D. *Elements of x-ray diffraction*; 3rd ed.; Upper saddle river, 2001.

77. Klotz, M.; Albouy, P.-A.; Ayral, A.; Ménager, C.; Grosso, D.; Van der Lee, A.; Cabuil, V.; Babonneau, F.; Guizard, C., The true structure of hexagonal mesophase-templated silica films as revealed by x-ray scattering: Effects of thermal treatments and of nanoparticle seeding. *Chemistry of Materials* **2000**, *12*, 1721-1728.

78. Hillhouse, H. W.; van Egmond, J. W.; Tsapatsis, M.; Hanson, J. C.; Larese, J. Z., The interpretation of x-ray diffraction data for the determination of channel orientation in mesoporous films. *Microporous and Mesoporous Materials* **2001**, *44–45*, 639-643.

79. Kacher, J.; Landon, C.; Adams, B. L.; Fullwood, D., Bragg's law diffraction simulations for electron backscatter diffraction analysis. *Ultramicroscopy* **2009**, *109*, 1148-1156.

80. Ruland, W.; Smarsly, B., Saxs of self-assembled oriented lamellar nanocomposite films: An advanced method of evaluation. *Journal of Applied Crystallography* **2004**, *37*, 575-584.

81. Urade, V. N.; Bollmann, L.; Kowalski, J. D.; Tate, M. P.; Hillhouse, H. W., Controlling interfacial curvature in nanoporous silica films formed by evaporation-induced self-assembly from nonionic surfactants. Ii. Effect of processing parameters on film structure. *Langmuir* **2007**, *23*, 4268-4278.

82. Tanaka, S.; Tate, M. P.; Nishiyama, N.; Ueyama, K.; Hillhouse, H. W., Structure of mesoporous silica thin films prepared by contacting peo106−ppo70−peo106 films with vaporized teos. *Chemistry of Materials* **2006**, *18*, 5461-5466.

83. Hillhouse, H. W.; van Egmond, J. W.; Tsapatsis, M., Highly oriented mesostructured thin films: Shear-induced deposition of optically anisotropic coatings of tungsten oxide/surfactant composites. *Langmuir* **1999**, *15*, 4544-4550.

84. *Electrochemical methods fundamentals and application*; Second edition ed.; Bard, A. J.; Faulkner, L. R., Eds.; John Wiley & Sons. Inc., 1944.

85. Winter, M.; Brodd, R. J., What are batteries, fuel cells, and supercapacitors? *Chemical Reviews* **2004**, *104*, 4245-4270.

86. Miller, J. R.; Simon, P., Electrochemical capacitors for energy management. *Science* **2008**, *321*, 651-652.

87. Xu, B.; Wu, F.; Chen, R.; Cao, G.; Chen, S.; Zhou, Z.; Yang, Y., Highly mesoporous and high surface area carbon: A high capacitance electrode material for edlcs with various electrolytes. *Electrochemistry Communications* **2008**, *10*, 795-797.

88. Cao, L.; Lu, M.; Li, H.-L., Preparation of mesoporous nanocrystalline co[sub 3]o[sub 4] and its applicability of porosity to the formation of electrochemical capacitance. *Journal of The Electrochemical Society* **2005**, *152*, A871-A875.

89. Mao-Wen, X.; Dan-Dan, Z.; Shu-Juan, B.; Hu-Lin, L., Mesoporous amorphous mno₂ as electrode material for supercapacitor. *Journal of Solid State Electrochemistry* **2007**, *11*, 1101-1107.

90. Subramanian, V.; Hall, S. C.; Smith, P. H.; Rambabu, B., Mesoporous anhydrous ruo2 as a supercapacitor electrode material. *Solid State Ionics* **2004**, *175*, 511-515.

91. Yuan, C.-Z.; Gao, B.; Zhang, X.-G., Electrochemical capacitance of nio/ru0.35v0.65o2 asymmetric electrochemical capacitor. *Journal of Power Sources* **2007**, *173*, 606-612.

92. Pandolfo, A. G.; Hollenkamp, A. F., Carbon properties and their role in supercapacitors. *Journal of Power Sources* **2006**, *157*, 11-27.

93. Simon, P.; Gogotsi, Y., Materials for electrochemical capacitors. *Nat Mater* **2008**, *7*, 845-854.

94. Zhai, Y.; Dou, Y.; Zhao, D.; Fulvio, P. F.; Mayes, R. T.; Dai, S., Carbon materials for chemical capacitive energy storage. *Advanced Materials* **2011**, *23*, 4828-4850.

95. Andrew, B., Ultracapacitors: Why, how, and where is the technology. *Journal of Power Sources* **2000**, *91*, 37-50.

96. Li, L.; Song, H.; Chen, X., Pore characteristics and electrochemical performance of ordered mesoporous carbons for electric double-layer capacitors. *Electrochimica Acta* **2006**, *51*, 5715-5720.

97. Korenblit, Y.; Rose, M.; Kockrick, E.; Borchardt, L.; Kvit, A.; Kaskel, S.; Yushin, G., High-rate electrochemical capacitors based on ordered mesoporous silicon carbide-derived carbon. *ACS Nano* **2010**, *4*, 1337-1344.

98. Zhou, H.; Zhu, S.; Hibino, M.; Honma, I., Electrochemical capacitance of self-ordered mesoporous carbon. *Journal of Power Sources* **2003**, *122*, 219-223.

99. Li, H.-Q.; Liu, R.-L.; Zhao, D.-Y.; Xia, Y.-Y., Electrochemical properties of an ordered mesoporous carbon prepared by direct tri-constituent co-assembly. *Carbon* **2007**, *45*, 2628-2635.

100. Xing, W.; Qiao, S. Z.; Ding, R. G.; Li, F.; Lu, G. Q.; Yan, Z. F.; Cheng, H. M., Superior electric double layer capacitors using ordered mesoporous carbons. *Carbon* **2006**, *44*, 216-224.

101. Huwe, H.; Fröba, M., Synthesis and characterization of transition metal and metal oxide nanoparticles inside mesoporous carbon cmk-3. *Carbon* **2007**, *45*, 304-314.

102. Moriguchi, I.; Hidaka, R.; Yamada, H.; Kudo, T.; Murakami, H.; Nakashima, N., A mesoporous nanocomposite of tio2 and carbon nanotubes as a high-rate li-intercalation electrode material. *Advanced Materials* **2006**, *18*, 69-73.

103. Guo, Y. G.; Hu, Y. S.; Sigle, W.; Maier, J., Superior electrode performance of nanostructured mesoporous tio2 (anatase) through efficient hierarchical mixed conducting networks. *Advanced Materials* **2007**, *19*, 2087-2091.

104. Zhu, S.; Zhou, H.; Miyoshi, T.; Hibino, M.; Honma, I.; Ichihara, M., Self-assembly of the mesoporous electrode material li3fe2(po4)3 using a cationic surfactant as the template. *Advanced Materials* **2004**, *16*, 2012-2017.

105. Prabaharan, S. R. S.; Vimala, R.; Zainal, Z., Nanostructured mesoporous carbon as electrodes for supercapacitors. *Journal of Power Sources* **2006**, *161*, 730-736.

106. Huang, J.; Sumpter, B. G.; Meunier, V., A universal model for nanoporous carbon supercapacitors applicable to diverse pore regimes, carbon materials, and electrolytes. *Chemistry – A European Journal* **2008**, *14*, 6614-6626.

107. Liang, C.; Dai, S., Synthesis of mesoporous carbon materials via enhanced hydrogen-bonding interaction. *Journal of the American Chemical Society* **2006**, *128*, 5316-5317.

108. Li, H.-Q.; Luo, J.-Y.; Zhou, X.-F.; Yu, C.-Z.; Xia, Y.-Y., An ordered mesoporous carbon with short pore length and its electrochemical performances in supercapacitor applications. *Journal of The Electrochemical Society* **2007**, *154*, A731-A736.

109. Taberna, P. L.; Simon, P.; Fauvarque, J. F., Electrochemical characteristics and impedance spectroscopy studies of carbon-carbon supercapacitors. *Journal of The Electrochemical Society* **2003**, *150*, A292-A300.

110. Wang, K.; Wang, Y.; Wang, Y.; Hosono, E.; Zhou, H., Mesoporous carbon nanofibers for supercapacitor application. *The Journal of Physical Chemistry C* **2008**, *113*, 1093-1097.

111. Li, H.; Wang, R.; Cao, R., Physical and electrochemical characterization of hydrous ruthenium oxide/ordered mesoporous carbon composites as supercapacitor. *Microporous and Mesoporous Materials* **2008**, *111*, 32-38.

112. Xiong, W.; Liu, M.; Gan, L.; Lv, Y.; Li, Y.; Yang, L.; Xu, Z.; Hao, Z.; Liu, H.; Chen, L., A novel synthesis of mesoporous carbon microspheres for supercapacitor electrodes. *Journal of Power Sources* **2011**, *196*, 10461-10464.

113. Lang, J.-W.; Yan, X.-B.; Yuan, X.-Y.; Yang, J.; Xue, Q.-J., Study on the electrochemical properties of cubic ordered mesoporous carbon for supercapacitors. *Journal of Power Sources* **2011**, *196*, 10472-10478.

114. Liu, P.; Tang, B.; Zhao, J.; Feng, J.; Xu, J., Ordered mesoporous carbon/sno₂ composites as the electrode material for supercapacitors. *Journal of Wuhan University of Technology--Materials Science Edition* **2011**, *26*, 407-411.

115. Gnanakan, S. R. P.; Karthikeyan, K.; Amaresh, S.; Cho, S. J.; Park, G. J.; Lee, Y. S., New application and electrochemical characterization of a nickel-doped mesoporous carbon for supercapacitors. *Journal of Alloys and Compounds* **2011**, *509*, 9858-9864.

116. Lang, J. W.; Yan, X. B.; Xue, Q. J., Facile preparation and electrochemical characterization of cobalt oxide/multi-walled carbon nanotube composites for supercapacitors. *Journal of Power Sources* **2011**, *196*, 7841-7846.

117. Liu, P.; Tang, B. J.; Zhao, J. C.; Feng, J. C.; Xu, J. L., Ordered mesoporous carbon/sno(2) composites as the electrode material for supercapacitors. *Journal of Wuhan University of Technology-Materials Science Edition* **2011**, *26*, 407-411.

118. Nagao, M.; Otani, M.; Tomita, H.; Kanzaki, S.; Yamada, A.; Kanno, R., New three-dimensional electrode structure for the lithium battery: Nano-sized gamma-fe(2)o(3) in a mesoporous carbon matrix. *Journal of Power Sources* **2011**, *196*, 4741-4746.

119. Yang, M.; Gao, Q. M., Copper oxide and ordered mesoporous carbon composite with high performance using as anode material for lithium-ion battery. *Microporous and Mesoporous Materials* **2011**, *143*, 230-235.

120. Chen, Y.; Lunsford, S. K.; Song, Y.; Ju, H.; Falaras, P.; Likodimos, V.; Kontos, A. G.; Dionysiou, D. D., Synthesis, characterization and electrochemical properties of mesoporous zirconia nanomaterials prepared by self-assembling sol-gel method with tween 20 as a template. *Chemical Engineering Journal* **2011**, *170*, 518-524.

121. Zhou, T. X.; Mo, S. S.; Zhou, S. L.; Zou, W. J.; Liu, Y. L.; Yuan, D. S., Mn(3)o(4)/worm-like mesoporous carbon synthesized via a microwave method for supercapacitors. *Journal of Materials Science* **2011**, *46*, 3337-3342.

122. Xia, N. N.; Yuan, D. S.; Zhou, T. X.; Chen, J. X.; Mo, S. S.; Liu, Y. L., Microwave synthesis and electrochemical characterization of mesoporous carbon@bi(2)o(3) composites. *Materials Research Bulletin* **2011**, *46*, 687-691.

123. Dong, X.; Shen, W.; Gu, J.; Xiong, L.; Zhu, Y.; Li, H.; Shi, J., Mno2-embedded-in-mesoporous-carbon-wall structure for use as electrochemical capacitors. *The Journal of Physical Chemistry B* **2006**, *110*, 6015-6019.

124. Lei, Y.; Fournier, C.; Pascal, J.-L.; Favier, F., Mesoporous carbon–manganese oxide composite as negative electrode material for supercapacitors. *Microporous and Mesoporous Materials* **2008**, *110*, 167-176.

125. Wu, Z.; Zhao, D., Ordered mesoporous materials as adsorbents. *Chemical Communications* **2011**, *47*.

126. Wan, Y.; Cui, X.; Wen, Z., Ordered mesoporous carbon coating on cordierite: Synthesis and application as an efficient adsorbent. *Journal of Hazardous Materials* **2011**, *198*, 216-223.

127. Ma, Y. Q.; Zhai, Q. Z.; Yu, H.; Yang, M. J., Removal of pb(ii) from water using nanoscale sba-15. *Asian Journal of Chemistry* **2011**, *23*, 5016-5024.

128. Bui, T. X.; Kang, S. Y.; Lee, S. H.; Choi, H., Organically functionalized mesoporous sba-15 as sorbents for removal of selected pharmaceuticals from water. *Journal of Hazardous Materials* **2011**, *193*, 156-163.

129. Idris, S. A.; Harvey, S. R.; Gibson, L. T., Selective extraction of mercury(ii) from water samples using mercapto functionalised-mcm-41 and regeneration of the sorbent using microwave digestion. *Journal of Hazardous Materials* **2011**, *193*, 171-176.

130. Mohammadi, N.; Khani, H.; Gupta, V. K.; Amereh, E.; Agarwal, S., Adsorption process of methyl orange dye onto mesoporous carbon material-kinetic and thermodynamic studies. *Journal of Colloid and Interface Science* **2011**, *362*, 457-462.

131. Tao, S.; Wang, C.; Ma, W.; Wu, S.; Meng, C., Designed multifunctionalized magnetic mesoporous microsphere for sequential sorption of organic and inorganic pollutants. *Microporous and Mesoporous Materials* **2012**, *147*, 295-301.

132. He, C.; Hu, X., Anionic dye adsorption on chemically modified ordered mesoporous carbons. *Industrial & Engineering Chemistry Research* **2011**, *50*, 14070-14083.

133. Barbosa, M.; Araujo, A.; Galvão, L.; Silva, E.; Santos, A.; Luz, G.; Fernandes, V., Carbon dioxide adsorption over dipa functionalized mcm-41

and sba-15 molecular sieves. *Journal of Thermal Analysis and Calorimetry* **2011**, *106*, 779-782.

134. Addorisio, V.; Pirozzi, D.; Esposito, S.; Sannino, F., Decontamination of waters polluted with simazine by sorption on mesoporous metal oxides. *Journal of Hazardous Materials* **2011**, *196*, 242-247.

135. Nunes, M. R.; Perez, G. M.; Loguercio, L. F.; Alves, E. W.; Carreno, N. L. V.; Martins, J. L.; Garcia, I. T. S., Active carbon preparation from treads of tire waste for dye removal in waste water. *Journal of the Brazilian Chemical Society* **2011**, *22*, 2027-2035.

136. Choi, J.-W.; Lee, S.-Y.; Chung, S.-G.; Hong, S.-W.; Kim, D.-J.; Lee, S.-H., Removal of phosphate from aqueous solution by functionalized mesoporous materials. *Water, Air, & Soil Pollution* **2011**, *222*, 243-254.

137. Yang, X.; Guan, Q.; Li, W., Effect of template in mcm-41 on the adsorption of aniline from aqueous solution. *Journal of Environmental Management* **2011**, *92*, 2939-2943.

138. Chen, H. M.; Chu, P. K.; He, J. H.; Hu, T.; Yang, M. Q., Porous magnetic manganese oxide nanostructures: Synthesis and their application in water treatment. *Journal of Colloid and Interface Science* **2011**, *359*, 68-74.

139. Song, J.; Kong, H.; Jang, J., Adsorption of heavy metal ions from aqueous solution by polyrhodanine-encapsulated magnetic nanoparticles. *Journal of Colloid and Interface Science* **2011**, *359*, 505-511.

140. Asuha, S.; Gao, Y. W.; Deligeer, W.; Yu, M.; Suyala, B.; Zhao, S., Adsorptive removal of methyl orange using mesoporous maghemite. *Journal of Porous Materials* **2011**, *18*, 581-587.

141. Deng, Y.; Cai, Y.; Sun, Z.; Gu, D.; Wei, J.; Li, W.; Guo, X.; Yang, J.; Zhao, D., Controlled synthesis and functionalization of ordered large-pore mesoporous carbons. *Advanced Functional Materials* **2010**, *20*, 3658-3665.

142. Lu, A.-H.; Li, W.-C.; Kiefer, A.; Schmidt, W.; Bill, E.; Fink, G.; Schüth, F., Fabrication of magnetically separable mesostructured silica with an open pore system. *Journal of the American Chemical Society* **2004**, *126*, 8616-8617.

143. Clark, L. C.; Lyons, C., Electrode systems for continuous monitoring in cardiovascular surgery. *Annals of the New York Academy of Sciences* **1962**, *102*, 29-45.

144. Wang, J., Electrochemical glucose biosensors. *Chemical Reviews* **2007**, *108*, 814-825.

145. Guilbault, G. G.; Lubrano, G. J., An enzyme electrode for the amperometric determination of glucose. *Analytica Chimica Acta* **1973**, *64*, 439-455.

146. Jiang, X.; Wu, Y.; Mao, X.; Cui, X.; Zhu, L., Amperometric glucose biosensor based on integration of glucose oxidase with platinum nanoparticles/ordered mesoporous carbon nanocomposite. *Sensors and Actuators B: Chemical* **2011**, *153*, 158-163.

147. Wang, L.; Bai, J.; Bo, X.; Zhang, X.; Guo, L., A novel glucose sensor based on ordered mesoporous carbon-au nanoparticles nanocomposites. *Talanta* **2011**, *83*, 1386-1391.

148. Dai, M.; Maxwell, S.; Vogt, B. D.; La Belle, J. T., Mesoporous carbon amperometric glucose sensors using inexpensive, commercial methacrylate-based binders. *Analytica Chimica Acta* **2012**, *738*, 27-34.

149. Su, C.; Zhang, C.; Lu, G.; Ma, C., Nonenzymatic electrochemical glucose sensor based on pt nanoparticles/mesoporous carbon matrix. *Electroanalysis* **2010**, *22*, 1901-1905.

150. Zhu, L.; Tian, C.; Zhu, D.; Yang, R., Ordered mesoporous carbon paste electrodes for electrochemical sensing and biosensing. *Electroanalysis* **2008**, *20*, 1128-1134.

CHAPTER 2

ORDERED MESOPOROUS CARBON COMPOSITE FILMS CONTAINING COBALT AND VANADIA FOR ELECTROCHEMICAL APPLICATIONS

2.1 Introduction

As discussed before ordered mesoporous carbon materials have garnered significant attention due to their attractive properties such as electrical conductivity, chemical inertness, high surface area, uniform pore size and biocompatibility.[1,2] These properties have led to proposed use of mesoporous carbons as catalyst supports,[3] sensors,[4] electrodes,[5] adsorbents for water remediation,[6] and active materials for energy storage[7] as examples. Ordered mesoporous carbon powders have been historically synthesized by nanocasting where a sacrificial (typically, silica) hard porous template is filled with the carbonizable precursor and then the template is dissolved after carbonization to yield an inverse replica.[8] More recently, soft templating approaches have been introduced that provide a more direct route to mesoporous carbons through organic-organic self-assembly.[9,10] These soft templating approaches can also be applied to fabricating mesoporous carbon films.[11,12]

There have been multiple routes developed to modify carbon to increase its functionality and/or performance especially for electrochemical applications.[3,13-18] Increasing the surface area (from 650 to 2390 m^2/g, BET surface area) through tri-constitute self assembly to form an ordered

mesoporous carbon-silica nanocomposite where the silica is subsequently removed yields significant improvements in the electrochemical performance.[19] Alternatively, the carbon can be doped with nitrogen, phosphorus or boron to significantly increase the electrochemical capacitance.[15,20] Similarly, incorporating metal oxide nanoparticles into the carbonizable precursor provides an alternative route to improved electrochemical performance.[3,14,21] However, the long term electrochemical performance of these mesoporous carbon based materials for reversible Li storage appears to be limited in comparison to alternatives such as hollow, carbon coated SnO_2 nanoparticles.[22] The increased Li capacity of some transition metal oxides, such as TiO_2, MnO_2, SnO_2 and V_2O_5, in comparison to carbon makes these metal oxides highly attractive for Li insertion battery electrodes.[23-27] However, their low electrical conductivity limits charge transfer and hence performance. Furthermore, the charge-discharge reversibility of bulk metal oxides is generally low due to the large volume changes that lead to pulverization of the active material upon successive cycling.[28] Addition of porosity in the material to enable expansion does provide some improvement in the cycling stability for Li battery applications,[29] but additional improvements in cyclability occur when the metal oxide is coated with a thin carbon layer because carbon can function as physical buffering layer for large volume change called cushion effect.[28] These results would suggest that mesoporous carbon composites could provide a route to high performance anodes for Li battery technology.

However, there are few reports of such mesoporous nanocomposite materials.[21,30,31] For example, Patel et al. illustrated that the electrochemical pseudocapacitance of disordered mesoporous carbon can be dramatically improved by the addition of MnO_2 nanoparticles.[21] Ordered mesoporous nanocomposites with well defined geometry and pore size could provide improvements in the ion transport and surface area, which in turn would lead to improved performance. Ordered mesoporous carbon-sulfur materials prepared by infiltration of sulfur into the micropores have exhibited high performance for Li/S battery applications.[13] Recently, Aksay and coworkers reported surfactant assembled graphene-tin oxide nanostructures that exhibit near theoretical specific energy density for Li insertion, as the electrochemical properties of the nanocomposites can be improved by increasing the conductivity of the electrode materials with graphene and by stabilizing the electrode structure with a good electric contact between SnO_2 and conductive graphene during the charge-discharge process.[32] However, this synthesis can be quite challenging due to multiple length scales of the building materials, but tri-constituent self-assembly to synthesize mesoporous nanocomposites is quite facile.[18] This self-assembly approach can also be applied to the assembly of carbonizable oligomers, metal alkoxides (sol-gel), and surfactants/block copolymers templates to yield ordered mesoporous materials with discrete metal oxide and carbon domains within the pore wall.[18,30] For the carbon-titania nanocomposites formed by tri-constituent self-assembly, modest reversible capacities are reported,[30] but to achieve a high capacity for Li

battery applications alternative metal oxides are required. One potential difficulty in extending this tri-constituent assembly approach is controlling the interactions between the carbonizable oligomer, metal oxide sol, and templating agent. For some transition metal oxides such as tin oxide, it is difficult to even obtain an ordered structure for the pure material without complex processing.[33] Alternatively, metal salts have been utilized to form nanoparticles within carbon aerogels,[34] but these salts could interfere with self assembly of the surfactant, which may lead to disordered carbon framework or decrease the porosity. Recently, Zhao and coworkers have demonstrated that ordered mesoporous carbon-MgO composites can be synthesized using magnesium nitrate, but the MgO nanoparticles can be larger than the pore walls and extend into the pores especially at high loadings.[35]

Alternatively, thermolysis of organometallic compounds is an effective route to synthesis of carbon coated metal nanoparticles,[27] but these are typically isolated large nanoparticles. The carbon shell and morphology of the nanoparticles are dependent upon the ligands and their carbonization. By proper selection of organic ligands on cobalt, thermolysis and controlled oxidation leads to carbon coated cobalt particles with excellent Li storage properties.[27] One such ligand is acetylacetonate (acac), which has also been utilized in controlling condensation rates for mixed metal oxides formed by sol gel chemistry.[36,37] This stability of metal (acac) should provide a wide processing window for incorporating transition metals into ordered mesoporous carbons.

In this chapter, the tri-constituent synthesis method for fabrication of ordered mesoporous carbon composites is extended to include cobalt and vanadium oxides by using $Co(acac)_3$ and $VO(acac)_2$ as precursors. Evaporation induced self-assembly (EISA) of low-molecular weight phenolic resin (resols),[38,39] commercially-available triblock copolymers (Pluronic F127) and metal (acac) is utilized to form highly ordered mesoporous carbon composite thin films after pyrolysis at 800 ℃. The porous morphology of the films is investigated by x-ray diffraction, transmission electron microscopy, and ellipsometric porosimetry. Additionally, the electrical and electrochemical properties of these films are examined as a function of composite film composition. These results illustrate the versatility of the triconstituent assembly approach for fabrication of ordered mesoporous carbon composites with potential applications in catalysis, energy storage and sensing.

2.2 Experimental

A triblock copolymer surfactant, Pluronic F127 (M_w = 12 600 g/mol, PEO_{106}-PPO_{70}-PEO_{106}, BASF), was used to template the carbon-based composite mesostructures. Sodium hydroxide (NaOH, Aldrich), phenol (Aldrich) and formaldehyde (37 wt% in H_2O) were used to synthesize the resol precursor.[38] Copper (III) acetylacetonate ($Co(C_5H_7O_2)_3$, 98+%, Strem Chemicals, Inc.) and vanadyl acetylacetonate ($VO(C_5H_7O_2)_2$, 98%, Strem Chemicals, Inc.) served as cobalt oxide and vanadium oxide precursors, respectively. Sodium sulfate (> 99%, Aldrich) was used as received and utilized as the salt in the electrolyte for electrochemical measurements.

Resol precursor was prepared by the polymerization of phenol and formaldehyde under a basic environment as described previously.[38] Following synthesis, the resol was dissolved in tetrahydrofuran (THF) at 30 wt-%. Mesostructured polymer-resins (similar to FDU-16)[38] were templated by using triblock copolymer F127 with molar compositions of phenol/formaldehyde/NaOH/F127 = 1:2:0.1:0.006.[38] For preparing nanocomposite film, $Co(acac)_3$ or $VO(acac)_2$ was added into resol and F127 in THF solution with fixed molar ratio of resol/F127=1:0.006. In order to maintain the same thickness range for all the films, all the solutions are diluted to 10 wt% of solids (i.e., F127 + resol + Metal(acac)). Silicon wafers were cleaned in piranha solution for 20 min at 90 ℃ and used as substrates. Films were prepared by spin-coating at 4000 rpm for 45 s on clean silicon wafer. The films were aged at room temperature for 1h, and subsequently the resol is thermopolymerized at 120 ℃ for 24 h to solidify the network. These as-made films are denoted as FDU16-am (pure carbon) and CM-X-am, where M represents the metal included in the composite and X lists the weight percent of M(acac) in the as-made (am) film. The pluronic template was removed thermally by pyrolysis in nitrogen. Mesoporous polymer composite films (CM-X-350) were obtained after pyrolysis at 350 ℃ for 3 h using a heating rate of 1 ℃/min, whereas mesoporous carbon composites (CM-X-800) were obtained after carbonization at 800 ℃ for 3 h, with heating rates of 1 ℃/min below 600 ℃, and 5 ℃/min above 600 ℃.

Table 1 Porosity, conductivity and chemical compositions of the mesoporous carbon/carbon-cobalt composite films.

Sample -800 ℃	M(acac) (g)	Resol (g)	F127 (g)	Porosity (%)	Co[a] (wt%)	Conductivity (S/cm)	C/M[b]/H[c] (Molar ratio)
FDU16	0.00	0.4	0.20	23	0.00	22	1/0/0.12
CCo-10	0.05	0.5	0.25	35	4.70	42	1/0.01/0.056
CCo-20	0.10	0.4	0.20	29	17.50	32	1/0.045/0.5
CCo-33	0.10	0.2	0.12	25	25.30	26	1/0.07/0.2
CV-10	0.05	0.5	0.25	30	2.90	41	1/0.007/0.08
CV-20	0.10	0.4	0.20	31	11.20	38	1/0.03/0.11
CV-33	0.10	0.2	0.12	24	20.00	33	1/0.06/0.22
CV-50	0.10	0.10	0.06	20	36.50	20	1/0.14/0.41

[a]Based upon only C, Co, V and H content while neglecting oxygen

[b] M = metal (either Co or V)

[c]Determined from RBS measurements of the thin films

X-ray diffraction (XRD) was performed in a θ/2θ geometry using Cu Kα source (Panalytical X'Pert PRO) with angle of incidence, θ, varied from 0.25 to 1.5 °. A parallel plate collimator (PPC) was used in combination with an incident beam optical module to provide an X-ray beam with very low divergence. Rutherford back scattering (RBS) was performed to obtain the elemental composition of the samples using IBeAM (Ion Beams for Analysis of Materials) facility at ASU with 1.7×10^6 tandem electrostatic accelerator sample analysis end stations. Elastic recoil detection (ERD) analysis was used to quantify hydrogen content.

Film thickness and the optical properties of the films were quantified using a UV-visible-NIR (240-1700 nm) variable angle spectroscopic ellipsometer (VASE M-2000, J.A. Woollam Co. These data provide a route to the optical properties of the films based upon Cauchy model with an Urbach adsorption for the as-made films and films after pyrolysis at 350 ℃, while an oscillator model based upon multiple Gaussian was used for films after pyrolysis at 800 ℃. Ellipsometric porosimetry (EP) was utilized to provide the pore size distribution and the porosity of the pyrolyzed films using the same M-2000 instrument. Toluene (Aldrich) was utilized as the probe molecule. The change in refractive index of films during the pore filling/empting provides vapor adsorption/desorption isotherms as a function of toluene partial pressure.[40-42] Assuming all pores were filled and neglecting the minor film swelling, the film porosity (P) was estimated from the refractive index of the film using the Bruggemann effective medium approximation (BEMA).[43] To quantify the pore size distribution (PSD), the radius of mesopore, $r_{p,}$ was calculated as the sum of the Kelvin radius and the thickness of the absorbed layer prior to capillary condensation. Each isotherm was fit to an arbitrary function based upon a series of Gaussian and Sigmoid functions[44] to provide a smooth curve for differentiation to estimate the population of pore sizes.[40-42]

Transmission electron microscopy (TEM) and scanning transmission electron microscopy (STEM) were performed on cross-sections of the films using JEOL 2010F microscope operating at 200 keV. TEM cross-section

samples were prepared by manually polishing, dimpling and then ion-milling. Fist, two same films on the Si wafer were face-to-face glued together. Then the the cross-section went through polishing and dimpling processes to make the thickness of the center under 10 μm. After that, ion milling was used to sputter a small hole in the center of the glue line. TEM images were obtained on the area next to the hole edge along the glue line of the two films.

The electrical conductivity of the films was determined using a four-point probe system (SP4-40045TFS, Lucas Labs). The current was sourced (Keithley 6221 AC and DC Current Source) across pins 1 and 4, while the potential was measured across the inner pins using an Agilent U1251A Digital Multimeter (DMM) according to typical protocols. The conductivity was corrected for the film thickness using typical geometric arguments.[45] Electrochemical measurements were carried out in a three electrode cell with a Pt wire counter electrode and Hg/Hg_2SO_4 reference electrode using a CHI630 electrochemical analyzer (CH Instruments Inc.). Molybdenum was sputtered onto the silicon substrate to serve as the current collector for electrochemical measurements. Electrochemical tests were conducted in 1M Na_2SO_4 at ambient temperature with aqueous potentials referenced against Hg/Hg_2SO_4.

2.3 Results and Discussion

Mesoporous carbon-cobalt oxide composite films are synthesized using resol and $Co(acac)_3$ as precursors with Pluronic F127 as the templating agent. Table 1 shows the formulations utilized to synthesize these mesoporous composite films. As the $Co(acac)_3$ content in the as-made films is increased

from 10 to 33 wt%, there is a corresponding increase in the final Co concentration in the carbonized films based on RBS results. One difficulty in fully quantifying the film composition is interference in the oxygen signal from the native oxide of the silicon wafer due to the film thickness being insufficient to fully adsorb scattering from the buried interface. For this reason, only the carbon, cobalt and hydrogen content is reported; for the films described previously the Co content increases from 4.7 wt % to 25.3 wt % when only considering element C, Co and H. As the cobalt is oxidized (as determined from EDX measurements of the cross section), this calculation overestimates the cobalt content, but underestimates the non-carbon content of the composite. Nonetheless, the addition of $Co(acac)_3$ to the casting solution provides a simple route to incorporation of heteroatoms in mesoporous carbon films.

To determine if the templated pore structure is preserved with the addition of $Co(acac)_3$ to the precursor, XRD is initially utilized as a screening tool for the ordered structure. For the as-made films, only a single diffraction peak is observed except for CCo-33-am, which does not show any evidence of an ordered structure (Figure 14A). The lack of higher order reflections may be resultant from the limited contrast in electron density between phenolic resol and surfactant in the as-made film; the addition of the $Co(acac)_3$ is expected to only slightly increase the contrast if segregated to the hydrophilic domain. A single diffraction peak for the as-made films is consistent with prior results for thicker films of resol-surfactant.[46] After removal of the template at 350 ℃,

two diffraction peaks are now observed for both FDU16-350 and CCo-10-350 (Figure 14B); additionally, the intensities of the primary peaks are substantially greater than the corresponding as-made films as expected from the increase in contrast. For all CCo-33 films, no diffraction peaks have been detected, which indicate no long range ordered mesostructure in these materials.

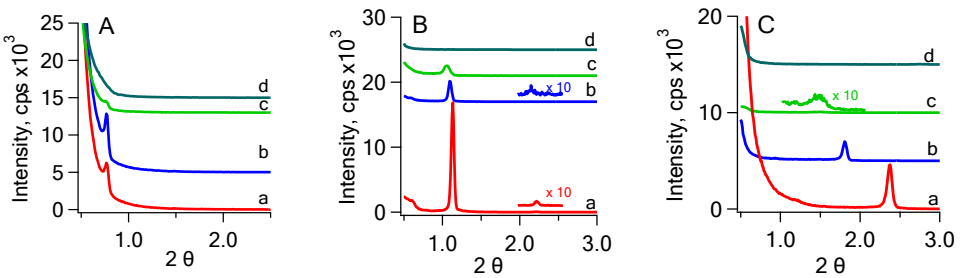

Figure 14 XRD profiles of mesoporous nanocomposite films: (a) FDU16, (b) Co-10, (c) Co-20 and (d) Co-33 for (A) as-made films, (B) films pyrolyzed at 350 ℃ and (C) films pyrolyzed at 800 ℃.

Changes in the mesostructure upon pyrolysis can be elucidated from the position of the primary diffraction peak; the primary peaks shift to larger 2θ after removal of template at 350 ℃. This shift is indicative of a decrease in d-spacing from contraction during pyrolysis process. The d-spacing is calculated using Bragg's Law, $\lambda = 2d \sin\theta$, where λ is wavelength (1.54Å for CuKα), d is d- spacing in angstroms (Table 2) and Θ is the diffraction angle. From the d-spacings of the as-made and mesoporous polymer composite films, the contraction, C, is calculated as $C= (d_{am}-d_{350})/d_{am}$, while d_{am} is the d-spacing for as-made films and d_{350} is the d-spacing for films pyrolyzed at 350 ℃.

Table 2 illustrates the difference in contraction for the mesoporous polymer composite films from the d-spacing. These contraction results show that addition of Co tends to reduce the contraction of mesoporous ordered structure films during pyrolysis at 350 ℃.

Table 2 d-spacing from primary diffraction peak and calculated contraction of carbon-cobalt/vanadium composite films.

Sample	d-spacing from as made (nm)	d-spacing after pyrolysis at 800 ℃ (nm)	Contraction (%)
FDU16-350	11.54	7.78	33
CCo-10-350	11.54	8.06	30
CCo-20-350	11.69	8.37	28
FDU16-800	11.54	3.72	68
CCo-10-800	11.54	4.89	58
CCo-20-800	11.69	6.15	47
CV-10-800	10.97	5.40	51
CV-20-800	10.09	4.95	51
CV-33-800	11.10	4.89	56

Carbonization of the film at 800 ℃ results in further contraction as evidenced by the primary diffraction peak shifting to even larger 2Θ (Figure 14C). However, it can be easily observed that this shift is decreased as Co concentration increases, indicating a larger d-spacing and lower contraction. Thus, the contraction is significantly decreased as Co concentration increases, similar effects result from adding Si into the film[46] as quantified in Table 2.

This compositional dependence of the d-spacing suggests that Co is distributed within the carbon framework.

To examine the mesostructure in more detail, transmission electron microscopy (TEM) is utilized as shown in Figure 15. In agreement with the previously discussed XRD results, micrographs of FDU16-350 (Figure 15a), CCo-10-350 (Figure 15b) and CCo-20-350 (Figure 15c) films show highly ordered mesostructure after pyrolysis at 350 ℃. In all cases, the mesopores appear to be nearly spherical in nature and distributed on a near cubic lattice. Further pyrolysis of these films to carbonize the phenolic resin at 800 ℃ indicate the highly ordered mesoporous structure is stable as shown in the micrographs of FDU16-800 (Figure 15d), Co-10-800 (Figure 15e) and CCo-20-800 (Figure 15f). One difference is for the CCo-20-800 film where the bottom layer of the film is only slightly porous, while the near surface has large domains of regular pores. Also examining the mesopores in detail, an obvious distortion of the pores is observed to an asymmetric elliptical shape with the pore dimension significantly smaller through the thickness of the film. Additionally, the pore size is significantly decreased in comparison to films pyrolyzed at 350 ℃. The short axis of the mesopores increases from 1.8 nm for FDU16-800 to 3.6 nm for CCo-10-800, which is consistent with the d-spacing changes determined from XRD. During pyrolysis process at 800 ℃, all the components in the precursor are “soft” organic compounds for FDU16-800 and a large contraction (68 %) is observed. However for carbon cobalt composites, the presence of rigid Cobalt oxide that forms from the

decomposition of $Co(acac)_3$ appears to effectively reduce the framework shrinkage (58% for CCo-10-800 and 47% for CCo-20-800), and hence the mesopores derived from degradation of F127 maintain a larger pore radius than FDU16-800.[19] This contraction can also be clearly observed from the cross-section TEM images. For example, the CCo-20-350 film that is 478 nm thick (Figure 15c) decreases to 183 nm upon carbonization (Figure 15f). This fractional thickness decrease (60 %) is much larger than expected from the decrease in d-spacing determined from XRD. The lack of mesopores in the lower fraction of the film could explain this discrepancy as collapse of the mesostructure would lead to a decrease in the film thickness, while not impacting the location of the primary diffraction peak that results solely from the ordered mesoporous regions. In addition to the mesopores, nanoparticles are also clearly visible in the micrographs for CCo-10-800 (Figure 15e) and CCo-20-800 (Figure 15f). For CCo-10-800, the nanoparticles are distributed throughout the film with the nanoparticle size less than 20 nm. Conversely for CCo-20-800, very large particles are observed that are greater than 80 nm in some cases. This suggests that the cobalt particles ripen during the carbonization process and could provide an explanation for the lack of ordered structure at high $Co(acac)_3$ loadings.

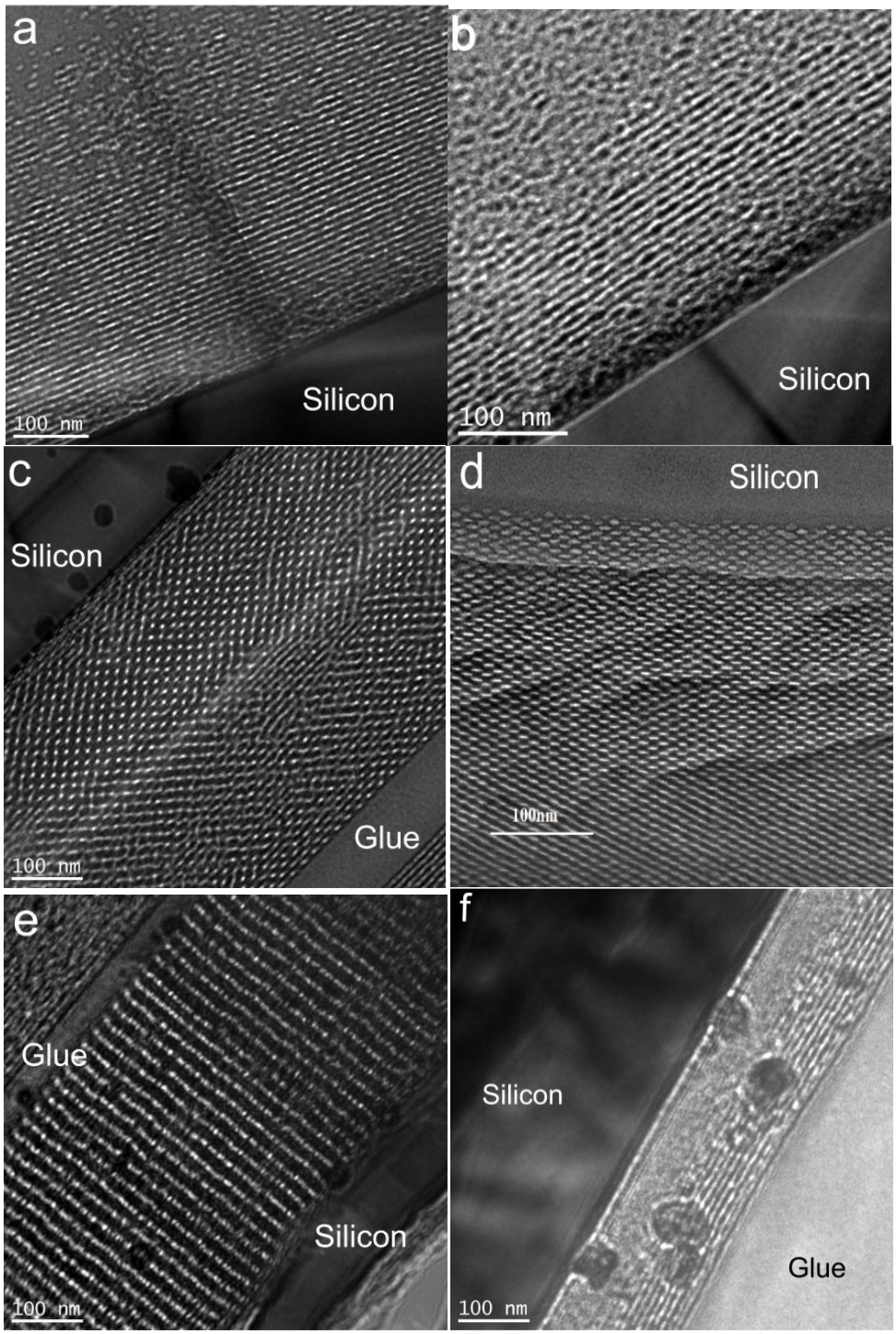

Figure 15 Cross-section TEM micrographs of mesoporous nanocomposite films after pyrolysis: (a) FDU16-350(b) Co-10-350, (c) Co-20-350, (d)

FDU16-800, and (e) Co-10-800. HR-TEM provides an enhanced view of the mesopores in (f) Co-10-800.

To further investigate the structure of these films, HR-TEM is employed. When examining the local structure of the ordered mesoporous region, HR-TEM illustrates small nanoparticles (1-2 nm) within the carbon framework (Figure 16a) of Co-10-800 film. These nanoparticles within the carbon framework are likely responsible for the decreased contraction in comparison to FDU16-800 film. Figure 16b shows a HR-TEM micrograph of a larger particle in Co-20-800 film; the micrograph shows randomly oriented lattice fringes in the darker area, but the bright area surrounding the dark nanoparticle also illustrates randomly oriented lattice fringes as well. Additionally, the live Fast Fourier Transform pattern also displays a ring diffraction pattern (inset in Figure 16b), which illustrate the polycrystalline structure of the particle. We hypothesize that the particles are carbon/cobalt oxide core-shell crystalline nanocomposites. This structure is consistent with the direct pyrolysis of $Co(acac)_3$ at 800 ℃ that yields a carbon/Co oxide core-shell structure nanocomposites.[47]

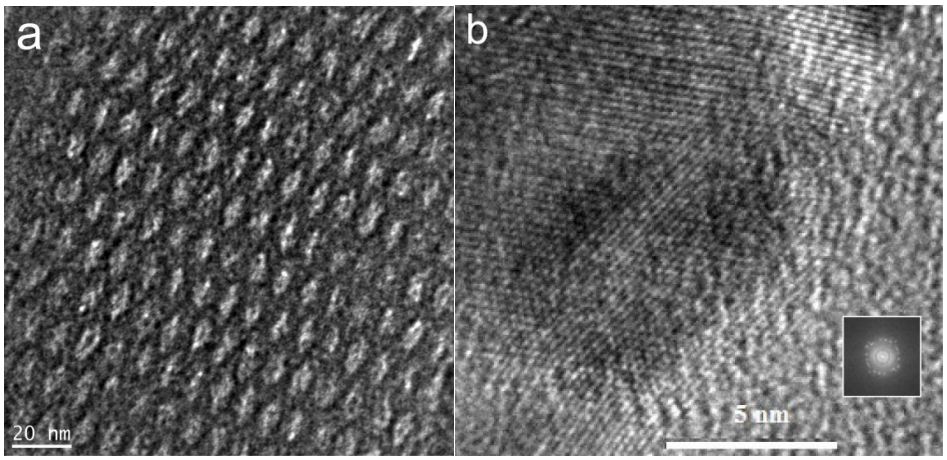

Figure 16 HR-TEM of (a) Co-10-800 and (b) Co-20-800 films.

To further investigate the structure of the Co-10-800 film as the nanoparticles are difficult to visualize in the HR-TEM micrographs, z-contrast STEM has been utilized to investigate the nanoparticles distribution as illustrated in Figure 17. The contrast in the system is based on the atomic number with lighter areas associated with larger atomic numbers; in this case, the bright white spots are attributed to Co-based nanoparticles. Although there are a few aggregated particles (approximately 10nm in diameter) in the film, most nanoparticles are dispersed throughout the wall framework as sub-1 nm particles based upon the micrograph. The is a significant difference in the distribution and size of the cobalt oxide nanoparticles between the Co-10-800 and Co-20-800; although the total cobalt content is larger for Co-20-800, there appear to be significantly more small nanoparticles for Co-10-800 based upon TEM and STEM micrographs.

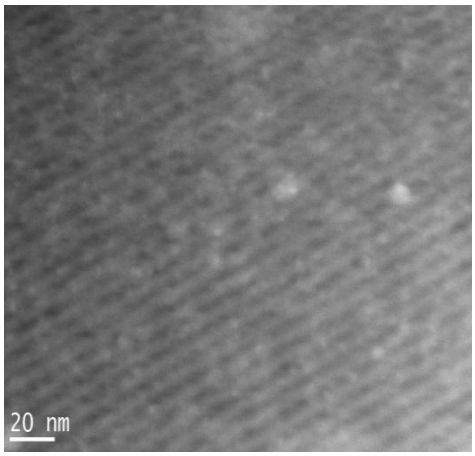

Figure 17 STEM micrograph of Co-10-800 film. The bright spots are Co, darker area is carbon and black areas are pores.

Pore size distribution and porosity play a vital role in mechanical, thermal and chemical properties of the porous films and their feasibility to be used in microelectronic technology.[37,38] Ellipsometric porosimetry (EP) method is a powerful technique to characterize the mesopores in thin films, which utilizes adsorption/desorption isotherms of the changes of refractive index caused by the various partial pressure of an organic solvent around a film.[37] Figure 18a shows the adsorption/desorption isotherms of Co-10-350 film, which is a typical type-IV isotherms with an H_1-type hysteresis loop. These isotherms are representative of those obtained for the mesoporous carbon composite films examined; adsorption/desorption isotherms for the other composite films are presented as Supplemental Information. The Kelvin equation is then utilized with the EP data to estimate the pore size distribution (PSD) of the films. The pore size distribution of Co-10-350 calculated from the desorption isotherm which is shown in Figure 18b.

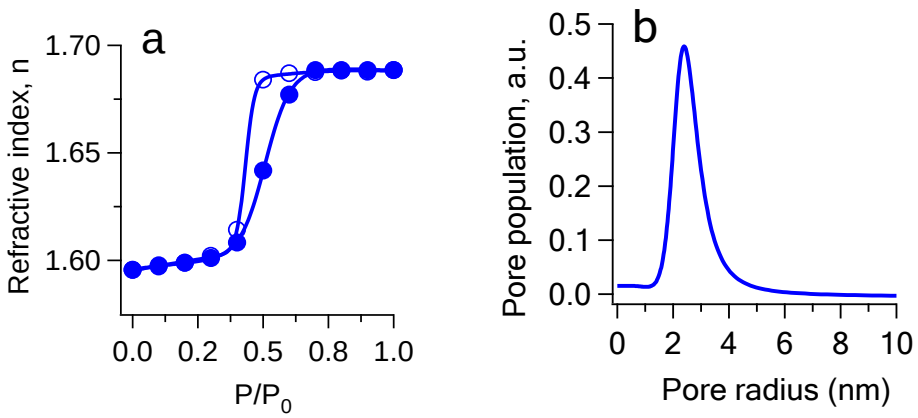

Figure 18 Toluene adsorption and desorption isotherms for in mesoporous nanocomposite films as determined through the changes in the refractive index (λ= 632.4 nm) of the Co-10-350 film as a function of the adsorbate (toluene) relative pressure. Closed symbol lines are for the adsorption process and the open symbol lines are desorption isotherms. (b) Pore size distribution of Co-10-350 film calculated by Kelvin equation using desorption isotherms.

Similarly, Figure 19a shows the pore size distribution for all the polymer-Co films after the removal of template at 350 ℃; a narrow distribution is found for all films as would be expected for a templated synthesis. The average pore radius increases from approximately 2 nm to 3 nm when $Co(acac)_3$ concentration increases in the precursor film from 0 to 20 wt-%. This increase in the average pore size is consistent with the decreased contraction determined from XRD, which would be expected to lead to larger pore size and higher porosity. The corresponding carbonized films also show a marked increase in the average pore size at larger Co concentration. Due to further contraction from pyrolysis at 800 ℃, the average pore size of all the

carbon-Co films (Figure 19d) is approximately 1 nm smaller than corresponding mesoporous polymer composite films (350 ℃).

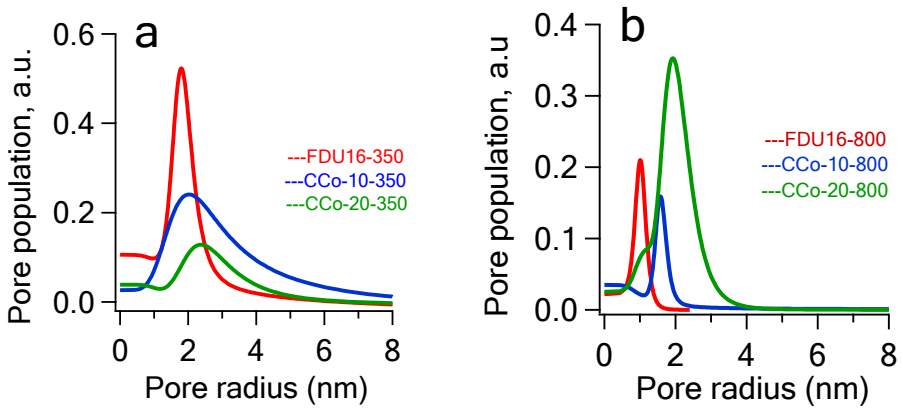

Figure 19 Pore size distributions of (a) polymer-Co films and (b) carbon-Co films.

To investigate the applicability of this tri-constituent assembly to other organometallics, similar materials are synthesized with $VO(acac)_2$ substituting for $Co(acac)_3$. The composition of the vanadium containing mesoporous composite films is shown in Table 1. Similar to carbon-cobalt films, the ordered structure of the films is examined using XRD. All as-made films of the carbon-vanadium-based nanocomposites exhibit a single diffraction peak that is similar to the vanadium free analog (FDU16-am film) when the $VO(acac)_2$ concentration is lower than 50% as shown in Figure 20a. Removal of the surfactant template results in a shift in the primary diffraction peaks to larger 2Θ. As the pyrolysis temperature is increased, the films contract further as evidenced by the shift in the primary diffraction peak (Figure 20b). The compositional dependence of the contraction and d-spacings are tabulated for

both vanadium and cobalt-based composite films in Table 2 for polymer and carbon composites, respectively. Both CV-10-350 and CV-20-350 films contract (30% for CV-10-350 and 28% for CV-20-350) less than FDU16-350; this is consistent with increasing mechanical rigidity of the porous framework from the incorporation of vanadium (or cobalt as discussed in the prior section). However, CV-33-350 film has slightly larger contraction than FDU16-350; this could be a result of long range order loss with high concentration of $VO(acac)_2$ in the film as CV-50-am does not appear to be ordered. After pyrolysis at 800 ℃ (Table 2), the increase in contraction for the composite films from the 350 ℃ is reduced in comparison to pure carbon. Both CV-10-800 and CV-33-800 films exhibit a single diffraction peak at relatively low 2Θ that corresponds to a d-spacing of 5.4 nm (2Θ=1.635°) and 4.9 nm(2Θ=1.805°), respectively. This suggests that addition of V into the carbon film significantly reduces the framework contract from stresses developed during carbonization process.

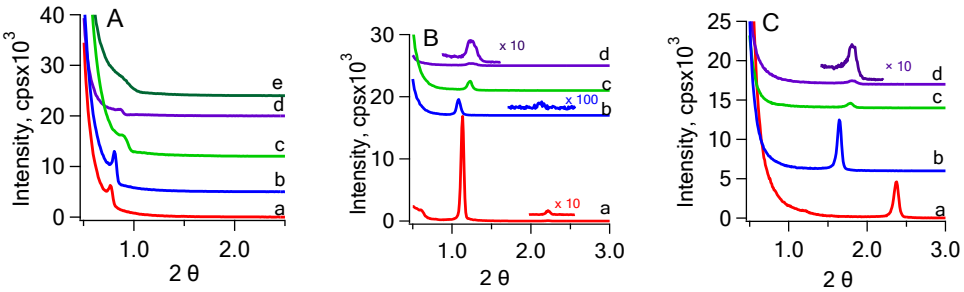

Figure 20 XRD profiles of mesoporous structure nanocomposite films: (a) FDU16, (b) CV-10, (c) CV-20, (d) CV-33 and (e) CV-50 for (A) polymer-V as-made films, (B) films pyrolyzed at 350 ℃ and (C) films pyrolyzed at 800 ℃.

To confirm the ordered mesoporous structure suggested from the XRD profiles, the films are examined using TEM for a real-space image. The polymer-vanadium films show a highly ordered mesoporous structure similar to polymer-cobalt films after pyrolysis at 350 ℃ (Figure 21a and 21b). However, it is interesting that after pyrolysis at 800 ℃ for 3h, the ordered mesostructure appears to be more wormhole-like, than a near cubic arrangement of isolated mesopores (Figures 21c and 21d). However, it would be highly unusual for a high temperature transition in the mesostructure to occur between 350 and 800 ℃ that could provide an explanation of the differences in the apparent mesostructures in the TEM micrographs shown in Figure 21. Unlike the carbon-cobalt oxide mesoporous composite films, the vanadium-based analogs do not show any large nanoparticles (or aggregates). To investigate the morphology of the films in most detail, z-contrast STEM has been utilized. Figure 22 illustrates the mesostructure of CV-10-800 as determined from STEM. The cross section shows most nanoparticles are small

(<5 nm, bright spots) and distributed within the carbon framework. Interestingly, the pores in the sample (dark spots) appear to actually be organized on a lattice as expected for a near cubic structure. The ordered structure of carbon-vanadium carbonized may appear to be wormhole-like in the TEM image due to the scattering and reflection of electrons from vanadium oxide nanoparticles that could be randomly distributed in the framework.

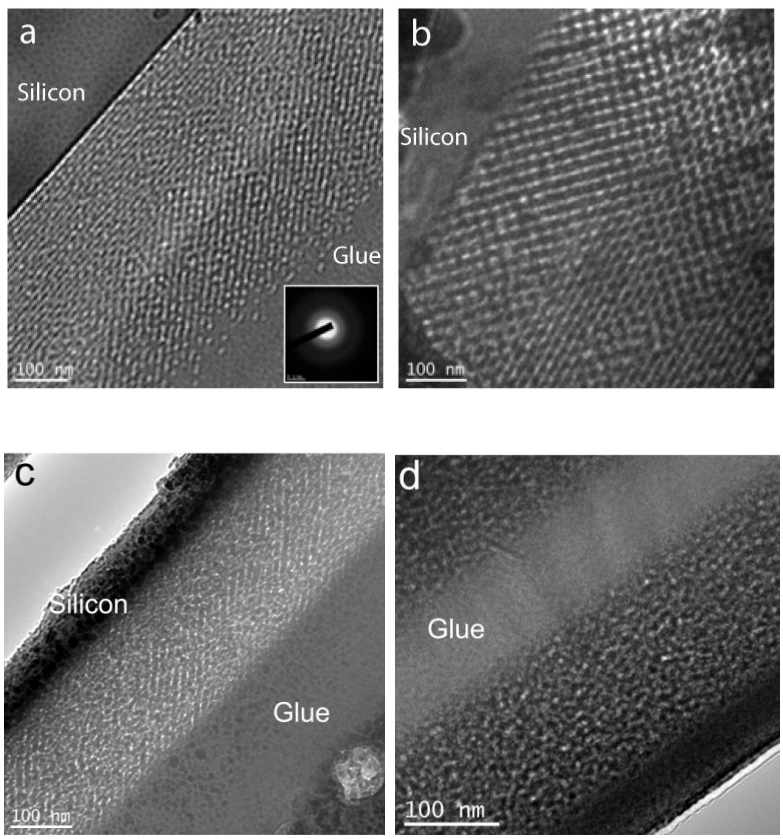

Figure 21 Cross-section TEM micrographs of mesoporous nanocomposite films: (a) CV-10-350, (b) CV-20-350, (c) CV-10-800 and (d) CV-33-800.

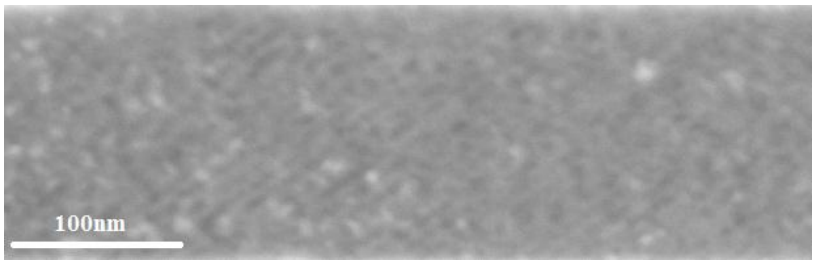

Figure 22 STEM micrograph of CV-10-800 film. The bright spots are vanadium, darker area is carbon and black area are pores.

For PSD in carbon-vanadium films, CV-10-350 film exhibits the largest average pore radius (2.7 nm, Figure 23a) among all the polymer-V composite films, which is supported by XRD results that CV-10-350 film has the smallest contraction. Corresponding to XRD results, CV-20-350 and CV-33-350 films maintain about the same pore size as pure FDU16-350 film. However, after pyrolysis at 800 ℃ (Figure 23b), from PSD results, all the carbon-V films show larger pore radius (1.4 nm for CV-10-800, 1.6 nm for CV-10-800 and 1.5 nm for CV-20-800) than FDU16-800 (1 nm), which is also consistent with contraction results that carbon-V films contract much less than pure carbon films.

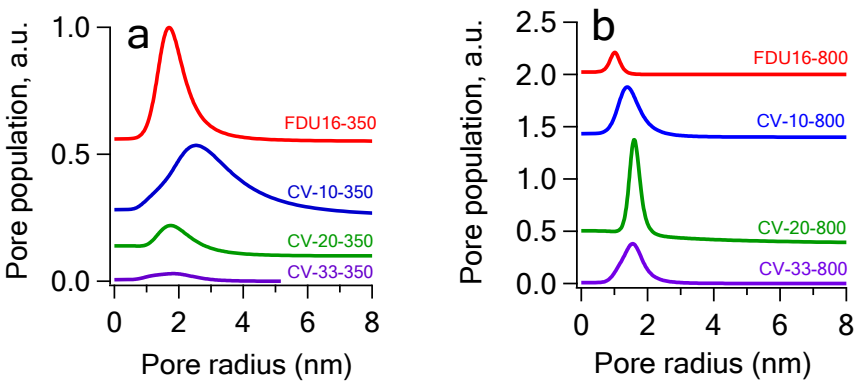

Figure 23 Pore size distributions of (a) polymer-V films and (b) carbon-V films.

Ordered mesoporous materials generally exhibit high specific surface areas, which are attractive for electrochemical applications. One issue in many cases is the poor electrical conductivity of the active material that necessitates addition of conductive filler such as carbon black.[19] To first assess any electrical conductivity limitations of the mesoporous composite films, a four-point probe test has been used and relatively high conductivity is found for all the films. As shown in Figure 24, the conductivity of the carbon film can be increased by addition of 10 wt% of either $Co(acac)_3$ or $VO(acac)_2$ into the precursor solution. The conductivity increases from approximately 22 S/cm for the pure mesoporous carbon film (in agreement with previous studies for FDU-16 carbonized at 800 ℃)[46,48] to approximately 40 S/cm. Addition of more organometallic decreases the electrical conductivity, but both Co-33-800 film (26 S/cm) and V-50-800 (20 S/cm) are comparable in conductivity to the neat carbon, FDU16-800. Interestingly, the conductivity of the cobalt-based composites decreases more at equivalent organometallic loading in

comparison to the vanadium-based composite films; the size of nanoparticle inclusions in the mesoporous films may be important to electrical conduction as the cobalt nanoparticles are larger. Previous studies of nickel oxide nanoparticles showed a significant increase in electrical conductivity for 5 nm nanoparticles in comparison to larger nanoparticles;[49] this enhancement was attributed to an increase in the defect density. A similar effect is likely responsible for the enhanced conductivity of the cobalt oxide and vanadium oxide – carbon mesoporous composite films. Additionally, there may also be some enhancement in the conductivity from the formation of a graphitic shell around the nanoparticles as suggested by the HR-TEM micrograph shown in Figure 17b. Nonetheless, all the mesoporous composite films exhibit relatively high electrical conductivity that should facilitate electrochemical processes.

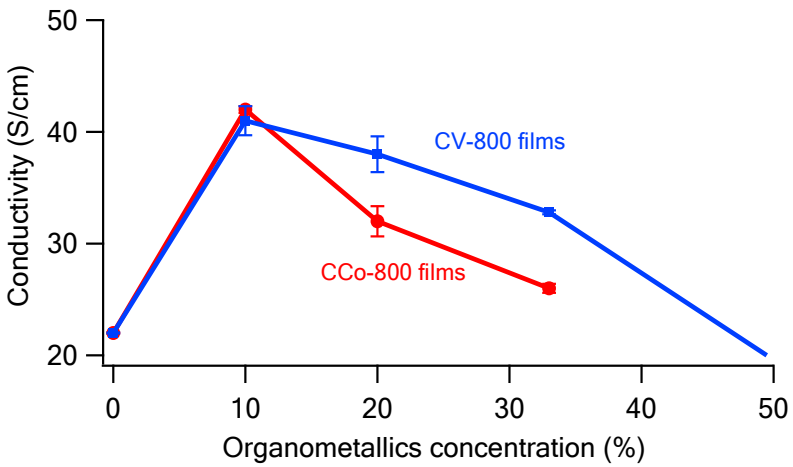

Figure 24 Electrical conductivity of films pyrolyzed at 800 ℃ is shown as a function of $Co(acac)_3/VO(acac)_2$ concentration in the precursor solution. Error bars represent standard deviation of 4 independent measurements.

To examine the (pseudo)capacitive properties of the films, cyclic voltammetry measurements are utilized for all the Co-C and V-C carbonized films at 100 mV s^{-1} using 1 M aqueous Na_2SO_4 for the electrolyte. Figure 25 illustrates the cyclic voltammograms for the composite films; the profiles are relatively flat and rectangular, which is typical for electrochemical double-layer capacitors.[19, 21] Even at relatively fast rates (100 mV/s), the capacitance of the films is appreciable. In order to quantify the capacitance of the films for direct comparison, the mass of films is estimated from the film area exposed to the electrolyte, film thickness and the film porosity using the density of graphite (2.27 g/cm^3). This calculation overestimates the mass of the film as the density of the amorphous carbon is generally between 1.8 and 2.1 g/cm^3; thus, the capacitance for the films reported here is a conservative estimate. By assuming the rate of electron transfer between the materials and solution is negligible, the capacitance of the films can be calculated as $C = dQ/dV$, where C is capacitance, Q is the charge and V is the potential.[43] For the pure mesoporous carbon film (FDU16-800), a capacitance of 22 F/g is observed for the first cycle. This capacitance agrees well with the capacitance for a mesoporous carbon powder with similar porosity and pore size (28 F/g at 2 mV/s).[21] The addition of the organometallic precursors can significantly increase the capacitance of the films; this is expected through the added pseodocapacitance of both cobalt oxide[50] and vanadium oxide.[51] For the cobalt-based films, the first cycle capacitance increases significantly with the added nanoparticles to 116 F/g for CCo-10-800 to 125 F/g for CCo-20-800.

This capacitance is actually larger than a pure Co_3O_4 film (74 F/g).[50] This enhanced capacitance is likely a result of both the accessibility of the cobalt oxide in the mesoporous carbon framework and the electrical conductivity imparted by the continuous carbon framework. Interestingly, the capacitance of the film actually decreases with further increases in the cobalt content, which also corresponds to a loss in the ordered mesostructure (see Figure 15). Major differences in these films are the ordered mesoporous framework (disordered at high $Co(acac)_3$ loadings and the size of the cobalt nanoparticles (increases at higher loadings), which might adversely impact the electrochemical performance. To further decouple the impact of nanoparticle size and film pore structure, the vanadium-based composite films can be examined as the nanoparticle size is relatively independent of $VO(acac)_2$ loading in the precursor film. Interestingly, the initial capacitance of the films increases steadily as the vanadium content is increased CV-10-800 (55 F/g), CV-20-800 (64 F/g), CV-33-800 (150 F/g), and CV-50-800 (215 F/g). This result suggests that the nanoparticle size may be a critical parameter for the capacitance of these mesoporous composites as the CV-50-800 film is disordered, but may maintain the small particle size as shown for CV-33-800. This increased capacitance for the smaller nanoparticles is consistent with results for hydrated RuO_2 powders;[52] the size dependence is attributed to surface utilization and mass transport limitations. We hypothesize similar origins to the observed capacitance behavior of the mesoporous carbon

composite films as the mesopores should provide minimial transport limitations at the scan rates examined.

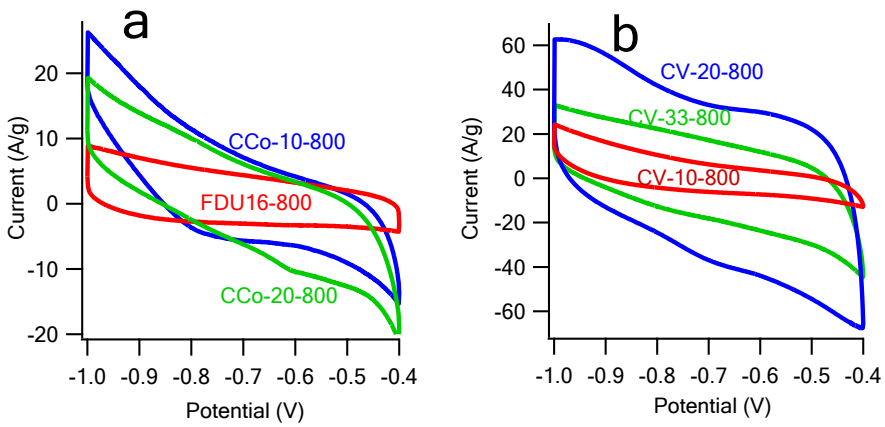

Figure 25 Cyclic voltammetry at 100 mV/s scan rate for (a) Co-based and (b) V-based composite mesoporous films in 1 M Na_2SO_4.

In addition to the initial capacitance of the films, the cyclic performance is critical to any electrochemical energy storage application. Figure 26 illustrates the capacitance for the different mesoporous carbon composite films for 500 charge/discharge cycles. For FDU16-800 and CCo-10-800, the specific capacitances are stable around 22 F/g and 115 F/g respectively for these 500 cycles. Conversely, the specific capacitance of Co-20-800 decreases rapidly to 83 F/g (maintains 66 % of initial capacitance) after 5 cycles, but then only decreases slightly further to 78 F/g (maintains 62 %) after 500 cycles. Further increasing the cobalt content results in a similar severe and rapid decrease in specific capacitance. For example, the capacitance of CCo-33-800 decreases from 99 F/g to 72 F/g after only 2 cycles; interestingly, this capacitance is not as stable with further decrease in

capacitance down to 40 F/g through 500 cycles. The capacitance loss is typically attributed to irreversible reactions of electrolyte with adsorbed impurities on the surface of the electrode. However, this instability is most pronounced for the higher Co loadings. For carbon-vanadium carbonized films (Figure 26b), the lower capacitance films (FDU16-800, CV-10-800 and CV-20-800) are nearly invariant with electrochemical cycling. However, the capacitance of CV-50-800 drops from 215 to 160 F/g (maintains 74%) and CV-33-800 drops from 150 to 103 F/g (maintains 69%) after only 10 cycles. However, the capacitance of these films is only slightly decreased upon further cycling (up to 500 cycles).

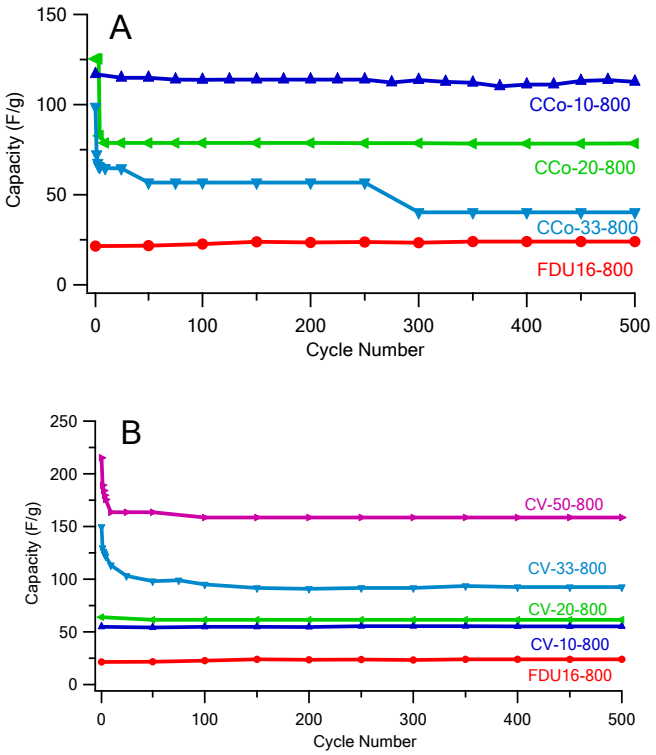

Figure 26 Cycle performance of (A) C-Co films and (B) C-V films.

An unusual observation from these electrochemical measurements on the mesoporous carbon composite films is that the specific capacitance does not necessarily always increase with the pseudocapacitive metal oxide content. Rather for the vanadium-based composites, there is a direct correlation between specific capacitance and vanadium content. Conversely for carbon-cobalt films, the average specific capacitance actually decreases with cobalt content. One major difference in these sample sets is the dispersion and size of the metal oxide nanoparticles. There is limited aggregation of nanoparticle in the carbon-vanadium films with the V is distributed relatively uniformly in the film. However for the carbon-cobalt films, higher Co concentration leads to larger (or aggregated) particles and a non-uniform texture is observed in these

films. Thus similar to traditional heterogeneous catalysts, good dispersion of small nanoparticles might be ideal for electrochemical applications based upon these limited results. Additional work that systematically varies the nanoparticle size in a conductive framework would be useful to understand the relationship between nanoparticle size and electrochemical performance. Nonetheless, these ordered mesoporous carbon composite films appear to possess attractive electrical and electrochemical properties for energy storage applications.

Two alternative methods have been utilized to identify the valence state for the Co and V. First from the TEM cross section, it is possible to obtain the chemical composition and binding information from electron energy loss spectroscopy (EELS) during the imaging. For the CCo-20-800 film (Figure 27), the cobalt is CoO on the basis of the binding energy which corresponds to Co-L2, 3 (780eV).

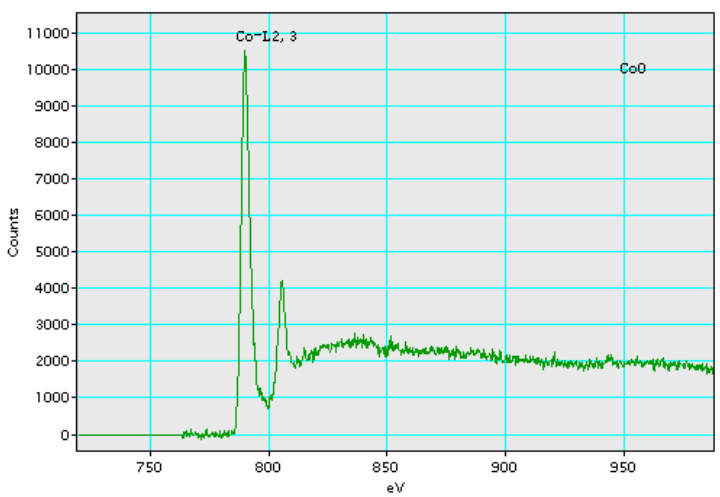

Figure 27 EELS of CCo-20-800 film.

Additionally, the unmanipulated film was examined using x-ray photoelectron spectroscopy (XPS) in ordere to further confirm the oxide state of Co (Figure 28). The strongest binding energy peak is at position 780.5eV, which corresponds to CoO $2P_{2/3}$. The results of both XPS and EELS showed the metal form is CoO.

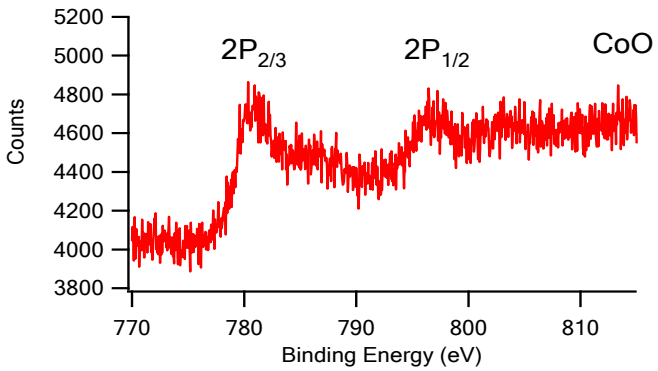

Figure 28 XPS of CCo-20-800 film.

As shown below for a vanadium-containing film, the bound oxygen appear to be associated with V_2O_5 (517.4eV, 2P2/3) in Figure 29. These results illustrate that the metal within the films is present as an oxide. We have included these data in the supplemental information file associated with the manscript.

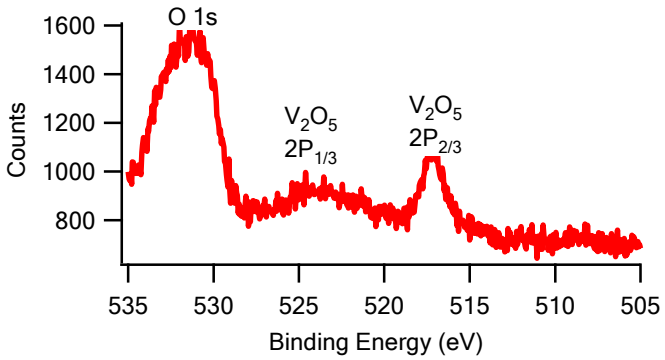

Figure 29 XPS of CV-33-800.

2.4 Conclusions

Ordered mesoporous carbon composite films are synthesized using tri-constituent self-assembly of resol (carbon precursor), an acac-based organometallic (metal oxide precursor) and Pluronic F127 (structure directing agent). The ordered morphology is confirmed using x-ray diffraction and transmission electron microscopy for both vanadium and cobalt containing composite films. There exists an upper limit for the organometallic content to maintain an ordered mesostructure that is precursor dependent. The size of the nanoparticle inclusions in the carbon framework is also dependent upon the organometallic precursor. For $Co(acac)_3$, small isolated nanoparticles are observed at low loading (10 wt %), but much larger aggregates/nanoparticles are observed at higher loadings(20 wt%). Conversely, small dispersed nanoparticles are observed for all compositions examined when using $VO(acac)_2$ as the organometallic precursor. These morphological differences appear to significantly impact the electrical and electrochemical properties of these films. The electrical conductivity increases initially with the introduction

of either V or Co to 10 wt % of the organometallic in the precursor film, but then decreases with further loading down to approximately the same conductivity as the initial pure carbon film at the highest $VO(acac)_2$ and $Co(acac)_3$ loadings examined. However, the conductivity of the films remains greater than 20 S/cm for all films and thus, electrical resistance should not be a limiting factor in electrochemical measurements. The capacitance of the mesoporous films is more strongly dependent upon the choice of organometallic precursor. As the concentration of $VO(acac)_2$ is increased in the precursor films, the composite carbon film capacitance is increased. There is a decrease in the electrochemical stability of the capacitance as $VO(acac)_2$ content is increased beyond 20 wt %; but even after 500 cycles, the capacitance is still greatest for the highest V content film. Conversely, the capacitance of the Co-C composite films is greatest for the 10 wt % $Co(acac)_3$ film. This result suggests that the small dispersed nanoparticles are most effective for increasing the capacitance of carbons.

2.5 Reference

1. Liang, C.; Li, Z.; Dai, S., Mesoporous carbon materials: Synthesis and modification. *Angewandte Chemie International Edition* **2008**, *47*, 3696-3717.

2. Schüth, F., Non-siliceous mesostructured and mesoporous materials†. *Chemistry of Materials* **2001**, *13*, 3184-3195.

3. Gao, P.; Wang, A.; Wang, X.; Zhang, T., Synthesis of highly ordered ir-containing mesoporous carbon materials by organic–organic self-assembly. *Chemistry of Materials* **2008**, *20*, 1881-1888.

4. Liu, C.-Y.; Chen, C.-F.; Leu, J.-P.; Lu, C.-C.; Liao, K.-H., Fabrication and carbon monoxide sensing characteristics of mesostructured carbon gas sensors. *Sensors and Actuators B: Chemical* **2009**, *143*, 12-16.

5. Wang, G.; Xing, W.; Zhuo, S., Application of mesoporous carbon to counter electrode for dye-sensitized solar cells. *Journal of Power Sources* **2009**, *194*, 568-573.

6. Baniamerian, M. J.; Moradi, S. E.; Noori, A.; Salahi, H., The effect of surface modification on heavy metal ion removal from water by carbon nanoporous adsorbent. *Applied Surface Science* **2009**, *256*, 1347-1354.

7. Lee, J.; Yoon, S.; Hyeon, T.; Oh, S. M.; Kim, K. B., Synthesis of a new mesoporous carbon and its application to electrochemical double-layer capacitors. *Chemical Communications* **1999**, 2177-2178.

8. Ryoo, R.; Joo, S. H.; Jun, S., Synthesis of highly ordered carbon molecular sieves via template-mediated structural transformation. *Journal of Physical Chemistry B* **1999**, *103*, 7743-7746.

9. Meng, Y.; Gu, D.; Zhang, F. Q.; Shi, Y. F.; Yang, H. F.; Li, Z.; Yu, C. Z.; Tu, B.; Zhao, D. Y., Ordered mesoporous polymers and homologous carbon frameworks: Amphiphilic surfactant templating and direct transformation. *Angewandte Chemie-International Edition* **2005**, *44*, 7053-7059.

10. Kosonen, H.; Valkama, S.; Nykanen, A.; Toivanen, M.; ten Brinke, G.; Ruokolainen, J.; Ikkala, O., Functional porous structures based on the pyrolysis of cured templates of block copolymer and phenolic resin. *Advanced Materials* **2006**, *18*, 201-+.

11. Liang, C. D.; Hong, K. L.; Guiochon, G. A.; Mays, J. W.; Dai, S., Synthesis of a large-scale highly ordered porous carbon film by self-assembly of block copolymers. *Angewandte Chemie-International Edition* **2004**, *43*, 5785-5789.

12. Tanaka, S.; Katayama, Y.; Tate, M. P.; Hillhouse, H. W.; Miyake, Y., Fabrication of continuous mesoporous carbon films with face-centered orthorhombic symmetry through a soft templating pathway. *Journal of Materials Chemistry* **2007**, *17*, 3639-3645.

13. Liang, C. D.; Dudney, N. J.; Howe, J. Y., Hierarchically structured sulfur/carbon nanocomposite material for high-energy lithium battery. *Chemistry of Materials* **2009**, *21*, 4724-4730.

14. Gorka, J.; Jaroniec, M., Incorporation of inorganic nanoparticles into mesoporous carbons synthesized by soft templating. *Journal of Physical Chemistry C* **2008**, *112*, 11657-11660.

15. Kwon, T.; Nishihara, H.; Itoi, H.; Yang, Q. H.; Kyotani, T., Enhancement mechanism of electrochemical capacitance in nitrogen-/boron-doped carbons with uniform straight nanochannels. *Langmuir* **2009**, *25*, 11961-11968.

16. Calvillo, L.; Moliner, R.; Lazaro, M. J., Modification of the surface chemistry of mesoporous carbons obtained through colloidal silica templates. *Materials Chemistry and Physics* **2009**, *118*, 249-253.

17. Hu, Q. Y.; Kou, R.; Pang, J. B.; Ward, T. L.; Cai, M.; Yang, Z. Z.; Lu, Y. F.; Tang, J., Mesoporous carbon/silica nanocomposite through multi-component assembly. *Chemical Communications* **2007**, 601-603.

18. Liu, R. L.; Shi, Y. F.; Wan, Y.; Meng, Y.; Zhang, F. Q.; Gu, D.; Chen, Z. X.; Tu, B.; Zhao, D. Y., Triconstituent co-assembly to ordered mesostructured polymer-silica and carbon-silica nanocomposites and large-pore mesoporous carbons with high surface areas. *Journal of the American Chemical Society* **2006**, *128*, 11652-11662.

19. Li, H. Q.; Liu, R. L.; Zhao, D. Y.; Xia, Y. Y., Electrochemical properties of an ordered mesoporous carbon prepared by direct tri-constituent co-assembly. *Carbon* **2007**, *45*, 2628-2635.

20. Zhao, X. C.; Wang, A. Q.; Yan, J. W.; Sun, G. Q.; Sun, L. X.; Zhang, T., Synthesis and electrochemical performance of heteroatom-incorporated ordered mesoporous carbons. *Chemistry of Materials* **2010**, *22*, 5463-5473.

21. Patel, M. N.; Wang, X.; Wilson, B.; Ferrer, D. A.; Dai, S.; Stevenson, K. J.; Johnston, K. P., Hybrid mno2-disordered mesoporous carbon nanocomposites: Synthesis and characterization as electrochemical pseudocapacitor electrodes. *Journal of Materials Chemistry* **2010**, *20*, 390-398.

22. Lou, X. W.; Deng, D.; Lee, J. Y.; Archer, L. A., Preparation of sno2/carbon composite hollow spheres and their lithium storage properties. *Chemistry of Materials* **2008**, *20*, 6562-6566.

23. Bruce, P. G.; Scrosati, B.; Tarascon, J. M., Nanomaterials for rechargeable lithium batteries. *Angewandte Chemie-International Edition* **2008**, *47*, 2930-2946.

24. Chou, S.-L.; Wang, J.-Z.; Sun, J.-Z.; Wexler, D.; Forsyth, M.; Liu, H.-K.; MacFarlane, D. R.; Dou, S.-X., High capacity, safety, and enhanced cyclability of lithium metal battery using a v2o5 nanomaterial cathode and

room temperature ionic liquid electrolyte. *Chemistry of Materials* **2008**, *20*, 7044-7051.

25. Das, S. K.; Darmakolla, S.; Bhattacharyya, A. J., High lithium storage in micrometre sized mesoporous spherical self-assembly of anatase titania nanospheres and carbon. *Journal of Materials Chemistry* **2010**, *20*, 1600-1606.

26. Jiao, F.; Bruce, P. G., Mesoporous crystalline beta-mno2- a reversible positive electrode for rechargeable lithium batteries. *Advanced Materials* **2007**, *19*, 657-+.

27. Zhi, L.; Hu, Y.-S.; Hamaoui, B. E.; Wang, X.; Lieberwirth, I.; Kolb, U.; Maier, J.; Müllen, K., Precursor-controlled formation of novel carbon/metal and carbon/metal oxide nanocomposites. *Advanced Materials* **2008**, *20*, 1727-1731.

28. Lou, X. W.; Li, C. M.; Archer, L. A., Designed synthesis of coaxial sno2@carbon hollow nanospheres for highly reversible lithium storage. *Advanced Materials* **2009**, *21*, 2536-2539.

29. Esmanski, A.; Ozin, G. A., Silicon inverse-opal-based macroporous materials as negative electrodes for lithium ion batteries. *Advanced Functional Materials* **2009**, *19*, 1999-2010.

30. Li, Q.; Xu, J.; Wu, Z.; Feng, D.; Yang, J.; Wei, J.; Wu, Q.; Tu, B.; Cao, Y.; Zhao, D., Facile synthesis of highly stable and well-dispersed mesoporous zro2/carbon composites with high performance in oxidative dehydrogenation of ethylbenzene. *Physical Chemistry Chemical Physics* **2010**, *12*, 10996-11003.

31. Ishii, Y.; Kanamori, Y.; Kawashita, T.; Mukhopadhyay, I.; Kawasaki, S., Mesoporous carbon–titania nanocomposites for high-power li-ion battery anode material. *Journal of Physics and Chemistry of Solids* **2010**, *71*, 511-514.

32. Wang, D.; Kou, R.; Choi, D.; Yang, Z.; Nie, Z.; Li, J.; Saraf, L. V.; Hu, D.; Zhang, J.; Graff, G. L.; Liu, J.; Pope, M. A.; Aksay, I. A., Ternary self-assembly of ordered metal oxide−graphene nanocomposites for electrochemical energy storage. *ACS Nano* **2010**, *4*, 1587-1595.

33. Urade, V. N.; Hillhouse, H. W., Synthesis of thermally stable highly ordered nanoporous tin oxide thin films with a 3d face-centered orthorhombic nanostructure. *The Journal of Physical Chemistry B* **2005**, *109*, 10538-10541.

34. Baumann, T. F.; Fox, G. A.; Satcher, J. H.; Yoshizawa, N.; Fu, R.; Dresselhaus, M. S., Synthesis and characterization of copper-doped carbon aerogels. *Langmuir* **2002**, *18*, 7073-7076.

35. She, L.; Li, J.; Wan, Y.; Yao, X.; Tu, B.; Zhao, D., Synthesis of ordered mesoporous mgo/carbon composites by a one-pot assembly of amphiphilic triblock copolymers. *Journal of Materials Chemistry* **2011**, *21*, 795-800.

36. Zhan, Z.; Zeng, H. C., A catalyst-free approach for sol–gel synthesis of highly mixed zro2–sio2 oxides. *Journal of Non-Crystalline Solids* **1999**, *243*, 26-38.

37. Breitscheidel, B.; Zieder, J.; Schubert, U., Metal-complexes in inorganic matrices .7. Nanometer-sized, uniform metal particles in a sio2 matrix by sol-gel processing of metal-complexes. *Chemistry of Materials* **1991**, *3*, 559-566.

38. Meng, Y.; Gu, D.; Zhang, F.; Shi, Y.; Cheng, L.; Feng, D.; Wu, Z.; Chen, Z.; Wan, Y.; Stein, A.; Zhao, D., A family of highly ordered mesoporous polymer resin and carbon structures from organic−organic self-assembly. *Chemistry of Materials* **2006**, *18*, 4447-4464.

39. Dai, M.; Song, L.; LaBelle, J. T.; Vogt, B. D., Ordered mesoporous carbon composite films containing cobalt oxide and vanadia for electrochemical applications. *Chemistry of Materials* **2011**, *23*, 2869-2878.

40. Baklanov, M. R.; Mogilnikov, K. P.; Polovinkin, V. G.; Dultsev, F. N., Determination of pore size distribution in thin films by ellipsometric porosimetry. *Journal of Vacuum Science & Technology B: Microelectronics and Nanometer Structures* **2000**, *18*, 1385-1391.

41. Sing, K. S. W.; Everett, D. H.; Haul, R. A. W.; Moscou, L.; Pierotti, R. A.; Rouquerol, J.; Siemieniewska, T., Reporting physisorption data for gas solid systems with special reference to the determination of surface-area and porosity (recommendations 1984). *Pure and Applied Chemistry* **1985**, *57*, 603-619.

42. Boissiere, C.; Grosso, D.; Lepoutre, S.; Nicole, L.; Bruneau, A. B.; Sanchez, C., Porosity and mechanical properties of mesoporous thin films assessed by environmental ellipsometric porosimetry. *Langmuir* **2005**, *21*, 12362-12371.

43. Song, L.; Feng, D.; Fredin, N. J.; Yager, K. G.; Jones, R. L.; Wu, Q.; Zhao, D.; Vogt, B. D., Challenges in fabrication of mesoporous carbon films

with ordered cylindrical pores via phenolic oligomer self-assembly with triblock copolymers. *ACS Nano* **2009**, *4*, 189-198.

44. Lee, H.-J.; Soles, C. L.; liu, D.-W.; Bauer, B. J.; Lin, E. K.; Wu, W.-l.; Grill, A., Structural characterization of porous low-k thin films prepared by different techniques using x-ray porosimetry. *Journal of applied physics* **2004**, *95*, 5.

45. Smits, F. M., Measurement of sheet resistivity with the four-point probe. *The Bell Symtem Technical Journal* **1958**, 7.

46. Song, L.; Feng, D.; Campbell, C. G.; Gu, D.; Forster, A. M.; Yager, K. G.; Fredin, N.; Lee, H.-J.; Jones, R. L.; Zhao, D.; Vogt, B. D., Robust conductive mesoporous carbon-silica composite films with highly ordered and oriented orthorhombic structures from triblock-copolymer template co-assembly. *Journal of Materials Chemistry* **2010**, *20*, 1691-1701.

47. Fabregat-Santiago, F.; Mora-Seró, I.; Garcia-Belmonte, G.; Bisquert, J., Cyclic voltammetry studies of nanoporous semiconductors. Capacitive and reactive properties of nanocrystalline tio2 electrodes in aqueous electrolyte. *The Journal of Physical Chemistry B* **2002**, *107*, 758-768.

48. Li, X.; Larson, A. B.; Jiang, L.; Song, L.; Prichard, T.; Chawla, N.; Vogt, B. D., Evolution of mechanical, optical and electrical properties of self-assembled mesostructured phenolic resins during carbonization. *Microporous and Mesoporous Materials* **2011**, *138*, 86-93.

49. Biju, V.; Abdul Khadar, M., Ac conductivity of nanostructured nickel oxide. *Journal of Materials Science* **2001**, *36*, 5779-5787.

50. Shinde, V. R.; Mahadik, S. B.; Gujar, T. P.; Lokhande, C. D., Supercapacitive cobalt oxide (co3o4) thin films by spray pyrolysis. *Applied Surface Science* **2006**, *252*, 7487-7492.

51. Jayalakshmi, M.; Rao, M. M.; Venugopal, N.; Kim, K.-B., Hydrothermal synthesis of sno2–v2o5 mixed oxide and electrochemical screening of carbon nano-tubes (cnt), v2o5, v2o5–cnt, and sno2–v2o5–cnt electrodes for supercapacitor applications. *Journal of Power Sources* **2007**, *166*, 578-583.

52. Sugimoto, W.; Iwata, H.; Yokoshima, K.; Murakami, Y.; Takasu, Y., Proton and electron conductivity in hydrous ruthenium oxides evaluated by electrochemical impedance spectroscopy: The origin of large capacitance. *The Journal of Physical Chemistry B* **2005**, *109*, 7330-7338.

CHAPTER 3

IMPACT OF COMPOSITION AND MICROPOROSITY ON ADSORPTION OF METHYLENE GREEN BY MAGNETIC MESOPOROUS CARBON-COBALT COMPOSITES

3.1 Introduction

Ordered mesoporous carbons have been proposed as adsorbents for chemical separations and electrodes in energy storage and sensors[1-5] due to their large surface area, narrow pore size distribution, chemically inert, mechanical stability and significant adsorption capability.[6-8] The first synthesis of ordered mesoporous carbon frameworks reported by Ryoo and coworkers[9] used sucrose as the carbon source and mesoporous silica molecular sieve MCM-4 [10] as a sacrificial hard template. However, a structural transformation occurs when etching the silica template.[11] For a mirror replica of the template in carbon, an alternative templates are used such as SBA-15[12] to yield a mesoporous carbon (CMK-3).[13] This hard templating route has been the preferred method for the fabrication of ordered mesoporous carbons, but several soft templating routes have been reported more recently.[14-17] These soft templating routes provide processing advantages by eliminating the synthesis of a template and its subsequent etching. However, the first reported soft templating route required a custom synthesized template and long processing times to achieve an ordered mesoporous film.[17] Further advances allow more traditional commercial surfactant templates in conjunction with a reactive resorcinol-formaldehyde mixture[15,16] or pre-synthesized oligomeric

phenolic resins (resol)[14] to be co-assembled to yield mesoporous carbons upon pyrolysis. This later methodology has the advantage that the precursor solution is stable and produces ordered mesostructures much more reproducibly than the former route in our hands. Moreover, the stable resol precursor enables co-assembly of multiple components to fabricate order mesoporous composite materials.[18] This versatility in the synthetic procedure provides a facile route to a variety of ordered mesoporous metal-carbon and metal oxide-carbon materials.[7,19-25]

These materials exhibit high specific surface area, regular pore size, and large pore volume along with tunable surface chemistry, which makes them attractive as adsorbents.[26,27] For example, bulky dyes in aqueous solution are readily adsorbed by mesoporous carbons, but subsequent separation of the fine powder from the suspension is difficult for *in-situ* applications.[18,28] One route for their separation is through the incorporation of magnetic nanoparticles for magnetically separable adsorbents.[6,29-31] For example, Zhang and Li[6] synthesized rattle-like structures with Fe_3O_4 nanoparticles in the interior of mesoporous carbon capsules, which exhibit high specific surface area (1570 m^2/g) and saturation magnetization (5.5 emu/g, 10.5 wt % Fe_3O_4). Similarly, oxidation of Fe^{3+} ions in FDU-18 produces Fe nanoparticles with a saturated magnetization of 4.2 emu/g.[29] Alternatively, Zhao and co-workers[30] used triconstituent cooperative assembly of triblock polymer F127, resol, and nickel chloride with polystyrene colloidal crystals to generate hierarchical magnetically-separable ordered porous carbons that exhibit high adsorption

capacity (100 mg/g) for methylene blue and a saturation magnetization of 3.8 emu/g (11 wt% Ni). Several shortcomings still exist in these materials for acceptable use in aqueous separations. First, the magnetic susceptibility of Ni is modest and thus either large Ni concentrations or high field magnets will be required for efficient separations. Second although Fe, Fe_3O_4, and Co have improved magnetic properties compared to Ni, acidic aqueous solutions can leach the transition metal into solution thereby decreasing the reuse potential of such materials.[32,33] Ryoo et al.[32] illustrated that the acidic media stability of embedded Co nanoparticles in mesoporous carbon can be significantly improved by a secondary treatment and subsequent carbonization to yield a graphitic shell. However, this procedure requires many steps through a hard template method with three >300 ℃ steps required for making the Co more resistant to etch in acidic media, but these Co-CMK materials exhibit the highest saturation magnetization (5.53 emu/g, 9.5 wt % Co on basis of residual after HF etching) of any reported mesoporous carbon composite. However, the multiple steps required to form this structure is not desired. Moreover, the typical route to increasing the accessible surface area is through silica-carbon co-assembly followed by HF or NaOH etching; the typical metal nitrate precursors will tend to segregate to the silica phase and be removed during etching. This appears to limit the surface area for these magnetically separable mesoporous carbon adsorbents, which is a key factor in the loading capacity.[8]

To overcome these limitations, two design rules are employed in this work: first, the metal precursor should be selected to minimize concentration

in the silica phase and second, the precursor should promote the formation of a carbon shell around the nanoparticle to provide stability in acidic aqueous media. For this second criteria, it is known that organometallic cobalt precursors yield a graphene shell around Co nanoparticle by simple heating in an inert atmosphere.[34] We have previously introduced Co into ordered carbon framework through tri-constituent self-assembly method by using $Co(acac)_3$ as precursor[35] where, a graphitic shell is obtained around nanoparticles dispersed in a mesoporous carbon matrix. This precursor may also be more apt to segregate into the resol phase to minimize the loss of Co nanoparticles when etching silica to increase surface area. Here, the co-assembly of pluronic F127, resol, $Co(acac)_3$, and tetraethyl orthosilicate (TEOS) is applied to the fabrication of high surface area, magnetic, order mesoporous carbon powders. The morphological properties of these mesoporous powders are investigated by X-ray diffraction (XRD), transmission electron microscopy (TEM) and Brunauer-Emmett-Teller (BET) N_2 porosimetry. Superconducting quantum interference device (SQUID) magnetometer measurements indicate that these Co-containing composites exhibit stronger magnetization than has been previously report for magnetic mesoporous carbons. The adsorption performance is evaluated using methylene green, which is slightly larger than the previously examined methylene blue. The adsorption of methylene green appears strongly dependent upon the Co content, although finite pore size effects may also be important. The adsorption capacity does not scale directly with surface area however. These results show that these mesoporous C-Co

materials are excellent candidate materials for magnetically-separable adsorbents.

3.2 Experimental Section

3.2.1 Materials

Sodium hydroxide (NaOH), phenol and formaldehyde (37 wt% in H_2O) were obtained from Sigma-Aldrich and used as received to synthesize the resol precursor as previously described. [14] Triblock copolymer surfactant, Pluronic F127 (M_w = 12 600 g/mol, PEO_{106}-PPO_{70}-PEO_{106}, BASF), was used to template the mesostructures, while Cobalt (III) acetylacetonate ($Co(C_5H_7O_2)_3$, 98+%, Strem Chemicals, Inc.) was the cobalt precursor. Tetraethyl orthosilicate (TEOS) was obtained from Sigma-Aldrich and used as silica precursor to increase the surface area of the composites.[36] Methylene green, $C_{16}H_{17}ClN_4O_2S$ (Sigma-Aldrich), was used as a model bulky dye for adsorption studies from aqueous solution.

3.2.2 Sample preparation

The synthesized resol was first dissolved in tetrahydrofuran (THF) at 30 wt%. Mesostructure polymer-resins (similar to FDU-16)[14] were templated by using triblock copolymer F127 with molar composition of phenol/formaldehyde/NaOH/F127 = 1:2:0.1:0.006. To incorporate Co nanoparticles (C-Co powders), $Co(acac)_3$ pre-dissolved at 2 wt% in THF solution was added into the polymer-resins solution. Additional THF was then added to the solution to maintain a constant 10 wt % solids for all compositions examined. Solutions were stirred for 20 min to obtain a dark

green homogeneous solution, which was spread onto watch-glasses to evaporate the THF for 5-8 h. The resol was then crosslinked by heating to 120 ℃ for 24 h to solidify the network.

Carbon-silica-cobalt (CS-Co) powders were synthesized using TEOS, resol, Pluronic F127 and $Co(acac)_3$ in ethanolic solution. The composition of the solution without $Co(acac)_3$ was formulated to match CS-68[37] as synthesized previously with all solutions at 10 wt % solids. Solutions were stirred for 1h under 45 ℃ and then were spread onto watch-glasses to evaporate ethanol for 5-8 h. Subsequently, the samples were thermopolymerized at 120 ℃ for 24 h.

Mesoporous carbon composites were obtained after carbonization at 800 ℃ for 3 h, with heating rates of 1 ℃/min below 600 ℃, and 5 ℃/min above 600 ℃. All the pyrolysis processes were under a nitrogen atmosphere with a flow rate of 140 $cm^3\,min^{-1}$. After carbonization, the obtained powders were denoted as FDU16 (pure carbon), CCo-X and CS-Co-X, where X is the wt % of $Co(acac)_3$ in the solids of casting solution. For the CS-Co powder, the silica was removed using 1M NaOH ethanol-water solution. The powders were soaked for three days and washed with distilled water at least five times prior to their subsequent characterization.

3.2.3 Characterization techniques

X-ray diffraction (XRD) was performed in a θ/2θ geometry using Cu Kα source (Panalytical X'Pert PRO) with 2θ varied from 0.5 to 3.0° for small angle XRD (mesostructure) and from 10 to 80 ° for wide angle XRD (crystal

structure). A parallel plate collimator (PPC) was used in combination with an incident beam optical module to provide an X-ray beam with very low divergence. Nitrogen adsorption–desorption isotherms at 77 K were measured using Tristar II 3020(Micromeritics). Prior to these measurements, the samples were degassed at 300 ℃ under vacuum for at least 1 h. Specific surface areas were calculated using the Brunauer–Emmett–Teller (BET) method in a relative pressure range of P/P_0 = 0.05–0.25. The pore size distribution (PSD) and pore volume were estimated from the adsorption branch of the isotherm using the Barrett–Joyner–Halenda (BJH) model. Transmission electron microscopy (TEM) was performed on powder materials using JEOL 2010F microscope operating at 200 keV. To prepare samples, the carbonized powder materials were ground in a marble mortar with a pestal and dispersed in ethanol using sonication for 5 min. One drop of the resulting slurry was placed on a TEM copper grid and dried for 30 min prior to imaging. Magnetic properties of the powders were elucidated using quantum interference device magnetometer (SQUID, Quantum Design, MPMS5) at ambient temperature. The absorbance spectra for methylene green adsorption quantification were measured using a UV-vis (Agilent 8453) spectrophotometer. The amount of adsorbed dye (mg/g) was calculated by $Q = \frac{(C-C_0)V}{W}$, where C is the concentration of the dye solution after adsorbed, C_o is the original concentration, and V is the volume of the dye solution and W is the mass of the adsorbent. Elemental compositions of the powders were obtained after the

powder was digested in a block digester. The composition of C and H in the all the powder samples was obtained using CHN Elemental Analysis - PE2400. Thermo iCAP 6300 ICP-OES was utilized to investigate the Co composition in the powder.

3.3 Results and discussion

3.3.1 Morphological characterization of mesoporous carbon and carbon-cobalt composite powders

The composition of these mesoporous powders is determined by elemental analysis after carbonization. As expected, increasing the concentration of $Co(acac)_3$ in the solids of casting solution leads to an increase in the Co content after carbonization as shown in Table 3. The Co content varies from 0 to 8.3 wt % in the samples examined. Interestingly for the two powders that initially contained 10 wt % $Co(acac)_3$ prior to carbonization, a similar Co content also remains in the powder after carbonization. The difference between these power sets (C-Co vs CS-Co) is the inclusion of silica during the synthesis in the CS powders that is subsequently extracted by NaOH. As the solids composition is initially the same, the Co is not strongly selectively segregated to either phase and some fraction of the Co is removed with the silica. Nonetheless, a significant Co concentration is still present in these powders. To understand how these compositional changes impacts the pore characteristics, BET analysis is performed as illustrated in Figure 27. Typical type IV isotherms of N_2 sorption with H_1 hysteresis loops at 77 K are found for both sets of materials. For both C-Co and CS-Co powders, the

surface area decreases as Co content is increased, while the average pore size and volume calculated using BJH model increases (Table 3). These results suggest that the Co acts to mechanically strengthen the framework during carbonization to partially supress volumetric contraction, similar to the role of silica in the CS powder.[36] Due to the removal of silica after carbonization to yield micropores, the CS powders exhibit much higher surface areas and pore volumes in comparison to the analogous C-Co powders.

Table 3 Physical characteristics of carbon, C-Co and CS-Co composite powders

Samples	Surface area (m^2/g)	Avg. pore diameter (nm)	Pore volume (cm^3/g)	Co content (wt %)
FDU16-800	671	2.9	0.14	0
CCo-10-800	441	4.2	0.21	4.2
CCo-20-800	355	4.8	0.24	8.3
CS-68-800	1520	3.6	1.51	0
CS-Co-1-800	1444	4.1	1.62	0.85
CS-Co-4-800	1393	4.2	1.68	2.09
CS-Co-10-800	1125	4.3	1.69	4.78

Further examining the pore characteristics through the pore size distribution (PSD) calculated using BJH model (Figures 30B and 30D), it is clear that the PSD is quite narrow as expected for a templated material. However, both cobalt containing powder sets have a distribution of pores that is not present for Co-free materials. For the C-Co powders, there is a broader distribution of large pores in the range of tens of nm. We hypothesize that

these larger pores are a result of the reduction of the cobalt precursor *in-situ*; recently, Zhao and coworkers have reported controlled activation of mesoporous carbon using copper oxide that is reduced by the carbon to yield larger and more interconnected mesopores.[38] Similarly, the incorporation of unreduced Co into the resol framework could lead to larger pores from the reduction during carbonization. Moreover, pore volume of CCo-10-800 and CCo-20-800 are 1.5 and 1.7 times (based upon integration of pores sizes from 1.7 to 300 nm determined from BJH model) greater than FDU16-800, respectively.

For the CS-Co powders, there is a bimodal distribution of pores with these two distributions straddling the distribution of the Co-free analog. The silica that is present in the framework likely limits interconnecting the mesopores through activation; during extraction of the silica, Co nanoparticles embedded in the silica are also removed, which lead to the smaller pores. The average pore size increases from 3.6 to 4.9 nm, and pore volume is also increased from 1.51 to 1.69 cm^3/g in comparing CS-68-800 to CS-Co-800 powders. Combined these results suggest that adding Co into carbon framework decreases contraction during carbonization at 800 ℃, leading to average larger pore size in the composite powders than analogous carbon powders. This larger pore size would yield a smaller surface area from geometric argument and larger pore volume, consistent with the results listed in Table 3.

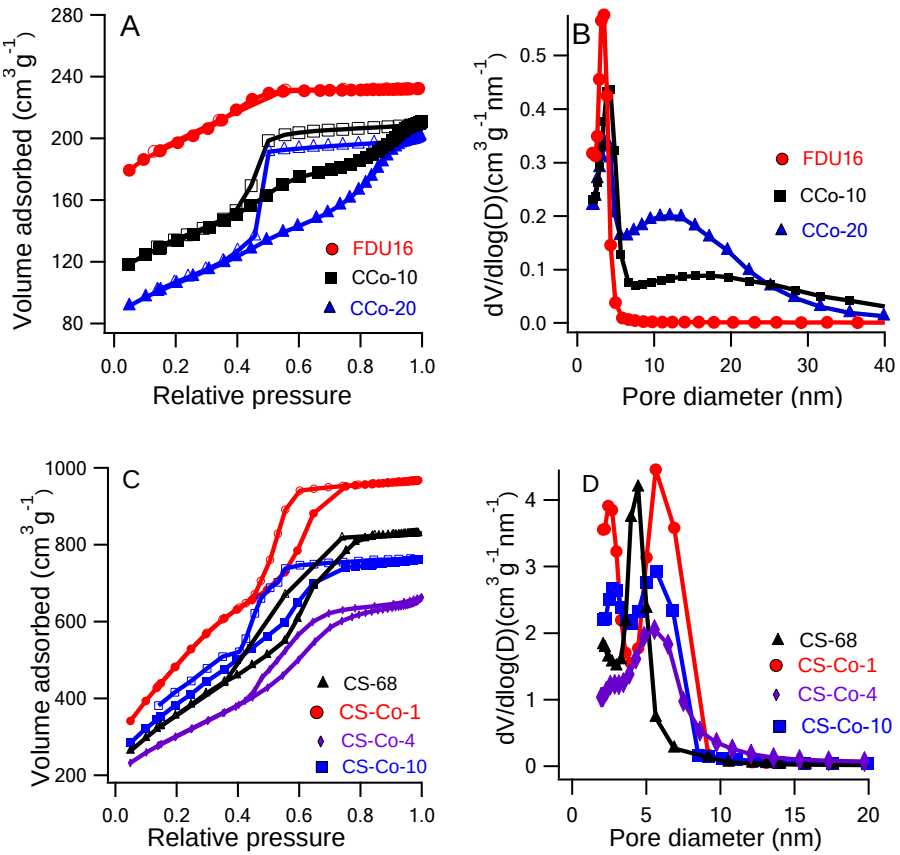

Figure 30 (A and C) Nitrogen adsorption-desorption isotherms, and (B and D) pore size distributions. The pore size distributions are calculated from the adsorption brand of the isotherms by using BJH model.

To further understand the structure of these materials, XRD is utilized to provide insight into the ordered mesophase and crystallinity of the framework. Figure 31 illustrates the low angle diffraction to examine the mesostructure; FDU16-800 exhibits a strong diffraction peak at 2θ = 1.05° (Figure 31A), which is consistent with prior reports for FDU16 powders 14. A second order reflection is also clearly present for this powder. The intensity of this primary diffraction peak becomes significantly weaker in CCo-10-800

with a slight shift to lower angle, which is consistent with decreased contraction of the powder. Interestingly, no diffraction peak can be readily observed for CCo-20-800 despite the narrow pore size distribution from BJH analysis. Similarly, the primary diffraction peak becomes weaker as Co content increases for the CS-Co-800 powders as illustrated in Figure 28B. No mesoscale diffraction peak is found for CS-Co-10-800, similar to the CCo-20-800 powder.

These changes in the diffraction patterns suggest that addition of $Co(acac)_3$ leads to a less ordered mesostructure. This behavior is consistent with previous results for Ni containing mesoporous carbons,[39] where a significant decrease in diffraction is observed when the Ni concentration exceeds 12 wt % and no diffraction is observed for higher concentrations. However, ordered morphologies were still observed for these Ni-C powders from TEM. As x-rays are sensitive to changes in electron density, the inclusion of random metal nanoparticles could significantly impact the local contrast. Additionally, the nanoparticles tend to be larger than the typical pore wall, which leads to distortion of the lattice of the mesostructure.

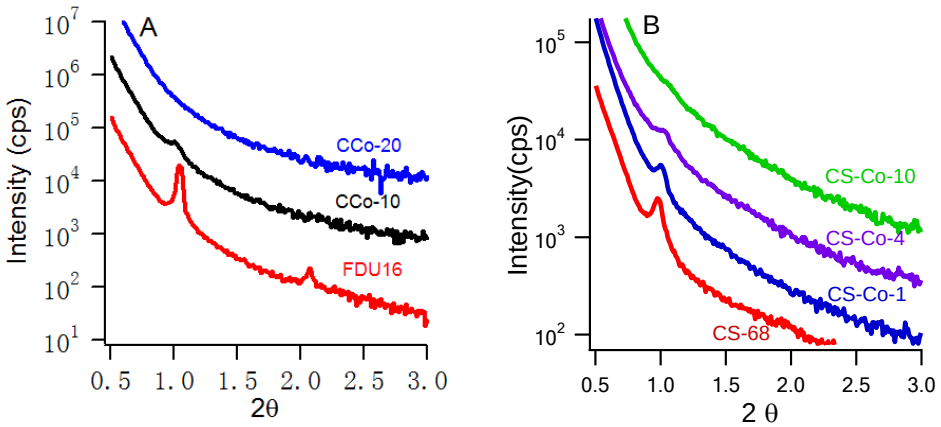

Figure 31 Small angle XRD profiles of (A) FDU16-800, CCo-10-800 and CCo-20-800 powders and (B) CS-68-800, CS-Co-1-800, CS-Co-4-800 and CS-Co-10-800 powders.

To investigate the morphology of these powders in more detail, TEM is utilized to directly observe the mesostructure of the carbon powders in real space as illustrated by representative micrographs in Figure 32. An ordered mesostructure is clearly present in the micrographs with the exceptions of CCo-10-800 (Figure 32c) and CS-Co-10-800 (Figure 32h). There appears to be degradation in the long range order of the mesopores as the Co content is increased. However, even for the powders that lack a well-defined mesostructure (Figure 32c and 32h), the pores appear uniform in size and resemble the worm-like micelle morphology observed in mesoporous silica 40. This morphology could provide transport advantages for large molecules over the cage-like structure in the more ordered materials.

In addition to the mesopores, nanoparticles are dispersed the composite materials as evidenced by the dark spots in the micrographs. At the lowest

concentration of $Co(acac)_3$ examined (1%), nanoparticles cannot be clearly observed in the micrograph (Figure 32f). This is likely due to the low concentration of Co and the small associated nanoparticle size. As the Co concentration increases, the size of the nanoparticles also increases. In many cases, the size of these nanoparticles after carbonization is much larger than the wall thickness and thus these nanoparticles will impact the long range ordered structure of the mesopores. This is likely the culprit for the very weak diffraction peak from CCo-10-800 and in CS-Co-4-800. Nonetheless, the pore size and morphology is fairly well defined for all the materials, which is consistent with the narrow pore size distributions determined from adsorption experiments.

To further investigate the nanoparticle morphology, HR-TEM is utilized to examine the crystal structure in Co-20-800. These nanoparticles are polycrystalline (Figure 32d) with an apparent graphitic carbon coating around the nanoparticle. This coating would be consistent with direct pyrolysis of $Co(acac)_3$[34] and our prior observations in thin films.[29] This coating type of coating has previously been shown to be important for material stability in acidic media,[32] but the coating of the Co in the prior case required multiple processing steps;[32] here, the mesostructure, nanoparticles and its coating are all formed in a one-pot approach with a single high temperature processing step.

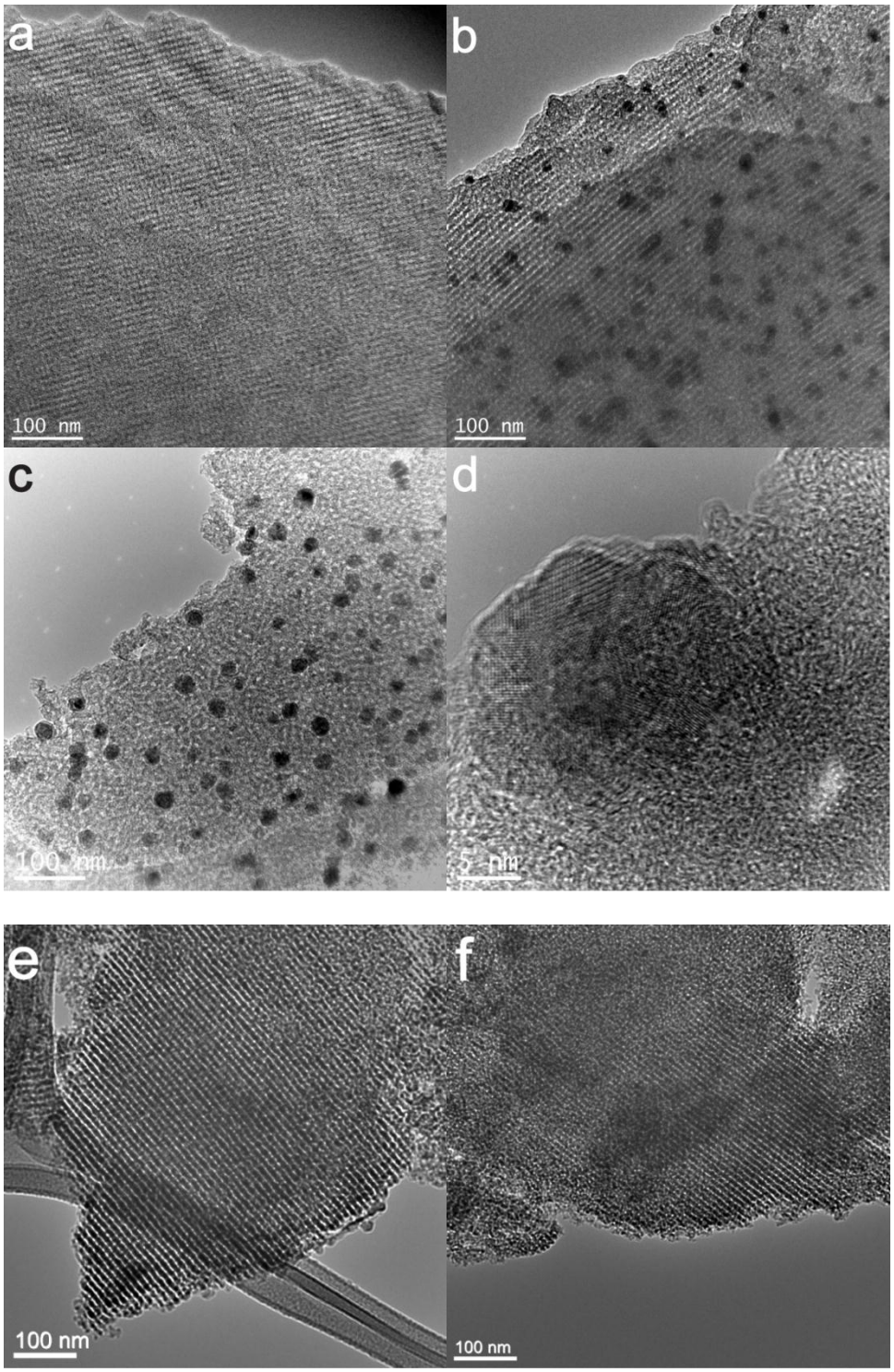
a
100 nm
b
100 nm
c
100 nm
d
5 nm
e
100 nm
f
100 nm

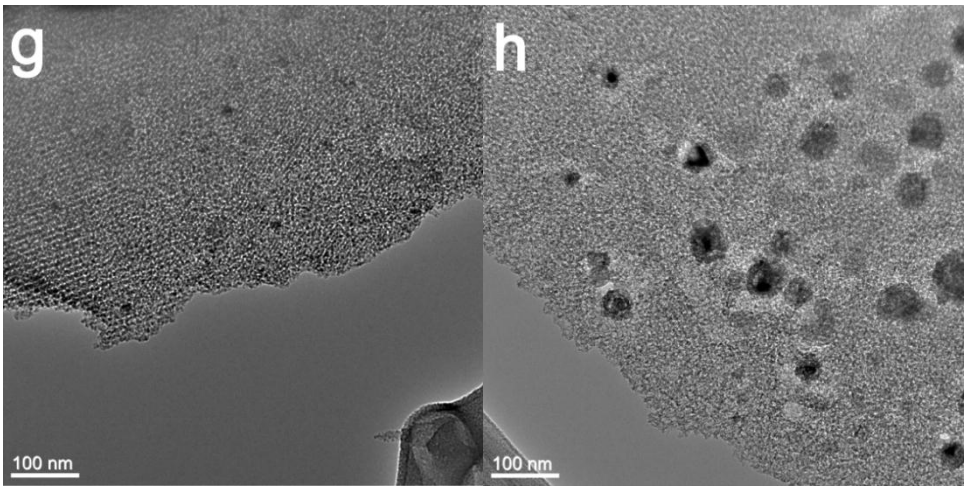

Figure 32 TEM micrographs of (a) FDU16-800, (b) CCo-10-800, (c) CCo-20-800, (e) CS-68-800, (f) CS-Co-1-800, (g) CS-Co-4-800 and (h) CS-Co-10-800; additionally, HR-TEM micrograph of (d) nanoparticle from CCo-20-800 illustrates the crystalline nature of the nanoparticle.

To understand the composition of the nanoparticles dispersed in both C-Co and CS-Co powders, wider angles (2Θ, 10 - 80 °) are utilized in XRD to determine the crystal structure as illustrated in Figure 33. For the two Co free powders, FDU16-800 and CS-68-800, a weak peak shoulder at ≈ 21° and a broad peak at ≈ 43° are observed, which correspond to (002) and (100) planes from typical graphitic carbons.[41] The calculated d-spacing of the (002) plane is 0.423 nm, which is larger than fully graphitic carbon formed at 2800 ℃ (0.343 nm).[41] This increased spacing and broad diffraction peak are consistent with an amorphous carbon framework as previously shown for FDU16-800.[15] In contrast, the powders that contain Co exhibit a shift in the (002) diffraction peak to lower angle (25.8 °) and this peak narrows significantly in comparison to the Co-free analogs. This sharper peak is consistent with graphitic carbon

and previous reports of formation of graphitic carbon upon doping carbonizable polymers with transition metals such as Ni and Co.[42,43] In addition to the diffraction related to the carbon structure, two additional diffraction peaks are observed for the C-Co composite materials, which match the (111) and (200) planes of metallic cobalt. Thus unlike thin films where CoO is formed,[35] metallic cobalt nanocrystals are formed in the powders. To explain this apparent contradiction, the relative reducing atmosphere must be considered. In order to efficiently open the mesopores,[44] approximately 1-2 % O_2 is present in the nitrogen gas stream during carbonization. For the thin films (< 200 nm thick), this is sufficient oxygen to prevent full reduction of the cobalt in the presence of carbon at elevated temperatures; additionally, there is oxygen present at the buried interface in the form of a thermal silicon oxide. Conversely for these powders, there is approximately 1 g of material initially such that a vast majority of the powder is exposed to a substantially more reducing environment, which likely leads to the formation of metallic cobalt. It should be noted that a small fraction of this material (exposed to sweep gas stream) might contain CoO nanoparticles; however, we see no evidence for CoO in these samples from XRD.

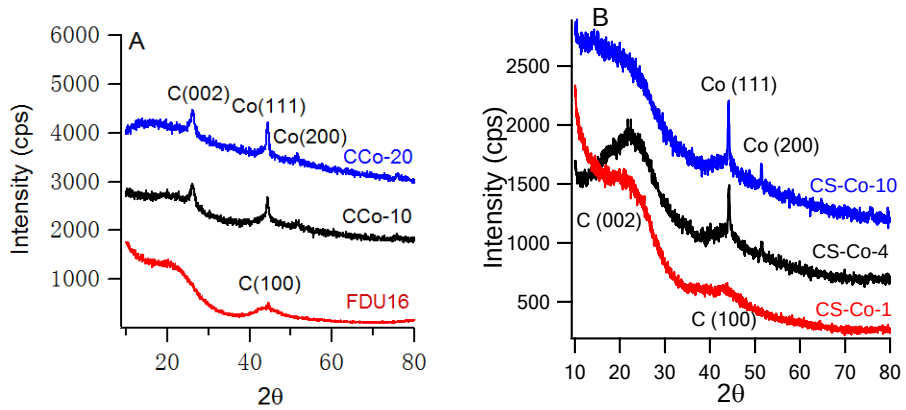

Figure 33 Wide-angle XRD profiles of (A) FDU16-800, CCo-10-800 and CCo-20-800 (B) CS-Co-1-800, CS-Co-4-800 and CS-Co-10-800 powders.

3.3.2 Adsorption properties

The hydrophobicity and (relatively) large pore size of mesoporous carbon makes them attractive as adsorbents of bulky organic molecules from aqueous solution.[14,16-18,28] Here to demonstrate the adsorption properties of these powders, the adsorption of methylene green from aqueous solution is examined, rather than the previously examined methylene blue.[30] There is an additional nitro- group on methylene green, which slightly increases its size in comparison to methylene blue. To quantify the adsorption behavior, UV-vis adsorption spectroscopy measurements are employed to determine the concentration of pollutants in the solution after addition of the mesoporous powders.

With the two sets of powders, we can distinguish the relative effects of pore size, surface area and cobalt on the adsorption capacity. In examining the C-Co powders, the maximum adsorption capacities increase as the Co content

increases: 2.0 mg/g for FDU16-800, 20 mg/g for CCo-10-800 and 90 mg/g for CCo-20-800. The 90 mg/g capacity is very similar to previous reports for mesoporous carbon with Ni nanoparticles for the adsorption of methylene blue.[30] However, the kinetics for the adsorption of the methylene green are quite slow in this case as nearly one week is required to saturate the adsorbent powders. From these adsorption measurements, it appears that the capacity is either limited by pore size or the presence of Co significantly increases the adsorption of methylene green; the surface area decreases with the methylene green capacity, which suggests that available surface adsorption sites are likely not the limiting factor.

The CS powders provide a route to try to deconvolute the pore size and Co content effect as the size of the mesopores in the CS-68-800 powder is significantly larger than that for FDU-16-800. In this case, the adsorption capacity increases from 2 mg/g for FDU-16-800 to 878 mg/g. This huge increase is somewhat unexpected given the maximum capacity for the C-Co powders is only 90 mg/g; this result demonstrates that the microporosity and its associated surface area formed by etching of the silica provides favorable sites for the adsorption of methylene green. The adsorption capacity can be even further increased by the incorporation of Co nanoparticles with maximum adsorption capacity of 1151 mg/g for the powders examined. Thus, the modification of the surface chemistry by the Co (and its catalyzed graphitization) appears to highly favor the adsorption of methylene green. The significantly higher the adsorption capacity in the CS-Co powders than in C-

Co powders can be explained by the higher surface area, which is able to accommodate more dye at the pore surface. It should be noted that the capacity of the CS-Co powders is significantly larger than other carbon adsorbents reported for bulky organic dyes. These include methyl orange (~300 mg/g) in mesoporous carbon CMK-3,[45] orange II (~650 mg/g) in CMK-3,[46] and methlylene blue (~100 mg/g) in Ni containing magnetic-separable hierarchially-ordered porous carbon.[30] One issue is the kinetics of adsorption for this system, but it could likely be improved by using a hierarchical design of porosity such as those introducted by Zhao and coworkers.[30]

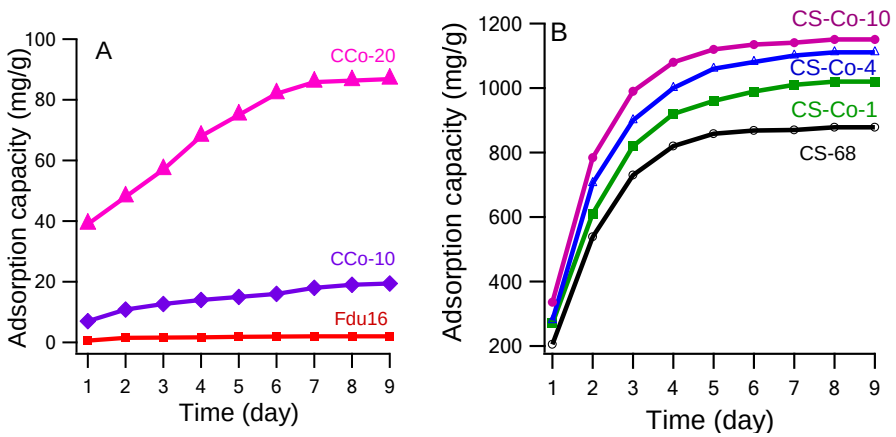

Figure 34 Adsorption capacity of methylene green for (A) FDU16-800, CCo-10-800 and CCo-20-800; (B) CS-68-800, CS-Co-1-800, CS-Co-4-800 and CS-Co-10-800 powders.

3.3.3 Magnetic properties

One issue with these carbon adsorbents is their recovery from suspension; historically, carbon has been notoriously difficult to remove from suspension.[47] However, the inclusion of Co nanoparticles in these powders

should enable their separation. Figure 35 illustrates pictorially the potential of these materials to be magnetically separated from suspension. Figure 35a shows the color of the initial methylene green solution. After addition of CCo-20-800 powder, the suspension was rapidly shaken (Figure 35b). These powders sediment is as shown in Figure 35c. However, these powders can more rapidly be removed from suspension by application of a magnetic field as shown in Figure 35d.

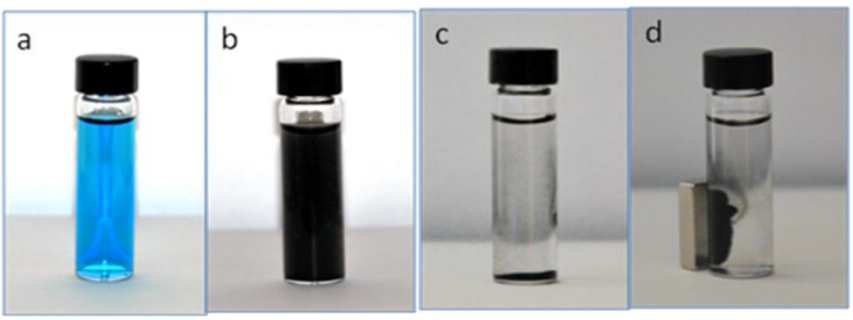

Figure 35 Images of (a) dye-polluted water; (b) after adding CCo-20-800 and vigorous shaking; (c) after sedimentation; and (d) after magnetic separation from the solution.

A SQUID magnetometer is utilized to quantify this magnetic behavior of the carbonized meosoporous composites. Figure 36 illustrates the field-dependent magnetization curve at room temperature for these composites. The magnetization curves of C-Co (Figure 36A) and CS-Co (Figure 36B) composites show an obvious hysteresis loop that result from the coercive force of cobalt nanoparticles. The saturation magnetizations for each composites is 4.8 emu/g for CCo-10-800 (4.2 wt% Co), 12.3 emu/g for CCo-20-800 (8.3 wt% Co), 0.01 emu/g for CS-Co-1-800 (0.85 wt% Co), 1.68 emu/g for CS-Co-

4-800 (2.09 wt% Co) and 3.83 emu/g for CS-Co-10-800 (4.78 wt% Co), respectively. To put these values in prospective, the ratio of saturation magnetization to the mass of Co is significantly greater than 4.98 emu/g of CoCMK with 9.5 wt% Co[32] except for the CS-Co-1-800 composite. The low saturation magnetization of CS-Co-1-800 might be expected, as no Co nanoparticles are obvious in the TEM micrographs (Figure 32f). Thus, there appears to be a lower limit for the Co loading to obtain powders sufficiently magnetic to be removed from suspension. A similar saturation magnetization (on mass basis of Co) was found using pre-formed cobalt nanoparticles with a multi-step, hard template approach (12.8 emu/g for 9 wt % Co).[48] Thus, the magnetic properties of these composite powders are better or comparable to prior literature reports and should be sufficient for recovery of the mesoporous powders from suspension using a magnetic field.

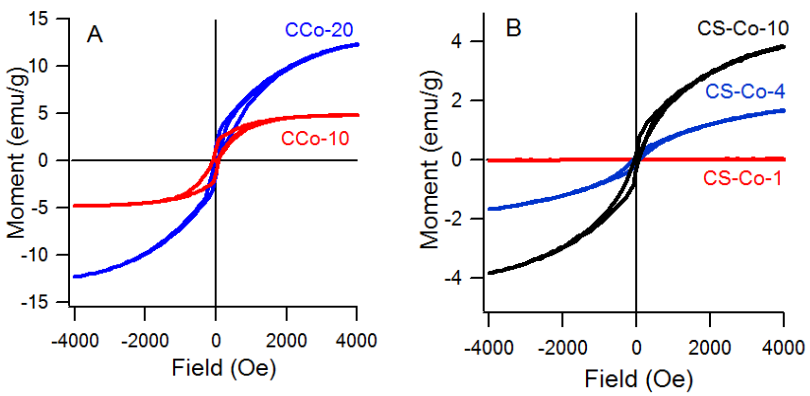

Figure 36 Magnetization of (A) CCo-800 and CCo-20-800; (B) CS-Co-1-800, CS-Co-4-800 and CS-Co-10-800 powders at room temperature.

One additional issue with Co nanoparticles is their low intrinsic

stability in acidic aqueous media. Similar mesoporous carbons with unprotected Co nanoparticles samples synthesized by Ryoo and co-workers[32] lose their magnetic properties completely after washing with dilute HCl. Similarly, Han and co-workers[49] showed Co nanoparticles quickly dissolve in 6M HCl with the appearance of light blue aqueous phase from Co. To test the stability of these Co nanoparticles, CCo-20-800 powders are soaked for 96 h in 2 M HCl. After this time, elemental analysis demonstrates 2.5 wt % Co remains in the powders, so approximately 1/3 of the Co remains after this extended leaching. As dissolution of unprotected Co is rapid, we hypothesize that approximately 1/3 of the carbon shells in our case are defect-free as Co remains in the sample after 96 h in 2 M HCl; further exposure to acid should not significantly alter the Co composition. Furthermore, the magnetic property of the powders is maintained such that the powders can be separated easily from solution by a magnet. These results are consistent with prior reports that carbon coating of Co nanoparticles prevents acid erosion.[48] However, this previous case utilized hard templating with the Co nanoparticles being preformed and an additional furfuryl alcohol treatment step was required to protect the Co prior to carbonization, but some nanoparticles are still observed to be leached to yield hollow carbon shells after using HF (72 h) to remove the hard silica template;[48] this was attributed to some defects in the carbon shells surrounding the Co nanoparticles. The large magnetic susceptibility and modest aqueous stability of the Co nanoparticles combined with the simple, single step synthesis make these materials attractive as magnetically separable

adsorbents.

3.4 Conclusions

Mesoporous carbon powders containing nanoparticles of polycrystalline cobalt are synthesized using multi-constituent self-assembly of resol (carbon precursor), $Co(acac)_3$ (metal precursor), TEOS (silica, optional) and Pluronic F127 (structure directing agent). The adsorption capacity of C-Co materials for methlylene green is strongly dependent upon the Co concentration with an increase from 2.0 to 90 mg/g when the powder contains 8.3 wt% Co; this powder also exhibits excellent magnetic properties (12.3 emu/g) that enable efficient separation of the powders from aqueous suspension. Addition of silica to the synthesis, followed by its etching in NaOH yields high surface area powders with much larger adsorption capacities (878 mg/g to 1151 mg/g). Moreover despite the decrease in surface area with addition of Co, the adsorption capacity increases with Co content. These results indicate that careful tuning of wall chemistry and microporosity could enable selective separations from aqueous mixtures. Additionally, the *in-situ* formed cobalt nanoparticles are encapsulated in carbon that imparts modest stability in aqueous acidic solutions.

3.5 References

1. Hou, Z.; Zeng, F.; He, B.; Tao, W.; Ge, C.; Kuang, Y.; Zeng, J., High rate capability of ordered mesoporous carbon with platelet graphitic pore walls for lithium ion anodes. *Materials Letters* **2011**, *65*, 897-900.

2. Huang, C.-h.; Doong, R.-a.; Gu, D.; Zhao, D., Dual-template synthesis of magnetically-separable hierarchically-ordered porous carbons by catalytic graphitization. *Carbon*, *49*, 3055-3064.

3. Sang, L. C.; Vinu, A.; Coppens, M. O., Ordered mesoporous carbon with tunable, unusually large pore size and well-controlled particle morphology. *Journal of Materials Chemistry* **2011**, *21*, 7410-7417.

4. Wang, L.; Bai, J.; Bo, X.; Zhang, X.; Guo, L., A novel glucose sensor based on ordered mesoporous carbon-au nanoparticles nanocomposites. *Talanta* **2011**, *83*, 1386-1391.

5. Zhang, Y.; Xu, S.; Luo, Y.; Pan, S.; Ding, H.; Li, G., Synthesis of mesoporous carbon capsules encapsulated with magnetite nanoparticles and their application in wastewater treatment. *Journal of Materials Chemistry*, *21*, 3664-3671.

6. Zhang, Y.; Xu, S.; Luo, Y.; Pan, S.; Ding, H.; Li, G., Synthesis of mesoporous carbon capsules encapsulated with magnetite nanoparticles and their application in wastewater treatment. *Journal of Materials Chemistry* **2011**, *21*, 3664-3671.

7. Zhai, Y.; Dou, Y.; Liu, X.; Park, S. S.; Ha, C.-S.; Zhao, D., Soft-template synthesis of ordered mesoporous carbon/nanoparticle nickel composites with a high surface area. *Carbon* **2011**, *49*, 545-555.

8. Levario, T. J.; Dai, M.; Yuan, W.; Vogt, B. D.; Nielsen, D. R., Rapid adsorption of alcohol biofuels by high surface area mesoporous carbons. *Microporous and Mesoporous Materials* **2012**, *148*, 107-114.

9. Ryoo, R.; Joo, S. H.; Jun, S., Synthesis of highly ordered carbon molecular sieves via template-mediated structural transformation. *The Journal of Physical Chemistry B* **1999**, *103*, 7743-7746.

10. Kresge, C. T.; Leonowicz, M. E.; Roth, W. J.; Vartuli, J. C.; Beck, J. S., Ordered mesoporous molecular sieves synthesized by a liquid-crystal template mechanism. *Nature* **1992**, *359*, 710-712.

11. Lee, J.-S.; Joo, S. H.; Ryoo, R., Synthesis of mesoporous silicas of controlled pore wall thickness and their replication to ordered nanoporous carbons with various pore diameters. *Journal of the American Chemical Society* **2002**, *124*, 1156-1157.

12. Zhao, D.; Feng, J.; Huo, Q.; Melosh, N.; Fredrickson, G. H.; Chmelka, B. F.; Stucky, G. D., Triblock copolymer syntheses of mesoporous silica with periodic 50 to 300 angstrom pores. *Science* **1998**, *279*, 548-552.

13. Jun, S.; Joo, S. H.; Ryoo, R.; Kruk, M.; Jaroniec, M.; Liu, Z.; Ohsuna, T.; Terasaki, O., Synthesis of new, nanoporous carbon with hexagonally ordered mesostructure. *Journal of the American Chemical Society* **2000**, *122*, 10712-10713.

14. Meng, Y.; Gu, D.; Zhang, F.; Shi, Y.; Cheng, L.; Feng, D.; Wu, Z.; Chen, Z.; Wan, Y.; Stein, A.; Zhao, D., A family of highly ordered mesoporous polymer resin and carbon structures from organic−organic self-assembly. *Chemistry of Materials* **2006**, *18*, 4447-4464.

15. Tanaka, S.; Nishiyama, N.; Egashira, Y.; Ueyama, K., Synthesis of ordered mesoporous carbons with channel structure from an organic-organic nanocomposite. *Chemical Communications* **2005**, 2125-2127.

16. Liang, C.; Dai, S., Synthesis of mesoporous carbon materials via enhanced hydrogen-bonding interaction. *Journal of the American Chemical Society* **2006**, *128*, 5316-5317.

17. Liang, C.; Hong, K.; Guiochon, G. A.; Mays, J. W.; Dai, S., Synthesis of a large-scale highly ordered porous carbon film by self-assembly of block copolymers. *Angewandte Chemie International Edition* **2004**, *43*, 5785-5789.

18. Zhuang, X.; Wan, Y.; Feng, C.; Shen, Y.; Zhao, D., Highly efficient adsorption of bulky dye molecules in wastewater on ordered mesoporous carbons. *Chemistry of Materials* **2009**, *21*, 706-716.

19. Wang, W.; Wang, H.-y.; Wei, W.; Xiao, Z.-G.; Wan, Y., Self-assembling and size-selective synthesis of ni and nio nanoparticles embedded in ordered mesoporous carbon and polymer frameworks. *Chemistry- A European Journal* **2011**, *17*, 13461-13472.

20. She, L.; Li, J.; Wan, Y.; Yao, X.; Tu, B.; Zhao, D., Synthesis of ordered mesoporous mgo/carbon composites by a one-pot assembly of amphiphilic triblock copolymers. *Journal of Materials Chemistry* **2011**, *21*, 795-800.

21. Li, Q.; Xu, J.; Wu, Z.; Feng, D.; Yang, J.; Wei, J.; Wu, Q.; Tu, B.; Cao, Y.; Zhao, D., Facile synthesis of highly stable and well-dispersed mesoporous zro2/carbon composites with high performance in oxidative dehydrogenation of ethylbenzene. *Phys. Chem. Chem. Phys.* **2010**, *12*, 10996-11003.

22. Gao, W.; Wan, Y.; Dou, Y.; Zhao, D., Synthesis of partially graphitic ordered mesoporous carbons with high surface areas. *Advanced Energy Materials* **2011**, *1*, 115-123.

23. Ji, Z.; Liang, S.; Jiang, Y.; Li, H.; Liu, Z.; Zhao, T., Synthesis and characterization of ruthenium-containing ordered mesoporous carbon with high specific surface area. *Carbon* **2009**, *47*, 2194-2199.

24. Zhai, Y.; Dou, Y.; Liu, X.; Tu, B.; Zhao, D., One-pot synthesis of magnetically separable ordered mesoporous carbon. *Journal of Materials Chemistry* **2009**, *19*, 3292-3300.

25. Liu, R.; Ren, Y.; Shi, Y.; Zhang, F.; Zhang, L.; Tu, B.; Zhao, D., Controlled synthesis of ordered mesoporous c−tio2 nanocomposites with crystalline titania frameworks from organic−inorganic−amphiphilic coassembly†. *Chemistry of Materials* **2007**, *20*, 1140-1146.

26. Hartmann, M., Ordered mesoporous materials for bioadsorption and biocatalysis. *Chemistry of Materials* **2005**, *17*, 4577-4593.

27. Wu, Z.; Zhao, D., Ordered mesoporous materials as adsorbents. *Chemical Communications* **2011**, *47*, 3332-3338.

28. Wu, Z.; Meng, Y.; Zhao, D., Nanocasting fabrication of ordered mesoporous phenol-formaldehyde resins with various structures and their adsorption performances for basic organic compounds. *Microporous and Mesoporous Materials* **2010**, *128*, 165-179.

29. Deng, Y.; Cai, Y.; Sun, Z.; Gu, D.; Wei, J.; Li, W.; Guo, X.; Yang, J.; Zhao, D., Controlled synthesis and functionalization of ordered large-pore mesoporous carbons. *Advanced Functional Materials* **2010**, *20*, 3658-3665.

30. Huang, C.-h.; Doong, R.-a.; Gu, D.; Zhao, D., Dual-template synthesis of magnetically-separable hierarchically-ordered porous carbons by catalytic graphitization. *Carbon* **2011**, *49*, 3055-3064.

31. Zhang, X.-l.; Niu, H.-y.; Li, W.-h.; Shi, Y.-l.; Cai, Y.-q., A core-shell magnetic mesoporous silica sorbent for organic targets with high extraction performance and anti-interference ability. *Chemical Communications* **2011**, *47*, 4454-4456.

32. Park, I.-S.; Choi, M.; Kim, T.-W.; Ryoo, R., Synthesis of magnetically separable ordered mesoporous carbons using furfuryl alcohol and cobalt nitrate in a silica template. *Journal of Materials Chemistry* **2006**, *16*, 3409-3416.

33. Lin, Y.-S.; Haynes, C. L., Synthesis and characterization of biocompatible and size-tunable multifunctional porous silica nanoparticles. *Chemistry of Materials* **2009**, *21*, 3979-3986.

34. Linjie, Z.; Yong-Sheng, H.; Bassem El, H.; Xuan, W.; Ingo, L.; Ute, K.; Joachim, M.; Klaus, M., Precursor-controlled formation of novel carbon/metal and carbon/metal oxide nanocomposites. *Advanced Materials* **2008**, *20*, 1727-1731.

35. Dai, M.; Song, L.; LaBelle, J. T.; Vogt, B. D., Ordered mesoporous carbon composite films containing cobalt oxide and vanadia for electrochemical applications. *Chemistry of Materials* **2011**, *23*, 2869-2878.

36. Liu, R. L.; Shi, Y. F.; Wan, Y.; Meng, Y.; Zhang, F. Q.; Gu, D.; Chen, Z. X.; Tu, B.; Zhao, D. Y., Triconstituent co-assembly to ordered mesostructured polymer-silica and carbon-silica nanocomposites and large-pore mesoporous carbons with high surface areas. *Journal of the American Chemical Society* **2006**, *128*, 11652-11662.

37. Song, L.; Feng, D.; Campbell, C. G.; Gu, D.; Forster, A. M.; Yager, K. G.; Fredin, N.; Lee, H.-J.; Jones, R. L.; Zhao, D.; Vogt, B. D., Robust conductive mesoporous carbon-silica composite films with highly ordered and oriented orthorhombic structures from triblock-copolymer template co-assembly. *Journal of Materials Chemistry* **2010**, *20*, 1691-1701.

38. Xue, C.; Lv, Y.; Zhang, F.; Wu, L.; Zhao, D., Copper oxide activation of soft-templated mesoporous carbons and their electrochemical properties for capacitors. *Journal of Materials Chemistry* **2012**, *22*, 1547-1555.

39. Yao, J.; Li, L.; Song, H.; Liu, C.; Chen, X., Synthesis of magnetically separable ordered mesoporous carbons from f127/[ni(h2o)6](no3)2/resorcinol-formaldehyde composites. *Carbon* **2009**, *47*, 436-444.

40. Bagshaw, S. A.; Prouzet, E.; Pinnavaia, T. J., Templating of mesoporous molecular sieves by nonionic polyethylene oxide surfactants. *Science* **1995**, *269*, 1242-1244.

41. Yang, H.; Yan; Liu, Y.; Zhang, F.; Zhang, R.; YanMeng, Y.; Li, M.; Xie, S.; Tu, B.; Zhao, D., A simple melt impregnation method to synthesize ordered mesoporous carbon and carbon nanofiber bundles with graphitized structure from pitches. *The Journal of Physical Chemistry B* **2004**, *108*, 17320-17328.

42. Cotet, L. C.; Gich, M.; Roig, A.; Popescu, I. C.; Cosoveanu, V.; Molins, E.; Danciu, V., Synthesis and structural characteristics of carbon aerogels with a high content of fe, co, ni, cu, and pd. *Journal of Non-Crystalline Solids* **2006**, *352*, 2772-2777.

43. Fu, R.; Baumann, T. F.; Cronin, S.; Dresselhaus, G.; Dresselhaus, M. S.; Satcher, J. H., Formation of graphitic structures in cobalt- and nickel-doped carbon aerogels. *Langmuir* **2005**, *21*, 2647-2651.

44. Yan, Y.; Wei, J.; Zhang, F.; Meng, Y.; Tu, B.; Zhao, D., The pore structure evolution and stability of mesoporous carbon fdu-15 under co2, o2 or water vapor atmospheres. *Micropor. Mesopor. Mater.* **2008**, *113*, 305-314.

45. Mohammadi, N.; Khani, H.; Gupta, V. K.; Amereh, E.; Agarwal, S., Adsorption process of methyl orange dye onto mesoporous carbon material–kinetic and thermodynamic studies. *J. Colloid and Interface Sci.* **2011**, *362*, 457-462.

46. He, C.; Hu, X., Anionic dye adsorption on chemically modified ordered mesoporous carbons. *Ind. Eng. Chem. Res.* **2011**, *50*, 14070-14083.

47. Teunissen, W.; de Groot, F. M. F.; Geus, J.; Stephan, O.; Tence, M.; Colliex, C., The structure of carbon encapsulated nife nanoparticles. *J. Catal.* **2001**, *204*, 169-174.

48. Lu, A.-H.; Schmidt, W.; Matoussevitch, N.; Bönnemann, H.; Spliethoff, B.; Tesche, B.; Bill, E.; Kiefer, W.; Schüth, F., Nanoengineering of a magnetically separable hydrogenation catalyst. *Angew. Chem.* **2004**, *116*, 4403-4406.

49. Zhou, Z.; Liu, G.; Han, D., Coating and structural locking of dipolar chains of cobalt nanoparticles. *ACS Nano* **2008**, *3*, 165-172.

CHAPTER 4

MESOPOROUS CARBON AMPEROMETRIC GLUCOSE SENSORS USING INEXPENSIVE, COMMERCIAL METHACRYLATE-BASED BINDERS

4.1 Introduction

In terms of worldwide public health problems, diabetes mellitus is one of the most rapidly growing issues with more than one quarter billion people affected and expectations that this number will more than double in the next 20 years.[1-4] With increasingly westernized diets, it is expected that many of these new cases will occur in Africa. Treatment of diabetes mellitus requires controlling the glucose levels in the patient; key to this control is facile routes to measure their glucose concentration.[3] Electrochemical enzymatic measurements involving with the glucose oxidase provide a suitable solution in many cases due to sensitivity, selectivity and simplicity of electrochemical measurements. Considerable attention has been paid to screen printed electrodes for these functions and they provide rapid and accurate measurements with additional attributes of being small, cheap and disposable, but their sensitivity can be limited by the measuring electronics due to relatively low current associated with the redox reactions. For developing nations, it would be useful to be able to increase this signal to decrease the cost of the disposable meter.

One factor that significantly impacts the performance of an electrochemical device is the material selection for the electrode.[5] Although many metals could act as electrodes, their chemical stability and biocompatibility are limited in comparison to carbon, which exhibits exceptional conductivity,

mechanical and chemical stabilities, and biocompatibility; thus carbon-based electrodes are commonly utilized for biological electrochemical sensing.[5,6] In addition to the simple material properties, increasing the accessible surface area can be used to enhance the signal. Thus, activated carbon has been utilized substantially in electrochemical applications, but its small pores generally create significant transport limitations for active sensing. Alternatively, ordered mesoporous carbon have more recently been examined as working electrodes in electrochemical biosensing applications; these materials still possess high specific surface area, but their pore size is controllable along with the transport paths through selection of the ordered mesostructure.[6-9] Interestingly, mesoporous carbon electrodes have been shown to display superior sensitivity to even high surface area carbon nanotubes in some cases, such as for electrochemical detection of p-nitrophenol.[10] Similarly, Zhu et al.[5] have demonstrated that ordered mesoporous carbon modified electrodes show lower over potential, better-defined peak shape and higher sensitivity in comparison to conventional carbon nanotubes and graphite powder modified electrodes for bioanalytical applications. These results illustrate the potential advantages of ordered mesoporous carbons for electrochemical sensing applications. Moreover, the synthesis of these mesoporous carbon has been shown to be scalable to the kilogram scale[11] and utilize relatively inexpensive, commodity chemicals in their synthesis.[12] These characteristics make mesoporous carbons attractive as the active material in disposable electrochemical sensors.

However in order to maintain mechanical integrity and enable facile fabrication of the electrode, a binder is typically utilized that comprises 10-20 wt % of the electrode.[13,14] Hence, binder selection is important for optimization of the mechanical and electrical properties of electrochemical sensors.[13] There are two common approaches to provide binding of the conductive particles into a compact electrode: direct bonding via interparticle bridges formed by the binder molecules (such as gelatin) and indirect binding through non-covalent interactions of the binder that acts like an adhesive to hold active electrode components in place(such as polymer binders).[15] For mesoporous carbon electrodes, an additional complication involves the binder entering or blocking the mesopores to decrease the accessible surface area. When examining common binders for electrochemical sensors are compatible within expensive screen printed processing, two factors emerge that could adversely impact the economics of these systems: first, many common polymer binders are fluoropolymers (Perfluorosulfonic acid (Nafion), polyvinylidene fluoride (PVDF) and polytetrafluoroethylene (PTFE)),[16] but these fluorinated binders are significantly more costly than commodity thermoplastics. Second in order to process these binders with the active electrode materials, volatile and often toxic organic solvents are required to dissolve the binder for the processing of the electrode [14,17], which adds both cost and environmental considerations. In addition to these considerations, good binding performance for a number of these polymers requires an additional heat treatment step that can exceed the temperature for dimensional stability of the substrate.[16,18] Higher temperatures can be achieved for

other plastic substrates, but the costs associated with these alternative substrates are typically higher. Therefore, alternative binders that still provide mechanical stability ease of processing and good electrochemical performance are desired if they can overcome the mentioned issues.

Recently, several alternative binders have been introduced for electrochemical electrodes. For example, PTFE can be replaced by butadiene/styrene copolymers as a binder for carbon black based electrochemical supercapacitors with stable performance.[19] Poly (acrylic acid) as binder actually improves the electrode performance in comparison to PVDF for silica composites.[13,20] Aqueous slurries based on sodium salt of carboxymethyl cellulose binder provide advantages such as higher compactness than PVDF and relatively low preparation temperature to achieve high performance.[14] However, these binders vary drastically in their relative hydrophobicity and ionic content, so it is unclear what polymer properties are important for determining their efficacy as a binder.

In this study, we systematically examined the role of binder physical properties using a series of poly (methacrylate)s for disposable screen printed electrode sensors based on mesoporous carbons for glucose measurement. The selection of the methylacrylates as binders is motivated by their commercial availability and low cost along with many derivatives available. Mesoporous carbons provide large surface area to enhance the sensing signals and well-defined transport paths for the analyte. Two distinct mesoporous carbons with cubic and hexagonal packing for the pores are investigated as the active electrode

materials with the impact of binder and its concentration in the formulation. The combination of mesoporous carbon and polymer binder that provided the best sensor response for neat glucose solution is shown to be effective for detecting the glucose concentration in whole rabbit blood. The performance of these sensor electrode formulations is directly compared to that of a commercial glucose meter.

4.2 Experiments

All reagents were obtained from Sigma or Sigma-Aldrich unless otherwise specified. Glucose oxidase (GOx) had an activity of 155.6 U/mg (type X–S from Aspergilus niger). Rabbit blood (female, New Zealand white) was purchased from Bioreclamation. All solutions were prepared in 10mM phosphate-buffered saline (PBS) at PH 7.4 unless otherwise specified.

Mesoporous carbons were synthesized by organic-organic self-assembly of a triblock copolymer surfactant, Pluronic F127 (PEO_{106}-PPO_{70}-PEO_{106}, BASF) with a low-molecular-weight, water soluble phenolic resin, resol. Resol was prepared by sodium hydroxide (NaOH, Aldrich) catalyzed polymerization of phenol and formaldehyde (37 wt% in H_2O) as described previously.[12] The morphology of the mesoporous carbon was controlled by the molar composition of phenol to Pluronic F127 in the initial ethanol solution; hexagonally packed (P6mm) cylindrical mesopores product (FDU-15) at molar composition of phenol/formaldehyde/NaOH/F127 = 1: 2: 0.1: 0.012[12] and body centered cubic packed (Im3m) spherical mesoporous product (FDU-16) at molar composition of phenol/formaldehyde/NaOH/F127 = 1: 2: 0.1: 0.006.[12] After evaporation of the ethanol, the phenolic resin was thermally crosslinked at 120 ℃ for 24 h.

Carbonization was performed in tubular furnace under nitrogen atmosphere with a flow rate of 140 cm^3/min at 800 ℃ for 2 h with heating rates of 1 ℃/min below 600 ℃, and 5 ℃/min above 600 ℃. After carbonization, the mesoporous carbon powder was ground with marble pestle and mortar to obtain a fine powder.

Four different polymers as illustrated in Figure 37, poly (2-hydroxyethyl methacrylate) (PHEMA), poly (hydroxybutyl methacrylate) (PHBMA), poly (tert-butyl methacrylate) (PTBMA) and poly (n-propyl methacrylate) (PPMA) (Scientific Polymer Products Inc.) were investigated as polymeric binders. For electrode formulation preparation, PHBMA, PHEMA, PTBMA were dissolved in ethanol, and PPMA was dissolved in toluene at 5 wt%. The polymer binder solution was added to the mesoporous carbon powder and mixed thoroughly with pestle until a homogeneous ink was achieved as shown in Figure 38. For the electrode base, a disposable, commercial screen-printed electrode was used (Zensor, Austin, TX), which featured a working (71.0 mm^2) and counter electrode made of conductive carbon ink, a pseudoreference electrode made of silver ink (-72 mV vs Ag/AgCl)[21,22]. The polymer-binder ink was printed over the working electrode of a Zensor; the printed sensor was dried in ambient for 1 h and subsequently at 80 ℃ for 1h. The total loading of the mesoporous carbon-binder on the Zensor is approximately 0.1 mg.

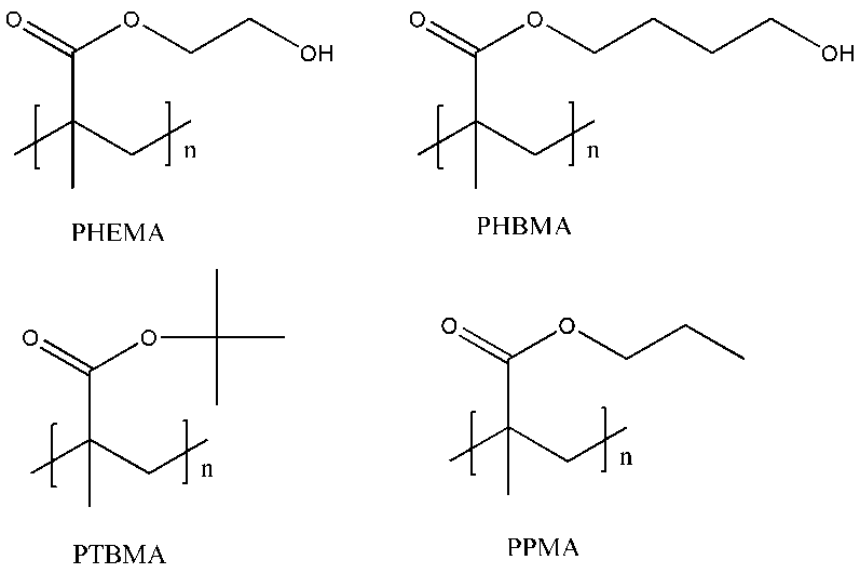

Figure 37 Structures of PHEMA, PHBMA, PTBMA and PPMA polymer binders.

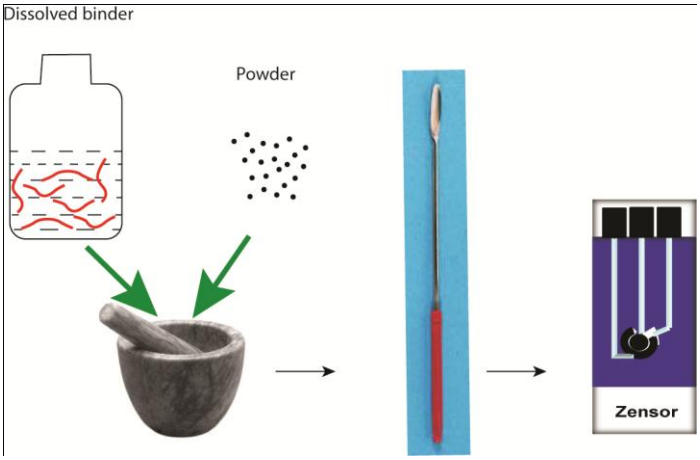

Figure 38 Scheme for the preparation of screen printed sensor.

The ordered mesostructure of the carbons was elucidated by X-ray diffraction (XRD) in θ/2θ geometry with Cu K_α source and parallel plate collimator in combination with an incident beam optical module to minimize beam divergence (PANalytical X'Pert PRO).The angle of incidence, θ, was varied from 0.25 to 1.5 degrees. For direct visualization of the pores, transmission

electron microscopy (TEM) (JEOL 2010F microscope operating at 200 kV) was used. Surface area and pore size information was determined using Nitrogen adsorption–desorption isotherms (Tristar II 3020 Micromeritics 77 K) application of Brunauer–Emmett–Teller (BET) method in a relative pressure range of P/P_0 = 0.05–0.25 and Barrett–Joyner–Halenda (BJH) model using the adsorption branch of the isotherm, respectively. The samples were degassed at 300 ℃ for at least 1h prior to the sorption measurements.

For electrochemical measurements, a CHI 1230A potentiostat electrochemical analyzer (CHI, Austin, TX) was used with chronoamperometric behavior examined under applied potential of + 0.6 V for all the samples. A ferricyanide-mediated system based on 1 mg mL^{-1} of enzyme (GOx) in 100 mM ferricyanide-PBS solution was used for all measurements. In a standard measurement, the contacts of the sensor were wetted by 90 μL of enzyme/mediator solution with the entire contact area for each electrode (working, reference and counter electrode) covered by the solution. Subsequently, 10 μL sample solution (glucose or blood) was injected into the center of the enzyme/mediator solution and allowed to settle for 20 s. For each set of amperometric i-t assays, pure-glucose-in-PBS concentration gradient was used with glucose concentrations of 0, 5, 10, 20, 40, 60, 80 and100 mg mL^{-1} (n=3), respectively. For all the concentration gradient measurements, glucose solutions were prepared ~24 h before use. The glucose in the whole blood is 0 mg mL^{-1} as measured by Yellow Springs Instrument glucometer (YSI) because of glucose loss from glycolysis by erythrocytes during transport and processing.[23] For the

detection of glucose level in blood, a calculated amount of glucose was added into whole blood to make 100 mg mL^{-1} concentration and then diluted to 10, 20, 40, 60 and 80 mg mL^{-1}, respectively. The amperometric i-t response under applied potential of +0.6V was then measured within 30 s for each concentration. Each glucose concentration gradient sensing measurement was repeated at least three times to obtain the average sensitivity and error range. Every sensor was washed with fresh PBS three times and gently dried by wipe between measurements to prevent contamination from prior measurement.

4.3 Results and Discussion

First to demonstrate the well-ordered mesostructure for these carbons, well defined low-angle diffraction peaks (Figure 39) from XRD suggest excellent textural uniformity of the materials[24] and illustrate the successful synthesis of both FDU-16 and FDU-15 with these peaks assigned to diffraction from (100) plane for hexagonal FDU-15 and (110) plane for cubic FDU-16.[12,25] Application of Bragg's law yields a d-spacing of 7.33 nm and 8.45 nm for FDU-15 and FDU-16, respectively. XRD provides a global average for the materials; the d-spacing can be compared to the local mesostructure from transmission electron microscopy (Figure 40). Consistent with XRD, the micrographs illustrate a highly ordered mesoporous structure for both powders. The d-spacing can be determined from image analysis of the TEM micrographs, which yields 7.31 nm and 8.40 nm for FDU-15 and FDU-16, respectively, in good agreement with XRD results.

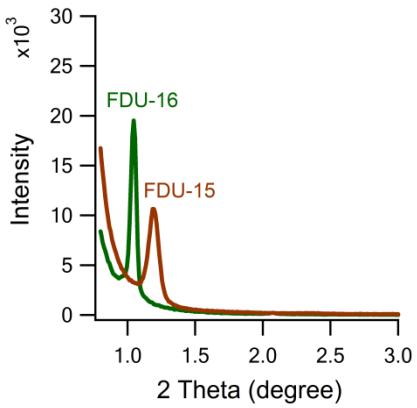

Figure 39 Low-angle powder XRD patterns for FDU-15 and FDU-16.

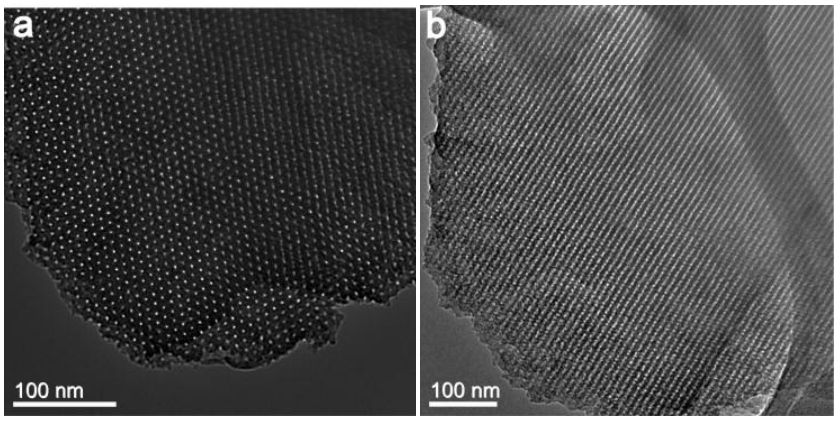

Figure 40 TEM micrographs of the mesoporous carbons of (a) FDU-15 viewed at [001] direction and (b) FDU-16 viewed a [100] plane.

To further investigate the structural characteristics of the mesoporous powders, adsorption/desorption isotherms of N_2 are utilized. These isotherms show typical type IV isotherms that are generally obtained for mesoporous materials (Figure 41a). Simply from the isotherms, it is clear that the pore volume in FDU-16 is greater than FDU-15, as evidenced by difference in the maximum absorbed N_2. By application of BJH model, the average pore size can be estimated to be 2.9 nm and 2.6 nm for FDU-16 and FDU-15, respectively. These pore sizes

are similar to those obtained from examination of the TEM micrographs[26] in Figure 40 (3.0 nm and 2.7 nm for FDU-16 and FDU-15, respectively). One additional critical physical characteristic for the electrochemical properties is the surface area that is estimated by application of standard BET methodology. FDU-16 exhibits a larger surface area in addition to pore size than FDU-15, which shows the same trend as in the literature.[12] Structure information obtained from the sorption isotherms for the two powders is summarized in Table 4.

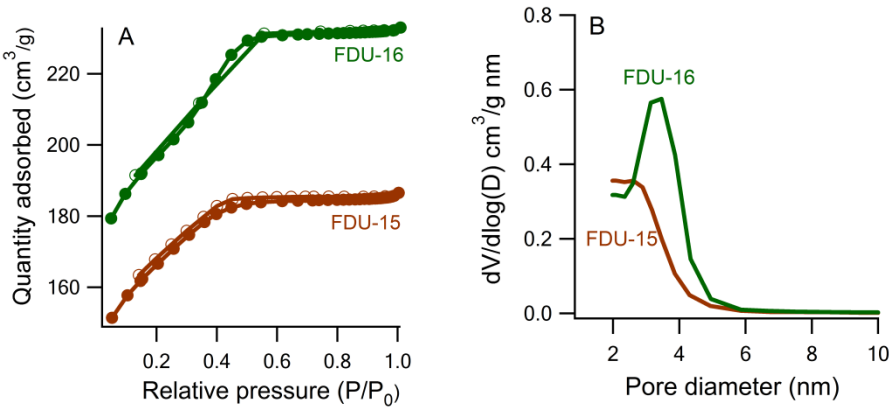

Figure 41 A) Adsorption (●)/desorption (○) isotherms and B) pore size distribution of FDU-15 and FDU-16.

Table 4 Structural properties of FDU-15 and FDU-16 obtained from N_2 sorption

	Surface area (m^2/g)	**Pore Diameter (nm)**	**d-spacing (nm)**	**Pore Volume (cm^3/g)**
FDU-15-800	544	2.6	7.33	0.09
FDU-16-800	671	2.9	8.45	0.14

To begin to examine the electrochemical properties of these electrodes, cyclic voltammograms are obtained in GOx ferricyanide-PBS solution (90 μL GOx solution + 10 μL PBS) without glucose present as shown in Figure 42. The use of mesoporous carbon with the PHBMA binder significantly increases the current in comparison to the Zensor. In all cases, the cyclic behavior is well-behaved with the reduction (oxidation) of the ferricyanide (ferrocyanide) well resolved. We chose + 0.6 V as electrode potential for both mesoporous carbon electrode when used as glucose sensor in order to obtain high current as shown in Figure 42.

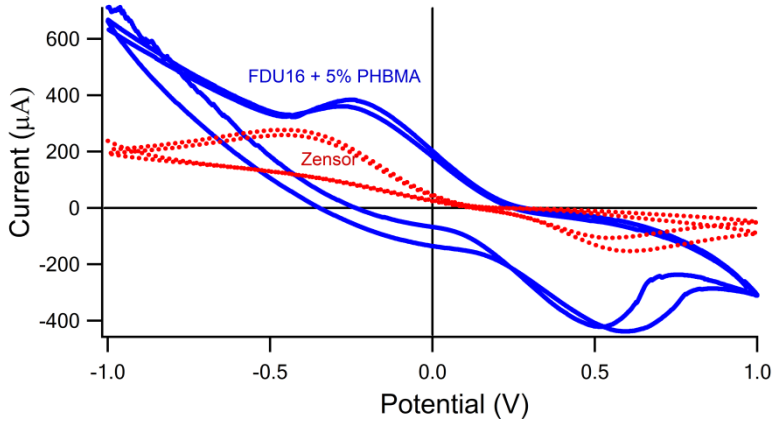

Figure 42 CV behaviors of A) Zensor and B) FDU-16 + 5% PHBMA electrodes.

As shown in Figure 43, in the presence of GOx, glucose is oxidized to gluconolactone with mediator in the enzyme reduced; this reduced redox mediator is then oxidized at the electrode in a heterogeneous reaction.[27-29] This charge transfer enables the amount of oxidized glucose to be directly proportional to the current measured at the electrode.[27] This simple relationship provides the basis for a calibration curve to relate the measured current to the glucose concentration in

the system. The redox mediator provides a steady-state response from amperometric i-t measurements.[28] Figure 44 shows typical current response for the two mesoporous carbon-based electrodes at various glucose concentrations. As the glucose concentration increases, the current increases for amperometric i-t measurement. In order to show the quick response of the sensor, current at 5s was selected to simulate calibration line.

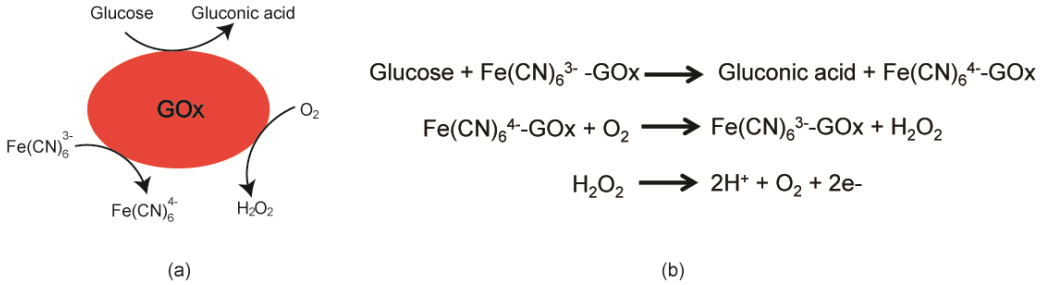

Figure 43 (a) Scheme and (b) equations of glucose reactions on the electrode.

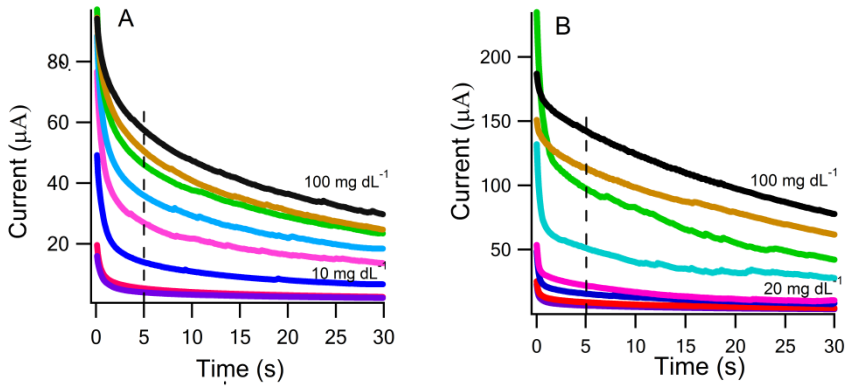

Figure 44 Steady-state stability current measurements of A) FDU-15 + 5%PHBMA and B) FDU-16 + 5% PHBMA for different concentrations of glucose. From bottom to top: 0, 5, 10, 20, 40, 60, 80, and 100 mg/dl at 5s, respectively.

The impact of the binder selection and its concentration in the electrode formulation on the sensitivity and signal of the sensors are investigated as shown in Figure 45 and Figure 46. The purpose of binder is to hold the electrically active materials together that comprising the electrode, but it also influences the performance of the electrode by reducing the effective accessible area of the electrode by introducing a barrier to access the electrode, introducing electrical resistance to the electrode by virtue of its poor conductivity and filling or otherwise blocking accessibility of the pores to the analyte.[30] There are several trade-offs associated with the binder selection in terms of mechanical rigidity, permeability to the analyte, processibility of the formulation to screen print the electrode, and the amount of binder required to hold the electrode together. Ideally, a minimum binder concentration would be used to hold the active materials together, while minimally impacting the electrical conductivity and accessibility of the electrode to the analyte. As binder compositions tend to range from 5-25 % in formulations for electrodes, initially the mesoporous carbons are tested with only 5 % of each binder, but the physical integrity of the electrodes after soaking in PBS is lost for all binders examined except PHBMA. However, by increasing the binder to 10 %, the physical integrity of the electrodes is maintained for almost all of the selected polymer binders. Figure 45 illustrates the performance of the electrodes for the various 10wt% binders using both FDU-15 and FDU-16 mesoporous carbon-based electrodes. It is obvious that PHBMA binder provides the largest signal and sensitivity for the binders examined. The signal for the electrode with the PTBMA binder is weak, but still an order of

magnitude greater than for the bare Zensor. Using PPMA as the binder, the signal is almost indistinguishable from the bare electrode Zensor. This dependence on the binder appears to scale with the relative hydrophobicity of the polymer binder. The t-butyl moiety in PTBMA is a common protecting group for polymer synthesis[31] and modern photoresists,[32] but it is acid and thermally labile. For the commercial product, some deprotection occurs that leads to a copolymer with a small fraction of poly (methacrylic acid). This enables the solubility of the polymer in ethanol as used here and provides for some hydrophilic domains for the transport of the analyte to the electrode. The PTBMA however is a glassy polymer that will resist transport and thus limits the accessibility to the carbon surface. PPMA conversely is a softer binder, but has very hydrophobic propyl side chains that act as a resistance for transport in this sensing system. The modulus of PPMA is similar to that of the butadiene/styrene copolymers that are effective binders for a different system.[19] We attribute the improved performance of the electrode with the PHBMA binder to the increased hydrophilicity on the basis of hydroxyl groups; these enable swelling by aqueous media and rapid transport of the glucose through the polymer to the carbon surface. However if the hydrophilicity is further increased by reducing the butyl (PHBMA) to ethyl (PHEMA) in the side chain, the electrode is unable to maintain cohesion in aqueous media even when the binder concentration is increased to 20 %. PHEMA is not water soluble, but can form a hydrogel with a significant water fraction.[33-35] These results suggest the water uptake in the binder is a critical factor in the performance dependencies associated with a specific binder; a binder

that is too hydrophobic can prevent analyte transport to the carbon surface for sensing, while too hydrophilic can leading swelling that mechanically weakens the system to the point of compromising the physical integrity of the electrode.

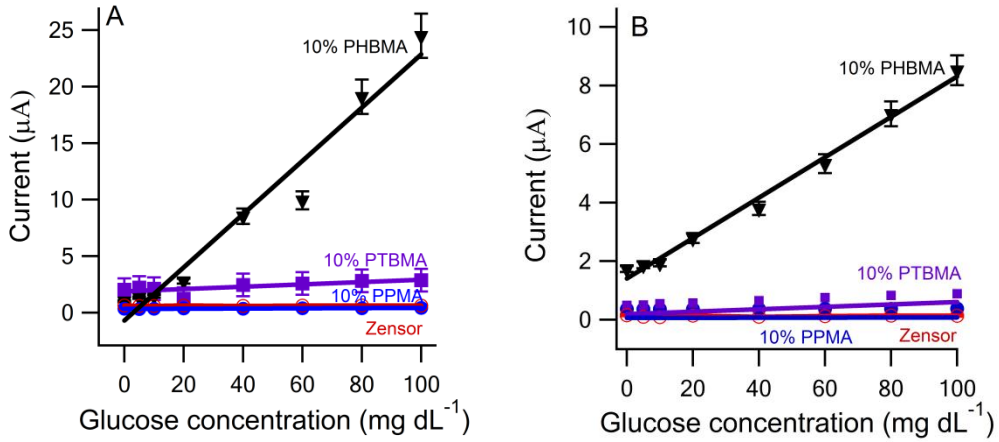

Figure 45 Glucose concentration gradient measurements on (A) FDU-15 and (B) FDU-16 with 10% binders (From top to bottom: PHBMA (▼), PTBMA (■), PPMA (●) binder and Zensor (○) as control)

In order to find the minimum amount of PHBMA binder and how the amount of the binder would affect the performance of the sensors, 2.5%, 5%, 7.5% and 10% of PHBMA were investigated on both mesoporous carbons as shown in Figure 46. Because 2.5% PHBMA wasn't enough to bind the carbons together, the data wasn't shown in the graph. For both mesoporous carbons, the current signal and sensitivity decreased significantly as the amount of binder increased. From the fitting equation in Table 5, the slope of the line dropped from 0.55 to 0.30 to 0.23 for FDU-15, while from 1.4 to 0.53 to 0.06 for FDU-16 when PHBMA amount increased from 5% to 7.5% to 10%. If just compare the performance of these two carbons with 5% and 7.5% binder, FDU-16 has higher

current signal and sensitivity (slope) than FDU-15, especially for 5% PHBMA, because of the higher surface area of FDU-16 than FDU-15. However, for 10% of each binder (Figure 46 and Table 5), the phenomenon is reversed. It means FDU-16 is more sensitive to the amount of binder than FDU-15, because the bottlenecks in the FDU-16 at pore-pore interconnections are blocked with high binder concentration.

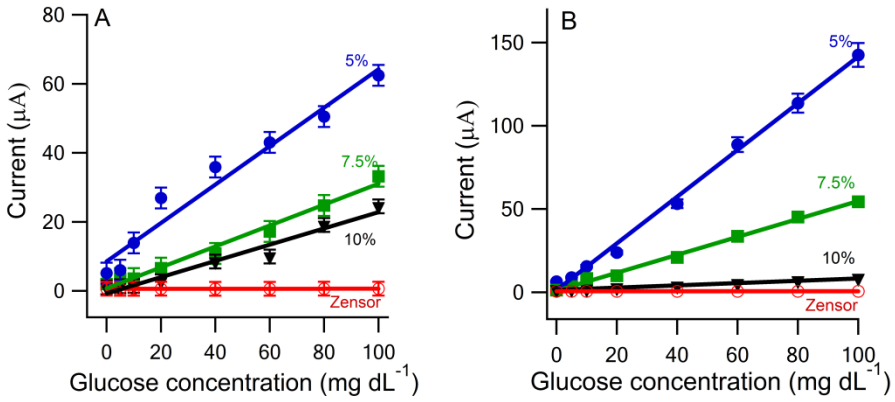

Figure 46 Glucose concentration gradient measurements on (A) FDU-15 and (B) FDU-16 with different amount of PHBMA binder (From top to bottom: 5% (●), 7.5% (■), 10% (▼) PHBMA and Zensor as control (○)).

Table 5 Calibration curves for the FDU-15 and FDU-16 glucose biosensors with comparison to 'standard' Zensor (current I is in μA and concentration C is in mg dL^{-1})

	Fitting equation	R^2	RSD
FDU-15 + 5% PHBMA	I = 0.55C + 8.575	0.958	0.14
FDU-15 + 7.5% PHBMA	I = 0.30C + 0.795	0.983	0.16
FDU-15 + 10% PHBMA	I = 0.23C - 0.668	0.962	0.03
FDU-15 + 10% PTBMA	I = 0.008C + 2.085	0.973	0.07
FDU-15 + 10% PPMA	I = 0.0008C + 0.342	0.806	0.05
FDU16 + 5% PHBMA	I = 1.40C + 1.314	0.995	0.4
FDU16 + 7.5% PHBMA	I = 0.53C + 0.956	0.995	0.06
FDU16 + 10% PHBMA	I = 0.06C + 1.408	0.991	0.18
FDU16 + 10% PTBMA	I = 0.004C + 0.190	0.993	0.03
FDU16 + 10% PPMA	I = 0.0002C + 0.059	0.974	0.07
Zensor	I = 0.00005C + 0.592	0.84	0.3

From these experiments examining the influence of binder and mesoporous carbon on the electrode performance for sensing glucose, it is clear that combination of FDU-16 and 5% PHBMA binder provides the best performance (signal and sensitivity). This electrode is further investigated for efficacy in detecting glucose in whole rabbit blood. We begin by comparing the measurement from this electrode to the commercial meter for the stock (120 mg

dL^{-1}) solution. Excellent agreement is found between the commercial meter and the FDU-16 based sensor at this concentration, which is within the reported range for this meter (105-140 mg dL^{-1}). As illustrated in Figure 47, the sensitivity of this mesoporous carbon based sensor is significantly improved with the measured glucose concentration corresponding well to the actual concentration even well below 100 mg dL^{-1}. However when the glucose concentration decreases below 20 mg dL^{-1}, interference from other components in the blood appears to adversely impact the performance of the mesoporous carbon based electrode at these low concentrations. Additionally, it should be noted that this electrode lacks a membrane that limits the transport of blood components to the electrode. We attribute the excellent performance at modest glucose concentrations to the large internal area, which limits the transport of undesired components to the active electrode surface by size exclusion. Only at low glucose levels is the background current from non-specific interactions sufficient to adversely impact the accuracy of these mesoporous carbon electrodes for glucose sensing.

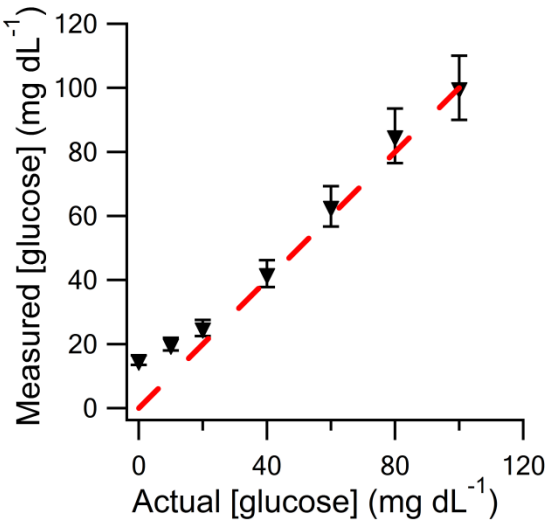

Figure 47 Glucose concentration measurements by FDU-16 + 5% PHBMA electrode in comparison to commercial glucose meter.

4.4 Conclusions

A screen printed glucose sensor with mesoporous carbon electrode has been prepared using a low cost and fluorine-free polymer binder (PHBMA) that provides high performance for the sensor by enabling aqueous media transport while maintaining mechanical stability in aqueous solutions. Despite similar surface areas and pore sizes, carbons with interconnected spherical mesopores yield significantly larger signal than carbons with cylindrical mesopores when used as amperometric glucose sensors. These mesoporous carbon-based sensors provide an accurate measure of the glucose concentration at levels far below the detection limit for a commercial glucose meter. The combined advantages of increased sensitivity ease of processing via screen printing, and relatively low cost components provide promise for future advances in electrochemical sensing by use of these mesoporous carbon-based electrodes.

4.5 References

1. Jiang, X.; Wu, Y.; Mao, X.; Cui, X.; Zhu, L., Amperometric glucose biosensor based on integration of glucose oxidase with platinum nanoparticles/ordered mesoporous carbon nanocomposite. *Sensors and Actuators B: Chemical* **2011**, *153*, 158-163.

2. Bo, X.; Bai, J.; Yang, L.; Guo, L., The nanocomposite of ptpd nanoparticles/onion-like mesoporous carbon vesicle for nonenzymatic amperometric sensing of glucose. *Sensors and Actuators B: Chemical* **2011**, *157*, 662-668.

3. Cash, K. J.; Clark, H. A., Nanosensors and nanomaterials for monitoring glucose in diabetes. *Trends in Molecular Medicine* **2010**, *16*, 584-593.

4. Wang, J., Electrochemical glucose biosensors. *Chemical Reviews* **2007**, *108*, 814-825.

5. Zhu, L.; Tian, C.; Yang, D.; Jiang, X.; Yang, R., Bioanalytical application of the ordered mesoporous carbon modified electrodes. *Electroanalysis* **2008**, *20*, 2518-2525.

6. Zhu, L.; Tian, C.; Zhu, D.; Yang, R., Ordered mesoporous carbon paste electrodes for electrochemical sensing and biosensing. *Electroanalysis* **2008**, *20*, 1128-1134.

7. You, C.; Yan, X.; Kong, J.; Zhao, D.; Liu, B., Bicontinuous gyroidal mesoporous carbon matrix for facilitating protein electrochemical and bioelectrocatalytic performances. *Talanta* **2011**, *83*, 1507-1514.

8. Li, H.; He, J.; Zhao, Y.; Wu, D.; Cai, Y.; Wei, Q.; Yang, M., Immobilization of glucose oxidase and platinum on mesoporous silica nanoparticles for the fabrication of glucose biosensor. *Electrochimica Acta* **2011**, *56*, 2960-2965.

9. Su, C.; Zhang, C.; Lu, G.; Ma, C., Nonenzymatic electrochemical glucose sensor based on pt nanoparticles/mesoporous carbon matrix. *Electroanalysis* **2010**, *22*, 1901-1905.

10. Lee, J. H.; Park, J. Y.; Min, K.; Cha, H. J.; Choi, S. S.; Yoo, Y. J., A novel organophosphorus hydrolase-based biosensor using mesoporous carbons and carbon black for the detection of organophosphate nerve agents. *Biosensors and Bioelectronics* **2010**, *25*, 1566-1570.

11. Wang, J.; Xue, C.; Lv, Y.; Zhang, F.; Tu, B.; Zhao, D., Kilogram-scale synthesis of ordered mesoporous carbons and their electrochemical performance. *Carbon* **2011**, *49*, 4580-4588.

12. Meng, Y.; Gu, D.; Zhang, F.; Shi, Y.; Cheng, L.; Feng, D.; Wu, Z.; Chen, Z.; Wan, Y.; Stein, A.; Zhao, D., A family of highly ordered mesoporous polymer resin and carbon structures from organic−organic self-assembly. *Chemistry of Materials* **2006**, *18*, 4447-4464.

13. Magasinski, A.; Zdyrko, B.; Kovalenko, I.; Hertzberg, B.; Burtovyy, R.; Huebner, C. F.; Fuller, T. F.; Luzinov, I.; Yushin, G., Toward efficient binders for li-ion battery si-based anodes: Polyacrylic acid. *ACS Appl. Mater. Interfaces* **2010**, *2*, 3004-3010.

14. Lux, S. F.; Schappacher, F.; Balducci, A.; Passerini, S.; Winter, M., Low cost, environmentally benign binders for lithium-ion batteries. *Journal of The Electrochemical Society* **2010**, *157*, A320-A325.

15. Pejovnik, S.; Dominko, R.; Bele, M.; Gaberscek, M.; Jamnik, J., Electrochemical binding and wiring in battery materials. *Journal of Power Sources* **2008**, *184*, 593-597.

16. Chen, Z.; Christensen, L.; Dahn, J. R., Comparison of pvdf and pvdf-tfe-p as binders for electrode materials showing large volume changes in lithium-ion batteries. *Journal of The Electrochemical Society* **2003**, *150*, A1073-A1078.

17. Fransson, L.; Eriksson, T.; Edström, K.; Gustafsson, T.; Thomas, J. O., Influence of carbon black and binder on li-ion batteries. *Journal of Power Sources* **2001**, *101*, 1-9.

18. Cheng, S.; Liu, H.; Logan, B. E., Power densities using different cathode catalysts (pt and cotmpp) and polymer binders (nafion and ptfe) in single chamber microbial fuel cells. *Environ. Sci. Technol.* **2005**, *40*, 364-369.

19. Beck, F.; Dolata, M., Fluorine-free binders for carbon black based electrochemical supercapacitors. *Journal of Applied Electrochemistry* **2001**, *31*, 517-521.

20. Komaba, S.; Shimomura, K.; Yabuuchi, N.; Ozeki, T.; Yui, H.; Konno, K., Study on polymer binders for high-capacity sio negative electrode of li-ion batteries. *The Journal of Physical Chemistry C* **2011**, *115*, 13487-13495.

21. Bishop, D. K.; La Belle, J. T.; Vossler, S. R.; Patel, D. R.; Cook, C. B., A disposable tear glucose biosensor---part 1: Design and concept testing. *Journal of Diabetes Science and Technology* **2010**, *4*, 299-306.

22. La Belle, J. T.; Bishop, D. K.; Vossler, S. R.; Patel, D. R.; Cook, C. B., A disposable tear glucose biosensor---part 2: System integration and model validation. *Journal of Diabetes Science and Technology* **2010**, *4*, 307-311.

23. Landt, M., Glyceraldehyde preserves glucose concentrations in whole blood specimens. *Clinical Chemistry* **2000**, *46*, 1144-1149.

24. Han, Y.-J.; Kim, J. M.; Stucky, G. D., Preparation of noble metal nanowires using hexagonal mesoporous silica sba-15. *Chemistry of Materials* **2000**, *12*, 2068-2069.

25. Yang, P.; Zhao, D.; Margolese, D. I.; Chmelka, B. F.; Stucky, G. D., Generalized syntheses of large-pore mesoporous metal oxides with semicrystalline frameworks. *Nature* **1998**, *396*, 152-155.

26. Song, L.; Feng, D.; Fredin, N. J.; Yager, K. G.; Jones, R. L.; Wu, Q.; Zhao, D.; Vogt, B. D., Challenges in fabrication of mesoporous carbon films with ordered cylindrical pores via phenolic oligomer self-assembly with triblock copolymers. *ACS Nano* **2009**, *4*, 189-198.

27. Harper, A.; Anderson, M. R., Electrochemical glucose sensors—developments using electrostatic assembly and carbon nanotubes for biosensor construction. *Sensors* **2010**, *10*, 8248-8274.

28. Vaillancourt, M.; Wei Chen, J.; Fortier, G.; Bédanger, D., Electrochemical and enzymatic studies of electron transfer mediation by ferrocene derivatives with nafion-glucose oxidase electrodes. *Electroanalysis* **1999**, *11*, 23-31.

29. Heller, A.; Feldman, B., Electrochemical glucose sensors and their applications in diabetes management. *Chemical Reviews* **2008**, *108*, 2482-2505.

30. Rosolen, J. M.; Matsubara, E. Y.; Marchesin, M. S.; Lala, S. M.; Montoro, L. A.; Tronto, S., Carbon nanotube/felt composite electrodes without polymer binders. *Journal of Power Sources* **2006**, *162*, 620-628.

31. Qin, S.; Saget, J.; Pyun, J.; Jia, S.; Kowalewski, T., Synthesis of block, statistical, and gradient copolymers from octadecyl (meth)acrylates using atom transfer radical polymerization. *Macromolecules* **2003**, *36*, 8969-8977.

32. Sinha, A.; Hess, D. W.; Henderson, C. L., A top surface imaging method using area selective ald on chemically amplified polymer photoresist films. *Electrochemical and Solid-State Letters* **2006**, *9*, G330-G333.

33. Holly, F. J.; Refojo, M. F., Wettability of hydrogels i. Poly(2-hydroxyethyl methacrylate). *Journal of Biomedical Materials Research* **1975**, *9*, 315-326.

34. Rao, J. K.; Ramesh, D. V.; Rao, K. P., Implantable controlled delivery systems for proteins based on collagen — phema hydrogels. *Biomaterials* **1994**, *15*, 383-389.

35. Roorda, W. E.; Bouwstra, J. A.; de Vries, M. A.; Junginger, H. E., Thermal behavior of poly hydroxy ethyl methacrylate (phema) hydrogels. *Pharmaceutical Research* **1988**, *5*, 722-725.

CHAPTER 5

SCREEN PRINTED BIOSENSORS USING HIGH SURFACE AREA MESOPOROUS CARBON INKS TO ENABLE AMPEROMETRIC SENSING OF NOREPINEPHRINE AT < 100 pg mL^{-1}

5.1 Introduction

Neurotransmitters play the crucial role of endogenous primary chemical messengers to transport information among biological cells in mammalian central nervous system and are indicative of health and disease [1]. One important catecholamine neurotransmitter is norepinephrine (NE), which is associated with stress, blood pressure regulation, heart rate immune system and glycogen metabolism.[2,3] Abnormal NE concentrations in blood can be indicators of diseases such as thyroid hormone deficiency, congestive heart failure, arrhythmias and idiopathic postural hypotension.[4,5] Thus, facile detection of NE could provide for advances in clinical diagnosis, study of disease pathologies and discovery of new drugs.[2,6]

Given the potential impact associated with understanding NE concentration *in vivo*, there has been significant interest in developing new techniques that provide fast and accurate measures of NE concentration as existing technologies (peroxidase-based spectrophotometric method,[7] high performance liquid chromatography technique,[8] stable-isotope dilution gas chromatography-tandem mass spectrometry[9] and capillary electrophoresis[10]) are limited in their speed and sensitivity. Electrochemical sensors with modified electrodes for NE provide significant advantages over these other techniques such

as quick response, simple procedure, high selectivity and direct information.[4,11] The electrochemical sensor electrode is often modified to promote the electrochemical reaction of the target in order to improve the sensitivity, selectivity and reproducibility of the sensor.[1] For example, gold nanoparticles deposited on an electrode exhibits potent and persistent electro-mediating behavior to detect NE.[2] Similarly, modifying activated glassy carbon with Ni and polyurethane increases the selectivity for NE.[12] However, these modification schemes add complexity and/or costly materials to the electrode design. Carbon materials are commonly utilized in the electrode for electrochemical sensors due to their high conductivity, chemical inertness, bio-compatibility, and low cost.[13-16] Electrodes based upon carbon nanotubes,[11] carbon paste,[5] Ag ion irradiated multi-walled carbon nanotube[3] and carbon fiber[17] have been used to detect NE successfully. However, current signal is generally low from those electrodes, leading to low sensitivity.

Increasing surface area of the electrode materials provides one effective method to significantly improve the sensitivity of the sensor.[18] Thus, carbon nanotubes with their large surface area[3,19] have been explored extensively as electrodes for electrochemical sensors, but their cost is high relative to other carbons. Alternatively to obtain high surface areas, ordered mesoporous carbon can be fabricated by simple organic-organic self-assembly of inexpensive phenolic resin and commercial surfactants and subsequent carbonization.[20] High surface area mesoporous carbon pastes have been demonstrated as active materials in electrochemical sensors,[4,13,21-23] but the detecting limit of these

sensors are above 1×10^4 pg mL^{-1} ($\sim7\times10^{-8}$ M) with current signal lower than 40 μA. To further increase the surface area of these mesoporous carbons, triconstituent assembly of surfactant, phenolic resin and a silica precursor can be utilized with removal of SiO_2 after carbonization; for the same materials, the surface area can be increased from 760 m^2 g^{-1} (no silica) to 2390 m^2 g^{-1} (46 % silica).[24] This increased surface area dramatically increases the electrochemical double layer capacitance[25-27] and enhances the adsorption capacity for bulky organics from aqueous solution.[28] The added pores to produce this high surface area are very small (<1 nm) and included within the wall framework of the ordered mesopores. We have recently demonstrated high efficacy, amperometric glucose sensors using modest surface area, mesoporous carbon with polymer binder of poly(hydroxybutyl methacrylate) that did not necessitate a Nafion membrane to achieve high sensitivity and selectivity in whole rabbit blood.[18] However for glucose, physiological concentrations (100 mg mL^{-1}) are orders of magnitude greater than for NE (90-220 pg mL^{-1}). This low concentration for NE provides a significant change for electrochemical sensing. Extensive efforts have focused on modifying the electrodes to decrease the detecting limit of NE concentration, such as macrocyclic Ni and hydrophilic polyurethane modified glass carbon,[12] carbon fiber and diamond microelectrodes,[17] Ag ion irradiated based nanotubes,[3] and ZrO^2 nanoparticles-modified carbon paste.[5] Nevertheless, all those electrodes were not able to detect NE concentration lower than 1×10^4 pg mL^{-1}. As to our knowledge, there is no electrode reported that shows detecting limitation of NE as low as 100 pg mL^{-1}.

In this work, we utilize mesoporous carbon inks to screen print electrodes for the detection of norepinephrine amperometrically. There are numerous advantages to amperometric sensing in terms of cost, simplicity and maturity of the technologies. However, the low concentration (90-220 pg mL^{-1}) of NE in human blood provides a significant challenge to obtaining an acceptable signal to noise when only the current is being measured to assess the concentration in blood. To overcome the lower concentration limits for the amperometric sensing, we increased the surface area of the mesoporous carbons to enhance the current signal by use of triconstituent assembly and silica etching; surface areas from 1500 to 2300 m^2/g can be produced depending upon the carbon-silica ratio during self-assembly. To assess the role of the small micropores, one control without silica is also examined. The performance of these screen printed mesoporous carbon electrodes is strongly dependent upon the surface area with greatest sensitivity for the highest surface area carbon. The sensors are effective at detecting NE concentrations as low as 100 pg mL^{-1} in rabbit whole blood. These results illustrate the potential of these high surface area carbons for use in electrodes for rapid and highly sensitive electrochemical detection of biological targets.

5.2 Materials/Methods

5.2.1 Chemicals

All reagents were obtained from Sigma or Sigma-Aldrich unless otherwise specified. Phenylethanolamine N-Methyl Transferase (PNMT) with an activity of 50-100 U mg^{-1} protein was obtained from Calzyme Laboratories, CA. Cofactor S-

(5′-Adenosyl)-L-methionine chloride dihydrochloride (SAM) and target norepinephrine (NE) were obtained from Sigma-Aldrich. Whole rabbit blood (female, New Zealand white) was purchased from Bioreclamation. All solutions were prepared in 10 mM phosphate-buffered saline (PBS) at PH 7.4 unless otherwise specified.

5.2.2 Mesoporous carbons preparation

Highly ordered mesoporous carbon powders were synthesized by the evaporation-induced triconstituent co-assembly method using a triblock copolymer surfactant Pluronic F127 (PEO106-PPO70-PEO106, BASF), low-molecular-weight, water soluble phenolic resin (resol) and Tetraethyl orthosilicate (TEOS) as silica template.[24] Resol was prepared by sodium hydroxide (NaOH, Aldrich) catalyzed polymerization of phenol and formaldehyde (37 wt% in H_2O) as described previously.[20] Hydrolysis of TEOS was performed at fixed mass ratio of TEOS/EtOH/HCl/H_2O at $2.08:12:7.3\times10^{-3}$:1.0. The morphology of the mesoporous carbon was controlled through the resol and TEOS ratio following procedure of Zhao and coworkers[24] with a phenol / formaldehyde / NaOH / F127 = 1:2:0.1:0.006 for the carbon synthesized without TEOS. In a typical preparation, 1.6 g F127 was dissolved initially in 8.0 g ethanol at 40 C° with adding 0.2g 2 M HCl, whereupon solutions of 5.0 g of 20 wt% resol in ethanol and 2.08 g TEOS were added and the mixture was stirred at 40 C° for 2 h. The preparation comditions of other samples are shown in Table 6. Then, the solution was spread into several watch glasses and allowed to dry overnight. After evaporation of the solvent, the phenolic resin was thermally crosslinked at 100 ℃ for 24 h.

Carbonization was performed in tubular furnace under nitrogen atmosphere with a flow rate of 140 $cm^3 min^{-1}$ at 900 ℃ for 2 h with heating rates of 1 ℃ min^{-1} below 600 ℃, and 5 ℃/min above 600 ℃. After carbonization, the mesoporous carbon powder was ground with marble mortar and pestle to obtain a fine powder.

The silica (when present) was removed after carbonization by soaking the carbonized powders in 1M NaOH Ethanol-H_2O (volume ratio 1:1) for 3 days,[29] followed by washing with distilled water three times. After dried overnight at 100 ℃, the powder was ready to use.

Table 6 Preparation compositions of high mesoporous carbons

	TEOS (g)	**Resol (g)**	**F127 (g)**
MP-C-36	2.08	0.5	1.0
MP-C-46	2.08	1.0	1.6
MP-C-61	2.08	2.0	2.3

5.2.3 Characterization of mesoporous carbons

The ordered mesostructure of the porous carbons was elucidated by X-ray diffraction (XRD) in θ/2θ geometry using Cu K_α source and parallel plate collimator in combination with an incident beam optical module to minimize beam divergence (PANalytical X'Pert PRO). The angle of incidence, θ, was varied from 0.25 to 1.5 degrees. For direct visualization of the pores, transmission electron microscopy (TEM, JEOL 2010F microscope operating at 200 kV) was used. Surface area and pore size information was determined using Nitrogen adsorption–desorption isotherms (Tristar II 3020 Micromeritics 77 K) by

application of Brunauer–Emmett–Teller (BET) method in a relative pressure range of P/P_0 = 0.05–0.25 and Barrett–Joyner–Halenda (BJH) model using the adsorption branch of the isotherm, respectively. The samples were degassed at 300 ℃ for at least 1 h prior to the gas sorption measurements.

5.2.4 Mesoporous carbon electrode preparation

The inks for the screen printing were fabricated by physically mixing the mesoporous carbon powder with 3 wt% poly (hydroxybutyl methacrylate) (PHMBA) in ethanol to form a consistent paste. The PHMBA functioned as the polymer binder as described previously[18] and was 15 wt % of the solids in the electrode. The paste was deposited on the working area on a screen printed electrode (CHI, Austin, TX) by a small spoon and allowed to dry (weight of ink in each electrode is less than 0.1mg after dried). A bake at 80 ℃ for 1 h was utilized to enhance the binder to ensure stable mesoporous carbon electrodes.

5.2.5 Electrochemical Detection

For electrochemical measurements, a CHI 1230A potentiostat electrochemical analyzer (CHI, Austin, TX) was used. The chronoamperometric behavior was examined under applied potential of -0.2 V for all the samples. A ferricyanide-mediated system based on 0.25 mg mL^{-1} of enzyme PNMT, 0.375 mg ml^{-1} cofactor SAM, 25 mM potassium hexacyanoferrate and 25 mM potassium ferricyanide in PBS solution were used for all measurements. In a standard measurement, the contacts of the sensor were wetted by 90 μL of enzyme/cofactor/mediator solution with the entire contact area for each electrode (working, reference and counter electrode) covered by the solution. Subsequently,

10 μL sample solution (NE in PBS or blood) was injected into the center of the enzyme/mediator solution and allowed to settle for 5 s. For each set of amperometric i-t assays, a NE-in-PBS concentration gradient was used with NE concentrations of 0, 100, 200, 300, 400 and 500 pg mL^{-1} (n=3), respectively. For the detection of NE level in blood, a known amount of NE was added into the whole blood to yield 1000 mg mL^{-1}. This stock solution was subsequently diluted to 100, 200, 300, 400 and 500 pg mL^{-1} for the detection measurements. The amperometric i-t response under applied potential of -0.2 V was then measured for 20 s for each concentration. Each NE concentration gradient sensing measurement was repeated at least three times to obtain the average sensitivity and error range. Every sensor was washed with fresh PBS three times and gently dried between measurements to prevent contamination from prior measurement.

5.3 Results and discussions

5.3.1Characterizations of mesoporous carbons

Figure 48 illustrates the XRD profile of the mesoporous carbons. A well-defined low-angle diffraction peak is observed for all the carbons, which indicates an ordered mesostructure. The XRD profile lacks higher order reflections and thus precludes space group identification from the diffraction pattern. However, the position of the primary diffraction peak is consistent with prior reports for similar materials[24] and shifts to lower angles as the silica content is increased (MP-C-36 to MP-C-61). The d-spacing of the framework is from 8.4 nm, 8.9 nm, 9.6nm and 10 nm for FDU-16, MP-C-36, MP-C-61 and MP-C-46, respectively, from application of Bragg's law. It should be noted that the contraction of the resol

during carbonization is significantly hindered by addition of TEOS from the d-space observed whereby the silica network supports the framework during carbonization. It is this structural reinforcement by the silica that leads to the shifts in the diffraction peaks. The ordered mesostructures of these carbons are confirmed by TEM (Figure 49) with a well ordered mesoporous structure that is consistent with the global average information from XRD patterns.

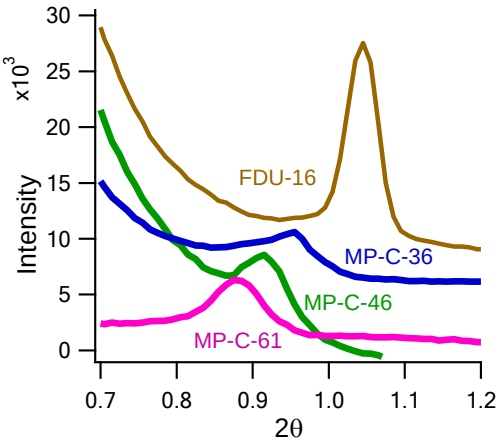

Figure 48 Low-angle powder XRD patterns for MP-C-36, MP-C-46 and MP-C-61.

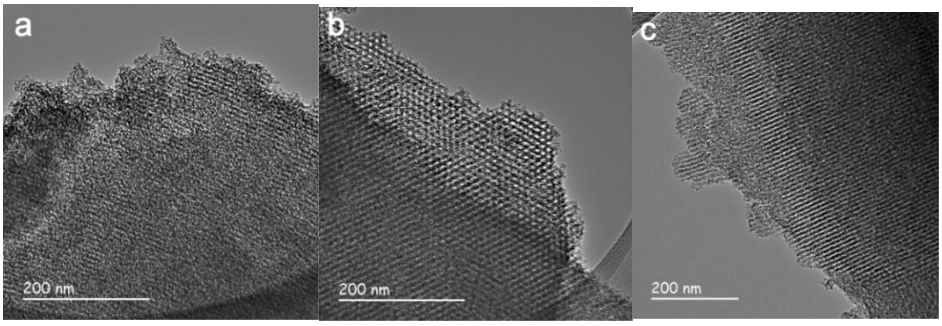

Figure 49 TEM micrographs of mesoporous carbons: (a) MP-C-36, (b) MP-C-46 and (c) MP-C-61. A well-defined ordered structure is found for all materials.

From the XRD and TEM, the difference between the mesoporous carbon materials appears minor, but the etched silica yields significant porosity in the mesostructure framework that can be readily assessed using N_2 sorption. Figure 50A illustrates the adsorption/desorption isotherms for the mesoporous carbons, which are typical type IV isotherm curves for mesoporous materials. The isotherms qualitatively can provide significant insight into the pore structure of the powders. First, the volume of adsorbed N_2 for the isotherms scales with the pore volume of the mesoporous materials with MP-C-46 obviously exhibiting the largest pore volume. Additionally, the slope of the isotherm between $P/P_0 = 0.05–0.25$ provides insight into the surface area with MP-C-46 exhibiting the largest slope and hence the greatest surface area of the mesoporous carbons examined. From analysis of the adsorption isotherms, the pore size distribution (Figure 50B) is calculated based upon BJH model. The average pore diameter is between 6 and 9 nm for all mesoporous carbons examined as shown in Table 7. These small differences in pore size are consistent with the previous reports for analogous mesoporous carbons.[24] When TEOS is not utilized in the synthesis of the mesoporous carbon (FDU-16), the pore diameter is 5.8 nm, which is not far removed from the 6 nm diameter for MP-C-36. However, the surface area is nearly triples from 671 m^2/g to 1734 m^2/g from FDU-16 to MP-C-36 due to the presence of micropores in the carbon framework from the etched silica. The surface area increases significantly again for MP-C-46 (2339 $m^2\ g^{-1}$), but then subsequently decreases when additional TEOS is added for MP-C-61 (1501 m^2/g). These pore characteristics are consistent with previous reports.[24]

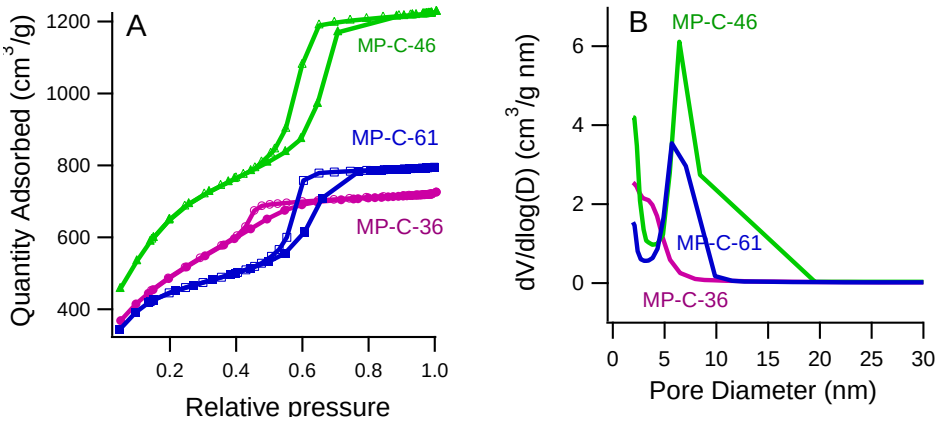

Figure 50 Adsorption (solid marker)/desorption (empty marker) isotherms and (B) pore size distribution of MP-CS-36, MP-CS-46 and MP-CS-61.

Table 7 Structural properties of mesoporous powders obtained from N_2 sorption.

	Surface area ($m^2 g^{-1}$)	**Pore diameter (nm)**	**Pore Volume ($cm^3 g^{-1}$)**
FDU-16	671	2.9	0.14
MP-C-36	1734	3.0	0.91
MP-C-46	2339	4.0	1.68
MP-C-61	1501	4.3	1.23

5.3.2 Electrochemical detection of Norepinephrine (NE)

Phenylethanolamine N-methyltransferase (PNMT) is mainly localized in the adrenal medulla, which can physiologically catalyze norepinephrine (NE) into epinephrine (EP).[30,31] During amperometric i-t measurements, with the presence of PNMT, NE is oxidized to EP,[2] meanwhile the reduction/oxidation of the mediator enables the charge transfer during the reaction to be measured at the

electrode, which is directly proportional to the oxidized amount of NE. In order to effectively determine concentrations from amperometric i-t measurements on the electrodes, cyclic voltammograms (CV) are obtained to select the potential for i-t tests. Figure 51 illustrates a representative CV curve using MP-C-36; the current obtained from 500 pg mL^{-1} NE solution is significantly greater than the blank solution. Moreover, the reduction/oxidation of ferricyanide/ferrocyanide from the oxidation of NE is clearly observed with a peak at - 0.2 V that is present only for 500 pg mL^{-1} NE solution but not for the blank. As this peak at - 0.2V appears directly related to the oxidation and detection of NE, this potential is selected for all the amperometric i-t measurements.

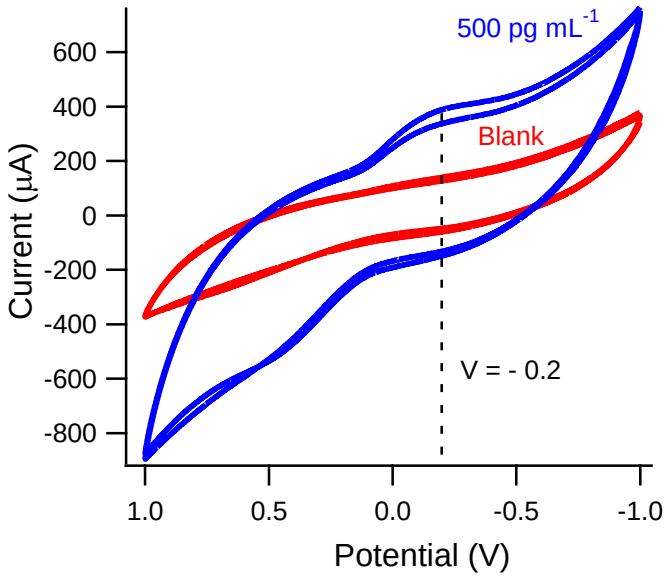

Figure 51 Cyclic voltammetry profile using MP-C-36 electrode containing PNMT, SAM and potassium ferri/ferro-cyanide with comparison of testing a blank (0 pg mL^{-1} NE) and 500 pg mL^{-1} NE sample.

Calibration curves are obtained on the basis of this current-concentration relationship with a steady-state response provided by redox mediator during amperometric i-t measurements. Figure 52 demonstrates a typical current response of i-t measurement using a MP-C-36 carbon electrode where the steady state current increases gradually as NE concentration increases. For the detection point and the calibration curve, the current at 5 s is utilized in order to show the response of the sensor can be rapid.

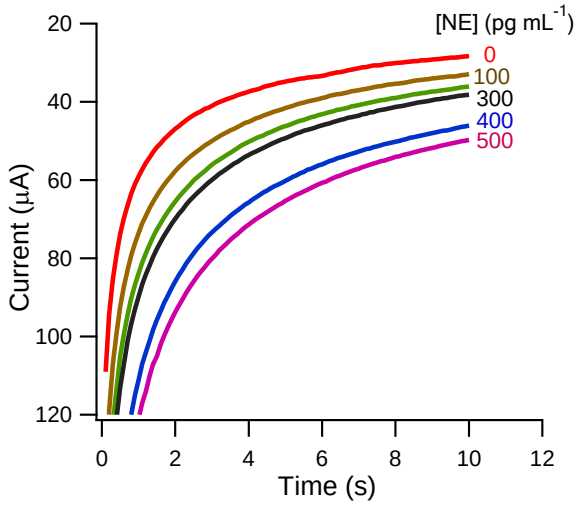

Figure 52 Steady-state stability current measurements of MP-C-36 electrode with different concentrations of NE. From bottom to top: 0, 100, 200, 300, 400, 500 pg mL^{-1}, respectively.

5.3.3 Impact of surface area/pore size on sensor performance

It is well established that surface area of the electrode materials is crucial for high sensitivity of electrochemical sensors. In addition to surface area, the pore size is also important to facilitate transport of the reactants for the bulk solution to the internal pores for collection of the electrons associated with the

redox reaction and thus increasing the current that potentially could improve the sensitivity of the sensor.[32,33] However for these self-assembled porous materials, increasing pore size generally leads to a decrease in surface area[33,34] Typically it is desired to use the minimum pore diameter that still allows enzyme infiltration to obtain maximum sensitivity for the sensor.[33,34] The hydrodynamic radius of PNMT is calculated to be 5 nm, but this size is dominated by three flexible arms and thus can easily enter into the smaller pores examined here with the mode peak size from BJH analysis (Figure 48B) being 3.8 nm (MP-C-36), 6.5 nm (MP-C-46), 5.8 nm (MP-C-61). The calculated average pore size is smaller due to large number of micropores produced by removing SiO_2 from the carbon framework. These small micropores are too small to accommodate PNMT, but these are accessible to the potassium ferri-/ferro-cyanide. As a result, these carbon powders have a hierarchical structure with large pores accessible to the enzyme PNMT and micropores, which enable charge transfer from the mediator with very large accessible surface area. To illustrate the importance of the high surface area micropores, the detection ability of these hierarchical porous carbons is compared with a control sample with similar mesopore size, but lacking micropores (FDU-16). As shown in Figure 53, the current from the FDU-16 is nearly invariant over the range of relevant NE concentrations (0-500 pg/ml); conversely, using MP-C-36, which exhibits a very similar pore size, as the active electrode material produces a clear linear increase in current as the NE concentration is increased over the same range. This is despite an order of magnitude greater FDU-16 (~ 1 mg) than MP-C-36 (~0.1 mg) for the electrodes in this case. Although FDU-16

exhibited excellent performance when used as electrode for glucose sensing,[18] it lacks surface area to enable high sensitivity for low concentration analytes such as NE ($6\frac{\mu A}{ng/ml}$). Of the mesoporous carbons examined, MP-C-46 shows the highest current signal (181-232 μA, <0.1 mg electrode); this might be expected as MP-C-46 has both the highest surface area (2339 m^2/g) and largest pore size (4.0) of the mesoporous carbons. However as the amount of mesoporous powder varies somewhat between electrodes, the absolute current is not an appropriate measure for the sensitivity. Rather, the change in current with increasing NE concentration provides a normalized route to assess the sensitivity of the mesoporous carbon-based sensors. To assess this sensitivity, the calibration curves illustrated in Figure 53A can be linearly fit. The most sensitive electrode is fabricated using MP-C-46 with sensitivity (slope) of $117\frac{\mu A}{ng/ml}$; this result is not surprising as this mesoporous carbon exhibits the largest pore size and surface area, both of which are important to detection of the PNMT as described previously. To further investigate the relative importance of pore size and surface area for the mesoporous carbons examined here, the detection sensitivity of NE using MP-C-36 (1734 m^2/g, 3 nm) and MP-C-61 (1501 m^2/g, 4.3 nm) are compared; despite the smaller pore size in MP-C-36, it has similar sensitivity $62\frac{\mu A}{ng/ml}$ as MP-C-61 ($67\frac{\mu A}{ng/ml}$), because of the similar surface area. If sensitivity is plotted against surface area in each case, as shown in Figure 53B, a linear relationship would occur. Sensitivity of the electrode is directly proportional to the surface area of mesoporous carbon.

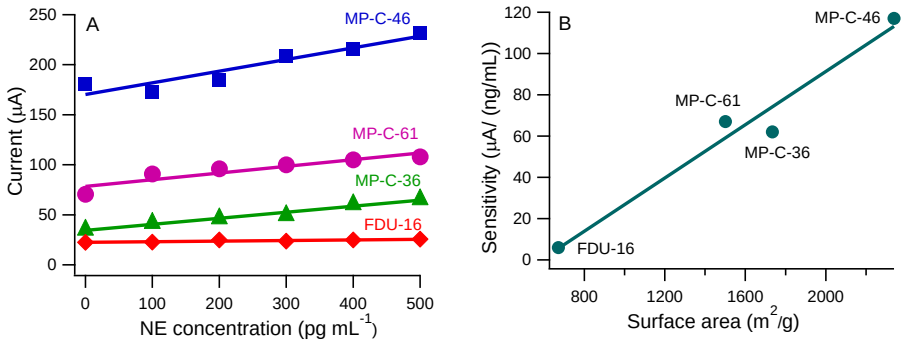

Figure 53 (A) NE concentration gradient calibration curves in PBS of MP-C-36 (▲), MP-C-46 (■), MP-C-61(●) and (D) FDU-16 (♦) as reference; (B) Relationship between sensitivity (slope of calibration curve) and surface area.

We have previously illustrated for glucose sensing that mesopores in FDU-16 provide efficient blocking of non-specific interactions to enable sensing without a Nafion membrane in whole blood.[18] However, the concentration of NE is significantly less than glucose at physiological conditions; thus, it is not clear if these mesoporous materials will be effective without use of a membrane to exclude other blood components from the active electrode. As MP-C-46 mesoporous carbon provides the best performance in electrochemical detection of NE, this electrode is further investigated for its efficacy in detecting NE in whole rabbit blood. Figure 54 illustrates the amperometric response of this electrode to NE in whole rabbit blood. A linear trend is clearly present in the current response of the sensor with the NE concentration in the blood. The lower detection limit of this sensor without a membrane appears to be approximately 100 pg mL^{-1} as the current does not deviate significantly from the control (no NE) at this lowest concentration, but the current at 100 pg mL^{-1} appears to be consistent with the

linear trend from higher concentrations. This result suggests that the high surface area coupled with small pores of ordered mesoporous carbon can be utilized to easily and rapidly detect electrochemically active components in blood via mediated enzymatic reaction using simple amperometric sensing protocols.

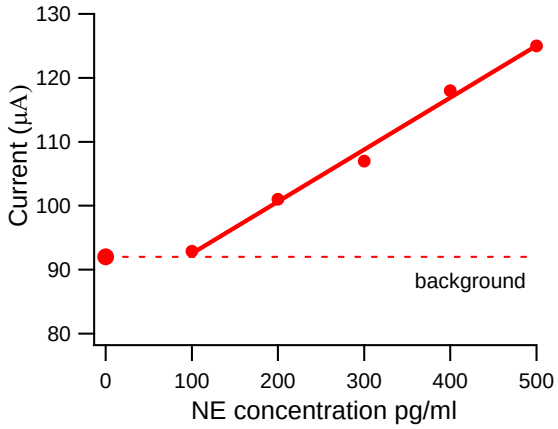

Figure 54 NE concentration measurements in blood by MP-C-46 screen printed electrode.

5.4 Conclusions

Screen printed sensors based on high surface area mesoporous carbon electrode and PHBMA binder can detect norepinephrine (NE) at low concentrations that are physiologically relevant. The sensitivity of these electrodes for NE is strongly dependent upon the surface area; to obtain sufficient surface area and pores compatible with PNMT, a hierarchical templating approach is utilized with mesopores (3-5 nm) to enable transport of PNMT templated by non-ionic surfactant and micropores (<1 nm) in the wall to provide high surface area templated by silica. Mesoporous carbon without the micropore template lacks sensitivity to accurately detect NE in the range of 100-500 pg mL^{-1}.

A mesoporous carbon with similar pore size by significantly larger surface area as a result of the micropores provides sufficient sensitivity to NE over this range. The best-performing sensor also provides similar performance when detecting NE in both PBS and whole rabbit blood. The lower detection limit without an exclusion membrane such as Nafion is approximately 100 pg mL^{-1} in whole rabbit blood; this high sensitivity without a membrane is attributed to the molecular sieving capabilities of the mesopores and the large internal surface area of the mesoporous carbons.

5.5 References

1. Mazloum-Ardakani, M.; Beitollahi, H.; Amini, M. K.; Mirkhalaf, F.; Mirjalili, B.-F., A highly sensitive nanostructure-based electrochemical sensor for electrocatalytic determination of norepinephrine in the presence of acetaminophen and tryptophan. *Biosensors and Bioelectronics* **2011**, *26*, 2102-2106.

2. Goyal, R. N.; Aziz, M. A.; Oyama, M.; Chatterjee, S.; Rana, A. R. S., Nanogold based electrochemical sensor for determination of norepinephrine in biological fluids. *Sensors and Actuators B: Chemical* **2011**, *153*, 232-238.

3. Goyal, R. N.; Agrawal, B., Ag ion irradiated based sensor for the electrochemical determination of epinephrine and 5-hydroxytryptamine in human biological fluids. *Analytica Chimica Acta* **2012**, *743*, 33-40.

4. Mazloum-Ardakani, M.; Sheikh-Mohseni, M. A.; Abdollahi-Alibeik, M.; Benvidi, A., Electrochemical sensor for simultaneous determination of norepinephrine, paracetamol and folic acid by a nanostructured mesoporous material. *Sensors and Actuators B: Chemical* **2012**, *171–172*, 380-386.

5. Mazloum-Ardakani, M.; Beitollahi, H.; Amini, M. K.; Mirkhalaf, F.; Abdollahi-Alibeik, M., New strategy for simultaneous and selective voltammetric determination of norepinephrine, acetaminophen and folic acid using zro2 nanoparticles-modified carbon paste electrode. *Sensors and Actuators B: Chemical* **2010**, *151*, 243-249.

6. Moraes, F. C.; Cesarino, I.; Coelho, D.; Pedrosa, V. A.; Machado, S. A. S., Highly sensitive neurotransmitters analysis at platinum-ultramicroelectrodes arrays. *Electroanalysis* **2012**, *24*, 1115-1120.

7. Zhu, M.; Huang, X.; Li, J.; Shen, H., Peroxidase-based spectrophotometric methods for the determination of ascorbic acid, norepinephrine, epinephrine, dopamine and levodopa. *Analytica Chimica Acta* **1997**, *357*, 261-267.

8. Carrera, V.; Sabater, E.; Vilanova, E.; Sogorb, M. A., A simple and rapid hplc–ms method for the simultaneous determination of epinephrine, norepinephrine, dopamine and 5-hydroxytryptamine: Application to the secretion of bovine chromaffin cell cultures. *Journal of Chromatography B* **2007**, *847*, 88-94.

9. Kuhlenbeck, D. L.; O'Neill, T. P.; Mack, C. E.; Hoke Ii, S. H.; Wehmeyer, K. R., Determination of norepinephrine in small volume plasma samples by stable-isotope dilution gas chromatography–tandem mass spectrometry with negative ion chemical ionization. *Journal of Chromatography B: Biomedical Sciences and Applications* **2000**, *738*, 319-330.

10. Wei, S.; Song, G.; Lin, J.-M., Separation and determination of norepinephrine, epinephrine and isoprinaline enantiomers by capillary electrophoresis in pharmaceutical formulation and human serum. *Journal of Chromatography A* **2005**, *1098*, 166-171.

11. Akhgar, M. R.; Beitollahi, H.; Salari, M.; Karimi-Maleh, H.; Zamani, H., Fabrication of a sensor for simultaneous determination of norepinephrine acetaminophen and tryptophan using a modified carbon nanotube paste electrode. *Anal. Methods* **2012**, *4*, 5.

12. Xu, G.-R.; Chang, H.-Y.; Cho, H.; Meng, W.; Kang, I.-K.; Bae, Z.-U., Macrocyclic nickel(ii) complex and hydrophilic polyurethane film electrodes for the electrocatalytic oxidation and selective detection of norepinephrine. *Electrochimica Acta* **2004**, *49*, 4069-4077.

13. Lee, J. H.; Park, J. Y.; Min, K.; Cha, H. J.; Choi, S. S.; Yoo, Y. J., A novel organophosphorus hydrolase-based biosensor using mesoporous carbons and carbon black for the detection of organophosphate nerve agents. *Biosensors and Bioelectronics* **2010**, *25*, 1566-1570.

14. Su, C.; Zhang, C.; Lu, G.; Ma, C., Nonenzymatic electrochemical glucose sensor based on pt nanoparticles/mesoporous carbon matrix. *Electroanalysis* **2010**, *22*, 1901-1905.

15. Cash, K. J.; Clark, H. A., Nanosensors and nanomaterials for monitoring glucose in diabetes. *Trends in Molecular Medicine* **2010**, *16*, 584-593.

16. Bo, X.; Bai, J.; Wang, L.; Guo, L., In situ growth of copper sulfide nanoparticles on ordered mesoporous carbon and their application as nonenzymatic amperometric sensor of hydrogen peroxide. *Talanta* **2010**, *81*, 339-345.

17. Dong, H.; Wang, S.; Liu, A.; Galligan, J. J.; Swain, G. M., Drug effects on the electrochemical detection of norepinephrine with carbon fiber and diamond microelectrodes. *Journal of Electroanalytical Chemistry* **2009**, *632*, 20-29.

18. Dai, M.; Maxwell, S.; Vogt, B. D.; La Belle, J. T., Mesoporous carbon amperometric glucose sensors using inexpensive, commercial methacrylate-based binders. *Analytica Chimica Acta* **2012**, *738*, 27-34.

19. Chicharro, M.; Sánchez, A.; Bermejo, E.; Zapardiel, A.; Rubianes, M. D.; Rivas, G. A., Carbon nanotubes paste electrodes as new detectors for capillary electrophoresis. *Analytica Chimica Acta* **2005**, *543*, 84-91.

20. Meng, Y.; Gu, D.; Zhang, F.; Shi, Y.; Cheng, L.; Feng, D.; Wu, Z.; Chen, Z.; Wan, Y.; Stein, A.; Zhao, D., A family of highly ordered mesoporous polymer resin and carbon structures from organic−organic self-assembly. *Chemistry of Materials* **2006**, *18*, 4447-4464.

21. Jiang, X.; Wu, Y.; Mao, X.; Cui, X.; Zhu, L., Amperometric glucose biosensor based on integration of glucose oxidase with platinum nanoparticles/ordered mesoporous carbon nanocomposite. *Sensors and Actuators B: Chemical* **2011**, *153*, 158-163.

22. Zhou, M.; Shang, L.; Li, B.; Huang, L.; Dong, S., The characteristics of highly ordered mesoporous carbons as electrode material for electrochemical sensing as compared with carbon nanotubes. *Electrochemistry Communications* **2008**, *10*, 859-863.

23. Zhou, M.; Shang, L.; Li, B.; Huang, L.; Dong, S., Highly ordered mesoporous carbons as electrode material for the construction of electrochemical dehydrogenase- and oxidase-based biosensors. *Biosensors and Bioelectronics* **2008**, *24*, 442-447.

24. Liu, R. L.; Shi, Y. F.; Wan, Y.; Meng, Y.; Zhang, F. Q.; Gu, D.; Chen, Z. X.; Tu, B.; Zhao, D. Y., Triconstituent co-assembly to ordered mesostructured polymer-silica and carbon-silica nanocomposites and large-pore mesoporous carbons with high surface areas. *Journal of the American Chemical Society* **2006**, *128*, 11652-11662.

25. Xu, B.; Wu, F.; Chen, R.; Cao, G.; Chen, S.; Zhou, Z.; Yang, Y., Highly mesoporous and high surface area carbon: A high capacitance electrode material

for edlcs with various electrolytes. *Electrochemistry Communications* **2008**, *10*, 795-797.

26. Li, H.-Q.; Luo, J.-Y.; Zhou, X.-F.; Yu, C.-Z.; Xia, Y.-Y., An ordered mesoporous carbon with short pore length and its electrochemical performances in supercapacitor applications. *Journal of The Electrochemical Society* **2007**, *154*, A731-A736.

27. Xing, W.; Qiao, S. Z.; Ding, R. G.; Li, F.; Lu, G. Q.; Yan, Z. F.; Cheng, H. M., Superior electric double layer capacitors using ordered mesoporous carbons. *Carbon* **2006**, *44*, 216-224.

28. Dai, M.; Vogt, B. D., High capacity magnetic mesoporous carbon–cobalt composite adsorbents for removal of methylene green from aqueous solutions. *Journal of Colloid and Interface Science* **2012**, *387*, 127-134.

29. Karandikar, P.; Patil, K. R.; Mitra, A.; Kakade, B.; Chandwadkar, A. J., Synthesis and characterization of mesoporous carbon through inexpensive mesoporous silica as template. *Microporous and Mesoporous Materials* **2007**, *98*, 189-199.

30. Axelrod, j., Purification and properties of phenylethanolamine-n-methyl transferase. *J. Biol. Chem.* **1962**, *237*, 1657-1660.

31. Fuller, R. W.; Molloy, B. B.; Day, W. A.; Roush, B. W.; Marsh, M. M., Inhibition of phenylethanolamine n-methyl transferase by benzylamines. 1. Structure-activity relations. *Journal of Medicinal Chemistry* **1973**, *16*, 101-106.

32. Hyodo, T.; Sasahara, K.; Shimizu, Y.; Egashira, M., Preparation of macroporous sno2 films using pmma microspheres and their sensing properties to nox and h2. *Sensors and Actuators B: Chemical* **2005**, *106*, 580-590.

33. Ouyang, H.; DeLouise, L. A.; Miller, B. L.; Fauchet, P. M., Label-free quantitative detection of protein using macroporous silicon photonic bandgap biosensors. *Analytical Chemistry* **2007**, *79*, 1502-1506.

34. Ouyang, H.; Striemer, C. C.; Fauchet, P. M., Quantitative analysis of the sensitivity of porous silicon optical biosensors. *Appl. Phys. Lett.* **2006**, *88*, 3.

CHAPTER 6

FUTURE WORK

For the future work, the research will be focusing on exploring the applications of porous materials on the structure control of macroporous carbon and fabrication of antibody biosensors with it. The goal in the future study is to synthesize three macroporous carbon materials with uniform pore size around 50, 100 and 200 nm for each, by using poly(methyl methacrylate) as structure template. This synthesis is difficult mainly because the carbon framework is easy to collapse due to the large pore size and the thin pore wall. But we propose to achieve the stable macroporous carbon framework by changing the wall thickness through proper adjustment of composition of the components in the precursor. If the macroporous carbons are successfully synthesize, we will apply them on the application of antibody biosensors and the impact of the pore size of the carbon, applied potential, pH value and temperature on the performance of the biosensors will be studied.

6.1 Three dimensional macroporous carbons with controllable uniform pore size

Poly(methyl methacrylate) (PMMA) colloid crystals have been extensively used as a template in fabricating three-dimensionally (3D) ordered pores structures with pore diameter range from tens to hundreds of nanometers.[1-6] Non-cross-linked, monodisperse PMMA spheres were firstly synthesized by using emulsifier-free emulsion polymerization as reported by Zhou et al. in 1992.[7] Since then, all kinds of 3D macroporous materials templated by PMMA spheres have attracted much attention for their wide potential applications in photonic crystals.[8] supports for catalytic agents,[9] electrochemical sensors,[10,11] separation,[12,13] and tissue engineering.[14]

Numerous approaches have been developed to synthesize 3D macroporous materials with different structures. For example, through the infiltration of Zr precursor solutions into PMMA colloidal crystals, a 3D ordered macroporous sulfated zirconia catalyst with pore diameters ~300nm was successfully synthesized.[15] With PMMA playing a dual-function templating role for generating both mesoporosity and spherical morphology, mesoporous microspheres of zeolite have been fabricated by direct self-assembly of aluminosilicate precursor and PMMA nanospheres, as a promising candidate of catalyst for industrial cracking of petroleum.[2] As reported by Stein and coworkers, by templating a concentrated triconstituent precursor solution with PMMA spheres, carbon monoliths contains hierarchical porosity of both macropores and mesopores were obtained.[1] However, the process is involving the use of triblock copolymer F127 and tetraethylorthosilicate. In the structure of this carbon material, macropores are resulted from PMMA; large mesopores are from F127 and probably micropores from the removal of the Si. The extremely nonuniformity of the pore size may limit some of the applications such as membrane for separation if want to separate certain size of material, or selective adsorption.

In this work, in order to achieve 3D macroporous carbon with uniform pore size with 50, 100 and 200 nm, respectively, we propose to infiltrate phenol-formaldehyde resol into close-paced PMMA crystal colloids with sphere size of 50, 100, 200 nm, without using other surfactant or other inorganic compounds.

6.1.1 PMMA spheres synthesis

As described in the reported synthesis,[7] first add 20g methyl methacrylate monomer (remove inhibitor by column first) and 185 g water in a flask. Then heat the

solution to 70 ℃ for 20 minutes under stirring. (Add 0.962g dodecyl trimethylamonium bromide (DTAB) only for synthesizing ~50nm PMMA spheres). Add 5g 2 wt% initiator 2,2'-Azobis [2- (2-imidazolin-2-yl) propane] dihydrochloride water solution into the flask. After stir at 70 ℃ for 8 h, remove the flask and cool down to room temperature. Transfer the resulting PMMA sphere suspension to a glass dish and store for several weeks at room temperature without agitation. After the evaporation of water, PMMA spheres will sediment on the bottom of the container, forming opalescent colloidal crystal pieces. PMMA spheres at size ~50nm and ~100nm will be obtained by using surfactant DTAB and ~200nm will be synthesized without using DTAB.

6.1.2 Synthesis of 3D macroporous carbon

As described in previous work, resol precursor was prepared by the polymerization of phenol and formaldehyde under a basic environment. Resol with concentration 50wt% in ethanol will be added to a small beaker with PMMA monoliths sitting in the bottom. Keep the solution level below the top of the PMMA monoliths and cover the beaker with Parafilm. Let the beaker sit for 24 h until the infiltration of resol into PMMA is completed. Then remove the extra solution and place the beaker in a vacuum chamber for 2-3 h at room temperature to remove the solvent. Followed by heating the beaker in an over at 100 ℃ for 24 h and carbonize the monoliths at 600 ℃ under N_2 to remove the PMMA template (PMMA can be removed at 450 ℃ under N_2 environment[4]). Three-dimensional macroporous carbon with uniform size 50nm, 100nm and 200nm will be obtained as illustrated in Figure 55.

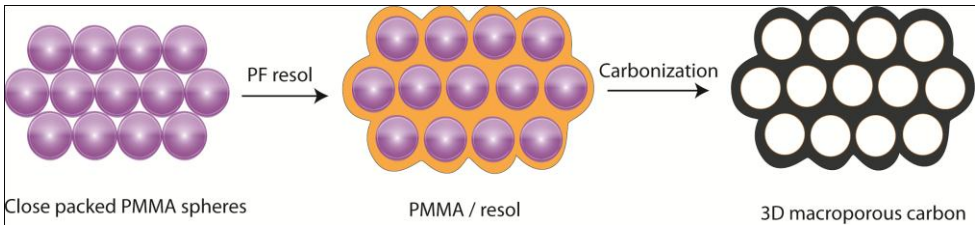

Figure 55 Synthesis steps for the 3D macroporous carbon monoliths.

6.1.3 Immobilize antibody by macroporous carbons

Since Leland C. Clark developed the first enzyme electrode with immobilized glucose oxidase at the New York Academy of Science Symposium in 1962,[16,17] many studies have been focused on searching the ways to immobilize various proteins in different biosensor electrodes to improve the stability, selectivity and sensitivity. Immobilization of protein in the sensor is to stabilize proteins by entrapping it in certain substrate, to retain its activity and specificity for longer time.[18] For immobilizing proteins, porous materials have attracted much attention as a good matrix because they have a large specific area, good adsorption and penetrability.[19] For example, mesoporous silica,[19] nanoporous glass carbon,[20] mesoporous titanium dioxide[21] and macroporous Au-Pt have been synthesized as immobilization hosts for all kinds of enzymes.[22] Macroporous silicon is normally used for entrapping large molecules such as bacteria and antibodies, since it's easy to fabricate macroporous silicon with large pores (1~2 μm) by etching with hydrofluoric acid. As to our knowledge, there is no report on using macroporous carbon as electrode for biosensors to entrap large antibodies. Considering the conductivity and surface area, porous carbons with smaller pore size (50 – 200 nm) may have higher sensitivity and better selectivity in comparison to porous silicon.

Besides the materials used, the pore size of the electrode is also important because it not only determines the size of the proteins that can enter into the pores but also impacts the sensitivity of the sensor.[23,24] Since the sensitivity of the biosensor decreases as the pore size increases because of the decreasing of surface area, the minimum acceptable pore diameter allowed for protein infiltration should be used to obtain maximum sensitivity.[23,25] However, for electrical biosensors, macroporous materials have their advantages such as less electrical noise due to the decreased density of surface state and easy for enzymes to locate the field lines through the pores near the electrodes[26]. Also, as reported by Steinhauer et al.,[27] macroporous silicon has higher binding capacity than nanoporous silicon.

Interleukin-12 (IL-12) is a protein that has been recognized as a central regulator of immune responses and it involves in the many diseases such as antibody-mediated autoimmune disease[28] and tumor.[29,30] It is important to detect IL-12 level to prevent those diseases in advance. In this work, in order to investigate the pore size of macroporous carbon on the sensitivity, mechanical stability and activity of the lifetime of immobilized enzymes, we propose to fabricate IL-12 biosensor using macroporous carbons with 50, 100 and 200 nm pore diameter to entrap the antibody (2 x 5 x 10 nm) against interleukin-12 (anti-IL-12). The performance of the sensor over time, temperature, PH and inteleukin-12 concentration will be investigated.

Step 1, antibody immobilization

Dissolve the anti-IL-12 in PBS buffer (10mM, PH=7.4) solution to get a final concentration of 2500 U/cm^{-3}. Then add the macroporous carbon into the enzyme solution, and allowed to adsorb enzyme for 20 h at room temperature as shown in Figure

56. Filter the carbon out and wash it with PBS solution to remove the unbound enzyme. The powder is allowed to dry under ambient conditions for overnight. Then the powder with entrapped anti-IL-12 is ready to deposit on the screen printed electrode.

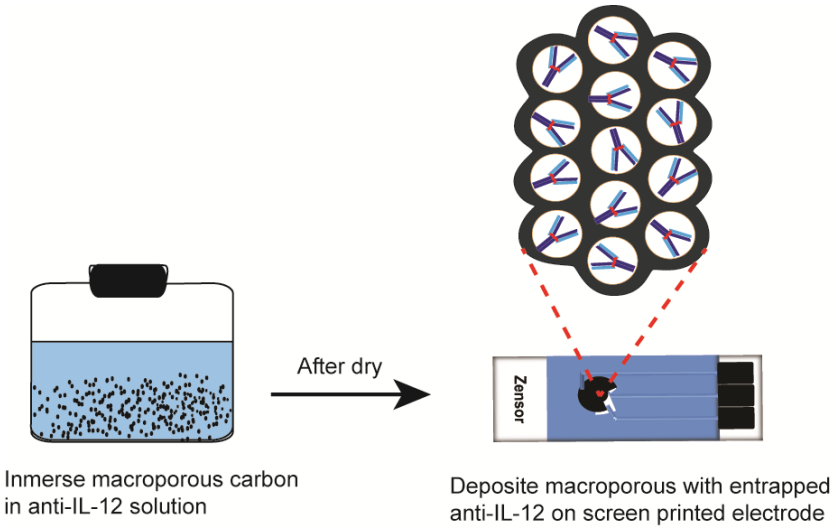

Figure 56 Schematic of preparation for macroporous carbon electrode with entrapped anti-IL-12.

Step 2, quantify the amount of adsorbed antibody

Measure the pore volume before and after adsorption of anti-IL-12 by BET method. The adsorption capacity will be calculated by

$$C = \frac{V_0 - V_1}{V_0} \tag{6.4}$$

where V_0 and V_1 are the pore volume before and after adsorption, respectively.[19]

Step 3, electrochemical analysis

First, the effect of applied potential on the amperometric response of the biosensor to the IL-12 will be examined. During the reaction, the anti-IL-12 only reacts with the antigen IL-12 as shown in Figure 57. The potential at the maximum value of current will be selected upon varying applied potential from -1 to 1 V. The pH value of

the target IL-12 solution is one important parameter affecting the response of the biosensor. The electrochemical current signal of the biosensor will be studied as the pH value varies from 4 to 9.0. The response is supposed to be maximum at pH 7.0 based on the assumption that other pH values would cause protein denaturation.[19] The activity of the biosensor will be investigated with temperature range from 15 to 60 ℃ (possible temperature in human body) based on the amperometric response. We hypothesize the signal will increase with temperature increasing from 15 to ~40 ℃ since the enzyme is more active at higher temperature, but higher than 40 ℃ would probably denature the antibody. Then the calibration curve of current versus IL-12 concentrations will be measured at optimal applied potential, pH value and temperature, and use the calibration curve to detect the IL-12 concentration in the blood sample. Also, the detecting performance versus time (~10 days) of the biosensor will be performed to determine the active time of entrapped anti-IL-12 to detect IL-12 in blood. Lastly, compare the performance of current signal, measurement accuracy and active lifetime of the biosensors composed by the different size of macroporous carbons.

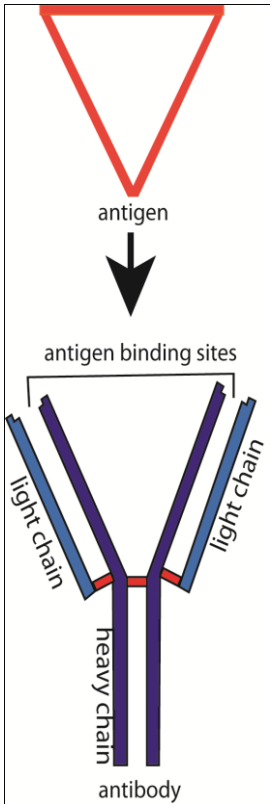

Figure 57 Schematic of reaction mechanism of antibody and antigen.

Through this study, it is expected to see that firstly macroporous carbons can be successfully synthesized. Then enough amount of anti-IL-12 can be entrapped in the macropores. By depositing the macroporous carbon with entrapped anti-IL-12 on to the screen printed electrode, the electrode is hypothesized to show high enough signal by responding to the target IL-12. Upon the study of response of the sensor to the target under different conditions, the optimum combination of pore size, pH value, environment temperature, and active time of the sensor. Finally, the sensor will be used to detect IL-12 in blood sample under optimum condition. This study would open a window of utilizing macroporous carbon in the application of amperometric antibody sensor and expand the application field of porous carbon on sensing other proteins with large size.

6.3 References

1. Wang, Z.; Stein, A., Morphology control of carbon, silica, and carbon/silica nanocomposites: From 3d ordered macro-/mesoporous monoliths to shaped mesoporous particles†. *Chemistry of Materials* **2007**, *20*, 1029-1040.

2. Zhao, J.; Zhou, J.; Chen, Y.; He, Q.; Ruan, M.; Guo, L.; Shi, J.; Chen, H., Fabrication of mesoporous zeolite microspheres by a one-pot dual-functional templating approach. *Journal of Materials Chemistry* **2009**, 7614-7616.

3. Sadakane, M.; Horiuchi, T.; Kato, N.; Takahashi, C.; Ueda, W., Facile preparation of three-dimensionally ordered macroporous alumina, iron oxide, chromium oxide, manganese oxide, and their mixed-metal oxides with high porosity. *Chemistry of Materials* **2007**, *19*, 5779-5785.

4. Yan, H.; Blanford, C. F.; Lytle, J. C.; Carter, C. B.; Smyrl, W. H.; Stein, A., Influence of processing conditions on structures of 3d ordered macroporous metals prepared by colloidal crystal templating. *Chemistry of Materials* **2001**, *13*, 4314-4321.

5. Wang, X.; Xu, S.; Xu, W., Luminescent properties of dye-pmma composite nanospheres. *Physical Chemistry Chemical Physics* **2011**, 1560-1567.

6. Sasahara, K.; Hyodo, T.; Shimizu, Y.; Egashira, M., Macroporous and nanosized ceramic films prepared by modified sol-gel method with pmma microsphere templates. *Journal of the European Ceramic Society* **2004**, *24*, 1961-1967.

7. Zou, D.; Ma, S.; Guan, R.; Park, M.; Sun, L.; Aklonis, J. J.; Salovey, R., Model filled polymers. V. Synthesis of crosslinked monodisperse polymethacrylate beads. *Journal of Polymer Science Part A: Polymer Chemistry* **1992**, *30*, 137-144.

8. Fu, M.; Deng, L.; Zhao, A.; Wang, Y.; He, D., Fabrication and optical properties of alq3 doped pmma microsphere arrays templated by zno inverse opal structure. *Optical Materials* **2010**, *32*, 1210-1215.

9. Zhang, J.; Zhang, Y.; Lian, S.; Liu, Y.; Kang, Z.; Lee, S.-T., Highly ordered macroporous carbon spheres and their catalytic application for methanol oxidation. *Journal of Colloid and Interface Science* **2011**, *361*, 503-508.

10. Simonis, A.; Ruge, C.; Müller-Veggian, M.; Lüth, H.; Schöning, M. J., A long-term stable macroporous-type eis structure for electrochemical sensor applications. *Sensors and Actuators B: Chemical* **2003**, *91*, 21-25.

11. Qiu, J.-D.; Peng, H.-Z.; Liang, R.-P.; Xiong, M., Preparation of three-dimensional ordered macroporous prussian blue film electrode for glucose biosensor application. *Electroanalysis* **2007**, *19*, 1201-1206.

12. Hosoya, K.; Ogata, T.; Watabe, Y.; Kubo, T.; Ikegami, T.; Tanaka, N.; Minakuchi, H.; Nakanishi, K., Silica monolithic membrane as separation medium: Summable property of different membranes for high-performance liquid chromatographic separation. *Journal of Chromatography A* **2005**, *1073*, 123-126.

13. Chen, X.; Yang, W.; Liu, J.; Lin, L., Synthesis of zeolite naa membranes with high permeance under microwave radiation on mesoporous-layer-modified macroporous substrates for gas separation. *Journal of Membrane Science* **2005**, *255*, 201-211.

14. Lévesque, S. G.; Lim, R. M.; Shoichet, M. S., Macroporous interconnected dextran scaffolds of controlled porosity for tissue-engineering applications. *Biomaterials* **2005**, *26*, 7436-7446.

15. Al-Daous, M. A.; Stein, A., Preparation and catalytic evaluation of macroporous crystalline sulfated zirconium dioxide templated with colloidal crystals. *Chemistry of Materials* **2003**, *15*, 2638-2645.

16. Clark, L. C.; Lyons, C., Electrode systems for continuous monitoring in cardiovascular surgery. *Annals of the New York Academy of Sciences* **1962**, *102*, 29-45.

17. Pohanka, M.; Skladal, P., Electrochemical biosensors - principles and applications. *J. Appl. Biomed.* **2008**, 6, 57-64.

18. Gavalas, V. G.; Chaniotakis, N. A.; Gibson, T. D., Improved operational stability of biosensors based on enzyme-polyelectrolyte complex adsorbed into a porous carbon electrode. *Biosensors and Bioelectronics* **1998**, *13*, 1205-1211.

19. Dai, Z.; Bao, J.; Yang, X.; Ju, H., A bienzyme channeling glucose sensor with a wide concentration range based on co-entrapment of enzymes in sba-15 mesopores. *Biosensors and Bioelectronics* **2008**, *23*, 1070-1076.

20. Haghighi, B.; Tabrizi, M. A., Direct electron transfer from glucose oxidase immobilized on a nano-porous glassy carbon electrode. *Electrochimica Acta* **2011**, *56*, 10101-10106.

21. Cosnier, S.; Senillou, A.; Grätzel, M.; Comte, P.; Vlachopoulos, N.; Jaffrezic Renault, N.; Martelet, C., A glucose biosensor based on enzyme entrapment within polypyrrole films electrodeposited on mesoporous titanium dioxide. *Journal of Electroanalytical Chemistry* **1999**, *469*, 176-181.

22. Lee, Y.-J.; Park, J.-Y., A coral-like macroporous gold–platinum hybrid 3d electrode for enzyme-free glucose detection. *Sensors and Actuators B: Chemical* **2011**, *155*, 134-139.

23. Ouyang, H.; DeLouise, L. A.; Miller, B. L.; Fauchet, P. M., Label-free quantitative detection of protein using macroporous silicon photonic bandgap biosensors. *Analytical Chemistry* **2007**, *79*, 1502-1506.

24. Hyodo, T.; Sasahara, K.; Shimizu, Y.; Egashira, M., Preparation of macroporous sno2 films using pmma microspheres and their sensing properties to nox and h2. *Sensors and Actuators B: Chemical* **2005**, *106*, 580-590.

25. Ouyang, H.; Striemer, C. C.; Fauchet, P. M., Quantitative analysis of the sensitivity of porous silicon optical biosensors. *Appl. Phys. Lett.* **2006**, *88*, 163108 0-3.

26. Das, R. D.; Maji, S.; Das, S.; RoyChaudhuri, C., Optimization of covalent antibody immobilization on macroporous silicon solid supports. *Applied Surface Science* **2010**, *256*, 5867-5875.

27. Steinhauer, C.; Ressine, A.; Marko-Varga, G.; Laurell, T.; Borrebaeck, C. A. K.; Wingren, C., Biocompatibility of surfaces for antibody microarrays: Design of macroporous silicon substrates. *Analytical Biochemistry* **2005**, *341*, 204-213.

28. Moiola, L.; Galbiati, F.; Martino, G.; Amadio, S.; Brambilla, E.; Comi, G.; Vincent, A.; Grimaldi, L. M. E., Il-12 is involved in the induction of experimental autoimmune myasthenia gravis, an antibody- mediated disease. *European Journal of Immunology* **1998**, *28*, 2487-2497.

29. Gillies, S. D.; Lan, Y.; Wesolowski, J. S.; Qian, X.; Reisfeld, R. A.; Holden, S.; Super, M.; Lo, K.-M., Antibody-il-12 fusion proteins are effective in scid mouse models of prostate and colon carcinoma metastases. *The Journal of Immunology* **1998**, *160*, 6195-6203.

30. Aloisi, F.; Penna, G.; Cerase, J.; Menendez Iglesias, B.; Adorini, L., Il-12 production by central nervous system microglia is inhibited by astrocytes. *The Journal of Immunology* **1997**, *159*, 1604-1612.

REFERENCES

1. Huang, C.-h.; Doong, R.-a.; Gu, D.; Zhao, D., Dual-template synthesis of magnetically-separable hierarchically-ordered porous carbons by catalytic graphitization. *Carbon* **2011**, *49*, 3055-3064.

2. Park, I.-S.; Choi, M.; Kim, T.-W.; Ryoo, R., Synthesis of magnetically separable ordered mesoporous carbons using furfuryl alcohol and cobalt nitrate in a silica template. *Journal of Materials Chemistry* **2006**, *16*, 3409-3416.

3. Vinu, A.; Streb, C.; Murugesan, V.; Hartmann, M., Adsorption of cytochrome c on new mesoporous carbon molecular sieves. *The Journal of Physical Chemistry B* **2003**, *107*, 8297-8299.

4. Gierszal, K. P.; Kim, T.-W.; Ryoo, R.; Jaroniec, M., Adsorption and structural properties of ordered mesoporous carbons synthesized by using various carbon precursors and ordered siliceous p6mm and ia3̄d mesostructures as templates. *The Journal of Physical Chemistry B* **2005**, *109*, 23263-23268.

5. Darmstadt, H.; Roy, C.; Kaliaguine, S.; Kim, T.-W.; Ryoo, R., Surface and pore structures of cmk-5 ordered mesoporous carbons by adsorption and surface spectroscopy. *Chemistry of Materials* **2003**, *15*, 3300-3307.

6. Zheng, D.; Ye, J.; Zhou, L.; Zhang, Y.; Yu, C., Simultaneous determination of dopamine, ascorbic acid and uric acid on ordered mesoporous carbon/nafion composite film. *Journal of Electroanalytical Chemistry* **2009**, *625*, 82-87.

7. Zhou, M.; Shang, L.; Li, B.; Huang, L.; Dong, S., Highly ordered mesoporous carbons as electrode material for the construction of electrochemical dehydrogenase- and oxidase-based biosensors. *Biosensors and Bioelectronics* **2008**, *24*, 442-447.

8. Zhou, M.; Shang, L.; Li, B.; Huang, L.; Dong, S., The characteristics of highly ordered mesoporous carbons as electrode material for electrochemical sensing as compared with carbon nanotubes. *Electrochemistry Communications* **2008**, *10*, 859-863.

9. Bo, X.; Bai, J.; Wang, L.; Guo, L., In situ growth of copper sulfide nanoparticles on ordered mesoporous carbon and their application as nonenzymatic amperometric sensor of hydrogen peroxide. *Talanta* **2010**, *81*, 339-345.

10. Dai, M.; Song, L.; LaBelle, J. T.; Vogt, B. D., Ordered mesoporous carbon composite films containing cobalt oxide and vanadia for electrochemical applications. *Chemistry of Materials* **2011**, *23*, 2869-2878.

11. Jia, N.; Wang, Z.; Yang, G.; Shen, H.; Zhu, L., Electrochemical properties of ordered mesoporous carbon and its electroanalytical application for selective determination of dopamine. *Electrochemistry Communications* **2007**, *9*, 233-238.

12. Ryoo, R.; Joo, S. H.; Kruk, M.; Jaroniec, M., Ordered mesoporous carbons. *Advanced Materials* **2001**, *13*, 677-681.

13. Zhou, M.; Guo, L.-p.; Lin, F.-y.; Liu, H.-x., Electrochemistry and electrocatalysis of polyoxometalate-ordered mesoporous carbon modified electrode. *Analytica Chimica Acta* **2007**, *587*, 124-131.

14. Zhou, M.; Ding, J.; Guo, L.-p.; Shang, Q.-k., Electrochemical behavior of l-cysteine and its detection at ordered mesoporous carbon-modified glassy carbon electrode. *Analytical Chemistry* **2007**, *79*, 5328-5335.

15. Levario, T. J.; Dai, M.; Yuan, W.; Vogt, B. D.; Nielsen, D. R., Rapid adsorption of alcohol biofuels by high surface area mesoporous carbons. *Microporous and Mesoporous Materials* **2012**, *148*, 107-114.

16. Ding, J.; Chan, K.-Y.; Ren, J.; Xiao, F.-s., Platinum and platinum–ruthenium nanoparticles supported on ordered mesoporous carbon and their electrocatalytic performance for fuel cell reactions. *Electrochimica Acta* **2005**, *50*, 3131-3141.

17. Joo, S. H.; Pak, C.; You, D. J.; Lee, S.-A.; Lee, H. I.; Kim, J. M.; Chang, H.; Seung, D., Ordered mesoporous carbons (omc) as supports of electrocatalysts for direct methanol fuel cells (dmfc): Effect of carbon precursors of omc on dmfc performances. *Electrochimica Acta* **2006**, *52*, 1618-1626.

18. Calvillo, L.; Lázaro, M. J.; García-Bordejé, E.; Moliner, R.; Cabot, P. L.; Esparbé, I.; Pastor, E.; Quintana, J. J., Platinum supported on functionalized ordered mesoporous carbon as electrocatalyst for direct methanol fuel cells. *Journal of Power Sources* **2007**, *169*, 59-64.

19. Tate, M. P.; Urade, V. N.; Kowalski, J. D.; Wei, T.-c.; Hamilton, B. D.; Eggiman, B. W.; Hillhouse, H. W., Simulation and interpretation of 2d diffraction patterns from self-assembled nanostructured films at arbitrary angles of incidence: From grazing incidence (above the critical angle) to transmission perpendicular to the substrate. *The Journal of Physical Chemistry B* **2006**, *110*, 9882-9892.

20. Meng, Y.; Gu, D.; Zhang, F.; Shi, Y.; Yang, H.; Li, Z.; Yu, C.; Tu, B.; Zhao, D., Ordered mesoporous polymers and homologous carbon frameworks: Amphiphilic surfactant templating and direct transformation. *Angewandte Chemie* **2005**, *117*, 7215-7221.

21. Hillmyer, M.; Abetz, V., Ed.; Springer Berlin / Heidelberg: 2005; Vol. 190, p 137-181.

22. Meng, Y.; Gu, D.; Zhang, F.; Shi, Y.; Cheng, L.; Feng, D.; Wu, Z.; Chen, Z.; Wan, Y.; Stein, A.; Zhao, D., A family of highly ordered mesoporous polymer resin and carbon structures from organic−organic self-assembly. *Chemistry of Materials* **2006**, *18*, 4447-4464.

23. Lu, G. Q.; Zhao, X. S. *Nanoporous materials science and engineering*; Imperial College Press, 2004; Vol. 4.

24. Beck, J. S.; Vartuli, J. C.; Roth, W. J.; Leonowicz, M. E.; Kresge, C. T.; Schmitt, K. D.; Chu, C. T. W.; Olson, D. H.; Sheppard, E. W., A new family of mesoporous molecular sieves prepared with liquid crystal templates. *Journal of the American Chemical Society* **1992**, *114*, 10834-10843.

25. Kresge, C. T.; Leonowicz, M. E.; Roth, W. J.; Vartuli, J. C.; Beck, J. S., Ordered mesoporous molecular sieves synthesized by a liquid-crystal template mechanism. *Nature* **1992**, *359*, 710-712.

26. Yang, P.,*The chemistry of nanostructured materials*; World Scientific Publishing Co. Pte. Ltd, 2003.

27. Firouzi, A.; Kumar, D.; Bull, L.; Besier, T.; Sieger, P.; Huo, Q.; Walker, S.; Zasadzinski, J.; Glinka, C.; Nicol, J.; et, a., Cooperative organization of inorganic-surfactant and biomimetic assemblies. *Science* **1995**, *267*, 1138-1143.

28. Huo, Q.; Margolese, D. I.; Ciesla, U.; Feng, P.; Gier, T. E.; Sieger, P.; Leon, R.; Petroff, P. M.; Schuth, F.; Stucky, G. D., Generalized synthesis of periodic surfactant/inorganic composite materials. *Nature* **1994**, *368*, 317-321.

29. Firouzi, A.; Atef, F.; Oertli, A. G.; Stucky, G. D.; Chmelka, B. F., Alkaline lyotropic silicate−surfactant liquid crystals. *Journal of the American Chemical Society* **1997**, *119*, 3596-3610.

30. Tanev, P. T.; Pinnavaia, T. J., A neutral templating route to mesoporous molecular-sieves. *Science* **1995**, *267*, 865-867.

31. Bagshaw, S. A.; Prouzet, E.; Pinnavaia, T. J., Templating of mesoporous molecular-sieves by nonionic polyethylene oxide surfactants. *Science* **1995**, *269*, 1242-1244.

32. Tanev, P. T.; Pinnavaia, T. J., Mesoporous silica molecular sieves prepared by ionic and neutral surfactant templating: A comparison of physical properties. *Chemistry of Materials* **1996**, *8*, 2068-2079.

33. Zentner, G. M.; Rathi, R.; Shih, C.; McRea, J. C.; Seo, M.-H.; Oh, H.; Rhee, B. G.; Mestecky, J.; Moldoveanu, Z.; Morgan, M.; Weitman, S., Biodegradable block copolymers for delivery of proteins and water-insoluble drugs. *Journal of Controlled Release* **2001**, *72*, 203-215.

34. Booth, C.; Attwood, D., Effects of block architecture and composition on the association properties of poly(oxyalkylene) copolymers in aqueous solution. *Macromolecular Rapid Communications* **2000**, *21*, 501-527.

35. Leibler, L., Theory of microphase separation in block copolymers. *Macromolecules* **1980**, *13*, 1602-1617.

36. Lodge, T. P.; Pudil, B.; Hanley, K. J., The full phase behavior for block copolymers in solvents of varying selectivity. *Macromolecules* **2002**, *35*, 4707-4717.

37. Zhao, D. Y.; Feng, J. L.; Huo, Q. S.; Melosh, N.; Fredrickson, G. H.; Chmelka, B. F.; Stucky, G. D., Triblock copolymer syntheses of mesoporous silica with periodic 50 to 300 angstrom pores. *Science* **1998**, *279*, 548-552.

38. Zhao, D.; Huo, Q.; Feng, J.; Chmelka, B. F.; Stucky, G. D., Nonionic triblock and star diblock copolymer and oligomeric surfactant syntheses of highly ordered, hydrothermally stable, mesoporous silica structures. *Journal of the American Chemical Society* **1998**, *120*, 6024-6036.

39. Komarneni, S.; Smith, D. M.; Beck, J. S. *Advances in porous materials*; Materials Research Society, 1994; Vol. 371.

40. Yang, P.; Zhao, D.; Margolese, D. I.; Chmelka, B. F.; Stucky, G. D., Generalized syntheses of large-pore mesoporous metal oxides with semicrystalline frameworks. *Nature* **1998**, *396*, 152-155.

41. Tian, B.; Liu, X.; Tu, B.; Yu, C.; Fan, J.; Wang, L.; Xie, S.; Stucky, G. D.; Zhao, D., Self-adjusted synthesis of ordered stable mesoporous minerals by acid-base pairs. *Nat Mater* **2003**, *2*, 159-163.

42. Braun, P. V.; Osenar, P.; Tohver, V.; Kennedy, S. B.; Stupp, S. I., Nanostructure templating in inorganic solids with organic lyotropic liquid crystals. *Journal of the American Chemical Society* **1999**, *121*, 7302-7309.

43. Frackowiak, E.; Béguin, F., Carbon materials for the electrochemical storage of energy in capacitors. *Carbon* **2001**, *39*, 937-950.

44. Planeix, J. M.; Coustel, N.; Coq, B.; Brotons, V.; Kumbhar, P. S.; Dutartre, R.; Geneste, P.; Bernier, P.; Ajayan, P. M., Application of carbon nanotubes as supports in heterogeneous catalysis. *Journal of the American Chemical Society* **1994**, *116*, 7935-7936.

45. Netzer, A.; Hughes, D. E., Adsorption of copper, lead and cobalt by activated carbon. *Water Research* **1984**, *18*, 927-933.

46. M, K., Removal of cr(vi) from aqueous solutions by adsorption onto hazelnut shell activated carbon: Kinetic and equilibrium studies. *Bioresource Technology* **2004**, *91*, 317-321.

47. Deck, C. P.; Vecchio, K., Prediction of carbon nanotube growth success by the analysis of carbon–catalyst binary phase diagrams. *Carbon* **2006**, *44*, 267-275.

48. Zouboulis, A. I.; Lazaridis, N. K.; Zamboulis, D., Powdered activated carbon separation from water by foam flotation. *Separation Science and Technology* **1994**, *29*, 385-400.

49. Zheng, M.; Jagota, A.; Semke, E. D.; Diner, B. A.; McLean, R. S.; Lustig, S. R.; Richardson, R. E.; Tassi, N. G., DNA-assisted dispersion and separation of carbon nanotubes. *Nat Mater* **2003**, *2*, 338-342.

50. Ishikawa, M.; Morita, M.; Ihara, M.; Matsuda, Y., Electric double-layer capacitor composed of activated carbon fiber cloth electrodes and solid polymer electrolytes containing alkylammonium salts. *Journal of The Electrochemical Society* **1994**, *141*, 1730-1734.

51. Liang, C.; Hong, K.; Guiochon, G. A.; Mays, J. W.; Dai, S., Synthesis of a large-scale highly ordered porous carbon film by self-assembly of block copolymers. *Angewandte Chemie International Edition* **2004**, *43*, 5785-5789.

52. Storck, S.; Bretinger, H.; Maier, W. F., Characterization of micro- and mesoporous solids by physisorption methods and pore-size analysis. *Applied Catalysis A: General* **1998**, *174*, 137-146.

53. Neimark, A. V.; Sing, K. S. W.; Thommes, M. In *Handbook of heterogeneous catalysis*; Wiley-VCH Verlag GmbH & Co. KGaA: 2008.

54. Brunauer, S.; Deming, L. S.; Deming, W. E.; Teller, E., On a theory of the van der waals adsorption of gases. *Journal of the American Chemical Society* **1940**, *62*, 1723-1732.

55. Lowel, S.; Shields, J. E. *Powder surface area and porosity*; Second ed.; Chapman and Hall, 1984.

56. Brunauer, S.; Emmett, P. H.; Teller, E., Adsorption of gases in multimolecular layers. *Journal of the American Chemical Society* **1938**, *60*, 309-319.

57. Harkins, W. D.; Jura, G., Surfaces of solids. Xiii. A vapor adsorption method for the determination of the area of a solid without the assumption of a molecular area, and the areas occupied by nitrogen and other molecules on the surface of a solid. *Journal of the American Chemical Society* **1944**, *66*, 1366-1373.

58. Anderson, R. B., Modifications of the brunauer, emmett and teller equation1. *Journal of the American Chemical Society* **1946**, *68*, 686-691.

59. Jerzy, H., Chapter 3.1 surface area and porosity. *Catalysis Today* **1994**, *20*, 11-16.

60. Boissiere, C.; Grosso, D.; Lepoutre, S.; Nicole, L.; Bruneau, A. B.; Sanchez, C., Porosity and mechanical properties of mesoporous thin films assessed by environmental ellipsometric porosimetry. *Langmuir* **2005**, *21*, 12362-12371.

61. Baklanov, M. R.; Mogilnikov, K. P.; Polovinkin, V. G.; Dultsev, F. N., Determination of pore size distribution in thin films by ellipsometric porosimetry. *Journal of Vacuum Science & Technology B: Microelectronics and Nanometer Structures* **2000**, *18*, 1385-1391.

62. Baklanov, M. R.; Mogilnikov, K. P., Non-destructive characterisation of porous low-k dielectric films. *Microelectronic Engineering* **2002**, *64*, 335-349.

63. Dultsev, F. N.; Baklanov, M. R., Nondestructive determination of pore size distribution in thin films deposited on solid substrates. *Electrochemical and Solid-State Letters* **1999**, *2*, 192-194.

64. Li, X.; Vogt, B. D., Carbon dioxide mediated synthesis of mesoporous silica films: Tuning properties using pressure. *Chemistry of Materials* **2008**, *20*, 3229-3238.

65. Morishige, K.; Tateishi, N., Adsorption hysteresis in ink-bottle pore. *The Journal of Chemical Physics* **2003**, *119*, 2301-2306.

66. Branton, P. J.; Hall, P. G.; Sing, K. S. W.; Reichert, H.; Schuth, F.; Unger, K. K., Physisorption of argon, nitrogen and oxygen by mcm-41, a model mesoporous adsorbent. *Journal of the Chemical Society, Faraday Transactions* **1994**, *90*, 2965-2967.

67. Thommes, M.; Smarsly, B.; Groenewolt, M.; Ravikovitch, P. I.; Neimark, A. V., Adsorption hysteresis of nitrogen and argon in pore networks and characterization of novel micro- and mesoporous silicas. *Langmuir* **2005**, *22*, 756-764.

68. Dongyuan, Z.; Peidong, Y.; Nick, M.; Jianglin, F.; Bradley, F. C.; Galen, D. S., Continuous mesoporous silica films with highly ordered large pore structures. *Advanced Materials* **1998**, *10*, 1380-1385.

69. Yang, Z. X.; Xia, Y. D.; Mokaya, R., Zeolite zsm-5 with unique supermicropores synthesized using mesoporous carbon as a template. *Advanced Materials* **2004**, *16*, 727-732.

70. Machin, W. D., Temperature dependence of hysteresis and the pore size distributions of two mesoporous adsorbents. *Langmuir* **1994**, *10*, 1235-1240.

71. Moro, F.; Böhni, H., Ink-bottle effect in mercury intrusion porosimetry of cement-based materials. *Journal of Colloid and Interface Science* **2002**, *246*, 135-149.

72. Štěpánek, F.; Šoóš, M.; Rajniak, P., Characterisation of porous media by the virtual capillary condensation method. *Colloids and Surfaces A: Physicochemical and Engineering Aspects* **2007**, *300*, 11-20.

73. Han, Y.-J.; Watson, J. T.; Stucky, G. D.; Butler, A., Catalytic activity of mesoporous silicate-immobilized chloroperoxidase. *Journal of Molecular Catalysis B: Enzymatic* **2002**, *17*, 1-8.

74. Ravikovitch, P. I.; Neimark, A. V., Experimental confirmation of different mechanisms of evaporation from ink-bottle type pores: Equilibrium, pore blocking, and cavitation. *Langmuir* **2002**, *18*, 9830-9837.

75. Williams, B. D.; Carter, B. C.,*Transmission electron microscopy: A textbook for material science* 2008.

76. Cullity, B. D. *Elements of x-ray diffraction*; 3rd ed.; Upper saddle river 2001.

77. Klotz, M.; Albouy, P.-A.; Ayral, A.; Ménager, C.; Grosso, D.; Van der Lee, A.; Cabuil, V.; Babonneau, F.; Guizard, C., The true structure of hexagonal mesophase-templated silica films as revealed by x-ray scattering: Effects of thermal treatments and of nanoparticle seeding. *Chemistry of Materials* **2000**, *12*, 1721-1728.

78. Hillhouse, H. W.; van Egmond, J. W.; Tsapatsis, M.; Hanson, J. C.; Larese, J. Z., The interpretation of x-ray diffraction data for the determination of channel orientation in mesoporous films. *Microporous and Mesoporous Materials* **2001**, *44–45*, 639-643.

79. Kacher, J.; Landon, C.; Adams, B. L.; Fullwood, D., Bragg's law diffraction simulations for electron backscatter diffraction analysis. *Ultramicroscopy* **2009**, *109*, 1148-1156.

80. Ruland, W.; Smarsly, B., Saxs of self-assembled oriented lamellar nanocomposite films: An advanced method of evaluation. *Journal of Applied Crystallography* **2004**, *37*, 575-584.

81. Urade, V. N.; Bollmann, L.; Kowalski, J. D.; Tate, M. P.; Hillhouse, H. W., Controlling interfacial curvature in nanoporous silica films formed by evaporation-induced self-assembly from nonionic surfactants. Ii. Effect of processing parameters on film structure. *Langmuir* **2007**, *23*, 4268-4278.

82. Tanaka, S.; Tate, M. P.; Nishiyama, N.; Ueyama, K.; Hillhouse, H. W., Structure of mesoporous silica thin films prepared by contacting peo106−ppo70−peo106 films with vaporized teos. *Chemistry of Materials* **2006**, *18*, 5461-5466.

83. Hillhouse, H. W.; van Egmond, J. W.; Tsapatsis, M., Highly oriented mesostructured thin films: Shear-induced deposition of optically anisotropic coatings of tungsten oxide/surfactant composites. *Langmuir* **1999**, *15*, 4544-4550.

84. Bard, A. J.; Faulkner, L. R. *Electrochemical methods fundamentals and application*; Second edition ed.; John Wiley & Sons. Inc., 1944.

85. Winter, M.; Brodd, R. J., What are batteries, fuel cells, and supercapacitors? *Chemical Reviews* **2004**, *104*, 4245-4270.

86. Miller, J. R.; Simon, P., Electrochemical capacitors for energy management. *Science* **2008**, *321*, 651-652.

87. Xu, B.; Wu, F.; Chen, R.; Cao, G.; Chen, S.; Zhou, Z.; Yang, Y., Highly mesoporous and high surface area carbon: A high capacitance electrode material for edlcs with various electrolytes. *Electrochemistry Communications* **2008**, *10*, 795-797.

88. Cao, L.; Lu, M.; Li, H.-L., Preparation of mesoporous nanocrystalline co[sub 3]o[sub 4] and its applicability of porosity to the formation of electrochemical capacitance. *Journal of The Electrochemical Society* **2005**, *152*, A871-A875.

89. Mao-Wen, X.; Dan-Dan, Z.; Shu-Juan, B.; Hu-Lin, L., Mesoporous amorphous mno₂ as electrode material for supercapacitor. *Journal of Solid State Electrochemistry* **2007**, *11*, 1101-1107.

90. Subramanian, V.; Hall, S. C.; Smith, P. H.; Rambabu, B., Mesoporous anhydrous ruo2 as a supercapacitor electrode material. *Solid State Ionics* **2004**, *175*, 511-515.

91. Yuan, C.-Z.; Gao, B.; Zhang, X.-G., Electrochemical capacitance of nio/ru0.35v0.65o2 asymmetric electrochemical capacitor. *Journal of Power Sources* **2007**, *173*, 606-612.

92. Pandolfo, A. G.; Hollenkamp, A. F., Carbon properties and their role in supercapacitors. *Journal of Power Sources* **2006**, *157*, 11-27.

93. Simon, P.; Gogotsi, Y., Materials for electrochemical capacitors. *Nat Mater* **2008**, *7*, 845-854.

94. Zhai, Y.; Dou, Y.; Zhao, D.; Fulvio, P. F.; Mayes, R. T.; Dai, S., Carbon materials for chemical capacitive energy storage. *Advanced Materials* **2011**, *23*, 4828-4850.

95. Andrew, B., Ultracapacitors: Why, how, and where is the technology. *Journal of Power Sources* **2000**, *91*, 37-50.

96. Li, L.; Song, H.; Chen, X., Pore characteristics and electrochemical performance of ordered mesoporous carbons for electric double-layer capacitors. *Electrochimica Acta* **2006**, *51*, 5715-5720.

97. Korenblit, Y.; Rose, M.; Kockrick, E.; Borchardt, L.; Kvit, A.; Kaskel, S.; Yushin, G., High-rate electrochemical capacitors based on ordered mesoporous silicon carbide-derived carbon. *ACS Nano* **2010**, *4*, 1337-1344.

98. Zhou, H.; Zhu, S.; Hibino, M.; Honma, I., Electrochemical capacitance of self-ordered mesoporous carbon. *Journal of Power Sources* **2003**, *122*, 219-223.

99. Li, H.-Q.; Liu, R.-L.; Zhao, D.-Y.; Xia, Y.-Y., Electrochemical properties of an ordered mesoporous carbon prepared by direct tri-constituent co-assembly. *Carbon* **2007**, *45*, 2628-2635.

100. Xing, W.; Qiao, S. Z.; Ding, R. G.; Li, F.; Lu, G. Q.; Yan, Z. F.; Cheng, H. M., Superior electric double layer capacitors using ordered mesoporous carbons. *Carbon* **2006**, *44*, 216-224.

101. Huwe, H.; Fröba, M., Synthesis and characterization of transition metal and metal oxide nanoparticles inside mesoporous carbon cmk-3. *Carbon* **2007**, *45*, 304-314.

102. Moriguchi, I.; Hidaka, R.; Yamada, H.; Kudo, T.; Murakami, H.; Nakashima, N., A mesoporous nanocomposite of tio2 and carbon nanotubes as a high-rate li-intercalation electrode material. *Advanced Materials* **2006**, *18*, 69-73.

103. Guo, Y. G.; Hu, Y. S.; Sigle, W.; Maier, J., Superior electrode performance of nanostructured mesoporous tio2 (anatase) through efficient hierarchical mixed conducting networks. *Advanced Materials* **2007**, *19*, 2087-2091.

104. Zhu, S.; Zhou, H.; Miyoshi, T.; Hibino, M.; Honma, I.; Ichihara, M., Self-assembly of the mesoporous electrode material li3fe2(po4)3 using a cationic surfactant as the template. *Advanced Materials* **2004**, *16*, 2012-2017.

105. Prabaharan, S. R. S.; Vimala, R.; Zainal, Z., Nanostructured mesoporous carbon as electrodes for supercapacitors. *Journal of Power Sources* **2006**, *161*, 730-736.

106. Huang, J.; Sumpter, B. G.; Meunier, V., A universal model for nanoporous carbon supercapacitors applicable to diverse pore regimes, carbon materials, and electrolytes. *Chemistry – A European Journal* **2008**, *14*, 6614-6626.

107. Liang, C.; Dai, S., Synthesis of mesoporous carbon materials via enhanced hydrogen-bonding interaction. *Journal of the American Chemical Society* **2006**, *128*, 5316-5317.

108. Li, H.-Q.; Luo, J.-Y.; Zhou, X.-F.; Yu, C.-Z.; Xia, Y.-Y., An ordered mesoporous carbon with short pore length and its electrochemical performances in supercapacitor applications. *Journal of The Electrochemical Society* **2007**, *154*, A731-A736.

109. Taberna, P. L.; Simon, P.; Fauvarque, J. F., Electrochemical characteristics and impedance spectroscopy studies of carbon-carbon supercapacitors. *Journal of The Electrochemical Society* **2003**, *150*, A292-A300.

110. Wang, K.; Wang, Y.; Wang, Y.; Hosono, E.; Zhou, H., Mesoporous carbon nanofibers for supercapacitor application. *The Journal of Physical Chemistry C* **2008**, *113*, 1093-1097.

111. Li, H.; Wang, R.; Cao, R., Physical and electrochemical characterization of hydrous ruthenium oxide/ordered mesoporous carbon composites as supercapacitor. *Microporous and Mesoporous Materials* **2008**, *111*, 32-38.

112. Xiong, W.; Liu, M.; Gan, L.; Lv, Y.; Li, Y.; Yang, L.; Xu, Z.; Hao, Z.; Liu, H.; Chen, L., A novel synthesis of mesoporous carbon microspheres for supercapacitor electrodes. *Journal of Power Sources* **2011**, *196*, 10461-10464.

113. Lang, J.-W.; Yan, X.-B.; Yuan, X.-Y.; Yang, J.; Xue, Q.-J., Study on the electrochemical properties of cubic ordered mesoporous carbon for supercapacitors. *Journal of Power Sources* **2011**, *196*, 10472-10478.

114. Liu, P.; Tang, B.; Zhao, J.; Feng, J.; Xu, J., Ordered mesoporous carbon/sno₂ composites as the electrode material for supercapacitors. *Journal of Wuhan University of Technology--Materials Science Edition* **2011**, *26*, 407-411.

115. Gnanakan, S. R. P.; Karthikeyan, K.; Amaresh, S.; Cho, S. J.; Park, G. J.; Lee, Y. S., New application and electrochemical characterization of a nickel-doped mesoporous carbon for supercapacitors. *Journal of Alloys and Compounds* **2011**, *509*, 9858-9864.

116. Lang, J. W.; Yan, X. B.; Xue, Q. J., Facile preparation and electrochemical characterization of cobalt oxide/multi-walled carbon nanotube composites for supercapacitors. *Journal of Power Sources* **2011**, *196*, 7841-7846.

117. Liu, P.; Tang, B. J.; Zhao, J. C.; Feng, J. C.; Xu, J. L., Ordered mesoporous carbon/sno(2) composites as the electrode material for supercapacitors. *Journal of Wuhan University of Technology-Materials Science Edition* **2011**, *26*, 407-411.

118. Nagao, M.; Otani, M.; Tomita, H.; Kanzaki, S.; Yamada, A.; Kanno, R., New three-dimensional electrode structure for the lithium battery: Nano-sized gamma-fe(2)o(3) in a mesoporous carbon matrix. *Journal of Power Sources* **2011**, *196*, 4741-4746.

119. Yang, M.; Gao, Q. M., Copper oxide and ordered mesoporous carbon composite with high performance using as anode material for lithium-ion battery. *Microporous and Mesoporous Materials* **2011**, *143*, 230-235.

120. Chen, Y.; Lunsford, S. K.; Song, Y.; Ju, H.; Falaras, P.; Likodimos, V.; Kontos, A. G.; Dionysiou, D. D., Synthesis, characterization and electrochemical properties of mesoporous zirconia nanomaterials prepared by self-assembling sol-gel method with tween 20 as a template. *Chemical Engineering Journal* **2011**, *170*, 518-524.

121. Zhou, T. X.; Mo, S. S.; Zhou, S. L.; Zou, W. J.; Liu, Y. L.; Yuan, D. S., Mn(3)o(4)/worm-like mesoporous carbon synthesized via a microwave method for supercapacitors. *Journal of Materials Science* **2011**, *46*, 3337-3342.

122. Xia, N. N.; Yuan, D. S.; Zhou, T. X.; Chen, J. X.; Mo, S. S.; Liu, Y. L., Microwave synthesis and electrochemical characterization of mesoporous carbon@bi(2)o(3) composites. *Materials Research Bulletin* **2011**, *46*, 687-691.

123. Dong, X.; Shen, W.; Gu, J.; Xiong, L.; Zhu, Y.; Li, H.; Shi, J., Mno2-embedded-in-mesoporous-carbon-wall structure for use as electrochemical capacitors. *The Journal of Physical Chemistry B* **2006**, *110*, 6015-6019.

124. Lei, Y.; Fournier, C.; Pascal, J.-L.; Favier, F., Mesoporous carbon–manganese oxide composite as negative electrode material for supercapacitors. *Microporous and Mesoporous Materials* **2008**, *110*, 167-176.

125. Wu, Z.; Zhao, D., Ordered mesoporous materials as adsorbents. *Chemical Communications* **2011**, *47*.

126. Wan, Y.; Cui, X.; Wen, Z., Ordered mesoporous carbon coating on cordierite: Synthesis and application as an efficient adsorbent. *Journal of Hazardous Materials* **2011**, *198*, 216-223.

127. Ma, Y. Q.; Zhai, Q. Z.; Yu, H.; Yang, M. J., Removal of pb(ii) from water using nanoscale sba-15. *Asian Journal of Chemistry* **2011**, *23*, 5016-5024.

128. Bui, T. X.; Kang, S. Y.; Lee, S. H.; Choi, H., Organically functionalized mesoporous sba-15 as sorbents for removal of selected pharmaceuticals from water. *Journal of Hazardous Materials* **2011**, *193*, 156-163.

129. Idris, S. A.; Harvey, S. R.; Gibson, L. T., Selective extraction of mercury(ii) from water samples using mercapto functionalised-mcm-41 and regeneration of the sorbent using microwave digestion. *Journal of Hazardous Materials* **2011**, *193*, 171-176.

130. Mohammadi, N.; Khani, H.; Gupta, V. K.; Amereh, E.; Agarwal, S., Adsorption process of methyl orange dye onto mesoporous carbon material-kinetic and thermodynamic studies. *Journal of Colloid and Interface Science* **2011**, *362*, 457-462.

131. Tao, S.; Wang, C.; Ma, W.; Wu, S.; Meng, C., Designed multifunctionalized magnetic mesoporous microsphere for sequential sorption of organic and inorganic pollutants. *Microporous and Mesoporous Materials* **2012**, *147*, 295-301.

132. He, C.; Hu, X., Anionic dye adsorption on chemically modified ordered mesoporous carbons. *Industrial & Engineering Chemistry Research* **2011**, *50*, 14070-14083.

133. Barbosa, M.; Araujo, A.; Galvão, L.; Silva, E.; Santos, A.; Luz, G.; Fernandes, V., Carbon dioxide adsorption over dipa functionalized mcm-41 and sba-15 molecular sieves. *Journal of Thermal Analysis and Calorimetry* **2011**, *106*, 779-782.

134. Addorisio, V.; Pirozzi, D.; Esposito, S.; Sannino, F., Decontamination of waters polluted with simazine by sorption on mesoporous metal oxides. *Journal of Hazardous Materials* **2011**, *196*, 242-247.

135. Nunes, M. R.; Perez, G. M.; Loguercio, L. F.; Alves, E. W.; Carreno, N. L. V.; Martins, J. L.; Garcia, I. T. S., Active carbon preparation from treads of tire waste for dye removal in waste water. *Journal of the Brazilian Chemical Society* **2011**, *22*, 2027-2035.

136. Choi, J.-W.; Lee, S.-Y.; Chung, S.-G.; Hong, S.-W.; Kim, D.-J.; Lee, S.-H., Removal of phosphate from aqueous solution by functionalized mesoporous materials. *Water, Air, & Soil Pollution* **2011**, *222*, 243-254.

137. Yang, X.; Guan, Q.; Li, W., Effect of template in mcm-41 on the adsorption of aniline from aqueous solution. *Journal of Environmental Management* **2011**, *92*, 2939-2943.

138. Chen, H. M.; Chu, P. K.; He, J. H.; Hu, T.; Yang, M. Q., Porous magnetic manganese oxide nanostructures: Synthesis and their application in water treatment. *Journal of Colloid and Interface Science* **2011**, *359*, 68-74.

139. Song, J.; Kong, H.; Jang, J., Adsorption of heavy metal ions from aqueous solution by polyrhodanine-encapsulated magnetic nanoparticles. *Journal of Colloid and Interface Science* **2011**, *359*, 505-511.

140. Asuha, S.; Gao, Y. W.; Deligeer, W.; Yu, M.; Suyala, B.; Zhao, S., Adsorptive removal of methyl orange using mesoporous maghemite. *Journal of Porous Materials* **2011**, *18*, 581-587.

141. Deng, Y.; Cai, Y.; Sun, Z.; Gu, D.; Wei, J.; Li, W.; Guo, X.; Yang, J.; Zhao, D., Controlled synthesis and functionalization of ordered large-pore mesoporous carbons. *Advanced Functional Materials* **2010**, *20*, 3658-3665.

142. Lu, A.-H.; Li, W.-C.; Kiefer, A.; Schmidt, W.; Bill, E.; Fink, G.; Schüth, F., Fabrication of magnetically separable mesostructured silica with an open pore system. *Journal of the American Chemical Society* **2004**, *126*, 8616-8617.

143. Clark, L. C.; Lyons, C., Electrode systems for continuous monitoring in cardiovascular surgery. *Annals of the New York Academy of Sciences* **1962**, *102*, 29-45.

144. Wang, J., Electrochemical glucose biosensors. *Chemical Reviews* **2007**, *108*, 814-825.

145. Guilbault, G. G.; Lubrano, G. J., An enzyme electrode for the amperometric determination of glucose. *Analytica Chimica Acta* **1973**, *64*, 439-455.

146. Jiang, X.; Wu, Y.; Mao, X.; Cui, X.; Zhu, L., Amperometric glucose biosensor based on integration of glucose oxidase with platinum nanoparticles/ordered mesoporous carbon nanocomposite. *Sensors and Actuators B: Chemical* **2011**, *153*, 158-163.

147. Wang, L.; Bai, J.; Bo, X.; Zhang, X.; Guo, L., A novel glucose sensor based on ordered mesoporous carbon-au nanoparticles nanocomposites. *Talanta* **2011**, *83*, 1386-1391.

148. Dai, M.; Maxwell, S.; Vogt, B. D.; La Belle, J. T., Mesoporous carbon amperometric glucose sensors using inexpensive, commercial methacrylate-based binders. *Analytica Chimica Acta* **2012**, *738*, 27-34.

149. Su, C.; Zhang, C.; Lu, G.; Ma, C., Nonenzymatic electrochemical glucose sensor based on pt nanoparticles/mesoporous carbon matrix. *Electroanalysis* **2010**, *22*, 1901-1905.

150. Zhu, L.; Tian, C.; Zhu, D.; Yang, R., Ordered mesoporous carbon paste electrodes for electrochemical sensing and biosensing. *Electroanalysis* **2008**, *20*, 1128-1134.

151. Liang, C.; Li, Z.; Dai, S., Mesoporous carbon materials: Synthesis and modification. *Angewandte Chemie International Edition* **2008**, *47*, 3696-3717.

152. Schüth, F., Non-siliceous mesostructured and mesoporous materials†. *Chemistry of Materials* **2001**, *13*, 3184-3195.

153. Gao, P.; Wang, A.; Wang, X.; Zhang, T., Synthesis of highly ordered ir-containing mesoporous carbon materials by organic–organic self-assembly. *Chemistry of Materials* **2008**, *20*, 1881-1888.

154. Liu, C.-Y.; Chen, C.-F.; Leu, J.-P.; Lu, C.-C.; Liao, K.-H., Fabrication and carbon monoxide sensing characteristics of mesostructured carbon gas sensors. *Sensors and Actuators B: Chemical* **2009**, *143*, 12-16.

155. Wang, G.; Xing, W.; Zhuo, S., Application of mesoporous carbon to counter electrode for dye-sensitized solar cells. *Journal of Power Sources* **2009**, *194*, 568-573.

156. Baniamerian, M. J.; Moradi, S. E.; Noori, A.; Salahi, H., The effect of surface modification on heavy metal ion removal from water by carbon nanoporous adsorbent. *Applied Surface Science* **2009**, *256*, 1347-1354.

157. Lee, J.; Yoon, S.; Hyeon, T.; Oh, S. M.; Kim, K. B., Synthesis of a new mesoporous carbon and its application to electrochemical double-layer capacitors. *Chemical Communications* **1999**, 2177-2178.

158. Ryoo, R.; Joo, S. H.; Jun, S., Synthesis of highly ordered carbon molecular sieves via template-mediated structural transformation. *Journal of Physical Chemistry B* **1999**, *103*, 7743-7746.

159. Meng, Y.; Gu, D.; Zhang, F. Q.; Shi, Y. F.; Yang, H. F.; Li, Z.; Yu, C. Z.; Tu, B.; Zhao, D. Y., Ordered mesoporous polymers and homologous carbon frameworks: Amphiphilic surfactant templating and direct transformation. *Angewandte Chemie-International Edition* **2005**, *44*, 7053-7059.

160. Kosonen, H.; Valkama, S.; Nykanen, A.; Toivanen, M.; ten Brinke, G.; Ruokolainen, J.; Ikkala, O., Functional porous structures based on the pyrolysis of cured templates of block copolymer and phenolic resin. *Advanced Materials* **2006**, *18*, 201-+.

161. Liang, C. D.; Hong, K. L.; Guiochon, G. A.; Mays, J. W.; Dai, S., Synthesis of a large-scale highly ordered porous carbon film by self-assembly of block copolymers. *Angewandte Chemie-International Edition* **2004**, *43*, 5785-5789.

162. Tanaka, S.; Katayama, Y.; Tate, M. P.; Hillhouse, H. W.; Miyake, Y., Fabrication of continuous mesoporous carbon films with face-centered orthorhombic symmetry through a soft templating pathway. *Journal of Materials Chemistry* **2007**, *17*, 3639-3645.

163. Liang, C. D.; Dudney, N. J.; Howe, J. Y., Hierarchically structured sulfur/carbon nanocomposite material for high-energy lithium battery. *Chemistry of Materials* **2009**, *21*, 4724-4730.

164. Gorka, J.; Jaroniec, M., Incorporation of inorganic nanoparticles into mesoporous carbons synthesized by soft templating. *Journal of Physical Chemistry C* **2008**, *112*, 11657-11660.

165. Kwon, T.; Nishihara, H.; Itoi, H.; Yang, Q. H.; Kyotani, T., Enhancement mechanism of electrochemical capacitance in nitrogen-/boron-doped carbons with uniform straight nanochannels. *Langmuir* **2009**, *25*, 11961-11968.

166. Calvillo, L.; Moliner, R.; Lazaro, M. J., Modification of the surface chemistry of mesoporous carbons obtained through colloidal silica templates. *Materials Chemistry and Physics* **2009**, *118*, 249-253.

167. Hu, Q. Y.; Kou, R.; Pang, J. B.; Ward, T. L.; Cai, M.; Yang, Z. Z.; Lu, Y. F.; Tang, J., Mesoporous carbon/silica nanocomposite through multi-component assembly. *Chemical Communications* **2007**, 601-603.

168. Liu, R. L.; Shi, Y. F.; Wan, Y.; Meng, Y.; Zhang, F. Q.; Gu, D.; Chen, Z. X.; Tu, B.; Zhao, D. Y., Triconstituent co-assembly to ordered mesostructured polymer-silica and carbon-silica nanocomposites and large-pore mesoporous carbons with high surface areas. *Journal of the American Chemical Society* **2006**, *128*, 11652-11662.

169. Li, H. Q.; Liu, R. L.; Zhao, D. Y.; Xia, Y. Y., Electrochemical properties of an ordered mesoporous carbon prepared by direct tri-constituent co-assembly. *Carbon* **2007**, *45*, 2628-2635.

170. Zhao, X. C.; Wang, A. Q.; Yan, J. W.; Sun, G. Q.; Sun, L. X.; Zhang, T., Synthesis and electrochemical performance of heteroatom-incorporated ordered mesoporous carbons. *Chemistry of Materials* **2010**, *22*, 5463-5473.

171. Patel, M. N.; Wang, X.; Wilson, B.; Ferrer, D. A.; Dai, S.; Stevenson, K. J.; Johnston, K. P., Hybrid mno2-disordered mesoporous carbon nanocomposites: Synthesis and characterization as electrochemical pseudocapacitor electrodes. *Journal of Materials Chemistry* **2010**, *20*, 390-398.

172. Lou, X. W.; Deng, D.; Lee, J. Y.; Archer, L. A., Preparation of sno2/carbon composite hollow spheres and their lithium storage properties. *Chemistry of Materials* **2008**, *20*, 6562-6566.

173. Bruce, P. G.; Scrosati, B.; Tarascon, J. M., Nanomaterials for rechargeable lithium batteries. *Angewandte Chemie-International Edition* **2008**, *47*, 2930-2946.

174. Chou, S.-L.; Wang, J.-Z.; Sun, J.-Z.; Wexler, D.; Forsyth, M.; Liu, H.-K.; MacFarlane, D. R.; Dou, S.-X., High capacity, safety, and enhanced cyclability of lithium metal battery using a v2o5 nanomaterial cathode and room temperature ionic liquid electrolyte. *Chemistry of Materials* **2008**, *20*, 7044-7051.

175. Das, S. K.; Darmakolla, S.; Bhattacharyya, A. J., High lithium storage in micrometre sized mesoporous spherical self-assembly of anatase titania nanospheres and carbon. *Journal of Materials Chemistry* **2010**, *20*, 1600-1606.

176. Jiao, F.; Bruce, P. G., Mesoporous crystalline beta-mno2- a reversible positive electrode for rechargeable lithium batteries. *Advanced Materials* **2007**, *19*, 657-+.

177. Zhi, L.; Hu, Y.-S.; Hamaoui, B. E.; Wang, X.; Lieberwirth, I.; Kolb, U.; Maier, J.; Müllen, K., Precursor-controlled formation of novel carbon/metal and carbon/metal oxide nanocomposites. *Advanced Materials* **2008**, *20*, 1727-1731.

178. Lou, X. W.; Li, C. M.; Archer, L. A., Designed synthesis of coaxial sno2@carbon hollow nanospheres for highly reversible lithium storage. *Advanced Materials* **2009**, *21*, 2536-2539.

179. Esmanski, A.; Ozin, G. A., Silicon inverse-opal-based macroporous materials as negative electrodes for lithium ion batteries. *Advanced Functional Materials* **2009**, *19*, 1999-2010.

180. Li, Q.; Xu, J.; Wu, Z.; Feng, D.; Yang, J.; Wei, J.; Wu, Q.; Tu, B.; Cao, Y.; Zhao, D., Facile synthesis of highly stable and well-dispersed mesoporous zro2/carbon composites with high performance in oxidative dehydrogenation of ethylbenzene. *Physical Chemistry Chemical Physics* **2010**, *12*, 10996-11003.

181. Ishii, Y.; Kanamori, Y.; Kawashita, T.; Mukhopadhyay, I.; Kawasaki, S., Mesoporous carbon–titania nanocomposites for high-power li-ion battery anode material. *Journal of Physics and Chemistry of Solids* **2010**, *71*, 511-514.

182. Wang, D.; Kou, R.; Choi, D.; Yang, Z.; Nie, Z.; Li, J.; Saraf, L. V.; Hu, D.; Zhang, J.; Graff, G. L.; Liu, J.; Pope, M. A.; Aksay, I. A., Ternary self-assembly of ordered metal oxide−graphene nanocomposites for electrochemical energy storage. *ACS Nano* **2010**, *4*, 1587-1595.

183. Urade, V. N.; Hillhouse, H. W., Synthesis of thermally stable highly ordered nanoporous tin oxide thin films with a 3d face-centered orthorhombic nanostructure. *The Journal of Physical Chemistry B* **2005**, *109*, 10538-10541.

184. Baumann, T. F.; Fox, G. A.; Satcher, J. H.; Yoshizawa, N.; Fu, R.; Dresselhaus, M. S., Synthesis and characterization of copper-doped carbon aerogels. *Langmuir* **2002**, *18*, 7073-7076.

185. She, L.; Li, J.; Wan, Y.; Yao, X.; Tu, B.; Zhao, D., Synthesis of ordered mesoporous mgo/carbon composites by a one-pot assembly of amphiphilic triblock copolymers. *Journal of Materials Chemistry* **2011**, *21*, 795-800.

186. Zhan, Z.; Zeng, H. C., A catalyst-free approach for sol–gel synthesis of highly mixed zro2–sio2 oxides. *Journal of Non-Crystalline Solids* **1999**, *243*, 26-38.

187. Breitscheidel, B.; Zieder, J.; Schubert, U., Metal-complexes in inorganic matrices .7. Nanometer-sized, uniform metal particles in a sio2 matrix by sol-gel processing of metal-complexes. *Chemistry of Materials* **1991**, *3*, 559-566.

188. Meng, Y.; Gu, D.; Zhang, F.; Shi, Y.; Cheng, L.; Feng, D.; Wu, Z.; Chen, Z.; Wan, Y.; Stein, A.; Zhao, D., A family of highly ordered mesoporous polymer resin and carbon structures from organic−organic self-assembly. *Chemistry of Materials* **2006**, *18*, 4447-4464.

189. Dai, M.; Song, L.; LaBelle, J. T.; Vogt, B. D., Ordered mesoporous carbon composite films containing cobalt oxide and vanadia for electrochemical applications. *Chemistry of Materials* **2011**, *23*, 2869-2878.

190. Baklanov, M. R.; Mogilnikov, K. P.; Polovinkin, V. G.; Dultsev, F. N., Determination of pore size distribution in thin films by ellipsometric porosimetry.

Journal of Vacuum Science & Technology B: Microelectronics and Nanometer Structures **2000**, *18*, 1385-1391.

191. Sing, K. S. W.; Everett, D. H.; Haul, R. A. W.; Moscou, L.; Pierotti, R. A.; Rouquerol, J.; Siemieniewska, T., Reporting physisorption data for gas solid systems with special reference to the determination of surface-area and porosity (recommendations 1984). *Pure and Applied Chemistry* **1985**, *57*, 603-619.

192. Boissiere, C.; Grosso, D.; Lepoutre, S.; Nicole, L.; Bruneau, A. B.; Sanchez, C., Porosity and mechanical properties of mesoporous thin films assessed by environmental ellipsometric porosimetry. *Langmuir* **2005**, *21*, 12362-12371.

193. Song, L.; Feng, D.; Fredin, N. J.; Yager, K. G.; Jones, R. L.; Wu, Q.; Zhao, D.; Vogt, B. D., Challenges in fabrication of mesoporous carbon films with ordered cylindrical pores via phenolic oligomer self-assembly with triblock copolymers. *ACS Nano* **2009**, *4*, 189-198.

194. Lee, H.-J.; Soles, C. L.; liu, D.-W.; Bauer, B. J.; Lin, E. K.; Wu, W.-l.; Grill, A., Structural characterization of porous low-k thin films prepared by different techniques using x-ray porosimetry. *Journal of applied physics* **2004**, *95*, 5.

195. Smits, F. M., Measurement of sheet resistivity with the four-point probe. *The Bell Symtem Technical Journal* **1958**, 7.

196. Song, L.; Feng, D.; Campbell, C. G.; Gu, D.; Forster, A. M.; Yager, K. G.; Fredin, N.; Lee, H.-J.; Jones, R. L.; Zhao, D.; Vogt, B. D., Robust conductive mesoporous carbon-silica composite films with highly ordered and oriented orthorhombic structures from triblock-copolymer template co-assembly. *Journal of Materials Chemistry* **2010**, *20*, 1691-1701.

197. Fabregat-Santiago, F.; Mora-Seró, I.; Garcia-Belmonte, G.; Bisquert, J., Cyclic voltammetry studies of nanoporous semiconductors. Capacitive and reactive properties of nanocrystalline tio2 electrodes in aqueous electrolyte. *The Journal of Physical Chemistry B* **2002**, *107*, 758-768.

198. Li, X.; Larson, A. B.; Jiang, L.; Song, L.; Prichard, T.; Chawla, N.; Vogt, B. D., Evolution of mechanical, optical and electrical properties of self-assembled mesostructured phenolic resins during carbonization. *Microporous and Mesoporous Materials* **2011**, *138*, 86-93.

199. Biju, V.; Abdul Khadar, M., Ac conductivity of nanostructured nickel oxide. *Journal of Materials Science* **2001**, *36*, 5779-5787.

200. Shinde, V. R.; Mahadik, S. B.; Gujar, T. P.; Lokhande, C. D., Supercapacitive cobalt oxide (co3o4) thin films by spray pyrolysis. *Applied Surface Science* **2006**, *252*, 7487-7492.

201. Jayalakshmi, M.; Rao, M. M.; Venugopal, N.; Kim, K.-B., Hydrothermal synthesis of sno2–v2o5 mixed oxide and electrochemical screening of carbon nano-tubes (cnt), v2o5, v2o5–cnt, and sno2–v2o5–cnt electrodes for supercapacitor applications. *Journal of Power Sources* **2007**, *166*, 578-583.

202. Sugimoto, W.; Iwata, H.; Yokoshima, K.; Murakami, Y.; Takasu, Y., Proton and electron conductivity in hydrous ruthenium oxides evaluated by electrochemical impedance spectroscopy: The origin of large capacitance. *The Journal of Physical Chemistry B* **2005**, *109*, 7330-7338.

203. Hou, Z.; Zeng, F.; He, B.; Tao, W.; Ge, C.; Kuang, Y.; Zeng, J., High rate capability of ordered mesoporous carbon with platelet graphitic pore walls for lithium ion anodes. *Materials Letters* **2011**, *65*, 897-900.

204. Huang, C.-h.; Doong, R.-a.; Gu, D.; Zhao, D., Dual-template synthesis of magnetically-separable hierarchically-ordered porous carbons by catalytic graphitization. *Carbon*, *49*, 3055-3064.

205. Sang, L. C.; Vinu, A.; Coppens, M. O., Ordered mesoporous carbon with tunable, unusually large pore size and well-controlled particle morphology. *Journal of Materials Chemistry* **2011**, *21*, 7410-7417.

206. Wang, L.; Bai, J.; Bo, X.; Zhang, X.; Guo, L., A novel glucose sensor based on ordered mesoporous carbon-au nanoparticles nanocomposites. *Talanta* **2011**, *83*, 1386-1391.

207. Zhang, Y.; Xu, S.; Luo, Y.; Pan, S.; Ding, H.; Li, G., Synthesis of mesoporous carbon capsules encapsulated with magnetite nanoparticles and their application in wastewater treatment. *Journal of Materials Chemistry*, *21*, 3664-3671.

208. Zhang, Y.; Xu, S.; Luo, Y.; Pan, S.; Ding, H.; Li, G., Synthesis of mesoporous carbon capsules encapsulated with magnetite nanoparticles and their application in wastewater treatment. *Journal of Materials Chemistry* **2011**, *21*, 3664-3671.

209. Zhai, Y.; Dou, Y.; Liu, X.; Park, S. S.; Ha, C.-S.; Zhao, D., Soft-template synthesis of ordered mesoporous carbon/nanoparticle nickel composites with a high surface area. *Carbon* **2011**, *49*, 545-555.

210. Levario, T. J.; Dai, M.; Yuan, W.; Vogt, B. D.; Nielsen, D. R., Rapid adsorption of alcohol biofuels by high surface area mesoporous carbons. *Microporous and Mesoporous Materials* **2012**, *148*, 107-114.

211. Ryoo, R.; Joo, S. H.; Jun, S., Synthesis of highly ordered carbon molecular sieves via template-mediated structural transformation. *The Journal of Physical Chemistry B* **1999**, *103*, 7743-7746.

212. Kresge, C. T.; Leonowicz, M. E.; Roth, W. J.; Vartuli, J. C.; Beck, J. S., Ordered mesoporous molecular sieves synthesized by a liquid-crystal template mechanism. *Nature* **1992**, *359*, 710-712.

213. Lee, J.-S.; Joo, S. H.; Ryoo, R., Synthesis of mesoporous silicas of controlled pore wall thickness and their replication to ordered nanoporous carbons with various pore diameters. *Journal of the American Chemical Society* **2002**, *124*, 1156-1157.

214. Zhao, D.; Feng, J.; Huo, Q.; Melosh, N.; Fredrickson, G. H.; Chmelka, B. F.; Stucky, G. D., Triblock copolymer syntheses of mesoporous silica with periodic 50 to 300 angstrom pores. *Science* **1998**, *279*, 548-552.

215. Jun, S.; Joo, S. H.; Ryoo, R.; Kruk, M.; Jaroniec, M.; Liu, Z.; Ohsuna, T.; Terasaki, O., Synthesis of new, nanoporous carbon with hexagonally ordered mesostructure. *Journal of the American Chemical Society* **2000**, *122*, 10712-10713.

216. Meng, Y.; Gu, D.; Zhang, F.; Shi, Y.; Cheng, L.; Feng, D.; Wu, Z.; Chen, Z.; Wan, Y.; Stein, A.; Zhao, D., A family of highly ordered mesoporous polymer resin and carbon structures from organic−organic self-assembly. *Chemistry of Materials* **2006**, *18*, 4447-4464.

217. Tanaka, S.; Nishiyama, N.; Egashira, Y.; Ueyama, K., Synthesis of ordered mesoporous carbons with channel structure from an organic-organic nanocomposite. *Chemical Communications* **2005**, 2125-2127.

218. Liang, C.; Dai, S., Synthesis of mesoporous carbon materials via enhanced hydrogen-bonding interaction. *Journal of the American Chemical Society* **2006**, *128*, 5316-5317.

219. Liang, C.; Hong, K.; Guiochon, G. A.; Mays, J. W.; Dai, S., Synthesis of a large-scale highly ordered porous carbon film by self-assembly of block copolymers. *Angewandte Chemie International Edition* **2004**, *43*, 5785-5789.

220. Zhuang, X.; Wan, Y.; Feng, C.; Shen, Y.; Zhao, D., Highly efficient adsorption of bulky dye molecules in wastewater on ordered mesoporous carbons. *Chemistry of Materials* **2009**, *21*, 706-716.

221. Wang, W.; Wang, H.-y.; Wei, W.; Xiao, Z.-G.; Wan, Y., Self-assembling and size-selective synthesis of ni and nio nanoparticles embedded in ordered

mesoporous carbon and polymer frameworks. *Chemistry- A European Journal* **2011**, *17*, 13461-13472.

222. She, L.; Li, J.; Wan, Y.; Yao, X.; Tu, B.; Zhao, D., Synthesis of ordered mesoporous mgo/carbon composites by a one-pot assembly of amphiphilic triblock copolymers. *Journal of Materials Chemistry* **2011**, *21*, 795-800.

223. Li, Q.; Xu, J.; Wu, Z.; Feng, D.; Yang, J.; Wei, J.; Wu, Q.; Tu, B.; Cao, Y.; Zhao, D., Facile synthesis of highly stable and well-dispersed mesoporous zro2/carbon composites with high performance in oxidative dehydrogenation of ethylbenzene. *Phys. Chem. Chem. Phys.* **2010**, *12*, 10996-11003.

224. Gao, W.; Wan, Y.; Dou, Y.; Zhao, D., Synthesis of partially graphitic ordered mesoporous carbons with high surface areas. *Advanced Energy Materials* **2011**, *1*, 115-123.

225. Ji, Z.; Liang, S.; Jiang, Y.; Li, H.; Liu, Z.; Zhao, T., Synthesis and characterization of ruthenium-containing ordered mesoporous carbon with high specific surface area. *Carbon* **2009**, *47*, 2194-2199.

226. Zhai, Y.; Dou, Y.; Liu, X.; Tu, B.; Zhao, D., One-pot synthesis of magnetically separable ordered mesoporous carbon. *Journal of Materials Chemistry* **2009**, *19*, 3292-3300.

227. Liu, R.; Ren, Y.; Shi, Y.; Zhang, F.; Zhang, L.; Tu, B.; Zhao, D., Controlled synthesis of ordered mesoporous c−tio2 nanocomposites with crystalline titania frameworks from organic−inorganic−amphiphilic coassembly†. *Chemistry of Materials* **2007**, *20*, 1140-1146.

228. Hartmann, M., Ordered mesoporous materials for bioadsorption and biocatalysis. *Chemistry of Materials* **2005**, *17*, 4577-4593.

229. Wu, Z.; Zhao, D., Ordered mesoporous materials as adsorbents. *Chemical Communications* **2011**, *47*, 3332-3338.

230. Wu, Z.; Meng, Y.; Zhao, D., Nanocasting fabrication of ordered mesoporous phenol-formaldehyde resins with various structures and their adsorption performances for basic organic compounds. *Microporous and Mesoporous Materials* **2010**, *128*, 165-179.

231. Deng, Y.; Cai, Y.; Sun, Z.; Gu, D.; Wei, J.; Li, W.; Guo, X.; Yang, J.; Zhao, D., Controlled synthesis and functionalization of ordered large-pore mesoporous carbons. *Advanced Functional Materials* **2010**, *20*, 3658-3665.

232. Huang, C.-h.; Doong, R.-a.; Gu, D.; Zhao, D., Dual-template synthesis of magnetically-separable hierarchically-ordered porous carbons by catalytic graphitization. *Carbon* **2011**, *49*, 3055-3064.

233. Zhang, X.-l.; Niu, H.-y.; Li, W.-h.; Shi, Y.-l.; Cai, Y.-q., A core-shell magnetic mesoporous silica sorbent for organic targets with high extraction performance and anti-interference ability. *Chemical Communications* **2011**, *47*, 4454-4456.

234. Park, I.-S.; Choi, M.; Kim, T.-W.; Ryoo, R., Synthesis of magnetically separable ordered mesoporous carbons using furfuryl alcohol and cobalt nitrate in a silica template. *Journal of Materials Chemistry* **2006**, *16*, 3409-3416.

235. Lin, Y.-S.; Haynes, C. L., Synthesis and characterization of biocompatible and size-tunable multifunctional porous silica nanoparticles. *Chemistry of Materials* **2009**, *21*, 3979-3986.

236. Linjie, Z.; Yong-Sheng, H.; Bassem El, H.; Xuan, W.; Ingo, L.; Ute, K.; Joachim, M.; Klaus, M., Precursor-controlled formation of novel carbon/metal and carbon/metal oxide nanocomposites. *Advanced Materials* **2008**, *20*, 1727-1731.

237. Dai, M.; Song, L.; LaBelle, J. T.; Vogt, B. D., Ordered mesoporous carbon composite films containing cobalt oxide and vanadia for electrochemical applications. *Chemistry of Materials* **2011**, *23*, 2869-2878.

238. Liu, R. L.; Shi, Y. F.; Wan, Y.; Meng, Y.; Zhang, F. Q.; Gu, D.; Chen, Z. X.; Tu, B.; Zhao, D. Y., Triconstituent co-assembly to ordered mesostructured polymer-silica and carbon-silica nanocomposites and large-pore mesoporous carbons with high surface areas. *Journal of the American Chemical Society* **2006**, *128*, 11652-11662.

239. Song, L.; Feng, D.; Campbell, C. G.; Gu, D.; Forster, A. M.; Yager, K. G.; Fredin, N.; Lee, H.-J.; Jones, R. L.; Zhao, D.; Vogt, B. D., Robust conductive mesoporous carbon-silica composite films with highly ordered and oriented orthorhombic structures from triblock-copolymer template co-assembly. *Journal of Materials Chemistry* **2010**, *20*, 1691-1701.

240. Xue, C.; Lv, Y.; Zhang, F.; Wu, L.; Zhao, D., Copper oxide activation of soft-templated mesoporous carbons and their electrochemical properties for capacitors. *Journal of Materials Chemistry* **2012**, *22*, 1547-1555.

241. Yao, J.; Li, L.; Song, H.; Liu, C.; Chen, X., Synthesis of magnetically separable ordered mesoporous carbons from f127/[ni(h2o)6](no3)2/resorcinol-formaldehyde composites. *Carbon* **2009**, *47*, 436-444.

242. Bagshaw, S. A.; Prouzet, E.; Pinnavaia, T. J., Templating of mesoporous molecular sieves by nonionic polyethylene oxide surfactants. *Science* **1995**, *269*, 1242-1244.

243. Yang, H.; Yan; Liu, Y.; Zhang, F.; Zhang, R.; YanMeng, Y.; Li, M.; Xie, S.; Tu, B.; Zhao, D., A simple melt impregnation method to synthesize ordered mesoporous carbon and carbon nanofiber bundles with graphitized structure from pitches. *The Journal of Physical Chemistry B* **2004**, *108*, 17320-17328.

244. Cotet, L. C.; Gich, M.; Roig, A.; Popescu, I. C.; Cosoveanu, V.; Molins, E.; Danciu, V., Synthesis and structural characteristics of carbon aerogels with a high content of fe, co, ni, cu, and pd. *Journal of Non-Crystalline Solids* **2006**, *352*, 2772-2777.

245. Fu, R.; Baumann, T. F.; Cronin, S.; Dresselhaus, G.; Dresselhaus, M. S.; Satcher, J. H., Formation of graphitic structures in cobalt- and nickel-doped carbon aerogels. *Langmuir* **2005**, *21*, 2647-2651.

246. Yan, Y.; Wei, J.; Zhang, F.; Meng, Y.; Tu, B.; Zhao, D., The pore structure evolution and stability of mesoporous carbon fdu-15 under co2, o2 or water vapor atmospheres. *Micropor. Mesopor. Mater.* **2008**, *113*, 305-314.

247. Mohammadi, N.; Khani, H.; Gupta, V. K.; Amereh, E.; Agarwal, S., Adsorption process of methyl orange dye onto mesoporous carbon material–kinetic and thermodynamic studies. *J. Colloid and Interface Sci.* **2011**, *362*, 457-462.

248. He, C.; Hu, X., Anionic dye adsorption on chemically modified ordered mesoporous carbons. *Ind. Eng. Chem. Res.* **2011**, *50*, 14070-14083.

249. Teunissen, W.; de Groot, F. M. F.; Geus, J.; Stephan, O.; Tence, M.; Colliex, C., The structure of carbon encapsulated nife nanoparticles. *J. Catal.* **2001**, *204*, 169-174.

250. Lu, A.-H.; Schmidt, W.; Matoussevitch, N.; Bönnemann, H.; Spliethoff, B.; Tesche, B.; Bill, E.; Kiefer, W.; Schüth, F., Nanoengineering of a magnetically separable hydrogenation catalyst. *Angew. Chem.* **2004**, *116*, 4403-4406.

251. Zhou, Z.; Liu, G.; Han, D., Coating and structural locking of dipolar chains of cobalt nanoparticles. *ACS Nano* **2008**, *3*, 165-172.

252. Jiang, X.; Wu, Y.; Mao, X.; Cui, X.; Zhu, L., Amperometric glucose biosensor based on integration of glucose oxidase with platinum nanoparticles/ordered mesoporous carbon nanocomposite. *Sensors and Actuators B: Chemical* **2011**, *153*, 158-163.

253. Bo, X.; Bai, J.; Yang, L.; Guo, L., The nanocomposite of ptpd nanoparticles/onion-like mesoporous carbon vesicle for nonenzymatic amperometric sensing of glucose. *Sensors and Actuators B: Chemical* **2011**, *157*, 662-668.

254. Cash, K. J.; Clark, H. A., Nanosensors and nanomaterials for monitoring glucose in diabetes. *Trends in Molecular Medicine* **2010**, *16*, 584-593.

255. Wang, J., Electrochemical glucose biosensors. *Chemical Reviews* **2007**, *108*, 814-825.

256. Zhu, L.; Tian, C.; Yang, D.; Jiang, X.; Yang, R., Bioanalytical application of the ordered mesoporous carbon modified electrodes. *Electroanalysis* **2008**, *20*, 2518-2525.

257. Zhu, L.; Tian, C.; Zhu, D.; Yang, R., Ordered mesoporous carbon paste electrodes for electrochemical sensing and biosensing. *Electroanalysis* **2008**, *20*, 1128-1134.

258. You, C.; Yan, X.; Kong, J.; Zhao, D.; Liu, B., Bicontinuous gyroidal mesoporous carbon matrix for facilitating protein electrochemical and bioelectrocatalytic performances. *Talanta* **2011**, *83*, 1507-1514.

259. Li, H.; He, J.; Zhao, Y.; Wu, D.; Cai, Y.; Wei, Q.; Yang, M., Immobilization of glucose oxidase and platinum on mesoporous silica nanoparticles for the fabrication of glucose biosensor. *Electrochimica Acta* **2011**, *56*, 2960-2965.

260. Su, C.; Zhang, C.; Lu, G.; Ma, C., Nonenzymatic electrochemical glucose sensor based on pt nanoparticles/mesoporous carbon matrix. *Electroanalysis* **2010**, *22*, 1901-1905.

261. Lee, J. H.; Park, J. Y.; Min, K.; Cha, H. J.; Choi, S. S.; Yoo, Y. J., A novel organophosphorus hydrolase-based biosensor using mesoporous carbons and carbon black for the detection of organophosphate nerve agents. *Biosensors and Bioelectronics* **2010**, *25*, 1566-1570.

262. Wang, J.; Xue, C.; Lv, Y.; Zhang, F.; Tu, B.; Zhao, D., Kilogram-scale synthesis of ordered mesoporous carbons and their electrochemical performance. *Carbon* **2011**, *49*, 4580-4588.

263. Meng, Y.; Gu, D.; Zhang, F.; Shi, Y.; Cheng, L.; Feng, D.; Wu, Z.; Chen, Z.; Wan, Y.; Stein, A.; Zhao, D., A family of highly ordered mesoporous polymer resin and carbon structures from organic−organic self-assembly. *Chemistry of Materials* **2006**, *18*, 4447-4464.

264. Magasinski, A.; Zdyrko, B.; Kovalenko, I.; Hertzberg, B.; Burtovyy, R.; Huebner, C. F.; Fuller, T. F.; Luzinov, I.; Yushin, G., Toward efficient binders for li-ion battery si-based anodes: Polyacrylic acid. *ACS Appl. Mater. Interfaces* **2010**, *2*, 3004-3010.

265. Lux, S. F.; Schappacher, F.; Balducci, A.; Passerini, S.; Winter, M., Low cost, environmentally benign binders for lithium-ion batteries. *Journal of The Electrochemical Society* **2010**, *157*, A320-A325.

266. Pejovnik, S.; Dominko, R.; Bele, M.; Gaberscek, M.; Jamnik, J., Electrochemical binding and wiring in battery materials. *Journal of Power Sources* **2008**, *184*, 593-597.

267. Chen, Z.; Christensen, L.; Dahn, J. R., Comparison of pvdf and pvdf-tfe-p as binders for electrode materials showing large volume changes in lithium-ion batteries. *Journal of The Electrochemical Society* **2003**, *150*, A1073-A1078.

268. Fransson, L.; Eriksson, T.; Edström, K.; Gustafsson, T.; Thomas, J. O., Influence of carbon black and binder on li-ion batteries. *Journal of Power Sources* **2001**, *101*, 1-9.

269. Cheng, S.; Liu, H.; Logan, B. E., Power densities using different cathode catalysts (pt and cotmpp) and polymer binders (nafion and ptfe) in single chamber microbial fuel cells. *Environ. Sci. Technol.* **2005**, *40*, 364-369.

270. Beck, F.; Dolata, M., Fluorine-free binders for carbon black based electrochemical supercapacitors. *Journal of Applied Electrochemistry* **2001**, *31*, 517-521.

271. Komaba, S.; Shimomura, K.; Yabuuchi, N.; Ozeki, T.; Yui, H.; Konno, K., Study on polymer binders for high-capacity sio negative electrode of li-ion batteries. *The Journal of Physical Chemistry C* **2011**, *115*, 13487-13495.

272. Bishop, D. K.; La Belle, J. T.; Vossler, S. R.; Patel, D. R.; Cook, C. B., A disposable tear glucose biosensor---part 1: Design and concept testing. *Journal of Diabetes Science and Technology* **2010**, *4*, 299-306.

273. La Belle, J. T.; Bishop, D. K.; Vossler, S. R.; Patel, D. R.; Cook, C. B., A disposable tear glucose biosensor---part 2: System integration and model validation. *Journal of Diabetes Science and Technology* **2010**, *4*, 307-311.

274. Landt, M., Glyceraldehyde preserves glucose concentrations in whole blood specimens. *Clinical Chemistry* **2000**, *46*, 1144-1149.

275. Han, Y.-J.; Kim, J. M.; Stucky, G. D., Preparation of noble metal nanowires using hexagonal mesoporous silica sba-15. *Chemistry of Materials* **2000**, *12*, 2068-2069.

276. Yang, P.; Zhao, D.; Margolese, D. I.; Chmelka, B. F.; Stucky, G. D., Generalized syntheses of large-pore mesoporous metal oxides with semicrystalline frameworks. *Nature* **1998**, *396*, 152-155.

277. Song, L.; Feng, D.; Fredin, N. J.; Yager, K. G.; Jones, R. L.; Wu, Q.; Zhao, D.; Vogt, B. D., Challenges in fabrication of mesoporous carbon films with ordered cylindrical pores via phenolic oligomer self-assembly with triblock copolymers. *ACS Nano* **2009**, *4*, 189-198.

278. Harper, A.; Anderson, M. R., Electrochemical glucose sensors—developments using electrostatic assembly and carbon nanotubes for biosensor construction. *Sensors* **2010**, *10*, 8248-8274.

279. Vaillancourt, M.; Wei Chen, J.; Fortier, G.; Bédanger, D., Electrochemical and enzymatic studies of electron transfer mediation by ferrocene derivatives with nafion-glucose oxidase electrodes. *Electroanalysis* **1999**, *11*, 23-31.

280. Heller, A.; Feldman, B., Electrochemical glucose sensors and their applications in diabetes management. *Chemical Reviews* **2008**, *108*, 2482-2505.

281. Rosolen, J. M.; Matsubara, E. Y.; Marchesin, M. S.; Lala, S. M.; Montoro, L. A.; Tronto, S., Carbon nanotube/felt composite electrodes without polymer binders. *Journal of Power Sources* **2006**, *162*, 620-628.

282. Qin, S.; Saget, J.; Pyun, J.; Jia, S.; Kowalewski, T., Synthesis of block, statistical, and gradient copolymers from octadecyl (meth)acrylates using atom transfer radical polymerization. *Macromolecules* **2003**, *36*, 8969-8977.

283. Sinha, A.; Hess, D. W.; Henderson, C. L., A top surface imaging method using area selective ald on chemically amplified polymer photoresist films. *Electrochemical and Solid-State Letters* **2006**, *9*, G330-G333.

284. Holly, F. J.; Refojo, M. F., Wettability of hydrogels i. Poly(2-hydroxyethyl methacrylate). *Journal of Biomedical Materials Research* **1975**, *9*, 315-326.

285. Rao, J. K.; Ramesh, D. V.; Rao, K. P., Implantable controlled delivery systems for proteins based on collagen — phema hydrogels. *Biomaterials* **1994**, *15*, 383-389.

286. Roorda, W. E.; Bouwstra, J. A.; de Vries, M. A.; Junginger, H. E., Thermal behavior of poly hydroxy ethyl methacrylate (phema) hydrogels. *Pharmaceutical Research* **1988**, *5*, 722-725.

287. Mazloum-Ardakani, M.; Beitollahi, H.; Amini, M. K.; Mirkhalaf, F.; Mirjalili, B.-F., A highly sensitive nanostructure-based electrochemical sensor for electrocatalytic determination of norepinephrine in the presence of acetaminophen and tryptophan. *Biosensors and Bioelectronics* **2011**, *26*, 2102-2106.

288. Goyal, R. N.; Aziz, M. A.; Oyama, M.; Chatterjee, S.; Rana, A. R. S., Nanogold based electrochemical sensor for determination of norepinephrine in biological fluids. *Sensors and Actuators B: Chemical* **2011**, *153*, 232-238.

289. Goyal, R. N.; Agrawal, B., Ag ion irradiated based sensor for the electrochemical determination of epinephrine and 5-hydroxytryptamine in human biological fluids. *Analytica Chimica Acta* **2012**, *743*, 33-40.

290. Mazloum-Ardakani, M.; Sheikh-Mohseni, M. A.; Abdollahi-Alibeik, M.; Benvidi, A., Electrochemical sensor for simultaneous determination of norepinephrine, paracetamol and folic acid by a nanostructured mesoporous material. *Sensors and Actuators B: Chemical* **2012**, *171–172*, 380-386.

291. Mazloum-Ardakani, M.; Beitollahi, H.; Amini, M. K.; Mirkhalaf, F.; Abdollahi-Alibeik, M., New strategy for simultaneous and selective voltammetric determination of norepinephrine, acetaminophen and folic acid using zro2 nanoparticles-modified carbon paste electrode. *Sensors and Actuators B: Chemical* **2010**, *151*, 243-249.

292. Moraes, F. C.; Cesarino, I.; Coelho, D.; Pedrosa, V. A.; Machado, S. A. S., Highly sensitive neurotransmitters analysis at platinum-ultramicroelectrodes arrays. *Electroanalysis* **2012**, *24*, 1115-1120.

293. Zhu, M.; Huang, X.; Li, J.; Shen, H., Peroxidase-based spectrophotometric methods for the determination of ascorbic acid, norepinephrine, epinephrine, dopamine and levodopa. *Analytica Chimica Acta* **1997**, *357*, 261-267.

294. Carrera, V.; Sabater, E.; Vilanova, E.; Sogorb, M. A., A simple and rapid hplc–ms method for the simultaneous determination of epinephrine, norepinephrine, dopamine and 5-hydroxytryptamine: Application to the secretion of bovine chromaffin cell cultures. *Journal of Chromatography B* **2007**, *847*, 88-94.

295. Kuhlenbeck, D. L.; O'Neill, T. P.; Mack, C. E.; Hoke Ii, S. H.; Wehmeyer, K. R., Determination of norepinephrine in small volume plasma samples by stable-isotope dilution gas chromatography–tandem mass spectrometry with negative ion chemical ionization. *Journal of Chromatography B: Biomedical Sciences and Applications* **2000**, *738*, 319-330.

296. Wei, S.; Song, G.; Lin, J.-M., Separation and determination of norepinephrine, epinephrine and isoprinaline enantiomers by capillary electrophoresis in pharmaceutical formulation and human serum. *Journal of Chromatography A* **2005**, *1098*, 166-171.

297. Akhgar, M. R.; Beitollahi, H.; Salari, M.; Karimi-Maleh, H.; Zamani, H., Fabrication of a sensor for simultaneous determination of norepinephrine acetaminophen and tryptophan using a modified carbon nanotube paste electrode. *Anal. Methods* **2012**, *4*, 5.

298. Xu, G.-R.; Chang, H.-Y.; Cho, H.; Meng, W.; Kang, I.-K.; Bae, Z.-U., Macrocyclic nickel(ii) complex and hydrophilic polyurethane film electrodes for the electrocatalytic oxidation and selective detection of norepinephrine. *Electrochimica Acta* **2004**, *49*, 4069-4077.

299. Lee, J. H.; Park, J. Y.; Min, K.; Cha, H. J.; Choi, S. S.; Yoo, Y. J., A novel organophosphorus hydrolase-based biosensor using mesoporous carbons and carbon black for the detection of organophosphate nerve agents. *Biosensors and Bioelectronics* **2010**, *25*, 1566-1570.

300. Su, C.; Zhang, C.; Lu, G.; Ma, C., Nonenzymatic electrochemical glucose sensor based on pt nanoparticles/mesoporous carbon matrix. *Electroanalysis* **2010**, *22*, 1901-1905.

301. Cash, K. J.; Clark, H. A., Nanosensors and nanomaterials for monitoring glucose in diabetes. *Trends in Molecular Medicine* **2010**, *16*, 584-593.

302. Bo, X.; Bai, J.; Wang, L.; Guo, L., In situ growth of copper sulfide nanoparticles on ordered mesoporous carbon and their application as nonenzymatic amperometric sensor of hydrogen peroxide. *Talanta* **2010**, *81*, 339-345.

303. Dong, H.; Wang, S.; Liu, A.; Galligan, J. J.; Swain, G. M., Drug effects on the electrochemical detection of norepinephrine with carbon fiber and diamond microelectrodes. *Journal of Electroanalytical Chemistry* **2009**, *632*, 20-29.

304. Dai, M.; Maxwell, S.; Vogt, B. D.; La Belle, J. T., Mesoporous carbon amperometric glucose sensors using inexpensive, commercial methacrylate-based binders. *Analytica Chimica Acta* **2012**, *738*, 27-34.

305. Chicharro, M.; Sánchez, A.; Bermejo, E.; Zapardiel, A.; Rubianes, M. D.; Rivas, G. A., Carbon nanotubes paste electrodes as new detectors for capillary electrophoresis. *Analytica Chimica Acta* **2005**, *543*, 84-91.

306. Meng, Y.; Gu, D.; Zhang, F.; Shi, Y.; Cheng, L.; Feng, D.; Wu, Z.; Chen, Z.; Wan, Y.; Stein, A.; Zhao, D., A family of highly ordered mesoporous polymer resin and

carbon structures from organic−organic self-assembly. *Chemistry of Materials* **2006**, *18*, 4447-4464.

307. Jiang, X.; Wu, Y.; Mao, X.; Cui, X.; Zhu, L., Amperometric glucose biosensor based on integration of glucose oxidase with platinum nanoparticles/ordered mesoporous carbon nanocomposite. *Sensors and Actuators B: Chemical* **2011**, *153*, 158-163.

308. Zhou, M.; Shang, L.; Li, B.; Huang, L.; Dong, S., The characteristics of highly ordered mesoporous carbons as electrode material for electrochemical sensing as compared with carbon nanotubes. *Electrochemistry Communications* **2008**, *10*, 859-863.

309. Zhou, M.; Shang, L.; Li, B.; Huang, L.; Dong, S., Highly ordered mesoporous carbons as electrode material for the construction of electrochemical dehydrogenase- and oxidase-based biosensors. *Biosensors and Bioelectronics* **2008**, *24*, 442-447.

310. Liu, R. L.; Shi, Y. F.; Wan, Y.; Meng, Y.; Zhang, F. Q.; Gu, D.; Chen, Z. X.; Tu, B.; Zhao, D. Y., Triconstituent co-assembly to ordered mesostructured polymer-silica and carbon-silica nanocomposites and large-pore mesoporous carbons with high surface areas. *Journal of the American Chemical Society* **2006**, *128*, 11652-11662.

311. Xu, B.; Wu, F.; Chen, R.; Cao, G.; Chen, S.; Zhou, Z.; Yang, Y., Highly mesoporous and high surface area carbon: A high capacitance electrode material for edlcs with various electrolytes. *Electrochemistry Communications* **2008**, *10*, 795-797.

312. Li, H.-Q.; Luo, J.-Y.; Zhou, X.-F.; Yu, C.-Z.; Xia, Y.-Y., An ordered mesoporous carbon with short pore length and its electrochemical performances in supercapacitor applications. *Journal of The Electrochemical Society* **2007**, *154*, A731-A736.

313. Xing, W.; Qiao, S. Z.; Ding, R. G.; Li, F.; Lu, G. Q.; Yan, Z. F.; Cheng, H. M., Superior electric double layer capacitors using ordered mesoporous carbons. *Carbon* **2006**, *44*, 216-224.

314. Dai, M.; Vogt, B. D., High capacity magnetic mesoporous carbon–cobalt composite adsorbents for removal of methylene green from aqueous solutions. *Journal of Colloid and Interface Science* **2012**, *387*, 127-134.

315. Karandikar, P.; Patil, K. R.; Mitra, A.; Kakade, B.; Chandwadkar, A. J., Synthesis and characterization of mesoporous carbon through inexpensive mesoporous silica as template. *Microporous and Mesoporous Materials* **2007**, *98*, 189-199.

316. Axelrod, j., Purification and properties of phenylethanolamine-n-methyl transferase. *J. Biol. Chem.* **1962**, *237*, 1657-1660.

317. Fuller, R. W.; Molloy, B. B.; Day, W. A.; Roush, B. W.; Marsh, M. M., Inhibition of phenylethanolamine n-methyl transferase by benzylamines. 1. Structure-activity relations. *Journal of Medicinal Chemistry* **1973**, *16*, 101-106.

318. Hyodo, T.; Sasahara, K.; Shimizu, Y.; Egashira, M., Preparation of macroporous sno2 films using pmma microspheres and their sensing properties to nox and h2. *Sensors and Actuators B: Chemical* **2005**, *106*, 580-590.

319. Ouyang, H.; DeLouise, L. A.; Miller, B. L.; Fauchet, P. M., Label-free quantitative detection of protein using macroporous silicon photonic bandgap biosensors. *Analytical Chemistry* **2007**, *79*, 1502-1506.

320. Ouyang, H.; Striemer, C. C.; Fauchet, P. M., Quantitative analysis of the sensitivity of porous silicon optical biosensors. *Appl. Phys. Lett.* **2006**, *88*, 3.

321. Wang, Z.; Stein, A., Morphology control of carbon, silica, and carbon/silica nanocomposites: From 3d ordered macro-/mesoporous monoliths to shaped mesoporous particles†. *Chemistry of Materials* **2007**, *20*, 1029-1040.

322. Zhao, J.; Zhou, J.; Chen, Y.; He, Q.; Ruan, M.; Guo, L.; Shi, J.; Chen, H., Fabrication of mesoporous zeolite microspheres by a one-pot dual-functional templating approach. *Journal of Materials Chemistry* **2009**, 7614-7616.

323. Sadakane, M.; Horiuchi, T.; Kato, N.; Takahashi, C.; Ueda, W., Facile preparation of three-dimensionally ordered macroporous alumina, iron oxide, chromium oxide, manganese oxide, and their mixed-metal oxides with high porosity. *Chemistry of Materials* **2007**, *19*, 5779-5785.

324. Yan, H.; Blanford, C. F.; Lytle, J. C.; Carter, C. B.; Smyrl, W. H.; Stein, A., Influence of processing conditions on structures of 3d ordered macroporous metals prepared by colloidal crystal templating. *Chemistry of Materials* **2001**, *13*, 4314-4321.

325. Wang, X.; Xu, S.; Xu, W., Luminescent properties of dye-pmma composite nanospheres. *Physical Chemistry Chemical Physics* **2011**, 1560-1567.

326. Sasahara, K.; Hyodo, T.; Shimizu, Y.; Egashira, M., Macroporous and nanosized ceramic films prepared by modified sol-gel method with pmma microsphere templates. *Journal of the European Ceramic Society* **2004**, *24*, 1961-1967.

327. Zou, D.; Ma, S.; Guan, R.; Park, M.; Sun, L.; Aklonis, J. J.; Salovey, R., Model filled polymers. V. Synthesis of crosslinked monodisperse polymethacrylate beads. *Journal of Polymer Science Part A: Polymer Chemistry* **1992**, *30*, 137-144.

328. Fu, M.; Deng, L.; Zhao, A.; Wang, Y.; He, D., Fabrication and optical properties of alq3 doped pmma microsphere arrays templated by zno inverse opal structure. *Optical Materials* **2010**, *32*, 1210-1215.

329. Zhang, J.; Zhang, Y.; Lian, S.; Liu, Y.; Kang, Z.; Lee, S.-T., Highly ordered macroporous carbon spheres and their catalytic application for methanol oxidation. *Journal of Colloid and Interface Science* **2011**, *361*, 503-508.

330. Simonis, A.; Ruge, C.; Müller-Veggian, M.; Lüth, H.; Schöning, M. J., A long-term stable macroporous-type eis structure for electrochemical sensor applications. *Sensors and Actuators B: Chemical* **2003**, *91*, 21-25.

331. Qiu, J.-D.; Peng, H.-Z.; Liang, R.-P.; Xiong, M., Preparation of three-dimensional ordered macroporous prussian blue film electrode for glucose biosensor application. *Electroanalysis* **2007**, *19*, 1201-1206.

332. Hosoya, K.; Ogata, T.; Watabe, Y.; Kubo, T.; Ikegami, T.; Tanaka, N.; Minakuchi, H.; Nakanishi, K., Silica monolithic membrane as separation medium: Summable property of different membranes for high-performance liquid chromatographic separation. *Journal of Chromatography A* **2005**, *1073*, 123-126.

333. Chen, X.; Yang, W.; Liu, J.; Lin, L., Synthesis of zeolite naa membranes with high permeance under microwave radiation on mesoporous-layer-modified macroporous substrates for gas separation. *Journal of Membrane Science* **2005**, *255*, 201-211.

334. Lévesque, S. G.; Lim, R. M.; Shoichet, M. S., Macroporous interconnected dextran scaffolds of controlled porosity for tissue-engineering applications. *Biomaterials* **2005**, *26*, 7436-7446.

335. Al-Daous, M. A.; Stein, A., Preparation and catalytic evaluation of macroporous crystalline sulfated zirconium dioxide templated with colloidal crystals. *Chemistry of Materials* **2003**, *15*, 2638-2645.

336. Clark, L. C.; Lyons, C., Electrode systems for continuous monitoring in cardiovascular surgery. *Annals of the New York Academy of Sciences* **1962**, *102*, 29-45.

337. Pohanka, M.; Skladal, P., Electrochemical biosensors - principles and applications. *J. Appl. Biomed.* **2008**, 6, 57-64.

338. Gavalas, V. G.; Chaniotakis, N. A.; Gibson, T. D., Improved operational stability of biosensors based on enzyme-polyelectrolyte complex adsorbed into a porous carbon electrode. *Biosensors and Bioelectronics* **1998**, *13*, 1205-1211.

339. Dai, Z.; Bao, J.; Yang, X.; Ju, H., A bienzyme channeling glucose sensor with a wide concentration range based on co-entrapment of enzymes in sba-15 mesopores. *Biosensors and Bioelectronics* **2008**, *23*, 1070-1076.

340. Haghighi, B.; Tabrizi, M. A., Direct electron transfer from glucose oxidase immobilized on a nano-porous glassy carbon electrode. *Electrochimica Acta* **2011**, *56*, 10101-10106.

341. Cosnier, S.; Senillou, A.; Grätzel, M.; Comte, P.; Vlachopoulos, N.; Jaffrezic Renault, N.; Martelet, C., A glucose biosensor based on enzyme entrapment within polypyrrole films electrodeposited on mesoporous titanium dioxide. *Journal of Electroanalytical Chemistry* **1999**, *469*, 176-181.

342. Lee, Y.-J.; Park, J.-Y., A coral-like macroporous gold–platinum hybrid 3d electrode for enzyme-free glucose detection. *Sensors and Actuators B: Chemical* **2011**, *155*, 134-139.

343. Ouyang, H.; DeLouise, L. A.; Miller, B. L.; Fauchet, P. M., Label-free quantitative detection of protein using macroporous silicon photonic bandgap biosensors. *Analytical Chemistry* **2007**, *79*, 1502-1506.

344. Hyodo, T.; Sasahara, K.; Shimizu, Y.; Egashira, M., Preparation of macroporous sno2 films using pmma microspheres and their sensing properties to nox and h2. *Sensors and Actuators B: Chemical* **2005**, *106*, 580-590.

345. Ouyang, H.; Striemer, C. C.; Fauchet, P. M., Quantitative analysis of the sensitivity of porous silicon optical biosensors. *Appl. Phys. Lett.* **2006**, *88*, 163108 0-3.

346. Das, R. D.; Maji, S.; Das, S.; RoyChaudhuri, C., Optimization of covalent antibody immobilization on macroporous silicon solid supports. *Applied Surface Science* **2010**, *256*, 5867-5875.

347. Steinhauer, C.; Ressine, A.; Marko-Varga, G.; Laurell, T.; Borrebaeck, C. A. K.; Wingren, C., Biocompatibility of surfaces for antibody microarrays: Design of macroporous silicon substrates. *Analytical Biochemistry* **2005**, *341*, 204-213.

348. Moiola, L.; Galbiati, F.; Martino, G.; Amadio, S.; Brambilla, E.; Comi, G.; Vincent, A.; Grimaldi, L. M. E., Il-12 is involved in the induction of experimental autoimmune myasthenia gravis, an antibody- mediated disease. *European Journal of Immunology* **1998**, *28*, 2487-2497.

349. Gillies, S. D.; Lan, Y.; Wesolowski, J. S.; Qian, X.; Reisfeld, R. A.; Holden, S.; Super, M.; Lo, K.-M., Antibody-il-12 fusion proteins are effective in scid mouse models of prostate and colon carcinoma metastases. *The Journal of Immunology* **1998**, *160*, 6195-6203.

350. Aloisi, F.; Penna, G.; Cerase, J.; Menendez Iglesias, B.; Adorini, L., Il-12 production by central nervous system microglia is inhibited by astrocytes. *The Journal of Immunology* **1997**, *159*, 1604-1612.